



UNIVERSITI PUTRA MALAYSIA

***DESIGN AND SYNTHESIS OF NEW 1-ALKYL-3-BUTYLIMIDAZOLIUM
BROMIDE IONIC LIQUIDS AS MEDIA FOR DNA SOLVATION***

KHAIRULAZHAR BIN JUMBRI

FS 2015 73



DESIGN AND SYNTHESIS OF NEW 1-ALKYL-3-BUTYLIMIDAZOLIUM BROMIDE IONIC LIQUIDS AS MEDIA FOR DNA SOLVATION

By

KHAIRULAZHAR BIN JUMBRI

**Thesis Submitted to the School of Graduate Studies,
Universiti Putra Malaysia, in Fulfilment of the
Requirements for the Degree of Doctor of Philosophy**

February 2015

All material contained within the thesis, including without limitation text, logos, icons, photographs and all other artwork, is copyright material of Universiti Putra Malaysia unless otherwise stated. Use may be made of any material contained within the thesis for non-commercial purposes from the copyright holder. Commercial use of material may only be made with the express, prior, written permission of Universiti Putra Malaysia.

Copyright © Universiti Putra Malaysia



Abstract of thesis presented to the Senate of Universiti Putra
Malaysia in fulfilment of the requirement for the degree of Doctor of
Philosophy

**DESIGN AND SYNTHESIS OF NEW 1-ALKYL-3-
BUTYLIMIDAZOLIUM BROMIDE IONIC LIQUIDS AS MEDIA FOR
DNA SOLVATION**

By

KHAIRULAZHAR BIN JUMBRI

February 2015

Chair: Mohd Basyaruddin Abdul Rahman, PhD

Faculty: Faculty of Science

The influence of ionic liquids (ILs) on the structural properties of DNA was revealed by experimental and molecular dynamics (MD) simulation. In the first part of experimental section, six new 1-alkyl-3-butylimidazolium bromide ILs ($[C_n\text{bim}][\text{Br}]$ where $n = 2, 4, 6, 8, 10$ and 12) were successfully synthesized. All of the ILs was obtained using simple alkylation reaction of 1-butylimidazole with various bromoalkanes, which gave high yield above 85%. Their physico-chemical properties, including the spectroscopic characteristics have been comprehensively studied. Three of these ILs (C_2, C_4, C_6) exist in liquid form while the others appear as semi solid at room temperature. Proton and carbon NMR and CHN elemental analysis were carried out to identify the molecular structure and purity of ILs produced. The thermal stability studied using TGA indicated that these new ILs were stable up to 270°C . As expected, the viscosity of three liquid salts hugely increased from $199 \text{ mPa}\cdot\text{s}$ ($[C_2\text{bim}][\text{Br}]$) to $1180 \text{ mPa}\cdot\text{s}$ ($[C_6\text{bim}][\text{Br}]$), while the density slightly decreased with increasing length of alkyl chains.

The properties of Calf thymus DNA in hydrated ILs were studied using spectroscopic analysis. The strong interactions between the P-O bond of DNA phosphate groups and the $[C_n\text{bim}]^+$ lead to compact DNA conformation, which excludes the intercalation of ethidium with DNA. Although the DNA stability is mainly due to the electrostatic attraction between DNA and ILs' cation, hydrophobic

interactions between hydrocarbon chains of $[C_n\text{bim}]^+$ and DNA bases also provided a major driving force for the binding of ILs to DNA. The effect of ILs concentration at 25°C shows that the DNA maintains its B-conformation in all solution of hydrated ILs despite the high concentration up to 75% (w/w). During heating process, hydrated ILs are observed to stabilize DNA helical structure up to $56^\circ\text{C} \pm 1.0^\circ\text{C}$, almost 11°C higher than DNA in water. The DNA melting temperature is found gradually increases with increasing length of alkyl chain from $56^\circ\text{C} \pm 1.0^\circ\text{C}$ (in $[C_2\text{bim}][\text{Br}]$) to $58^\circ\text{C} \pm 1.0^\circ\text{C}$ in the presence of $[C_6\text{bim}][\text{Br}]$.

In the first part of MD simulation, the force fields (FFs) parameter for these three liquid ILs ($[C_n\text{bim}][\text{Br}]$ where $n = 2, 4$ and 6) was validated based on experimental evidences. The modified collision parameter (σ) to 0.369 nm for the anion shows the simulation data obtained were in agreement with experimental density and viscosity with the percentage error below $\pm 2.0\%$ and $\pm 10.0\%$, respectively. The validated FFs were then applied for simulation of DNA in these ILs. The MD data offers clear evidence that the DNA maintains its B-conformation in all $[C_4\text{bim}]\text{Br}$ systems (25, 50 and 75% w/w). The hydration layer around the DNA phosphate group was the main factor in determining DNA stabilization. Stronger hydration shells in 25% $[C_4\text{bim}][\text{Br}]$ in water (w/w) reduced the binding ability of ILs' cations to the DNA phosphate groups. The computed energy shows that the electrostatic energy between $[C_4\text{bim}]^+ - [\text{PO}_4]^-$ (-46.55 ± 4.75 kcal mol $^{-1}$) is lower than water- $[\text{PO}_4]^-$ (-12.78 ± 2.12 kcal mol $^{-1}$). Effect of temperature revealed that ILs was able to retain DNA native conformation at high temperature up to 373.15 K in the presence of 75% $[C_4\text{bim}]\text{Br}$. All the simulations findings were in agreement with experimental evidences. The prediction solvation free energy of nucleic acids bases performed in last part of MD simulation revealed that the nucleic acid bases were better solvated in ILs rather than in aqueous solution.

Abstrak tesis yang dikemukakan kepada Senat Universiti Putra
Malaysia sebagai memenuhi keperluan untuk Ijazah Doktor
Falsafah

**REKABENTUK DAN SINTESIS CECAIR IONIK BAHARU 1-ALKIL-
3-BUTILIMIDAZOLIUM BROMIDA SEBAGAI MEDIA UNTUK
SOLVASI DNA**

Oleh

KHAIRULAZHAR BIN JUMBRI

Febuari 2015

Pengerusi: Mohd Basyaruddin Abdul Rahman, PhD

Fakulti: Fakulti Sains

Pengaruh cecair ionik (ILs) pada sifat-sifat struktur DNA telah didedahkan oleh eksperimen dan simulasi molekul dinamik (MD). Dalam bahagian pertama seksyen experiment, enam 1-alkil-3-butylimidazolium bromida ILs baharu ($[C_n\text{bim}][\text{Br}]$ di mana $n = 2, 4, 6, 8, 10$ dan 12) telah berjaya disintesis. Kesemua ILs diperolehi menggunakan tindak balas pengalkilan mudah 1-butylimidazol dengan pelbagai bromoalkana, yang memberi hasil tinggi di atas 85%. Sifat-sifat fiziko-kimia termasuk ciri-ciri spektroskopi telah dikaji secara menyeluruh. Tiga daripada ILs ini (C_2, C_4, C_6) wujud dalam bentuk cecair manakala yang lain muncul sebagai separuh pepejal pada suhu bilik. Proton dan karbon NMR dan analisis elemen CHN dilakukan untuk mengenal pasti struktur molekul dan ketulenan ILs yang dihasilkan. Kestabilan terma yang telah dikaji menggunakan TGA menunjukkan bahawa ILs baharu ini stabil sehingga suhu 270°C . Seperti yang dijangka, kelikatan tiga garam cecair meningkat mendadak daripada $199 \text{ mPa}\cdot\text{s}$ ($[C_2\text{bim}][\text{Br}]$) kepada $1180 \text{ mPa}\cdot\text{s}$ ($[C_6\text{bim}][\text{Br}]$), manakala data ketumpatan sedikit menurun dengan peningkatan rantai alkil.

Sifat-sifat DNA daripada Calf thymus dalam ILs terhidrat telah dikaji menggunakan analisis spektroskopi. Interaksi kuat antara ikatan P-O kumpulan fosfat DNA dan $[C_n\text{bim}]^+$ membawa kepada bentuk DNA yang padat, yang mana menyingkirkan interkalasi etidium dengan DNA. Walaupun kestabilan DNA terutamanya adalah

disebabkan oleh tarikan elektrostatik antara DNA dan kation ILs, interaksi hidrofobik antara rantai hidrokarbon $[C_n\text{bim}]^+$ dan bes DNA juga memberikan daya pendorong utama untuk pengikatan ILs kepada DNA. Kesan kepekatan ILs pada suhu 25°C menunjukkan bahawa DNA mengekalkan konformasi-B dalam semua larutan ILs terhidrat meskipun dalam kepekatan yang tinggi sehingga 75% (w/w). Semasa proses pemanasan, larutan ILs terhidrat diperhatikan menstabilkan struktur helix DNA sehingga suhu $56^\circ\text{C} \pm 1.0^\circ\text{C}$, hampir 11°C lebih tinggi daripada DNA di dalam air. Suhu lebur DNA didapati beransur-ansur meningkat dengan peningkatan panjang rantai alkil daripada $56^\circ\text{C} \pm 1.0^\circ\text{C}$ (di dalam $[C_2\text{bim}][\text{Br}]$) kepada $58^\circ\text{C} \pm 1.0^\circ\text{C}$ dalam kehadiran $[C_6\text{bim}][\text{Br}]$.

Dalam bahagian pertama simulasi MD, parameter medan daya (FFs) untuk tiga cecair ILs ($[C_n\text{bim}][\text{Br}]$ di mana $n = 2, 4$ dan 6) telah disahkan berdasarkan bukti-bukti eksperimen. Parameter perlanggaran (σ) untuk anion yang telah diubahsuai kepada 0.369 nm menunjukkan bahawa data simulasi yang diperolehi didapati bersetuju dengan data eksperimen ketumpatan dan kelikatan dengan peratus ralat masing-masing di bawah $\pm 2.0\%$ and $\pm 10.0\%$. FFs yang telah disahkan kemudiannya digunakan untuk simulasi DNA dalam ILs ini. MD data menunjukkan bukti yang jelas bahawa DNA mengekalkan konformasi-B di dalam semua sistem $[C_4\text{bim}]\text{Br}$ (25%, 50% dan 75% w/w). Lapisan penghidratan sekitar kumpulan fosfat DNA adalah faktor utama dalam menentukan kestabilan DNA. Lapisan penghidratan lebih kuat dalam 25% $[C_4\text{bim}][\text{Br}]$ (w/w) di dalam air telah mengurangkan keupayaan pengikatan kation ILs kepada kumpulan fosfat DNA. Tenaga yang dikira menunjukkan bahawa tenaga elektrostatik antara $[C_4\text{bim}]^+ - [\text{PO}_4]^-$ (-46.55 ± 4.75 kcal mol $^{-1}$) adalah lebih rendah berbanding air- $[\text{PO}_4]^-$ (-12.78 ± 2.12 kcal mol $^{-1}$). Kesan suhu mendedahkan bahawa ILs telah berupaya mengekalkan konformasi asal DNA pada suhu tinggi sehingga 373.15 K dalam kehadiran 75% $[C_4\text{bim}][\text{Br}]$. Semua penemuan simulasi didapati bersetuju dengan bukti-bukti eksperimen. Ramalan tenaga bebas pensolvatan bes nukleik acid yang dilakukan dalam bahagian akhir simulasi MD mendedahkan bahawa bes nukleik acid lebih mudah terlarut di dalam ILs berbanding di dalam larutan akues.

ACKNOWLEDGEMENTS

In the Name of Allah, The Most Merciful and Most Beneficent

Alhamdulillah, praise to ALLAH s.w.t., for giving me the strength to endure all challenges and complete this research. First and foremost, I'd like to thank my supervisor, Prof. Dr. Mohd Basyaruddin Abdul Rahman for all of his support, guidance and advice from the very early stage of this research as well as giving me extraordinary experiences throughout the work. Above all and the most needed, he provided me unflinching encouragement and support in various ways.

I am also indebted to my committee members, Dr. Emilia Abdul Malek, Dr. Haslina Ahmad and Dr. Nuno Micaelo for their invaluable guidance, encouragement and criticism, which kept me in a right track. Without these people, this research would not have been possible. Many thanks go to member of EMTech Research Centre and all of lab mates in the Organics and Synthetic Chemistry Lab. Without your presence and support, the lab experience would not have been complete. Many thanks also for member of Computational and Theoretical Chemistry Lab who really help through this study. For my good friends Mohd Azlan, Muhammad Alif, Asrul Farris, Mohd Rizal and others, thanks for the strong bonding of friendship and support during my research.

A special appreciation goes to all lecturers and staff in the Department of Chemistry, for their help and advice. Thank to Ministry of Science, Technology and Innovation Malaysia (MOSTI) for *National Science Fellowship* (NSF) scholarship and Universiti Putra Malaysia for financial support and facilities.

Finally and most importantly, I would like to express my appreciation to my wife, Noor Alifah Abdul Rahim whose dedication, love and persistent confidence in me. Thank you for being a good listener and accompany in my "Research World". Not to forget my sons, Muhammad Dayyan and Muhammad Zayyad Iman. Ayah loves both of you so much. For my parents and my family in-law who always show their endured me during difficult time and supported me in all my pursuits. Thanks you so much!

I certify that a Thesis Examination Committee has met on 23 February 2015 to conduct the final examination of Khairulazhar bin Jumbri on his thesis entitled “Design and Synthesis of New 1-Alkyl-3-Butylimidazolium Bromide Ionic Liquids as Media for DNA Solvation” in accordance with the Universities and University Colleges Act 1971 and the Constitution of the Universiti Putra Malaysia [P.U.(A) 106] 15 March 1998. The Committee recommends that the student be awarded the Doctor of Philosophy.

Members of the Thesis Examination Committee were as follows:

Mohamed Ibrahim bin Mohamed Tahir, PhD

Senior lecturer
Faculty of Science
Universiti Putra Malaysia
(Chairman)

Nor Azah binti Yusof, PhD

Professor
Faculty of Science
Universiti Putra Malaysia
(Internal Examiner)

Yatimah binti Alias, PhD

Professor
Faculty of Science
Universiti Malaya
(External Examiner)

Luis Paulo S.N.M Rebelo, PhD

Professor
Estacao Agronomica Nacional
Spain
(External Examiner)



ZULKARNAIN ZAINAL, PhD

Professor and Deputy Dean
School of Graduate Studies
Universiti Putra Malaysia

Date: 15 April 2015

This thesis was submitted to the Senate of Universiti Putra Malaysia and has been accepted as fulfilment of the requirement for the degree of Doctor of Philosophy. The members of the Supervisory Committee were as follows:

Mohd Basyaruddin Abdul Rahman, PhD

Professor
Faculty of Science
Universiti Putra Malaysia
(Chairman)

Emilia Abdul Malek, PhD

Senior Lecturer
Faculty of Science
Universiti Putra Malaysia
(Member)

Haslina Ahmad, PhD

Senior Lecturer
Faculty of Science
Universiti Putra Malaysia
(Member)

Nuno Miguel da Silva Micaelo, PhD

Senior Lecturer
Chemistry Centre
Minho University, Campus de Gualtar
Braga, Portugal
(Member)

BUJANG KIM HUAT, PhD

Professor and Dean
School of Graduate Studies
Universiti Putra Malaysia

Date:

Declaration by graduate student

I hereby confirm that:

- this thesis is my original work;
- quotations, illustrations and citations have been duly referenced;
- this thesis has not been submitted previously or concurrently for any other degree at any other institutions;
- intellectual property from the thesis and copyright of thesis are fully-owned by Universiti Putra Malaysia, as according to the Universiti Putra Malaysia (Research) Rules 2012;
- written permission must be obtained from supervisor and the office of Deputy Vice-Chancellor (Research and Innovation) before thesis is published (in the form of written, printed or in electronic form) including books, journals, modules, proceedings, popular writings, seminar papers, manuscripts, posters, reports, lecture notes, learning modules or any other materials as stated in the Universiti Putra Malaysia (Research) Rules 2012;
- there is no plagiarism or data falsification/fabrication in the thesis, and scholarly integrity is upheld as according to the Universiti Putra Malaysia (Graduate Studies) Rules 2003 (Revision 2012-2013) and the Universiti Putra Malaysia (Research) Rules 2012. The thesis has undergone plagiarism detection software.

Signature: _____ Date: _____

Name and Matric No.: KHAIRULAZHAR BIN JUMBRI (GS 27792)

Declaration by Members of Supervisory Committee

This is to confirm that:

- the research conducted and the writing of this thesis was under our supervision;
- supervision responsibilities as stated in the Universiti Putra Malaysia (Graduate Studies) Rules 2003 (Revision 2012-2013) are adhered to.

Signature: _____
Name of Chairman
of Supervisory
Committee: _____

Signature: _____
Name of Member of
Supervisory
Committee: _____

Signature: _____
Name of Member of
Supervisory
Committee: _____

Signature: _____
Name of Member of
Supervisory
Committee: _____

TABLE OF CONTENTS

	Page
ABSTRACT	i
ABSTRAK	iii
ACKNOWLEDGEMENTS	v
APPROVAL	vi
DECLARATION	vii
LIST OF TABLES	xv
LIST OF FIGURES	xviii
LIST OF SCHEME	xxv
LIST OF ABBREVIATIONS	xxvi
CHAPTER	
1 INTRODUCTION	1
1.1 Background of Research	1
1.2 Problem Statements	2
1.3 Research Objectives	4
2 LITERATURE REVIEW	5
2.1 History of Ionic Liquids	5
2.2 Properties of Ionic Liquids	9
2.2.1 Density	10
2.2.2 Viscosity	10
2.2.3 Thermal Stability and Liquid Range	11
2.2.4 Solubility and Polarity	12
2.3 Molecular Modeling Studies of Ionic Liquids	13
2.4 DNA	16
2.5 Non-covalent Binding to DNA	17
2.5.1 Electrostatic Attraction	17
2.5.2 Groove Binding	18
2.5.3 Intercalation	18
2.6 Ionic Liquids in DNA Biotechnology	19
2.7 Molecular Modeling Study of DNA in Ionic Liquids	22
2.8 Principles of Computational Chemistry	24
2.9 Molecular Dynamics	24
2.9.1 Pressure Coupling	26
2.9.2 Temperature Coupling	26
2.10 Optimization of Simulations	27
2.10.1 Periodic Boundary Condition	27
2.10.2 Long-range Electrostatic Interaction	28
2.11 Force Fields	28

	2.11.1	Bonded Interaction	30
	2.11.2	Non-Bonded Interaction	31
3		MATERIALS AND METHODS	33
	3.1	General Flow of Research Design	33
	3.2	Chemicals and Materials	36
	3.3	Hardware	36
	3.4	Software	36
	3.5	Experimental Methods	37
	3.5.1	Synthesis of New Ionic Liquids	37
		3.5.1.1 Distillation of 1-butylimidazole	37
		3.5.1.2 General Procedure	37
	3.5.2	Physico-Chemical Characterization	39
		3.5.2.1 Proton and Carbon NMR	39
		3.5.2.2 CHN Elemental Analysis	39
		3.5.2.3 Thermogravimetric Analysis	39
		3.5.2.4 Density Measurement	39
		3.5.2.5 Viscosity Measurement	40
	3.5.3	Biophysical Analysis of DNA in Ionic Liquids	40
		3.5.3.1 Preparation of DNA Stock Solution	40
		3.5.3.2 Purity of DNA	40
		3.5.3.3 Fluorescence Emission	41
		3.5.3.4 Circular Dichroism	41
		3.5.3.5 UV-visible	42
	3.6	Computational Procedures	42
	3.6.1	Geometry Optimization	42
	3.6.2	Partial Atomic Charges	44
	3.6.3	Force Fields	45
	3.6.4	System Setup	46
		3.6.4.1 Ionic Liquids	46
		3.6.4.2 DNA in Ionic Liquids	46
		3.6.4.3 Solvation Free Energy	50
	3.6.5	Molecular Dynamics Parameters	50
	3.6.6	Simulation Details	51
		3.6.6.1 Systems of Ionic Liquids	51
		3.6.6.2 Systems of DNA in Ionic Liquids	51
		3.6.6.3 Free Energy Systems	52
	3.6.7	Data Analysis	52
		3.6.7.1 Density	52
		3.6.7.2 Shear Viscosity	53
		3.6.7.3 Self-diffusion Coefficient	54
		3.6.7.4 Molecular Structure	54

	3.6.7.5	Root Mean Square Deviation	55
	3.6.7.6	Root Mean Square Fluctuation	55
	3.6.7.7	Hydrogen Bonds	56
	3.6.7.8	Free Energy Calculation	56
4	RESULTS AND DISCUSSION		59
	4.1	Design, Synthesis and Characterization of New Ionic Liquids	59
	4.1.1	Screening of Ionic Liquids	59
	4.1.2	Proton and Carbon NMR	62
	4.1.2.1	1-ethyl-3-butylimidazolium bromide ([C ₂ bim][Br])	62
	4.1.2.2	1,3-dibutylimidazolium bromide ([C ₄ bim][Br])	63
	4.1.2.3	1-hexyl-3-butylimidazolium bromide ([C ₆ bim][Br])	64
	4.1.2.4	1-octyl-3-butylimidazolium bromide ([C ₈ bim][Br])	65
	4.1.2.5	1-decyl-3-butylimidazolium bromide ([C ₁₀ bim][Br])	66
	4.1.2.6	1-dodecyl-3-butylimidazolium bromide ([C ₁₂ bim][Br])	67
	4.1.3	Physico-Chemical Properties	68
	4.1.3.1	Elemental Analysis (CHN) Studies	68
	4.1.3.2	Thermal Analysis	69
	4.1.3.3	Density	71
	4.1.3.4	Viscosity	71
	4.2	Biophysical Properties of DNA in Ionic Liquids	73
	4.2.1	Ionic liquid-DNA Binding	73
	4.2.2	Effect of Hydrocarbon Length of Ionic Liquids	77
	4.2.3	Structural Stability of DNA	82
	4.2.3.1	DNA in Aqueous Solution	82
	4.2.3.2	DNA in Ionic Liquids	84
	4.2.4	Melting Temperature of DNA	88
	4.3	Molecular Dynamics Simulation of Ionic Liquids	91
	4.3.1	Density	92
	4.3.2	Shear Viscosity	94
	4.3.3	Self-diffusion Coefficient	97
	4.3.4	Molecular Structure	100
	4.3.5	Polar and Non-Polar Regions	104

4.4	DNA Molecular Solvation in Ionic Liquids	106
4.4.1	Structural Modeling of DNA in Ionic Liquids	106
4.4.2	Role of Hydration Shells	111
4.4.3	Water Stripped from DNA Surface	115
4.4.4	Binding Characteristics of Ionic Liquid-DNA	117
4.4.5	Flexibility of DNA in Ionic Liquids	119
4.4.6	Hydrogen Bonding Interaction	121
4.5	Free Energies Solvation	123
4.5.1	Nucleic Acids Bases in Aqueous System	123
4.5.2	Nucleic Acids Bases in Ionic Liquids	125
5	SUMMARY, CONCLUSION AND RECOMMENDATIONS FOR FUTURE RESEARCH	128
5.1	Summary and Conclusion	128
5.2	Recommendations for Future Research	130
	REFERENCES	131
APPENDIX A1	Non-bonded parameters	153
APPENDIX A2	Bonds and angles parameters	154
APPENDIX A3	Dihedral and improper dihedral parameters	155
APPENDIX B1	Steepest Descent method	156
APPENDIX B2	Conjugate Gradient method	157
APPENDIX B3	NVT pre-equilibration	158
APPENDIX B4	NPT production simulation	159
APPENDIX B5	NVT non-equilibration for viscosity	160
APPENDIX C1	Steepest Descent method for free energy	161
APPENDIX C2	Conjugate Gradient method for free energy	162
APPENDIX C3	Stochastic dynamics NVT	163
APPENDIX C4	Stochastic dynamics NPT	165
APPENDIX D1	¹ H NMR spectrum of 1-ethyl-3-butylimidazolium bromide ([C ₂ bim][Br])	167
APPENDIX D2	¹³ C NMR spectrum of 1-ethyl-3-butylimidazolium bromide ([C ₂ bim][Br])	168
APPENDIX D3	¹ H NMR spectrum of 1,3-dibutylimidazolium bromide ([C ₄ bim][Br])	169
APPENDIX D4	¹³ C NMR spectrum of 1,3-dibutylimidazolium bromide ([C ₄ bim][Br])	170
APPENDIX D5	¹ H NMR spectrum of 1-hexyl-3-butylimidazolium bromide ([C ₆ bim][Br])	171
APPENDIX D6	¹³ C NMR spectrum of 1-hexyl-3-butylimidazolium bromide ([C ₆ bim][Br])	172
APPENDIX D7	¹ H NMR spectrum of 1-octyl-3-butylimidazolium bromide ([C ₈ bim][Br])	173

APPENDIX D8	¹³ C NMR spectrum of 1-octyl-3-butylimidazolium bromide ([C ₈ bim][Br])	174
APPENDIX D9	¹ H NMR spectrum of 1-decyl-3-butylimidazolium bromide ([C ₁₀ bim][Br])	175
APPENDIX D10	¹³ C NMR spectrum of 1-decyl-3-butylimidazolium bromide ([C ₁₀ bim][Br])	176
APPENDIX D11	¹ H NMR spectrum of 1-dodecyl-3-butylimidazolium bromide ([C ₁₂ bim][Br])	177
APPENDIX D12	¹³ C NMR spectrum of 1-dodecyl-3-butylimidazolium bromide ([C ₁₂ bim][Br])	178
APPENDIX E	Fluorescence emission spectra of A) [C ₂ bim][Br] and B) [C ₆ bim][Br] in the absence (bottom curve) and presence of calf thymus DNA in aqueous solution of deionized water. The arrow indicates that the emission intensity of increases with the addition of DNA. Excitation wavelength was set at 320 nm.	179
APPENDIX F1	Circular dichroism (A) and UV absorbance (B) spectra of 60 μM Calf thymus DNA in the presence of [C ₂ bim][Br] at different temperatures. Concentration [C ₂ bim][Br] was fixed at 0.1 M.	180
APPENDIX F2	Circular dichroism (A) and UV absorbance (B) spectra of 60 μM Calf thymus DNA in the presence of [C ₆ bim][Br] at different temperatures. Concentration [C ₆ bim][Br] was fixed at 0.1 M.	181
LIST OF PUBLICATIONS / SEMINAR / CONFERENCE BIODATA OF AUTHOR		182 184

LIST OF TABLES

Table		Page
2.1	The effect of cation size on the melting point.	11
2.2	Structural features of ideal A-, B- and Z-DNA (Source: Dickerson <i>et al.</i> , 1982).	17
3.1	Starting materials and abbreviated names for newly synthesized ILs.	38
3.2	Partial atomic charges for each set of atoms derived using RESP calculation. Atom type of opls_071 and opls_068 represent the UA model for CH_2 and CH_3 groups, respectively. For clarity, refer Figure 3.2 (page 43) for the position of each atom name. The charge for bromide anion ($[Br^-]$) is also shown.	45
3.3	Number of molecules used in the simulation of DNA.	48
3.4	Number of molecules used in the free energy simulation.	50
4.1	Physical properties and solubility of $[C_n\text{bim}][Br]$ ILs.	61
4.2	1H and ^{13}C NMR assignments of $[C_2\text{bim}][Br]$.	62
4.3	1H and ^{13}C NMR assignments of $[C_4\text{bim}][Br]$.	63
4.4	1H and ^{13}C NMR assignments of $[C_6\text{bim}][Br]$.	64
4.5	1H and ^{13}C NMR assignments of $[C_8\text{bim}][Br]$.	65
4.6	1H and ^{13}C NMR assignments of $[C_{10}\text{bim}][Br]$.	66
4.7	1H and ^{13}C NMR assignments of $[C_{12}\text{bim}][Br]$.	67
4.8	Quantitative analysis of carbon, hydrogen and nitrogen in $[C_n\text{bim}][Br]$ ILs compared with calculated theoretical values (shown in bracket).	68

4.9	Physico-chemical properties of [C _n bim][Br] ILs.	69
4.10	Predicted density obtained from MD simulation using different collision parameter (σ) in comparison to the experimental density of [C _n bim][Br] ILs at 298.15 K.	92
4.11	Calculated viscosities with different amplitude parameter.	95
4.12	The self-diffusion coefficient (D) from the slope of MSD plots (with standard deviation values in parentheses) and cationic (t_+) and anionic (t_-) anionic transference numbers for cations and anion in [C _n bim]Br ILs. The collision parameter (σ) of 0.369 for bromine atom was used.	97
4.13	Average number of [C ₄ bim][Br] ions and water molecules within 0.35 nm from the DNA surface at different temperatures. Data averaged from the last 2 ns of MD simulations.	113
4.14	The calculated of interaction energies between different parts in the simulation systems. The contribution of electrostatic and <i>van der Waals</i> interactions are shown.	119
4.15	Average number of Watson-Crick hydrogen bonds of DNA strands at different percentages of [C ₄ bim]Br (% w/w) and various temperatures. Hydrogen bonds are considered when the distances between the donor and the acceptor less than 0.35 nm and the angle hydrogen-donor-acceptor are lower than 30°. Average hydrogen bonds of DNA strands in aqueous system were also calculated for the purpose of comparison. Data averaged over the last 2 ns of MD simulations.	121
4.16	Average hydrogen bonds formed between DNA bases and ILs' cations and anions at different temperatures. H-bonds are considered to occur when the distances between the donor and the acceptor are less than 0.35 nm is and the angle hydrogen-donor-acceptor is lower than 30°. The hydrogen bond is considered between a proton in an imidazolium ring and the DNA	122

bases. Data is averaged over the last 2 ns of MD simulations.

- | | | |
|------|--|-----|
| 4.17 | Solvation free energy (kcal mol^{-1}) of nucleic acids bases in water. | 124 |
| 4.18 | Solvation free energy (kcal mol^{-1}) of nucleic acids bases in ILs from this work. Solvation free energy of nucleic acids in water was also depicted for comparison. | 127 |



LIST OF FIGURES

Figure		Page
2.1	Comparison between lattice energy of NaCl and [C ₂ mim][Cl] (Source: Wilkes <i>et al.</i> , 1982).	5
2.2	Structure of earliest [EtNH ₃][NO ₃] IL synthesized by Walden (1914).	6
2.3	Structure of [C ₂ mim][AlCl ₄].	6
2.4	Second generation ILs containing <i>N,N</i> -dialkylimidazolium and water stable or weakly coordinating anions.	7
2.5	Examples of cations and anions of "3 rd generation ILs".	8
2.6	Typical structures of cations and anions that are widely used in synthesizing various ILs.	9
2.7	Different types of anions responsible for water miscibility and immiscibility of ILs.	12
2.8	Position of C ² atom in [C _n mim] ⁺ cation.	14
2.9	RDF of ionic liquid [bmim][PF ₆] showing the longer-range ordered structure (Source: Micaelo <i>et al.</i> , 2006).	15
2.10	Snapshot from a MD simulation of [C ₆ mim][PF ₆] in which polar regions are colored red and non-polar regions are colored green (Source: Kioupis <i>et al.</i> , 2002).	16
2.11	Major DNA duplex conformations from left to right: A-DNA (PDB ID: 440D) (Yi-Gui <i>et al.</i> , 1999), B-DNA (PDB ID: 1FQ2) and Z-DNA (PDB ID: 2F8W) (Sines <i>et al.</i> , 2000).	16
2.12	Schematic representation of IL-coated capillary surface (Source: Qin and Li, 2003).	20
2.13	Schematic illustration of the interactions of [C ₄ mim] ⁺ cation with DNA phosphate groups	20

	during the extraction of dsDNA by [C ₄ mim][PF ₆] (Source: Wang <i>et al.</i> , 2007a).	
2.14	The DNA–ethidium bromide interaction in aqueous phase (top) and the IL–DNA–ethidium bromide interaction in [C ₄ mim][PF ₆] phase (bottom) (Source: Cheng <i>et al.</i> , 2007).	21
2.15	Schematic illustration of the mechanism of interaction between [C ₄ mim][Cl] and DNA (Source: Ding <i>et al.</i> , 2010).	22
2.16	Non-bonded interactions between polar atoms in alkylimidazolium cation with DNA bases (Source: Cardoso and Micaelo, 2011).	23
2.17	Distribution of [C ₄ mim] ⁺ cations around DNA surface. The cations were interact with DNA backbone, minor groove and major groove (Source: Chandran <i>et al.</i> , 2012).	23
2.18	Flow chart of steps performed in molecular dynamics program.	25
2.19	Schematics picture represents the PBC.	28
2.20	Type of the interactions exists in liquid system.	29
3.1	General flow of research design.	35
3.2	Geometry optimized cations with atom names. Structure of (a) [C ₂ bim] ⁺ (b) [C ₄ bim] ⁺ and (c) [C ₆ bim] ⁺ were model based on UA in which the hydrogen atoms are not explicitly considered. Proton HAR, HA4 and HA5 located at imidazolium ring were model AA description.	43
3.3	Snapshot of initial box of simulation for Calf thymus DNA in TIP4P model of water (top) and neat [C ₂ bim][Br] (bottom).	47
3.4	The initial box of simulation for the DNA in hydrated [C ₄ bim][Br] systems. A) 25%; B) 50% and C) 75% (w/w) [C ₄ bim][Br] in water. View from top of cubic simulation box.	49

3.5	Replicating previously equilibrated system along the z-axis.	54
3.6	Thermodynamic cycle used to determine the absolute solvation free energy (ΔG_{solv}) of given molecules A or B.	57
4.1	Different alkyl halides used in synthesizing of new $[\text{C}_n\text{bim}][\text{Br}]$ ILs.	60
4.2	Thermograms of $[\text{C}_n\text{bim}][\text{Br}]$ ILs detected by TGA.	70
4.3	The geometry structure of $[\text{C}_4\text{bim}]^+$ cation. The dashed line shows the symmetrical point.	72
4.4	Fluorescence emission spectra of $[\text{C}_4\text{bim}][\text{Br}]$ in the absence (bottom curve) and presence of Calf thymus DNA in aqueous solution of deionized water. The arrow indicates that the emission intensity of $[\text{C}_4\text{bim}][\text{Br}]$ increases with the addition of DNA. Excitation wavelength for $[\text{C}_4\text{bim}][\text{Br}]$ was set at 320 nm.	74
4.5	Hydrogen bond recognition sites accessible from the DNA major and minor grooves. Arrow outside the major and minor grooves represent the hydrogen bond receptors while arrow inside represents hydrogen bond donors.	76
4.6	The fluorescence profile of EB exhibits both increased emission intensity and hypsochromic shift in the presence of Calf thymus DNA. Excitation wavelength of EB was set at 510 nm.	78
4.7	Fluorescence emission spectra of EB-bound DNA complex in the presence of different concentration of ILs: (a) 2.5×10^{-3} M, (b) 5.0×10^{-3} M, (c) 7.5×10^{-3} M, (d) 1.0×10^{-2} M, (e) 1.25×10^{-2} M, (f) 1.5×10^{-2} M, (g) 2.5×10^{-2} M, (h) 5.0×10^{-1} M, (i) 7.5×10^{-1} M, (j) 1.0 M, (k) 1.25 M, (l) 1.5 M and (m) 2.0 M. The arrow shows the decreased emission intensity of EB-bound DNA upon the addition of (A) $[\text{C}_2\text{bim}][\text{Br}]$; (B) $[\text{C}_4\text{bim}][\text{Br}]$ and (C) $[\text{C}_6\text{bim}][\text{Br}]$. Excitation wavelength of EB was set at 510 nm.	80

4.8	Normalized emission intensity of EB-bound DNA complex with the continuous addition of different concentration of $[C_n\text{bim}][\text{Br}]$ ILs. The excitation wavelength of EB was set at 510 nm while the emission intensity was observed at λ_{max} 618 nm.	81
4.9	Circular dichroism spectra of Calf thymus DNA (300 μM) in deionized water at different temperatures.	83
4.10	UV-absorbance spectra of Calf thymus DNA in deionized water at different temperatures. Concentration of DNA was fixed at 300 μM .	84
4.11	Circular dichroism spectra of Calf thymus DNA (300 μM) in deionized water and in different percentages of hydrated $[C_4\text{bim}][\text{Br}]$ at 25°C. Control was Calf thymus DNA (300 μM) in aqueous solution at 25°C.	85
4.12	Absorbance of Calf thymus DNA (300 μM) in deionized water (control, black line) and in different percentages of hydrated $[C_4\text{bim}][\text{Br}]$ at 25°C. Control was calf thymus DNA (300 μM) in aqueous solution at 25°C.	86
4.13	Circular dichroism spectra of Calf thymus DNA (300 μM) in the presence of 25% $[C_4\text{bim}][\text{Br}]$ solution at different temperatures. Control DNA spectrum was Calf thymus DNA (300 μM) in deionized water at 25°C.	87
4.14	UV-absorbance spectra of Calf thymus DNA (300 μM) in the presence of 25% $[C_4\text{bim}][\text{Br}]$ solution at different temperatures.	88
4.15	Effects of alkyl chain lengths of $[C_n\text{bim}][\text{Br}]$ ILs towards the thermal stability of Calf thymus DNA. The Calf thymus DNA (60 μM) was dissolved in 25% $[C_n\text{bim}][\text{Br}]$ ILs in aqueous solution.	89
4.16	Schematic representation of duplex DNA view from the top showing the cylindrical model of DNA. DNA phosphate groups on the outside and amine groups on the inside show the hydrophilic regions, whereas the sugar groups in between	90

phosphate and amine groups form a partly hydrophobic region (Source: Hammouda, 2009).

- 4.17 A representative 10 ns graph of density of $[C_n\text{bim}][\text{Br}]$ ILs using new collision diameter (σ) of 0.369 nm at 298.15 K. 94
- 4.18 Graph of shear viscosities for A) $[C_2\text{bim}][\text{Br}]$, B) $[C_4\text{bim}][\text{Br}]$ and C) $[C_6\text{bim}][\text{Br}]$ obtained using acceleration amplitude 0.02 nm ps^{-2} . 96
- 4.19 MSD as a function of time for A) $[C_2\text{bim}][\text{Br}]$; B) $[C_4\text{bim}][\text{Br}]$ and C) $[C_6\text{bim}][\text{Br}]$. 98
- 4.20 RDF for the cation-anion (ca), cation-cation (cc) and anion-anion (aa) interactions in A) $[C_2\text{bim}][\text{Br}]$, B) $[C_4\text{bim}][\text{Br}]$ and C) $[C_6\text{bim}][\text{Br}]$. 101
- 4.21 RDF of cation-anion (ca) of each $[C_n\text{bim}]\text{Br}$ ILs. 102
- 4.22 Spatial distribution probability density of anions around cations in $[C_2\text{bim}][\text{Br}]$ (top), $[C_4\text{bim}][\text{Br}]$ (mid) and $[C_6\text{bim}][\text{Br}]$ (bottom) at 298.15 K. Anions at a maximum distance of 0.45 nm from the imidazole geometric center were selected. 103
- 4.23 Snapshots of simulation boxes of $[C_2\text{bim}][\text{Br}]$ (left) and $[C_6\text{bim}][\text{Br}]$ (right) in which atoms belonging to the polar domains of the cation (imidazolium ring) and to the anion were colored in red and atoms belonging to the non-polar domains (alkyl side chain) were colored in green. 104
- 4.24 RDF of anion-anion (aa) correlation for each of $[C_n\text{bim}][\text{Br}]$ ILs. 105
- 4.25 RMSD (nm) of duplex Calf thymus B-DNA conformation (all heavy atoms) solvated by three $[C_n\text{bim}][\text{Br}]$ ILs at 298.15 K. 106
- 4.26 Comparison of Calf thymus B-DNA structures after solvated in different neat ILs at 298.15 K. Initial crystal structure of DNA (A), structure of DNA in neat $[C_2\text{bim}]\text{Br}$ (B), $[C_4\text{bim}]\text{Br}$ (C) and $[C_6\text{bim}]\text{Br}$ (D). The circles show that the bases in DNA strands located at head and tail were most

disturbed by ILs molecules in comparison to the bases in the middle of DNA strands. The backbone of DNA consists of phosphate groups is able to maintain its helical shape due to the strong electrostatic attraction formed between ILs' cation and DNA phosphate groups. Colour schemes are as follow: red, oxygen; magenta, phosphorus; orange, backbone of DNA and gray, DNA bases. The structure of DNA in each ILs was taken from the final conformations of a 10 ns MD simulation trajectory.

- 4.27 RMSD (nm) of duplex DNA (all heavy atoms) simulated in neat [C₄bim][Br] at various temperatures. 108
- 4.28 Average RMSD (nm) of DNA (all heavy atoms) solvated in different percentages of hydrated [C₄bim][Br] solution (25%, 50% and 75% w/w) at various temperatures. For comparison, simulation of DNA in aqueous system is shown at zero percentage of [C₄bim][Br]. Values are averages over the last 2 ns of MD simulation. 109
- 4.29 Representative distribution of [C₄bim]⁺ molecules showing their association with the DNA phosphate groups, major and minor grooves. The distribution of anion ([Br]⁻) molecules was not shown here. Colour schemes are as follow: red, oxygen; magenta, phosphorus; gray, DNA structure; green, carbon; blue; nitrogen and white; proton. Figure made from the final conformations of a 10 ns MD simulation trajectory. 110
- 4.30 Representative populations of cations and water molecules within 0.35 nm of DNA surface. A) 25%, B) 50% and C) 75% (w/w) [C₄bim]Br solutions at 298.15 K. Colour scheme are as follow: white, water; blue, cation. Figures were taken from the final conformations of a 10 ns MD simulation trajectory. 111

- 4.31 DNA conformations obtained from last 10 ns simulation trajectories. A) Structure of DNA in pure water system; B) 25%; C) 50%; D) 75%; E) Neat (100%) [C₄bim]Br and F) Initial crystal structure of DNA. 112
- 4.32 Spin of hydration layers of water in the minor groove of DNA from control simulation (left). Penetration of hydration layers by [C₄bim]⁺ cations at the minor groove in 25% (mid) and 75% (right) of [C₄bim]Br solutions. 114
- 4.33 Percentage of water stripped from the DNA surface at different percentages of [C₄bim]Br in solution and at different temperatures. A) 298.15 K, B) 323.15 K, C) 343.15 K and D) 373.15 K. Colour scheme: black, 75%; gray, 50% and cyan, 25% (w/w) [C₄bim]Br solution. The percentage of water molecules stripped from DNA surface was calculated from the fraction of water present within 0.35 nm located from DNA surface divided with the initial water count in the same distance. Data for analysis was taken from the last 2 ns simulation trajectories. 116
- 4.34 (A) ILs' cations (head charge group) COM-RDF around DNA phosphate groups. (B) Exclusion of ILs' anions COM-RDF in the same region. Colour scheme: gray, [C₂bim]Br; orange, [C₄bim]Br and magenta, [C₆bim]Br. 118
- 4.35 RMSF of DNA bases (all heavy atoms) in different hydrated [C₄bim]Br systems including DNA in neat [C₄bim]Br at various temperatures. DNA in 25% (w/w) [C₄bim]Br, (A); 50%, (B); 75%, (C) and neat [C₄bim]Br (D). Colour scheme are as follow: black, 298.15 K; blue, 323.15 K; yellow, 343.15 K and red, 373.15 K. Bases of DNA strand A pair with bases of DNA strand B with the following combination A-T and C-G pairs. RMSF averaged over the last 2 ns of MD simulation. 120

LIST OF SCHEMES

Scheme		Page
3.1	Preparation of 1-alkyl-3-butylimidazolium bromide ILs ($[C_n\text{bim}][\text{Br}]$).	38
4.1	Mechanism of alkylation reaction of 1-butylimidazole with bromoalkanes.	61
4.2	Pyrolysis of alkylimidazolium with different alkyl chains length attached to nitrogen atoms via S_N2 mechanism in the presence of nucleophilic bromide (Source: Awad <i>et al.</i> , 2004).	70

LIST OF ABBREVIATIONS

$[\text{AlCl}_4]^-$	Tetrachloroaluminate
$[\text{BF}_4]^-$	Tetrafluoroborate
$[\text{C}_{10}\text{mim}][\text{Cl}]$	1-decyl-3-methylimidazolium chloride
$[\text{C}_{10}\text{mim}][\text{PF}_6]$	1-decyl-3-methylimidazolium hexafluorophosphate
$[\text{C}_1\text{mim}][\text{Cl}]$	1,3-dimethylimidazolium chloride
$[\text{C}_2\text{mim}][\text{AlCl}_4]$	1-ethyl-3-methylimidazolium tetrachloroaluminate
$[\text{C}_2\text{mim}][\text{BF}_4]$	1-ethyl-3-methylimidazolium tetrafluoroborate
$[\text{C}_2\text{mim}][\text{Cl}]$	1-ethyl-3-methylimidazolium chloride
$[\text{C}_2\text{mim}][\text{N}(\text{SO}_2\text{CF}_3)_2]$	1-ethyl-3-methylimidazolium bis(trifluoromethanesulfonate)imide
$[\text{C}_2\text{mim}][\text{PF}_6]$	1-ethyl-3-methylimidazolium hexafluorophosphate
$[\text{C}_2\text{mim}]^+$	1-ethyl-3-methylimidazolium
$[\text{C}_4\text{mim}][\text{BF}_4]$	1-butyl-3-methylimidazolium tetrafluoroborate
$[\text{C}_4\text{mim}][\text{Cl}]$	1-butyl-3-methylimidazolium chloride
$[\text{C}_4\text{mim}][\text{PF}_6]$	1-butyl-3-methylimidazolium hexafluorophosphate
$[\text{C}_4\text{mim}]^+$	1-butyl-3-methylimidazolium
$[\text{C}_6\text{mim}][\text{PF}_6]$	1-hexyl-3-methylimidazolium hexafluorophosphate
$[\text{CF}_3\text{O}_3\text{S}]^-$	Trifluoromethanesulfonate
$[\text{C}_n\text{bim}][\text{Br}]$	1-alkyl-3-butylimidazolium bromide

[C _n mim][BF ₄]	1-alkyl-3-methylimidazolium tetrafluoroborate
[C _n mim][PF ₆]	1-alkyl-3-methylimidazolium hexafluorophosphate
[C _n mim] ⁺	1-alkyl-3-methylimidazolium
[E] ⁺	Ethidium
[EtNH ₃][NO ₃]	Ethylammonium nitrate
[Ms ₂ N] ⁻	Bis(methanesulfonyl)amide
[N(SO ₂ CF ₃) ₂] ⁻	Bis(trifluoromethanesulfonate)imide
[NO ₃] ⁻	Nitrate
[PF ₆] ⁻	Hexafluorophosphate
[SO ₄] ²⁻	Sulfate
[TF]	Trifluoromethylsulfonate
³¹ P NMR	³¹ Phosphorus NMR
A ₂₆₀	Absorbance at wavelength 260 nm
AA	All-atom
AM1 / SM2	Austin Model 1 / Semiempirical quantum chemical solvation Model 2
AM1-MST	Austin Model 1 / Miertus–Scrocco–Tomasi
AMBER	Assisted Model Building with Energy Refinement
A-T	Adenine-Thymine
B3LYP	Becke's Three-parameter Hybrid Functional
BAR bp	Bennet Acceptance Ratio Base pairs

Br	Bromine
CD	Circular dichroism
C-G	Cytosine-Guanine
CH_2	Methylene
CH_3	Methyl
CHARM	Chemistry at HARvard Molecular Mechanics
CHN	Carbon, Hydrogen, Nitrogen
COM	Centre-of-mass
d_5 -CDCl ₃	Deuterated chloroform
DESO	Diethylsulfoxide
DFT	Density Functional Theory
DMF	Dimethylformamide
DMSO	Dimethylsulfoxide
DPSO	Dipropylsulfoxide
dsDNA	Double-stranded DNA
EB	Ethidium bromide
ESP	Electrostatic potential
FDPB	Finite Difference Poisson-Boltzmann
FEP	Free Energy Perturbation
FFs	Force Fields
FRET	Fluorescence resonance energy transfer
FT-IR	Fourier transform-Infrared
GROMOS	GRONingen Molecular Simulation

IL	Ionic liquid (singular)
ILs	Ionic liquids (plural)
kbp	Kilo base pairs
KCl	Potassium chloride
LINCS	Linear Constraint Solver
LJ	Lennard-Jones
MC	Monte Carlo
MD	Molecular dynamics
mdeg	Milidegree
MSD	Mean square displacement
MST	Miertus–Scrocco–Tomasi
NaCl	Sodium chloride
NDB	Nucleic Acids Database
NEMD	Non-equilibrium molecular dynamics
NMR	Nuclear Magnetic Resonance
NPT	Isobaric-isothermal ensemble
NVT	Canonical ensemble
OPLS	Optimized Potential for Liquid Simulation
PBC	Periodic boundary condition
PCR	Polymerase chain reaction
PDB	Protein Data Bank
PME	Particle Mesh-Ewald
QM	Quantum mechanics
QM/MM	Quantum mechanics / Molecular mechanics

RDF	Radial distribution function
RES-COM	Residue-centre of mass
RESP	Restrained electrostatic potential
RMSD	Root mean square deviation
RMSF	Root mean square fluctuation
RTILs	Room temperature ionic liquids
S1	Vibrational level 1
SCRFF	Self consistent reaction field
SDF	Spatial distribution function
SF ₆	Sulfur hexafluoride
SFE	Solvation free energy
S ₀	Ground state
ssDNA	Single-stranded DNA
TGA	Thermogravimetric Analysis
TI	Thermodynamics Integration
T _m	Melting temperature
T _{onset}	Onset temperature
UA	United-atom
w/w	Weight over weight
ΔG _{solv}	Absolute solvation free energy

CHAPTER 1

INTRODUCTION

1.1 Background of Research

Since the discovery of DNA over half a century ago, doing research on DNA has become a subject of intense interest. In many aspects of nucleic acid metabolism, the stability of double helical DNA structure is extremely important and plays a main role especially in biomedical applications. The specificity of hybridization is at the core of many molecular biology techniques including the DNA sequencing, polymerase chain reaction (PCR), microarray technology as well as an essential material in the development of advanced molecular devices (Krishnan and Simmel, 2011; Kutzler and Weiner, 2008; Jobling and Gill, 2004).

For many years, the solution environment strongly influences the stability of DNA. Both aqueous and organic solvents are widely used as an extraction media or molecular solvent for DNA solvation. The stability of biological structure of DNA mainly depends on the water molecules. Particularly, the conformational and stability of DNA are controlled by the interactions between DNA and nearby water molecules (Westhof, 1988; Saenger, 1987; Texter, 1978). Since there is a close connection between DNA structure and their biological function, understanding the water-DNA relationship is significantly important. Other than water, the ambient environment such as different buffer conditions (pH, types of buffer solutions), concentrations of molecules, higher salt concentrations or even different type of non-aqueous solvents may all affect the stability of DNA conformation (Bonner and Klibanov, 2000). Previous studies of DNA in non-aqueous solutions have revealed that most organic solvents such as methanol, phenols, chloroform and DMSO, whether neat or in a mixture with water, all spontaneously denature DNA.

The dry storage of DNA, utilizing the basic concept of anhydrobiosis or "life without water" is an alternative to old-style DNA storage (Bonnet *et al.*, 2009). The development of other non-aqueous media which can stabilize and maintain native DNA structure for a long period especially at ambient temperature is increasing. Recently, huge attention is directed to the development of specific solvent for DNA. Ionic liquids (ILs) which is one of the non-aqueous ionic solvent have attracted many attentions due to their interesting

properties. The usage of ILs is attractive as they are almost non-toxic, having good solubility and high conductivity (Sun *et al.*, 2008a; He *et al.*, 2006; Nishimura *et al.*, 2005; Qin and Li, 2003). They offer unique opportunities as alternatives to aqueous and non-aqueous solvents in DNA biotechnology.

The behavior of DNA structure in ILs is of both practical and fundamental interest. Structural studies using crystallography and NMR provide tremendous amounts of information with the determination of three-dimensional pictures of various complexes. From a historical point of view, the first structure of DNA solved by single crystal x-ray analysis was a tetramer reported by Viswamitra *et al.* (1978). Until now, there are many ligand/compound-DNA structures deposited to the Nucleic Acids Database (NDB) and also Protein Data Bank (PDB) (Berman *et al.*, 2000). However, these techniques only provide static pictures and often it is desirable to follow the progression of molecules as a function of time. Additionally, not all structures are possible to obtain via these methods due to technical issues. Molecular dynamics (MD) simulation technique provides another way to look at the structures and interactions and complements the experimental evidences nicely.

This study focused on understanding of how the ILs influence the dynamics and structural stability of DNA from both experimental and computational point of views. The results of our work may provide more insight into the studied system, allowing a better understanding of the IL-DNA binding and expanding the overall capabilities and applications of ILs in biological and biomedical applications. This study is also vital for future development of specific solvent especially for DNA and RNA solutes.

1.2 Problem Statements

The problems in current DNA technology are related to the use of aqueous and conventional organic solvents as a media for DNA solvation. Although DNA is considered stable in aqueous solution, it is susceptible to slow hydrolytic reaction such as deamination and depurination, which caused serious damage to DNA helical structure (Lukin and de los Santos, 2006). Furthermore, aqueous solution is not able to stabilize DNA helical structure over a long period especially at room temperature (several days up to 1 month) (Vijayaraghavan *et al.*, 2010a) due to the degradation by contaminating nucleases (Sasaki *et al.*, 2007) and inherent chemical instability.

Moreover, DNA in various organic solvents such as DMSO, DMF, formamide, methanol or pyridine is found to have lost its native structure, undergo strand separation or formation of toroid-like conformations (Ke *et al.*, 2010; Hammouda and Worcester, 2006; Montesi *et al.*, 2004; Bonner and Klibanov, 2000). Even worse, addition of ethanol to an aqueous solution induces drastic changes in the duplex structure, forcing a B- to A-DNA transition (Herskovits and Harrington, 1972). Traditional extractions using chloroform/phenol (Muller *et al.*, 1983) can also cause denaturation of DNA during the extraction process. More importantly, the contamination of extracted DNA by organic solvents is unavoidable and creates vital problems for the biological investigations as the traditional organic solvents are known to be toxic to bioprocesses (Matsumoto *et al.*, 2004; Albarino and Romanowski, 1994). Physical factors such as ionic strength, pH and temperature can also disturb the helical structure and cause denaturation (Cheng and Pettitt, 1992; Lindahl and Nyberg, 1972). Therefore, the development of potential molecular solvent is aimed to overcome these limitations and its application especially in the DNA biotechnology.

Therefore, there is a great need to introduce other solvent for DNA such as ILs. Based on their remarkable properties, ILs have proved to be preferred solvents to replace traditional organic solvents and aqueous solution in many types of reactions. Over the last few years, several authors have reported the use of ILs in extraction and separation/purification of traces species of interest from complex matrixes including metal and organic compounds as well as amino acids (Han and Armstrong, 2007). ILs also have been used for gene delivery vectors, capillary electrophoresis and DNA isolation (Zhang *et al.*, 2009b; Wang *et al.*, 2007a; Qin and Li, 2003). It has been reported that ILs are able to extract DNA without any contamination from proteins and metal species during the extraction process (Wang *et al.*, 2007a). This finding provides an alternate approach for the measurement of DNA in ILs as well as for the separation/purification of trace amounts of DNA in real-world biological matrices.

1.3 Research Objectives

This research was embarked with the main goal to show that ionic liquids (ILs) have good properties as molecular solvent for DNA. Hence, the experimental and computational studies were performed to fulfill the objectives as below:

i) Experimental part

1. To design and synthesize new alkylimidazolium-based ILs.
2. To characterize the physico-chemical properties of the synthesized ILs.
3. To elucidate the IL-DNA interaction using biophysical characterizations.

ii) Computer modeling via MD simulation

4. To study the properties and behavior of ILs and IL-DNA at molecular level.
5. To determine the solvation free energy of nucleic acid bases in ILs.

CHAPTER 2

LITERATURE REVIEW

2.1 History of Ionic Liquids

Ionic liquids (ILs), also known as room temperature ionic liquids (RTILs) or classically called “molten salts” have been studied for about a century ago. However, the definition of “molten salts” refers in general to any ionic compound with a high melting temperature. A simple example of a molten salt is sodium chloride (NaCl), which melts at 801°C. These high temperature melts are often highly corrosive, which makes them difficult to handle.

In order to distinguish low temperature molten salts or room temperature molten salts from the classical “molten salts”, the upcoming “ionic liquids community” in the 1990s decided to introduce a new term, “ionic liquids” because the low-temperature molten salts were often associated with high operating temperatures. It is also important to emphasize that ILs are not solutions of ions in water. The definition of “ionic liquids” stated that:

“Any ionic compound can be classified as ionic liquids if they composed only ions and can exist as a liquid or solid with the melting temperature below 100°C”

The considerable difference in melting temperature between molten salt NaCl and ILs, for example 1-ethyl-3-methylimidazolium chloride ([C₂mim][Cl]) lies in the asymmetric and large cation of ILs, leading to a difficult packing structure of the cations and anions as well as weak ionic bond between them as shown in Figure 2.1.

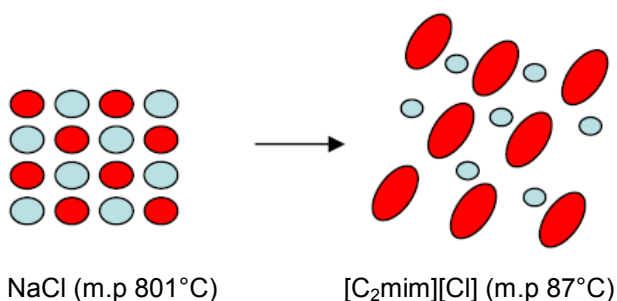


Figure 2.1. Comparison between lattice energy of NaCl and [C₂mim][Cl] (Source: Wilkes *et al.*, 1982).

An early example of low temperature molten salts or ILs was published by Walden (1914). This compound was obtained as “red oil” in Friedel-Craft reaction by addition of concentrated nitric acid to ethylamine followed by removal of water, to produce a pure liquid salt at room temperature (Herfort and Schneider, 1991). The structure of the salt was confirmed using spectroscopy techniques as ethylammonium nitrate ($[\text{EtNH}_3][\text{NO}_3]$) with a melting point of 12°C (Figure 2.2).

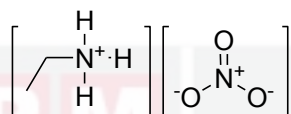


Figure 2.2. Structure of earliest $[\text{EtNH}_3][\text{NO}_3]$ IL synthesized by Walden (1914).

Since then, there were almost no publications about ILs until 1982, where the first dialkylimidazolium-based ILs, 1-ethyl-3-methylimidazolium tetrachloroaluminate ($[\text{C}_2\text{mim}][\text{AlCl}_4]$) was synthesized by Wilkes *et al.* (1982) (Figure 2.3). These types of ILs were mainly formed through a combination of alkylimidazolium cations with chloroaluminate or other metal halide anions and have been called as “1st generation ILs”. These ILs are sensitive to moisture and reactive toward various organic compounds and were therefore not suitable for many organics reactions (Dupont *et al.*, 2004). However, they were successfully used as both catalyst and solvent in many inorganic reactions such as in Friedel-Crafts (Boon *et al.*, 1986) and oligomerization reactions (Ellis *et al.*, 1999).

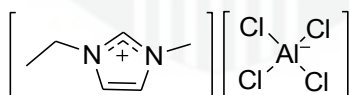


Figure 2.3. Structure of $[\text{C}_2\text{mim}][\text{AlCl}_4]$.

Since the successful use of $[\text{C}_2\text{mim}][\text{AlCl}_4]$ in many reactions, a numbers of research projects were carried out to synthesis new ILs based on *N,N*-dialkylimidazolium cation. A decade later in 1992, the same researcher who synthesized $[\text{C}_2\text{mim}][\text{AlCl}_4]$ developed the so called “2nd generation ILs” which are stable in air and water (Wilkes

and Zaworotko, 1992). These types of ILs were formed by combination of 1-ethyl-3-methylimidazolium cation ($[\text{C}_2\text{mim}]^+$) with water stable or weakly coordinating anions such as $[\text{BF}_4]^-$, $[\text{PF}_6]^-$, $[\text{SO}_4]^{2-}$, $[\text{NO}_3]^-$ and $[\text{CF}_3\text{O}_3\text{S}]^-$ (Figure 2.4). These types of ILs can be adjusted by varying the choice of *N,N*-dialkylimidazolium substituent and/or the anions. Some advantages properties of these ILs are moderate polarity as well as air and water tolerance. Most of them are hydrophobic and immiscible in water. However, they also have some disadvantages such as having similar toxicity level with chlorinated and aromatic solvents, high cost and lack of large-scale production (Docherty and Kulpa, 2005).

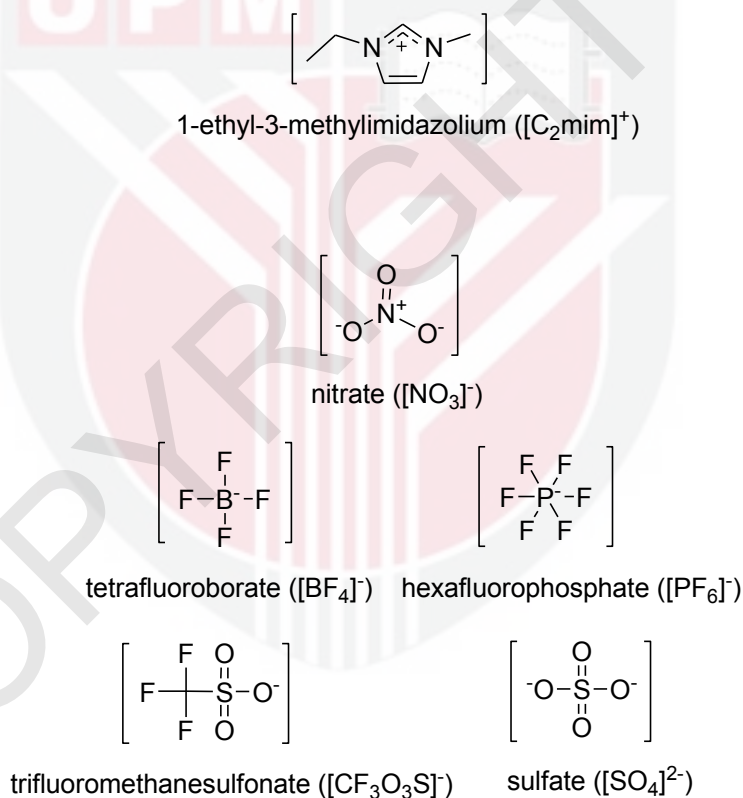


Figure 2.4. Second generation ILs containing *N,N*-dialkylimidazolium and water stable or weakly coordinating anions.

The research exploring of new ILs has gained much interest in community of researchers. During the last few years, “3rd generation ILs” especially those based on 1,3-dialkylimidazolium, quaternary ammonium and choline cations have found several applications; some of them are used as eutectic solvents (Gorke *et al.*, 2010). These ILs maintain its stability, lower toxicity, biodegradable and have moderate polarity. For example, the cation may be choline and the anions for example may be sugars, amino acids, organic acids or sulfuric acid (Figure 2.5).

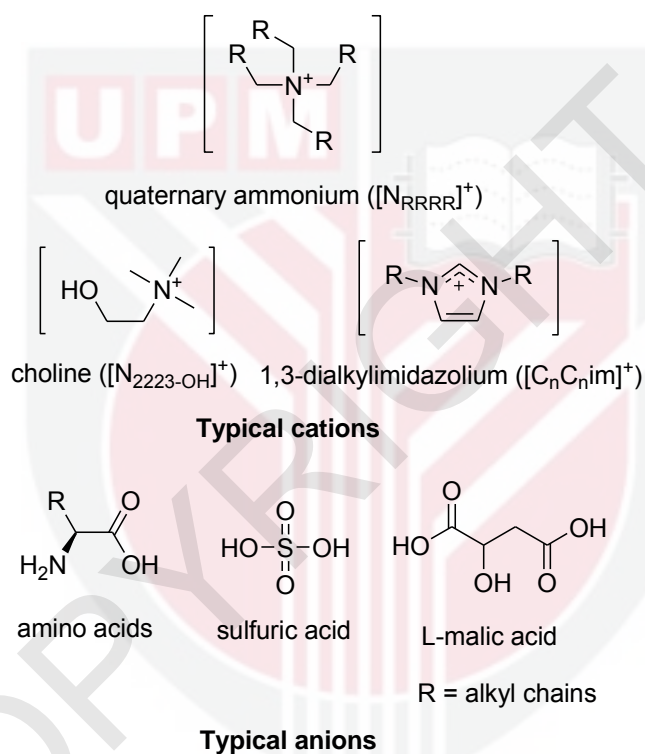


Figure 2.5. Examples of cations and anions of “3rd generation ILs”.

In our previous studies, a series of “3rd generations ILs” that have chiral component on anions derived from plant acids (Abdul Rahman *et al.*, 2009; Abdul Rahman *et al.*, 2008) and amino acids analogs (Abdul Rahman *et al.*, 2010) were successfully synthesized. These tetraethylammonium-based ILs are highly miscible in water and polar organics solvents. However, they suffer in terms of low thermal stability and some of them show higher viscosities compared to 2nd generation ILs.

2.2 Properties of Ionic Liquids

Generally, ILs are complex salts that composed of large organic cations and organic/inorganic anions. There are many of possible combinations of cations and anions, allowing the synthesis of specific ILs for specific applications. The typical structures of ILs cations and anions widely used are presented in Figure 2.6. Their properties can be fine-tuned either by selecting suitable cation-anion or by adding functional groups in the cation or in the anion. For example by attach linear or branching alkyl chain lengths in the structure of cation.

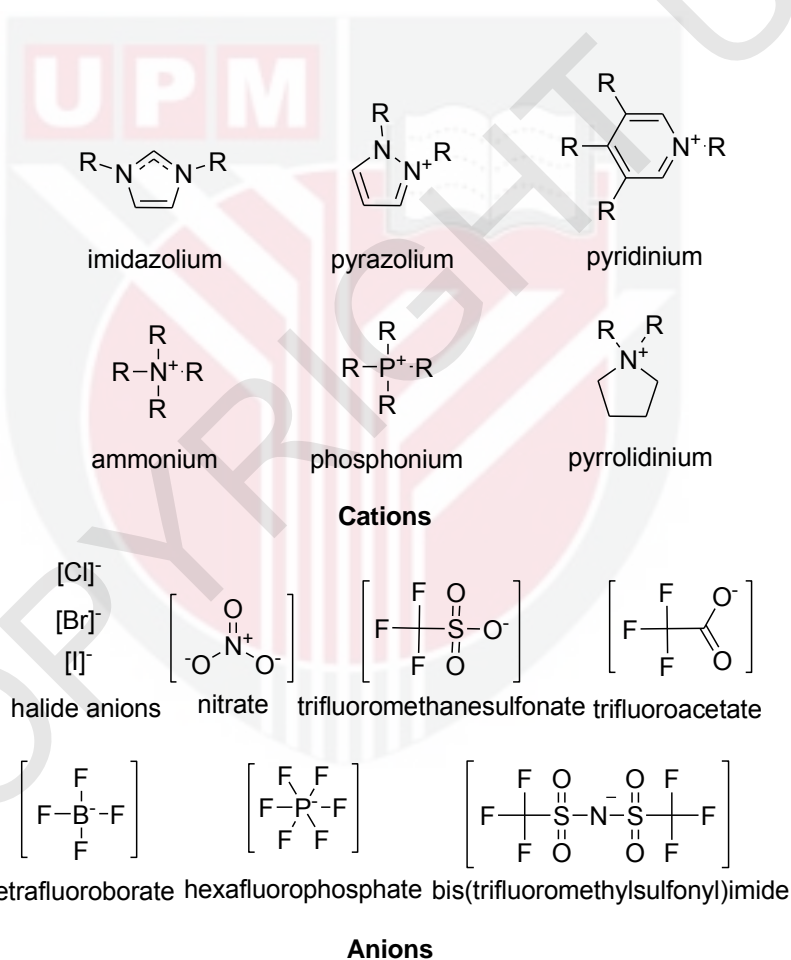


Figure 2.6. Typical structures of cations and anions which are widely used in synthesizing various ILs.

2.2.1 Density

Density is one of the most often measured properties of ILs, probably because most application requires information of the density. Generally, ILs are denser than water and most of the volatile organic solvents. The mass of cation and anion are significantly affects the density of ILs. For example, the $[\text{Ms}_2\text{N}]^+$ species have lower densities than the $[\text{TF}_2\text{N}]^+$ salts. Although the molecular volume for both anions is almost similar, but the mass of the fluorine is greater than oxygen in $[\text{Ms}_2\text{N}]^+$ anion (Chiappe and Pieraccini, 2005; Pringle *et al.*, 2003). This behavior may be attributed to the fact that packing structure becomes more compact as the cations and anions become more equal in size (Chiappe and Pieraccini, 2005).

2.2.2 Viscosity

Almost all ILs have a high viscosity due to their ionic nature. Some are not suitable for use as a solvent. Typically, ILs are more viscous (comparable to the viscosities of oils) than most common molecular solvents, varying over a range of 10 to > 1000 mPa·s at ambient temperature. A few factors affect the viscosity of ILs, but these are strongly dependent on the temperature, their strength of their *van der Waals* interactions and tendency to form hydrogen bonds (Bonhôte *et al.*, 1996).

In general, an increased in formation of intermolecular hydrogen bonding between cation-anion will result in higher viscosity of ILs. The influence of hydrogen bonding can be diminished by fluorinating the ILs (Pomaville and Poole, 1990). The viscosity of ILs may also increase when using longer or fluorinated alkyl chains on the cations, due to stronger *van der Waals* interactions for ILs with the same anion (Bonhôte *et al.*, 1996). In order to counter these problems, low viscosity ILs can be synthesized using more asymmetry cations than symmetry cations (Jiang *et al.*, 2008) or by using highly branched and compact alkyl chains (Swartling *et al.*, 2000).

The choices of cations and anions also have a major impact on the viscosity of ILs. In general, shorter alkyl chains lead to lower viscosity, while longer alkyl chains will increase the viscosity of ILs. This is mainly attributed to the *van der Waals* forces between the cations which will increase the energy required for molecular motion (Chaudhary *et al.*, 2013). The general trend is an increase in the molecular size and the molar mass of ILs leading to an increase in viscosity.

2.2.3 Thermal Stability and Liquid Range

The structure of ILs also has an impact on its physico-chemicals properties, in particular the thermal stability such as melting temperature and liquids ranges. The main factors which influence melting temperature of ILs are the charges, the size of cations and anions, the distribution of charges on the ions, the symmetry of the structure, hydrogen bonding ability and *van der Waals* interactions (Wasserscheid and Welton, 2003). To obtain a low melting point for ILs, the overall lattice energy of the ionic compound should be as low as possible. A reduction of the melting point can also be achieved by choosing asymmetric ions, which disturb the efficient packing of the ions in the crystal lattice (Wilkes *et al.*, 1982).

Furthermore, increasing hydrocarbon length of cation will decrease the melting temperature of ILs. For example, increasing the length of alkyl chain beyond a certain point, between 8 to 10 carbons in $[C_n\text{mim}]^+$ cations (where n = number of carbon), the melting temperature tends to increase due to an effect on the efficiency of ion packing (Ajam, 2005). For example, the effect of changes in the cation for different chloride salts is shown in Table 2.1. Alkaline metal salts are known to have high melting points. These melting points are reduced to temperatures at or below the room temperature by replacing the simple inorganic cations with unsymmetrical organic cations (Lide, 1992). Similarly, an increase in anions size reduces the melting point of ILs. However, not all ILs follow the pattern of decreasing melting point with increasing anion size.

Table 2.1. The effect of cation size on the melting point.

Cation	Melting point (°C)	Reference
NaCl	801	(Lide, 1992)
KCl	772	(Lide, 1992)
$[C_1\text{mim}][\text{Cl}]$	125	(Wasserscheid and Keim, 2000)
$[C_2\text{mim}][\text{Cl}]$	87	(Wasserscheid and Keim, 2000)
$[C_4\text{mim}][\text{Cl}]$	65	(Wasserscheid and Keim, 2000)

An interesting feature of ILs that common molecular solvents do not possess is their exceptionally wide liquid range. For an example, water has a liquid range of 100°C (0 to 100°C) and dichloromethane of 145°C (-95 to 40°C) at ambient pressure. In comparison, $[C_4\text{mim}][\text{BF}_4]$ and $[C_4\text{mim}][\text{PF}_6]$ have liquids range of

400°C. They also possess a high thermal stability which is dependent on both the cation and anion (Fredlake *et al.*, 2004). The upper limit of the liquid range normally signifies thermal decomposition rather than vaporization since ILs are non-volatile.

The decomposition temperature of ILs varies with the type of anions. For example, $[\text{C}_2\text{mim}][\text{BF}_4]$ has been reported to be stable up to 300°C and $[\text{C}_2\text{mim}][\text{N}(\text{SO}_2\text{CF}_3)_2]$ is stable to more than 400°C (Bonhôte *et al.*, 1996). The thermal stability of ILs also depends on the nucleophilicity of the anion. Weaker coordinating anions are more susceptible to high temperature decomposition (Ngo *et al.*, 2000).

2.2.4 Solubility and Polarity

The solubility of ILs in water is mainly dependent on the three factors namely the temperature, the length of alkyl chain and nature of the anion (Wasserscheid and Welton, 2003). As an example, Figure 2.7 shows the anions responsible for water miscibility and immiscibility for $[\text{C}_4\text{mim}]^+$ cation. In general, an increase in the organic character of the cation results to a decrease of water solubility in ILs (Wasserscheid and Welton, 2003).



Figure 2.7. Different types of anions responsible for water miscibility and immiscibility of ILs.

The solubility of water in ILs increases when using more coordinating anions. Increasing the alkyl chain length of cations as well as anions increases the hydrophobicity of the ILs (Seddon *et al.*, 2000). For example, $[\text{C}_n\text{mim}][\text{BF}_4]$ salts with alkyl chain length less than six are miscible with water at 25°C, but with a chain length greater than six the ILs are immiscible with water (Holbrey and Seddon, 1999). Most of ILs are considered to be highly polar due to their ionic character. They have a polarity that lies between those of water and chlorinated organic solvents (Wasserscheid and Welton, 2003). Due to the presence of the cation and the anion in ILs, a much wider range of solvent-solute interactions is expected in

comparison with conventional organic solvents. The results reported by Muldoon *et al.* (2001) indicated that the polarities of 1,3-dialkylimidazolium-based ILs contain the $[\text{PF}_6]^-$, $[\text{BF}_4]^-$, $[\text{CF}_3\text{SO}_3]^-$ and $[\text{N}(\text{SO}_2\text{CF}_3)_2]^-$ anions can be compared to those of short chain alcohols (such as ethanol and methanol) and other polar organic solvents such as DMF and DMSO. In addition, the polarity decreases as the alkyl chain length increases.

2.3 Molecular Modeling Studies of Ionic Liquids

One of the first computer simulation studies of ILs systems was conducted by Hanke *et al.* (2001) using molecular dynamics (MD) simulation to simulate ILs $[\text{C}_{10}\text{mim}][\text{Cl}]$, $[\text{C}_2\text{mim}][\text{Cl}]$, $[\text{C}_{10}\text{mim}][\text{PF}_6]$ and $[\text{C}_2\text{mim}][\text{PF}_6]$. Most of the force fields (FFs) parameters required, especially parameters for the *van der Waals* interaction terms were taken from the literature. The quantities included liquid structures in terms of radial distribution function (RDF), crystal structures, densities, self-diffusivities and rotational dynamics of the cations and anions were computed for the first time.

They examined the system of these ILs by computing two different models which are united-atom (UA) and all-atom (AA) models. The UA model treats the hydrogen and carbon atoms in each terminal methyl (CH_3) and each methylene (CH_2) on the alkyylimidazolium cations as a single interaction center. While the AA model shows fully explicit methyl and methylene groups (all hydrogen are shown). They found that the density of ILs using UA model is higher in the liquid and crystalline states. Also, the dynamics of the UA system are slower than the AA model. Before not too long after this early study, several groups reported the simulation studies of another alkyylimidazolium-based ILs using UA models.

de Andrade *et al.* (2002a) reported a study of the ionic liquid $[\text{C}_2\text{mim}][\text{AlCl}_4]$. They performed MD simulation of this salt over 100 ps in order to obtain density, enthalpy of vaporization and RDF. Later, Shah *et al.* (2002) published a Monte Carlo study of $[\text{C}_4\text{mim}][\text{PF}_6]$ using UA models for both ions. In their studied, the Lennard-Jones (LJ) parameter for the $[\text{PF}_6]^-$ anion was derived via scaling arguments using a widely-used SF_6 model as a reference. Structural properties and various volumetric data for $[\text{C}_4\text{mim}][\text{PF}_6]$ were computed and compared with available experimental results. They found that density of this salt is 5% higher than the experiment, even though the density as a function of pressure and temperature change were obtained reasonably well.

Soon, the FFs parameters for another alkyimidazolium-based ILs which is $[C_4mim][PF_6]$ based on AA models were developed by Margulis *et al.* (2002), while de Andrade *et al.* (2002b) published a FFs for the $[C_2mim]^+$ and $[C_4mim]^+$ cations paired with $[AlCl_4]^-$ and $[BF_4]^-$ anions. Later, Lopes and Pádua, (2004) have developed FFs for the $[TF]^-$ and $[TF_2N]^-$ anions. There has also been work devoted toward the development of FFs parameters, especially based on OPLS for other types of ILs cations including pyridinium (Cadena *et al.*, 2006), alkylammonium (Lopes *et al.*, 2004) and alkylphosphonium cations (Lopes and Pádua, 2006a). Currently, a range of potentials based upon each of the main FFs codes appeared. Some of the FFs shows more details representation of the ions and improved flexibility of ILs.

Almost all MD simulations involving the 1-alkyl-3-methylimidazolium cations ($[C_nmim]^+$) show that the anion is predicted close to the C^2 carbon of the imidazole ring as shown in Figure 2.8. The reason for this is because the hydrogen covalently bonded to the C^2 carbon atom is the most acidic site (Hardacre *et al.*, 2008). The anion interacts more strongly with the cation at this position. This behavior is consistent with the results of *ab initio* calculations (Meng *et al.*, 2002) and experimental evidence of Hardacre *et al.* (2003a). In 2004, Margulis had shown that as the length of alkyl chains increases from $n = 6$ to $n = 12$ on $[C_nmim][PF_6]$, the first and second solvation shells become slightly more ordered for the anion about the C^2 position of the cation (Margulis, 2004). While Cadena *et al.* (2004) found that when a CH_3 group is substituted for the acidic hydrogen, the anion is no longer exhibits a preference for this position and appears to associate equally with all of the carbon atoms in the ring.

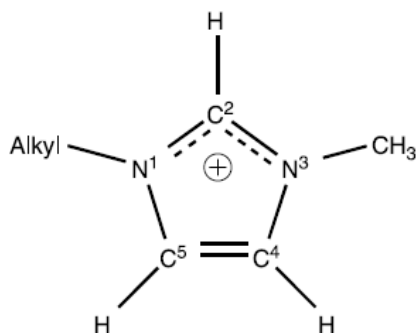


Figure 2.8. Position of C^2 atom in $[C_nmim]^+$ cation.

Besides the tendency of anions to localize close to the cation, ILs also exhibit long-range liquid order as compared to the simple molecular liquids as shown by RDF in Figure 2.9. The strong Coulombic forces between cation and anion lead to charge ordering over at least three coordination shells. This behavior is quite consistent with experimental studies which have also found long range liquid order in ILs (Hardacre *et al.*, 2003a; Hardacre *et al.*, 2003b; Takahashi *et al.*, 1999).

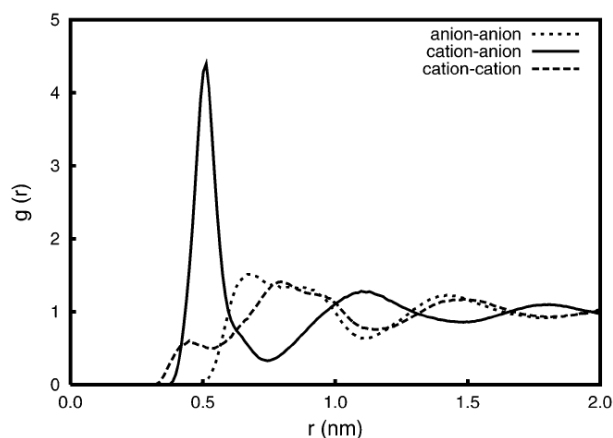


Figure 2.9. RDF of $[\text{C}_4\text{mim}][\text{PF}_6]$ showing the longer-range ordered structure. (Source: Micaelo *et al.*, 2006)

MD simulations carried out by Lopes *et al.* (2006) suggested that some ILs are not homogeneous, but instead show separation into continuous and semi-continuous domains of polar and non-polar regions. By visualizing the MD simulations results by using color-coding scheme (red = polar region; green = non-polar region), this type of phase segregation is possible to observe. As shows in Figure 2.10, there is clearly extensive ordering of the alkyl chains of $[\text{C}_6\text{mim}][\text{PF}_6]$ and the charged groups into domains that appear to percolate through the entire simulation box. Wang and Voth (2005), who used a coarse-grained model for the ILs also saw ordering of alkyl tails but not of charged groups in their simulation.

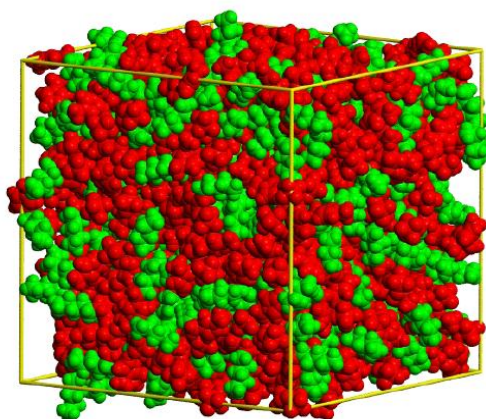


Figure 2.10. Snapshot from a MD simulation of $[C_6mim][PF_6]$ in which polar regions are colored red and non-polar regions are colored green (Source: Kioupis *et al.*, 2002).

2.4 DNA

Nucleic acids, including DNA and RNA, are polymeric macromolecules which are essential for all known forms of life. DNA is a chemical repository for the genetic information of an organism and widely used in life science application. This apparently simple biopolymer consisting of four distinct building blocks is capable of storing, retrieving and processing immense amounts of genetic information quickly and efficiently upon cellular demand. There are three main possible conformations of DNA, which are A-DNA, B-DNA and Z-DNA (Figure 2.11).

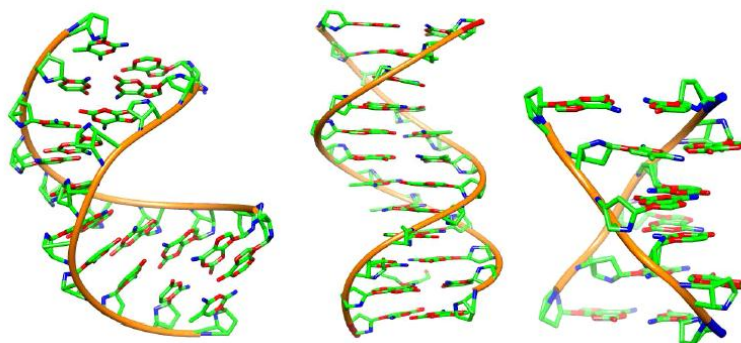


Figure 2.11. Major DNA duplex conformations from left to right: A-DNA (PDB ID: 440D) (Yi-Gui *et al.*, 1999), B-DNA (PDB ID: 1FQ2) and Z-DNA (PDB ID: 2F8W) (Sines *et al.*, 2000).

Whilst the first two conformations are right handed helices, the latter is left-handed helix. However, the most common conformation found under physiological conditions is B-DNA (Dickerson *et al.*, 1982). There are some noticeable differences between these conformations; diameter, the helical orientation, size and shape of the grooves. These features are summarized in Table 2.2.

Table 2.2. Structural features of ideal A-, B- and Z-DNA
(Source: Dickerson *et al.*, 1982).

Property	A-DNA	B-DNA	Z-DNA
Helix Sense	Right	Right	Left
Repeating Unit	1 base pair	1 base pair	2 base pair
Diameter	23 Å	20 Å	18 Å
Rotation per base pair	33°	36°	30°
Base pairs per turn	11	10.5	11.6
Helix rise per base	2.6 Å	3.4 Å	3.7 Å
Sugar pucker	C3' Endo	C2' Endo	C3' Endo at C C3' Endo at G
Major groove	Narrow and deep	Wide and deep	Narrow and deep
Minor groove	Wide and shallow	Narrow and deep	Narrow and deep

2.5 Non-covalent Binding to DNA

2.5.1 Electrostatic Attraction

DNA is a highly negative charged polymer which must be neutralized by a certain number of cations from solution to exist in stable conformations. The electrostatic interaction involves binding of cations to the negatively charged phosphates located in the DNA backbone through interactions which are generally non-specific and reversible. This interaction results in an increase in the stability of the DNA conformation. For example, polyamines bind to DNA through such interactions. They are usually fully protonated at physiological conditions; thus the negative charged phosphate DNA serves as the complementary site for interactions.

2.5.2 Groove Binding

The grooves resulting from the helical strands of duplex DNA serve as an alternative binding mode for ligands with DNA. Groove binding involves the direct interactions of the bound molecules with the edges of the base pair in both major and minor grooves of DNA. Unlike other binding modes, groove binding can span many base-pairs and hence very high level of DNA sequence specific recognition can occur. For example, many large oligonucleotide and protein molecules exhibit primarily binding through major groove while small molecules in general prefer to form interaction in the minor groove. Usually, groove-binding molecules have several simple aromatic rings connected by bonds with torsional freedom so that they can twist and fit into the helical curve of the DNA grooves (Bhattacharya and Chaudhuri, 2008). These molecules may fit better at A-T rather than G-C rich-sequences and they form *van der Waals* contact with the walls of the groove. Lower binding specificity to G-C rich sequence results from the fact that the presence of N2 amine group found in guanine sterically inhibits penetration of molecules into this groove in G-C rich regions (Goodsell *et al.*, 1995; Wartell *et al.*, 1974).

2.5.3 Intercalation

Intercalation is a process where a molecule can insert and stack between the DNA base pair. This process typically results in a substantial change in DNA structure, causes lengthening, unwinding and stiffening of the DNA helix as a result of rotation about torsional bonds in the DNA backbone in order to accommodate the intercalator (Satyanarayana *et al.*, 1993; Lerman, 1963; Lerman, 1961). The intercalator and adjacent base pairs are sandwiched tightly on the intercalating surface and the intercalator is stabilized in the helix by dipole-dipole interactions and a π - π stacking.

A number of physical methods are well established to determine intercalative binding (Erkkila *et al.*, 1999; Chaires and Dongchul, 1995; Long and Barton, 1990). For example hypochromism and red shift of the UV-visible absorption spectrum of the ligand, quenching/enhancement of the steady-state emission for substrates that luminesce and also an increase in length of the base pair which can be monitored by hydrodynamic methods such as viscosity and sedimentation measurement. In general, drugs such as pyrene and ethidium bromide are well known to be intercalator.

2.6 Ionic Liquids in DNA Biotechnology

Although interest in ILs has recently surged, there have already been several cases in which ILs have been utilized in conjunction with DNA. Many of these examples deal with electrochemistry, where the DNA is stabilized within an ILs network. ILs present a good environment for electrochemical applications due to high conductivity and good solubility (Sun *et al.*, 2008a; Sun *et al.*, 2008b; Guo *et al.*, 2007; Nishimura *et al.*, 2005; Qin and Li, 2003; Leone *et al.*, 2001). They have also been used to create DNA films with high conductivity (Nishimura and Ohno, 2002; Ohno and Nishimura, 2001).

One application of electrochemistry is the ability to detect hybridization of double-stranded DNA (dsDNA) without the use of a label or dye. Upon hybridization, the impedance change. If the probe DNA strand is first immobilized onto an electrode, the hybridization can be detected through the increase in electron transfer resistance. Although this is possible without the use of ILs, their presence could largely enhance the sensitivity (Zhang *et al.*, 2009a). They can also be used to enhance the detection of specific bases. Both adenine and guanine show characteristic oxidation peaks. This allows for a comparison of the ratio between the peaks, such that a single strand of DNA (ssDNA) can be measured for both adenine and guanine content (Sun *et al.*, 2008b). It has been found that the presence of ILs in these sensors can greatly enhance the peak, essentially increasing the sensitivity of the probe (Sun *et al.*, 2008a).

Although ILs are considered inert, this does not infer that there is no interaction between DNA and ILs. In the past few years, a number of publications have reported the use of ILs in DNA extraction/separation process. Qin and Li (2003) were the first group to study the extraction of DNA in ILs. They observed that the electrostatic attraction was formed between DNA fragments and 1,3-dialkylimidazolium based ILs, which then was used to design an IL-coated capillary for DNA separation (Figure 2.12). Similar studies have also reported the use of ILs in designing ion conductive DNA films. The so called "IL-robed DNA strands" with the characteristics of both ILs and DNA have been formed by fixing $[C_n\text{mim}]^+$ cations on the phosphate groups of DNA (Nishimura *et al.*, 2005).

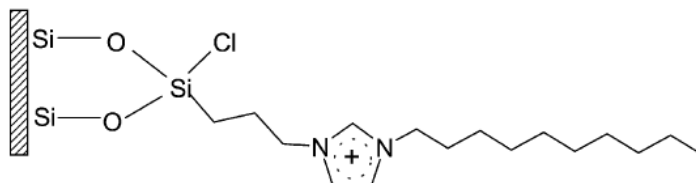


Figure 2.12. Schematic representation of IL-coated capillary surface (Source: Qin and Li, 2003).

Later studies explored the extraction of trace amounts of dsDNA by using ILs from an aqueous solution (Wang *et al.*, 2007a). They found that $[\text{C}_4\text{mim}][\text{PF}_6]$ could be successfully utilized to extract the DNA and showed potential to become an appropriate medium for bioprocessing. Interestingly, they identified that protein and metal species do not interfere with the extraction process by using $[\text{C}_4\text{mim}][\text{PF}_6]$ as compared to organics solvent where some protein impurities was found during extraction of DNA by phenol/chloroform. These finding provide an alternate approach for the measurement of DNA in ILs. The interaction between the P-O bonds of phosphate groups in the DNA strands (Figure 2.13) were confirmed through ^{31}P NMR and FT-IR.

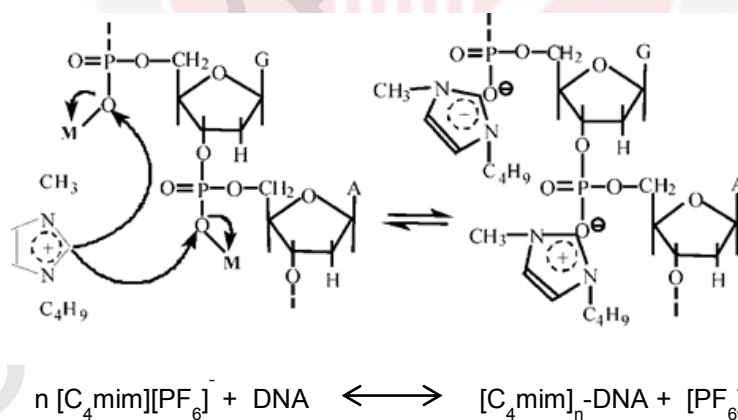


Figure 2.13. Schematic illustration of the interactions of $[\text{C}_4\text{mim}]^+$ cation with DNA phosphate groups during the extraction of dsDNA by $[\text{C}_4\text{mim}][\text{PF}_6]$ (Source: Wang *et al.*, 2007a).

A year later, detailed study was carried out to determine the interaction characteristics between DNA and $[C_4mim][BF_4]$. It was found that the ILs molecules could interact with DNA through electrostatic interactions, going so far as to be able to replace some molecules already bound to the DNA (Xie *et al.*, 2008). A schematic of this interaction is shown in Figure 2.14. ILs can also interact with DNA through hydrophobic interactions with the hydrophobic bases of DNA, resulting in compacting of the DNA coil and a lower hydrodynamic radius.

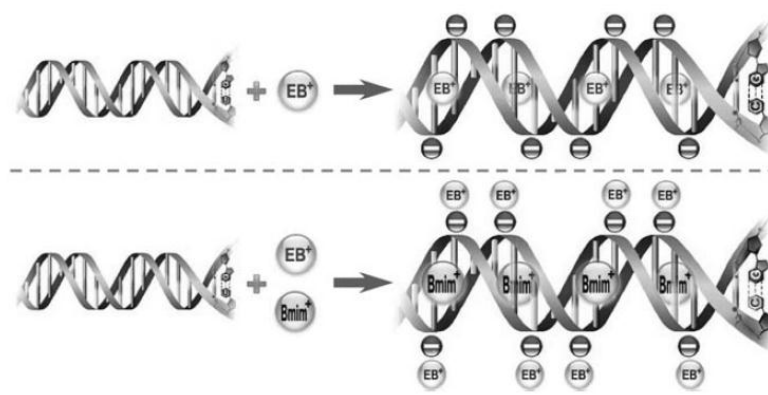


Figure 2.14. The DNA–ethidium bromide interaction in aqueous phase (top) and the IL–DNA–ethidium bromide interaction in $[C_4mim][PF_6]$ phase (bottom) (Source: Cheng *et al.*, 2007).

In 2010, Ding and his group studied the mechanism of interaction and binding characteristic between $[C_4mim][Cl]$ and DNA by using spectroscopic method. They found that the $[C_4mim][Cl]$ can bind to DNA and formed IL-DNA complexes through electrostatic attraction between the $[C_4mim]^+$ cation and phosphates groups of DNA (Figure 2.15) (Ding *et al.*, 2010). Although electrostatic attraction is necessary in the binding of this ILs to DNA, the hydrophobic interaction between the hydrocarbon chains of $[C_4mim]^+$ and the DNA bases also plays a significant role. They showed that the addition of $[C_4mim][Cl]$ with the DNA dye conjugate could cause a decrease in fluorescence. It has been hypothesized that this IL bound competitively with the DNA, eventually being able to displace the EB completely.

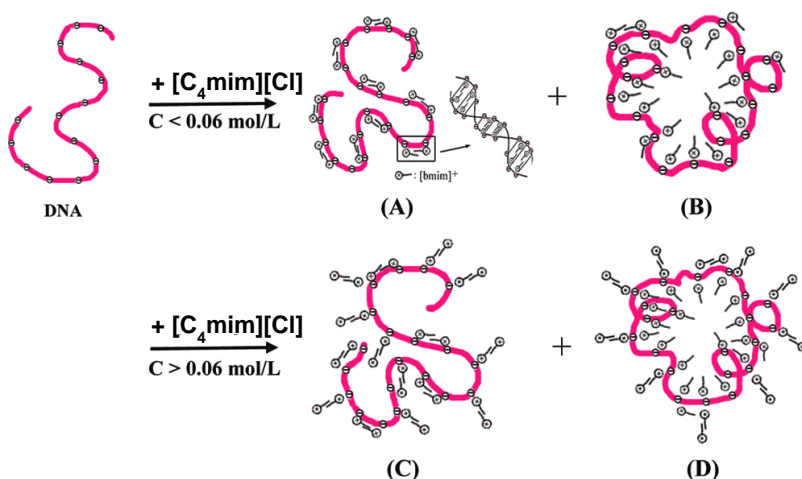


Figure 2.15. Schematic illustration of the mechanism of interaction between $[C_4mim][Cl]$ and DNA (Source: Ding *et al.*, 2010).

Some ILs such as choline dihydrogen phosphate has been found to significantly increase DNA stability. Usually, DNA is stored under refrigeration, as the double helix structure is disrupted by just one month of storage at room temperature. However, if stored in this IL, the DNA structure remains uncompromised even if left at room temperature for up to six months (Vijayaraghavan *et al.*, 2010a). Additionally, it has been reported that ILs can also improve temperature stability of the duplex by preventing denaturation at higher temperatures as compared to an aqueous medium. In some hydrated ILs, DNA can be stabilized up to a temperature of 100°C, which is significantly higher than in a fully aqueous medium (Vijayaraghavan *et al.*, 2010a).

2.7 Molecular Modeling Study of DNA in Ionic Liquids

There have been fewer publications regarding the topic of computational studies on DNA in ILs. So far, only two groups have successfully performed computer simulation on this topic. Cardoso and Micaelo, (2011) were the first researchers who studied the interaction between ILs and DNA using MD simulation. Their MD results show the interactions of ILs cations with the DNA bases and main chain, and also interactions between ILs anions and DNA bases (Figure 2.16). Based on the findings, they stressed the importance of the hydrogen-bonding interactions between ILs cations and the bases of DNA as well as the role of anions towards the stability of Drew Dickerson B-DNA.

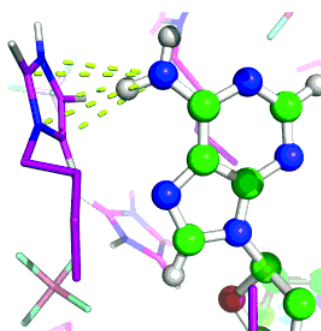


Figure 2.16. Non-bonded interactions between polar atoms in alkyimidazolium cation with DNA bases (Source: Cardoso and Micaelo, 2011).

One year later, Chandran *et al.* (2012) employed the MD simulations with the support of spectroscopic evidences to reveal the important factors that stabilize DNA in hydrated ILs. Both simulation and experimental results showed that DNA maintains its native B-conformation in ILs. They suggested that from a computational point of view, apart from the electrostatic association of ILs cations with the DNA backbone, groove binding of ILs cations through hydrophobic and polar interactions significantly contributes to DNA stability (Figure 2.17). They concluded that partial dehydration by ILs is able to stabilize duplex DNA for the long term and prevent the hydrolytic reactions that denature DNA.

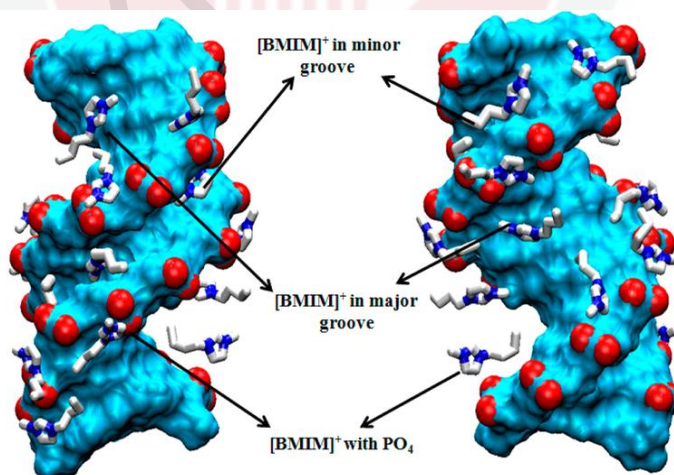


Figure 2.17. Distribution of $[\text{C}_4\text{mim}]^+$ cations around DNA surface. The cations were interact with DNA backbone, minor groove and major groove (Source: Chandran *et al.*, 2012).

2.8 Principles of Computational Chemistry

Computational chemistry is a part of chemistry that uses principles of computer science to help in solving chemical problems. Basically, it uses theoretical chemistry data in efficient computer programs to calculate the properties of molecules. In the field of computational chemistry, computational methods are used to solve chemical problems using a structure model to describe real systems. This does not mean that computer simulation can simply replace experimental work, but both fields can be used and support each other to efficiently solve theoretical questions. Computer simulation has many advantages; a few are listed below:

1. Uncertainty exists in the interpretation of the presented experimental results. By performing computer simulation, uncertainty can be well explained in terms of theoretical chemistry.
2. Efficiently use to minimize the time required and optimize the design and experimental programs.
3. Safety and useful methods to predict the properties of certain molecules which might be difficult, dangerous or costly if measured experimentally.

2.9 Molecular Dynamics

Molecular dynamics, generally known as MD, is one of the computational methods that are widely used in computer simulations. Molecular dynamics is a powerful technique which allows computing properties of many systems. In this framework, classical MD means that the motion of the particles of the system obeys the laws of classical mechanics (Newton's Laws). By using the MD technique, the trajectory of the molecular system as a function of time is generated by simultaneous integration of Newton's equations of motion for all atoms in the system. This can be written as follows:

$$\frac{\delta r_i(t)}{\delta t} = v_i(t) \quad (2.1)$$

$$\frac{\delta v_i(t)}{\delta t} = \frac{F_i(t)}{m_i} \quad (2.2)$$

where m_i is the mass and $r_i(t)$, $v_i(t)$ and $F_i(t)$ are the Cartesian position, velocity and total force acting on the atoms i , respectively. Both equations can also be applied to a center of mass of a molecule and then, F_i represents the total force on molecule i , m_i is the molecular mass, $r_i(t)$ is the Cartesian position of the center of mass and $v_i(t)$ is the velocity of the center of mass. These equations are solved on a step-by-step basis and the time interval δt is typically between 1-10 fs for molecular system. For example, δt will be significantly smaller than the typical time required for a molecule to travel its own length. To better understand what a MD program does at each timestep along a simulation. Figure 2.18 shows the flow stories code in MD simulation.

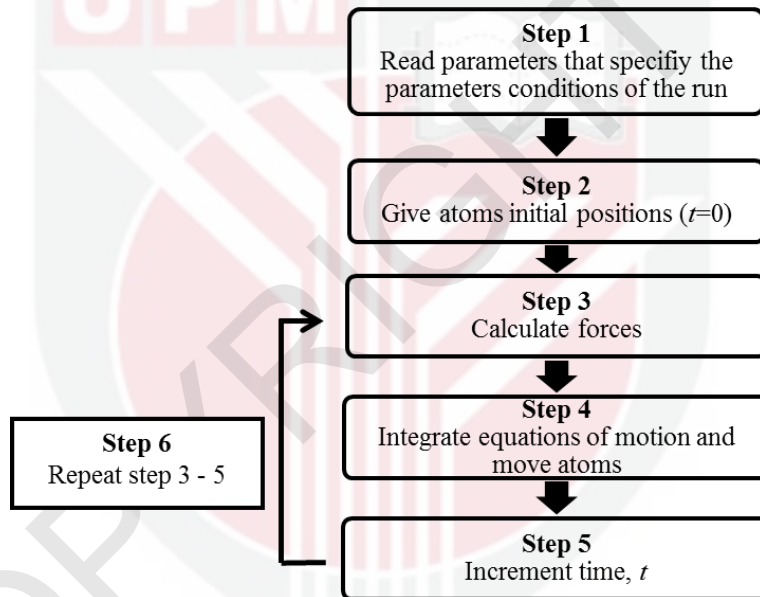


Figure 2.18. Flow chart of steps performed in molecular dynamics program.

MD simulations are in many respects similar to real experiments. The latter starts with a sample and a setup preparation. This is followed by the connection of the sample to a measuring instrument which will be used to measure the property of interest during a specified period of time. The measurement can experience some statistical noise, therefore the longer the acquisition period, the more accurate the measurement becomes.

In a simulation, the same approach is followed. First is the preparation of the sample (consisting of number of particles) with the selection of the appropriate interaction model potential, followed by the setup of the system properties (initial temperature, pressure, volume, and so on). Newton's equations of motion are then solved until the properties of the system are no longer change with time. This process is known as equilibration. The actual measurement is performed after the equilibration process, along simulation times are required to obtain accurate property estimation.

The simulations are usually performed as near to experimental conditions as possible. Therefore, physical conditions such as pressure and temperature are carefully chosen. In computer simulation part in this research, MD simulations were performed under two different conditions. The first condition is canonical ensemble (also known as NVT) in which the number of particles (N), volume (V) and temperature (T) are fixed. The other condition is an isobaric-isothermal ensemble (also known as NPT) in which N, pressure (P) and T are fixed value.

2.9.1 Pressure Coupling

In real experiments, the NPT situation instead of NVT ensemble is often given should a system be able to perform mechanical work by a change of its volume. However in an MD simulation, pressure is usually fluctuated. In order to maintain constant pressure during a course of simulation, all the simulation systems under study were coupled to a pressure bath using Berendsen barostat algorithm, as shown in Equation 2.3. Pressure is relaxed according to a couple time T_p towards a reference pressure P_0 . This equation is the simplest equation to simulate constant pressure introduced by Berendsen *et al.* (1984).

$$\frac{dP}{dt} = \frac{P_0 - P}{T_p} \quad (2.3)$$

2.9.2 Temperature Coupling

For some reasons such as drift during equilibration and drift as a result of integration error or due to the external forces, it is necessary to control the temperature of the system during simulation. Similar to pressure coupling, a Berendsen thermostat was chosen to be used in all simulations to maintain the

temperature. Berendsen *et al.* (1984) introduced the Berendsen thermostat algorithm which mimics weak coupling with first-order kinetics to an external heat bath with given temperature T_0 . The effect of this algorithm is that a deviation of the system temperature from T_0 becomes slowly corrected, according to Equation 2.4.

$$\frac{dT}{dt} = \frac{T_0 - T}{\tau} \quad (2.4)$$

which states that a temperature deviation decays exponentially with a time constant τ . This method was chosen in this computational study due to several advantages. It allows equilibrating the system in a reliable and fast manner and the coupling strength can be varied and adapted to user requirements.

2.10 Optimization of Simulations

The MD simulations are a powerful tool to investigate macromolecular systems, but finite size effects and long-range interactions are major factors to be concerned. Finite size effects are typically circumvented by periodic boundary conditions (PBC), but this requires an efficient and appropriate treatment of the long-range interactions.

2.10.1 Periodic Boundary Condition

The molecules of interest were randomly packed in a given cubic simulation box. This will create a finite system at the boundary, with molecules on one side and vacuum at the other. In order to minimize the edge effects involved in a finite system, PBC was employed in all directions (x , y , z) in box of simulation systems to represent an infinite system as shown in Figure 2.19. This means surrounding the simulation box with replicas of itself. During the course of the simulation, if an atom leaves the simulation box, attention can be switched to the incoming image.

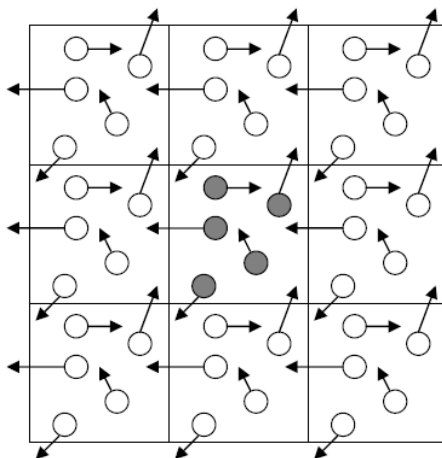


Figure 2.19. Schematics picture represents the PBC.

2.10.2 Long-range Electrostatic Interaction

As soon as the atoms are charged, long-range forces arise. The evaluation of long-range electrostatic interactions can be difficult. These interactions were most often ignored beyond a specified cut-offs. With the introduction of the Particle Mesh-Ewald (PME), the calculations became more accurate. PME is a method which was proposed by Darden *et al.* (1993) to improve the performance of the reciprocal sum. The charges are assigned to a grid using cardinal B-spline interpolation instead of directly summing wave vectors. This grid is then fourier transformed with a 3D FFT algorithm and the reciprocal energy term is obtained by a single sum over the grid in k-space.

2.11 Force Fields

Force fields (FFs) are used to describe the potential energy of a system of particles. There are two main components of FFs, namely the potential energy function and the parameters used in the function. The parameters which are included are derived from experimental work or from the high level quantum mechanics (QM) calculation on small model molecules. An accurate way to calculate the potential energy of a given system by describing nuclear and electronic interaction is to use QM calculation. However, in molecular simulation, QM demands more time for calculation of potential energy.

As an alternative, semi-empirical methods such as the classical FFs can be used. Such mathematical models represent the attempt to approximate the QM interactions in a system. The total potential energy of a system of N particles is given by the sum of the potential energy associated to all interactions occurring in the system as shown in Equation 2.5 below. Based on the equation, interactions can be divided into the following two categories: bonded interaction (u_{ij}^B) and non-bonded interaction (u_{ij}^{NB}). Figure 2.20 shows the available interaction in a liquid system.

$$U(r_1, r_2, \dots, r_N) = \sum_{i=1}^{N-1} \sum_{j>i}^N u_{ij}^B + u_{ij}^{NB} \quad (2.5)$$

$$= \sum_{i=1}^{N-1} \sum_{j>i}^N u_{ij}^{bond} + u_{ij}^{angle} + u_{ij}^{dihedral} + u_{ij}^{LJ} + u_{ij}^{Coulomb}$$

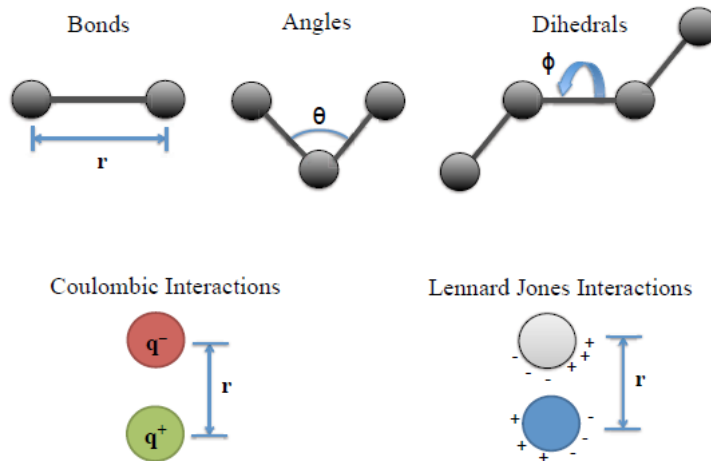


Figure 2.20. Type of the interactions exist in liquid system.

2.11.1 Bonded Interaction

Bonded interactions (u_{ij}^B) are associated to the interactions occurring between atoms within the same molecule. They describe the stretching of covalent bonds (u_{ij}^{bond}), the angles (u_{ij}^{angle}) and the torsion around dihedral angles ($u_{ij}^{dihedral}$). Typically, harmonic functions are used for modeling bonds, angles and improper torsions. The bond stretching potential can be written as:

$$U(r_{ij}) = k_b(|r_{ij}| - r_0)^2 \quad (2.6)$$

where $r_{ij} = r_i - r_j$ is the distance between the two bonded atoms i and j , k_b is the stretching force constant and r_0 is the nominal bond length. It is worthy to note that this model works well in close to the nominal bond length and reproducing the correct geometry in a molecular simulation. The potential of the angle between atom i , j and k represent as θ_{ijk} can be expressed as:

$$U(\theta_{ijk}) = k_\theta(\theta_{ijk} - \theta_0)^2 \quad (2.7)$$

where θ_0 is the nominal bond angle and k_θ is the bending force constant. Similarly, for improper torsions the harmonic potential which keeps planarity in ring is shown in Equation 2.8, where φ_0 is the nominal improper torsion angle and k_φ is the improper torsion force constant.

$$U(\varphi) = k_\varphi(\varphi - \varphi_0)^2 \quad (2.8)$$

The potential of dihedral torsion angle between atom i, j, k and l can be expressed using a truncated cosine series (Equation 2.9), where Φ_{ijkl} is the dihedral torsion angle formed by consecutively bonded atoms i, j, k and l , k is the barrier energy associated with term n and δ_n is the phase angle. n is an important parameter that determines the multiplicity, indicating the number of minima that are separated by 180° .

$$U(\Phi_{ijkl}) = \sum_{n=1}^N k_n [1 + \cos(n\Phi_{ijkl} - \delta_n)] \quad (2.9)$$

2.11.2 Non-Bonded Interaction

Meanwhile, the non-bonded interaction (u_{ij}^{NB}) have contributions from electrostatic and *van der Waals* interactions. The latter interaction account for the attraction of induced dipoles at longer range and the repulsion of electronic clouds at close range. The most popular functional form for *van der Waals* represented by Lennard-Jones (LJ) (u_{ij}^{LJ}) interactions due to its computational advantages and efficiency. The LJ equation is expressed as shown in Equation 2.10, where r_{ij} is the distance between atoms i and j , ϵ_{ij} is the well depth or maximum attractive energy and σ_{ij} is the collision diameter at which there is no interaction energy. In the LJ potential, there are two distinct terms: $(1/|r_{ij}|)^{12}$ and $(1/|r_{ij}|)^6$, corresponding to repulsive and attractive interactions, respectively.

$$U(r_{ij}) = 4\epsilon_{ij} \left(\left(\frac{\sigma_{ij}}{|r_{ij}|} \right)^{12} - \left(\frac{\sigma_{ij}}{|r_{ij}|} \right)^6 \right) \quad (2.10)$$

While the attractive part of the *van der Waals* forces takes care of interactions between induced dipoles, a model for electrostatic interactions is needed to account for the attraction of permanent dipoles or multipoles inherent to the species in a system. Partial point charges are a convenient way to represent the electrostatic surface of molecules that generates dipoles and higher order multipoles. Coulombic ($u_{ij}^{Coulomb}$) potentials can provide the energy between atomic charges, q_i separated by a distance, r_{ij} and ϵ_0 is the vacuum permittivity as shown in Equation 2.11.

$$U(r_{ij}) = \frac{1}{4\pi\epsilon_0} \frac{q_i q_j}{|r_{ij}|} \quad (2.11)$$

Lennard Jones and the Coloumb terms describe the short range non-bonded interaction which is 1–4 bonded and corresponds to the two outer most atoms in a dihedral, also contributing to the non-bonded term.

A lot of FFs development for ILs have been performed and the parameters along with their validation have been reported in many papers. Generally, parameterization takes place by tuning each kind of interaction with the main goal of reproducing certain experimental properties such as density, viscosity and self-diffusion

coefficient. The accuracy to predict the thermophysical properties depends upon the quality of the FFs used. Thus, with all of the above Equation 2.6 – 2.11, a complete standard molecular mechanics FFs (Leach, 2001) can be summarized as:

$$\begin{aligned}
 U(|r_{ij}|)_{total} = & \sum_{bonds} k_b (|r_{ij}| - r_0)^2 + \sum_{angles} k_\theta (\theta_{ijk} - \theta_0)^2 \\
 & + \sum_{dihedrals} \sum_{n=1}^N k_x [1 + \cos(n\chi_{ijkl} - \delta_n)] \\
 & + \sum_{impropers} k_\varphi (\varphi - \varphi_0)^2 \\
 & + \sum_{i=j}^{N-1} \sum_{j>1}^N \left\{ 4\epsilon_{ij} \left(\left(\frac{\sigma_{ij}}{|r_{ij}|} \right)^{12} - \left(\frac{\sigma_{ij}}{|r_{ij}|} \right)^6 \right) \right. \\
 & \left. + \frac{1}{4\pi\epsilon_0} \frac{q_i q_j}{|r_{ij}|} \right\} \quad (2.12)
 \end{aligned}$$

This FFs have been shown in many number of studies (Lopes and Padua, 2006a; Lopes *et al.*, 2004; Del Pópolo and Voth, 2004; Margulis *et al.*, 2002; Morrow and Maginn, 2002; Hanke *et al.*, 2001) to be effective in modeling the thermodynamic properties of alkylimidazolium-based ILs as well as biomolecules such as proteins and nucleic acids. Thus, it is expected that this equation also performs well for our MD simulations of ILs and DNA.

They are few numbers of empirical FFs used for the simulation of organics liquids and biomolecules such as CHARMM (Foloppe and MacKerell, 2000; MacKerell *et al.*, 1998), OPLS (Jorgensen *et al.*, 1996), AMBER (Pérez *et al.*, 2007; Cornell *et al.*, 1995) and GROMOS (Oostenbrink *et al.*, 2004). The functional form to describe specific interactions is quite similar between those FFs. In the present work of our computer simulation study, the FFs parameters for simulation of ILs and DNA were taken from the OPLS with large parameters sets that represent different classes of organics molecules.

CHAPTER 3

MATERIALS AND METHODS

3.1 General Flow of Research Design

Overview of the work for this study is illustrated in Figure 3.1. The research conducted was divided into two major sections, which are experimental and computer simulation. The computational section via MD simulation technique was performed to support and to further understand at molecular level the findings from experimental work.

The experimental section was separated into two parts. In the first part, the design and synthesis of new ILs specifically as a media for DNA solvation were carried out. The designing of new ILs was started with synthesizing of various 1-alkyl-3-butylimidazolium bromide ILs ($[C_n\text{bim}][\text{Br}]$). The main idea is to synthesize as many as possible hydrophilic ILs having different linear hydrocarbon chains and they must exist as a liquid form at room temperature. The properties of these ILs were characterized using modern techniques such as NMR, CHN, TGA, density and viscosity measurements.

In the second part, the suitable ILs was then utilized as a potential molecular solvent for DNA. Few parameters were studied such as temperature, effect of alkyl chain length and concentration of ILs towards the DNA conformation. Biophysical analyses through fluorescence, UV-visible and circular dichroism were employed to evaluate the properties of DNA in order to ensure its structure's stability as well as to understand the IL-DNA interaction.

Meanwhile, the computational section was separated into three parts. In the first part, parameterization and validation of the ILs FFs were performed. Parameterization involving geometry optimization of ILs' cations and partial atomic charge of each atom in ILs cations and anion were done using *ab initio* methods. Validation of the FFs including atomic charges, bonded and non-bonded interactions were based on the agreement between predicted simulation data such as density and viscosity with the experimental findings.

The second part of the computational modeling was the MD simulations of DNA in ILs. The simulation conditions used are similar to experimental parameters as possible. Few steps of MD simulation started with energy minimization, pre-equilibration and 10 ns production equilibration simulation were employed in order to obtain reliable results. The simulation data were discussed and correlated with experimental evidences. The last part was the free energy simulation of nucleic acids bases. Bennet acceptance ratio (BAR) method was used in the simulation in order to predict the solvation free energy of DNA and RNA bases in these [C_nbim][Br] ILs



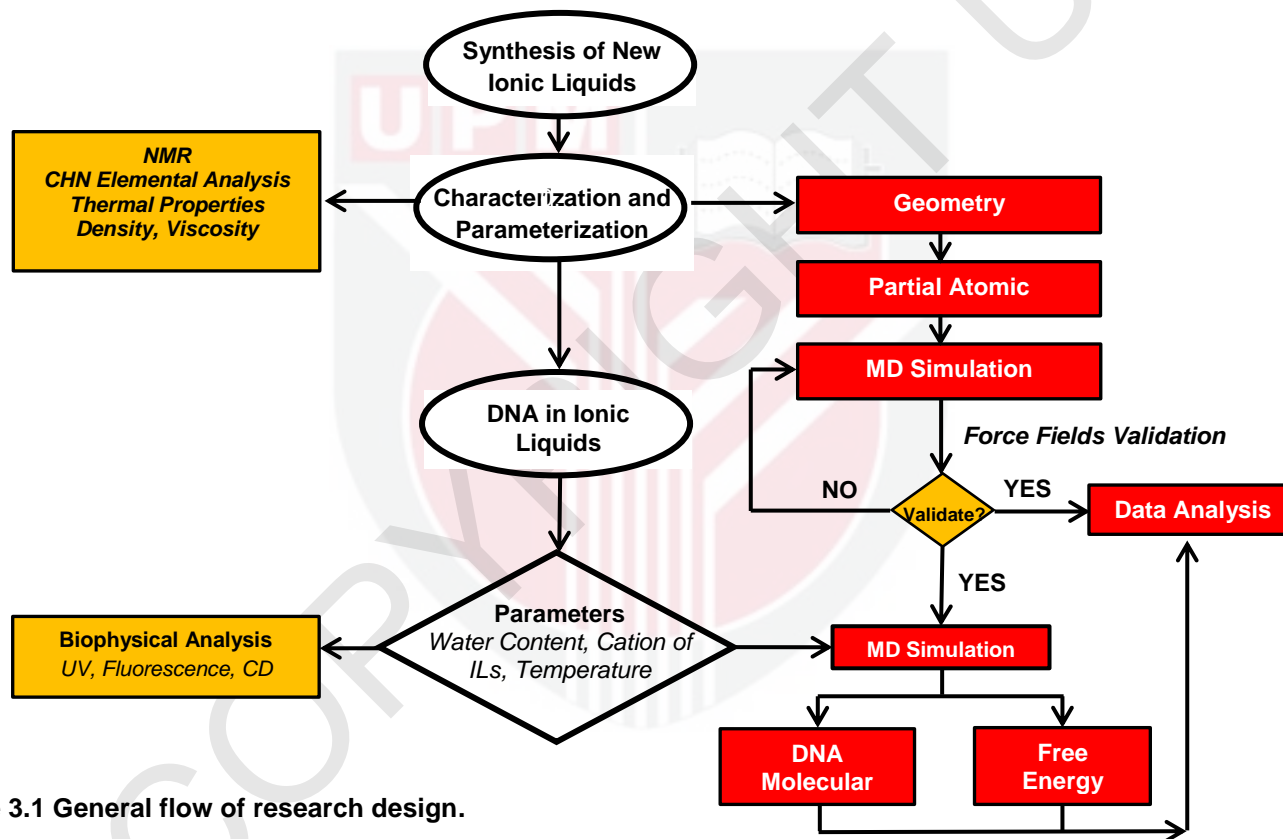


Figure 3.1 General flow of research design.

3.2 Chemicals and Materials

The chemical 1-butylimidazole (98% purity), bromoethane (99% purity), bromobutane (99% purity), bromohexane (98% purity), bromooctane (98% purity) bromodecane (98% purity), bromododecane (97% purity), potassium hydroxide (99% purity) and deuterated chloroform for NMR analysis (d_4 -CDCl₃, 99.9% purity) were purchased from Sigma-Aldrich, respectively. The solvents diethyl ether (99% purity) and chloroform (99% purity) were obtained from Merck.

Calf thymus DNA (~10 kbp, D1501, 99% purity) was purchased from Sigma-Aldrich. The DNA contained 41.9% mole cytosine-guanine (C-G) and 58.1% mole adenine-thymine (A-T) pairs, as experimentally measured by Marmur and Doty (1962). Ethidium bromide (EB, 99% purity) was used as a fluorescence probe, was also purchased from Sigma-Aldrich. Deionized water type III (Super Q Millipore system) was used with conductivity lower than 18 $\mu\text{S cm}^{-1}$. All chemicals and materials are commercially available and of higher analytical grade unless otherwise specified. The chemicals were used without purification, unless otherwise stated.

3.3 Hardware

A Dell Precision Workstation equipped with Intel® Xeon® Processor, 4 gigabyte (GB) of DDR2 memory and 1.5 terabyte (TB) of hard disk. The operating system (OS) was Fedora 17 Linux Desktop Edition with MPICH v.1.2.7pl, installed for parallel calculations up to 4 nodes. Most of the computer simulation results presented in this work was performed at Minho University, Braga, Portugal using Minho University GRIUM cluster. The cluster was linked to an ASUS Desktop equipped with Intel® Core™ i3 Processor, 4 GB of DDR2 memory and 1.0 TB of hard disk. Fedora 17 Linux was used as the OS for the ASUS Desktop.

3.4 Software

GROMACS software version 4.5 developed by University of Groningen, Netherlands. PyMOL, a molecular visualization software manufactured by Warren Lyford DeLano, DeLano Scientific LLC, San Carlos, CA, USA. This software is an open source foundation, which maintained and distributed by Schrödinger. Operating system used was Fedora 17 Linux Edition sponsored by Red Hat Enterprise Linux, USA. Packing Optimization for Molecular Dynamics Simulations (Packmol) was developed by University of

Campinas (UNICAMP), Brazil. MacMolPlt version 7.3 developed by Scalable Computing Laboratory, Iowa State University. The winGAMESS software is a general *ab initio* quantum chemistry package. This software is maintained by the members of the Gordon research group, also from Iowa State University. AMBER is originally developed by Peter Kollman's group, University of California, San Francisco, USA. GNU Emacs Editor Version 23.3 sponsored by Free Software Foundation, Boston, USA. All of the softwares are available and freely obtained from the sources.

3.5 Experimental Methods

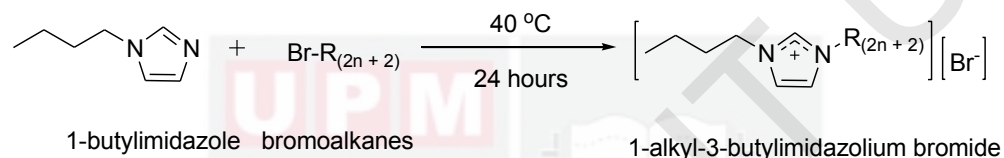
3.5.1 Synthesis of New Ionic Liquids

3.5.1.1 Distillation of 1-butylimidazole

Potassium hydroxide (0.25 mol, 14.02 g) was added to 1-butylimidazole (1.0 mol, 124.18 mL) in a 250 mL round-bottom flask. The mixture was then refluxed at 150°C under reduced pressure for several hours until no more unpurified yellowish 1-butylimidazole was observed. The distilled 1-butylimidazole was collected as a colourless liquid and was freshly used. For storage purpose, distilled 1-butylimidazole was stored in a dark place to avoid colour changes.

3.5.1.2 General Procedure

A general procedure obtained from Wang *et al.* (2007b) was used to synthesize 1-alkyl-3-butylimidazolium bromide ILs ($[C_n\text{bim}][\text{Br}]$, where $n = 2, 4, 6, 8, 10$ and 12). The distilled 1-butylimidazole (0.1 mol, 12.42 mL) was mixed with bromoethane (0.15 mol, 11.20 mL) in a 50 mL round-bottom flask and the mixture was stirred at 40°C for 24 hours. After cooling to room temperature, the mixture was extracted with diethyl ether (3×50 mL) to remove traces of bromoethane. The solvent was then removed by evaporation at 40°C under vacuum. Finally, the product appeared as a colourless liquid after being dried in vacuum oven for 1 day at 65°C. Scheme 3.1 shows the reaction scheme for preparation of $[C_n\text{bim}][\text{Br}]$ ILs using alkylation reaction. The same procedure was followed for all ILs derived from bromoalkanes as listed in Table 3.1.



R_(2n+2), where n = 0, R₂ = ethyl
= 1, R₄ = butyl
= 2, R₆ = hexyl
= 3, R₈ = octyl
= 4, R₁₀ = decyl
= 5, R₁₂ = dodecyl

Scheme 3.1 Preparation of 1-alkyl-3-butylimidazolium bromide ILs ([C_nbim][Br]).

Table 3.1 Starting materials and abbreviated names for newly synthesized ILs.

Entry	Alkylimidazole	Bromoalkane	ILs	Abbreviation
1	1-butylimidazole	Bromoethane	1-ethyl-3-butylimidazolium bromide	[C ₂ bim][Br]
2	1-butylimidazole	Bromobutane	1-butyl-3-butylimidazolium bromide	[C ₄ bim][Br]
3	1-butylimidazole	Bromohexane	1-hexyl-3-butylimidazolium bromide	[C ₆ bim][Br]
4	1-butylimidazole	Bromooctane	1-octyl-3-butylimidazolium bromide	[C ₈ bim][Br]
5	1-butylimidazole	Bromodecane	1-decyl-3-butylimidazolium bromide	[C ₁₀ bim][Br]
6	1-butylimidazole	Bromododecane	1-dodecyl-3-butylimidazolium bromide	[C ₁₂ bim][Br]

3.5.2 Physico-Chemical Characterization

3.5.2.1 Proton and Carbon NMR

Proton and carbon NMR spectra of each ILs were recorded at 25°C on 500 MHz JEOL NMR. The solvent used was deuterated chloroform (d_6 -CDCl₃). NMR spectra of presented compounds were available and chemical shifts were reported in ppm. A 5 mm NMR tube was used. The following abbreviations were used in the annotation of proton NMR spectra: singlet (s), doublet (d), triplet (t) and multiplet (m).

3.5.2.2 CHN Elemental Analysis

A quantitative analysis of carbon, hydrogen and nitrogen in ILs was performed using the LECO CHNS-932 Elemental Analyzer. About 1.5 to 2.0 mg of each ILs sample was analyzed and the results were then interpreted, allowing a deviation of $\pm 1.0\%$.

3.5.2.3 Thermogravimetric Analysis

The ILs samples were run on Mettler-Toledo TGA/SDTA 851^e TGA instrument and Mettler-Toledo STAR^e software version 8.10 was used to record and analyze the data. The samples were run in alumina pans under nitrogen atmosphere at a heating rate of 10°C min⁻¹ and the temperature was programmed from 25 to 400°C. The onset temperature (T_{onset}), which is the intersection of the baseline determined from the beginning of the experiment and the tangent of the weight versus temperature, was defined as the temperature for decomposition to occur.

3.5.2.4 Density Measurement

A density measurement of the new synthesized ILs was carried out with a digital densitometer at 25°C. The apparatus is precise to within 1.0×10^{-5} g cm⁻¹ and the uncertainty of the measurement was estimated to be better than $\pm 1.0 \times 10^{-4}$ g cm⁻¹. Calibration of the densitometer was performed at atmospheric pressure using distilled water, followed by standard fluid. The results were run in triplicate in order to assure the correct value.

3.5.2.5 Viscosity Measurement

Viscosities of ILs were measured at 25°C using the LVDV-II+Pro Viscometer manufactured by Brookfield Engineering Laboratories, Ins, USA, which was also equipped with CPE-52 spindle for high viscosity measurement. The instrument was connected to a computer using Rheocalc32 software. The viscosity data obtained were averaged over three measurements and recorded in mPa·s unit.

3.5.3 Biophysical Analysis of DNA in Ionic Liquids

3.5.3.1 Preparation of DNA Stock Solution

A stock solution of Calf thymus DNA was prepared by dissolving small amount of solid sodium salt in 20 mL deionized water type III without addition of buffer solution. An average chain length of 150-200 bp (Chaires, 1983) was achieved by subjecting the DNA solution to 30 minutes of discontinuous sonication using a Sanyo Soniprep 150 ultrasonic disintegrator. The prepared DNA solution was stored at 4°C with gentle shaking to achieve homogeneity within 24 hours.

3.5.3.2 Purity of DNA

The prepared DNA stock solution was subjected to absorbance analysis to check the presence of any unwanted contaminants especially proteins. The purity of the DNA was determined based on the ratio of absorbance of the DNA stock solution at wavelength of 260 nm (A_{260}) and 280 nm (A_{280}). The concentration of the DNA stock solution was determined by UV-visible spectroscopy using the Beer-Lambert Law equation:

$$A = \epsilon cl \quad (3.1)$$

where, A is absorbance value (no unit), ϵ is extinction coefficient constant, c is concentration of substance (M) and l is light path length (in cm). The extinction coefficient constant of $6600 \text{ M}^{-1} \text{ cm}^{-1}$ at wavelength of 260 nm was used and concentration was expressed in terms of base molarity (Reichmann *et al.*, 1954). It was found that the ratio of A_{260}/A_{280} is 1.9, indicating that the DNA was free from protein contaminants and pure enough to use for biophysical experiments. The DNA stock solution was kept in the freezer at -20°C and was used within a month.

3.5.3.3 Fluorescence Emission

The interaction between $[C_n\text{bim}][\text{Br}]$ ILs and Calf thymus DNA was determined using fluorescence emission spectroscopy. A 5.0 mL of 4.0 M stock solution of $[C_2\text{bim}][\text{Br}]$, $[C_4\text{bim}][\text{Br}]$ and $[C_6\text{bim}][\text{Br}]$ was prepared in deionized water. Then, 1.0 mL of each ILs stock solution was then diluted in order to obtain a final concentration of 0.5 M. The solution of DNA in deionized water with a final concentration of 0.3 mM was prepared from a 3.0 mM of DNA stock solution. The prepared DNA solution was slowly titrated into a cuvette filled with 1.5 mL of 0.5 M $[C_n\text{bim}][\text{Br}]$ solution and the emission intensity of $[C_n\text{bim}][\text{Br}]$ was observed. The excitation wavelength for $[C_n\text{bim}][\text{Br}]$ was set at 320 nm and maximum emission was observed at 358 nm.

The fluorescence displacement analysis of ethidium bromide-bound DNA (EB-bound DNA) quenched by $[C_n\text{bim}][\text{Br}]$ ILs was also recorded. The concentration of EB in aqueous solution was kept constant at 0.5 μM . Both the excitation and emission of EB were set at the wavelengths of 510 and 595 nm, respectively. The EB-bound DNA solution was prepared by titrating aqueous solution of DNA into the EB solution. The $[C_n\text{bim}][\text{Br}]$ solution was then slowly titrated with the portion of 1.0 μL for each titration into the solution of EB-bound DNA and the changes in intensity were recorded. The fluorescence emission spectra were recorded using the Cary Eclipse Fluorescence spectrophotometer. Band slits were fixed at 5.0 nm and 1.0 cm light-path quartz cuvette was used. The fluorescence spectra were corrected for the background intensities of the solution without DNA. All the titrations were performed at 25°C.

3.5.3.4 Circular Dichroism

The circular dichroism (CD) spectra of Calf thymus DNA's secondary structure in different percentages of $[C_n\text{bim}][\text{Br}]$ ILs (12.5%, 25.0%, 37.5%, 50.0% and 75.0% w/w) in deionized water were recorded using the Jasco J-815 spectrometer equipped with a Peltier temperature controller (PTC-423s) and water circulation unit. A rectangular quartz cell of 1.0 cm path length detachable cell was used to minimize DNA spectrum interference from $[C_n\text{bim}][\text{Br}]$ spectrum.

The titrations of $[C_n\text{bim}][\text{Br}]$ solution into a aqueous solution of DNA were performed with a fixed concentration of DNA (300 μM). As a control experiment, the solution of DNA in deionized water with the same concentration of 300 μM was also analyzed. The presented

spectrum was averaged over three scans recorded at a scan speed of 50 nm min^{-1} and was operated from a wavelength of 320 to 235 nm. The bandwidth was set at 1.0 nm and standard sensitivity was used. An appropriate blank was subtracted from respective spectra and the data were subjected to the noise reduction analysis. All analysis was performed at 25°C, 50°C, 70°C and 90°C.

3.5.3.5 UV-visible

AV-650 UV-Vis spectrophotometer, equipped with a temperature-controller sample holder and connected to a water circulation unit was used. The melting analysis was performed to study the effect of alkyl chain lengths of $[\text{C}_n\text{bim}][\text{Br}]$ ILs on the thermal stability of Calf thymus DNA. For this experiment, the percentage of each $[\text{C}_n\text{bim}][\text{Br}]$ (where $n = 2, 4, 6$) in deionized water was 25% (w/w) and the concentration of DNA was fixed at 60 μM . The melting temperature of DNA in aqueous solution was also observed. The temperature effect on the absorbance of DNA was detected at absorbance of 260 nm (A_{260}). A rectangular quartz cell of 1.0 cm path length was used. Heating experiments were conducted with heating rate set at $1.0^\circ\text{C min}^{-1}$. The temperature range was set from 25 to 90°C. The T_m value was calculated as the temperature at which the absorbance change was one half of the total A_{260} of DNA solution during melting (Bonner and Klivanov, 2000).

3.6 Computational Procedures

3.6.1 Geometry Optimization

The initial structure of three different 1-alkyl-3-butylimidazolium cations ($[\text{C}_n\text{bim}]^+$ where $n = 2, 4, 6$) used in this work was developed using PyMOL (DeLano, 2008). The cations were modeled using UA description for CH_2 and CH_3 groups of alkyl chains as shown in Figure 3.2. In case of imidazole rings, the inclusion of a proton attached to the ring (HAR, HA4 and HA5) was considered due to its polar character, as evidenced from partial atomic charge calculation. These protons from other *ab initio* calculation (Del Pópolo *et al.*, 2005) and experimental (Antony *et al.*, 2003; Headley and Jackson, 2002; Fuller *et al.*, 1994) data showed that they play an important role in forming hydrogen bonds with anions species.

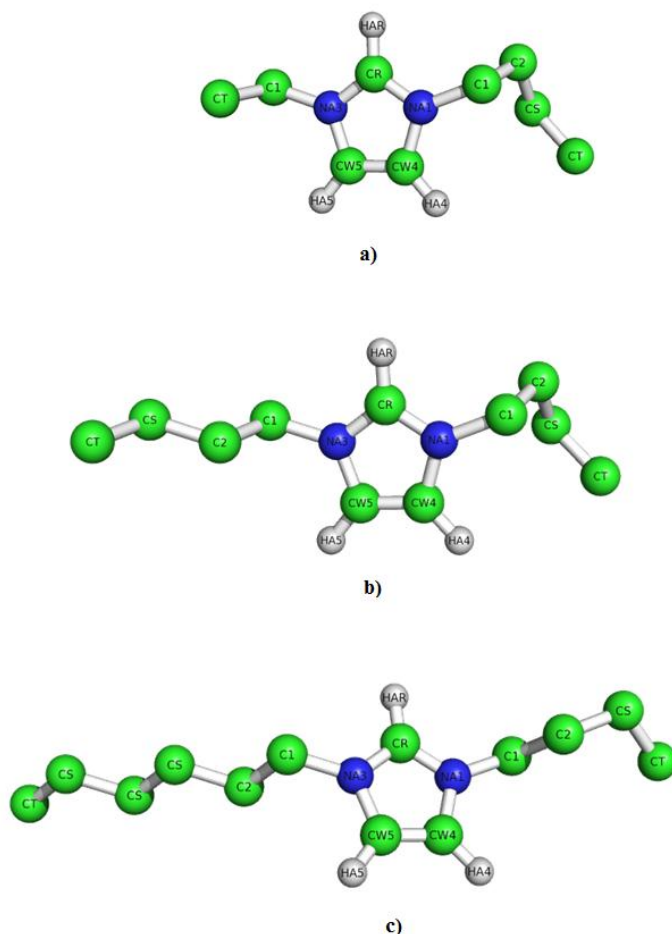


Figure 3.2. Geometry optimized cations with atom names. Structure of (a) $[C_2bim]^+$ (b) $[C_4bim]^+$ and (c) $[C_6bim]^+$ were model based on UA in which the hydrogen atoms are not explicitly considered. Proton HAR, HA4 and HA5 located at imidazolium ring were model AA description.

The structures of cations were geometrically optimized through *ab initio* calculations using winGAMESS software (Schmidt *et al.*, 1993) prior to MD simulation. The initial charges for cations were set to +1. The DFT with the popular Becke's Three-parameter Hybrid Functional (B3LYP) method (Becke, 1993; Lee *et al.*, 1988) was used. The B3LYP equation is shown in Equation 3.2.

$$E_{XC} = E_{XC}^{LSDA} + a_0(E_X^{exact} - E_X^{LSDA}) + a_x \Delta E_X^{B88} + a_c \Delta E_C^{PW91} \quad (3.2)$$

Where, the E_{XC}^{LSDA} is the uniform electron gas exchange-correlation energy, E_X^{exact} term corresponds to the exact exchange energy, ΔE_X^{B88} is Becke's 1988 gradient correction (to the LSDA) for exchange and ΔE_C^{PW91} is the 1991 gradient correction for correlation of Perdew and Wang (Perdew *et al.*, 1992). The coefficients a_0 , a_x , and a_c were determined by a linear least squares fit to 42 ionization potentials, 56 atomization energies and 8 proton affinities obtained from Becke, 1993. The values thus obtained, which are in some sense semi-empirical, were $a_0 = 0.20$, $a_x = 0.72$, and $a_c = 0.81$. The minimum energy of geometry of the structures studied were determined by performing calculations at the B3LYP/6-311++G** level of theory in the gas phase. This basis set was chosen as the molecules of cations are relatively small and acceptable for this calculation. A polarization function was included in the geometry optimization, since the inclusions of polarizable and diffuse functions for the hydrogen atom are important for descriptions of hydrogen-bonded interaction (Wu and Zhang, 2009; Mou *et al.*, 2008).

3.6.2 Partial Atomic Charges

Partial atomic charges for selected atoms in cationic molecules were calculated using the Restrained Electrostatic Potential (RESP) method developed by Bayly *et al.* (1993) based on electrostatic potentials obtained previously with the B3LYP/6-311++G** basis set. RESP is an *ab initio* method that does not include any empirical or semi empirical parameters in the equation and lacks inclusion of any experimental data. This method has previously worked well in tests of small molecules (Gundertofte *et al.*, 1996). This method fits the quantum mechanically calculated ESP at molecular surfaces using an atom-centered point charge model. The least square procedure was used to fit the charges q_j to atomic center j , in the molecule. The ESP equation is shown below:

$$\tilde{V}_i = \sum_j \frac{q_j}{r_{ij}} \quad (3.3)$$

The charges were computed using a single step and were distributed only to all of the atoms in alkylimidazolium ring including the hydrogen atoms attached to the ring and two carbon atoms in

alkyl chains near to the imidazole ring (carbon C1, refer Figure 3.2 page 43). The charges for alkyl chains except for carbon C1 were forced to have a zero charge. As in unrestrained calculations, it has been shown that the total charge of atoms in group CH_2 and CH_3 displayed to have zero charge. Based on previous studies, forcing those groups to have zero charges does not have any major effects on the properties obtained (Micaelo *et al.*, 2006). Table 3.2 shows the complete charge groups of each atom in alkyimidazolium cations and bromide anion.

Table 3.2 Partial atomic charges for each set of atoms derived using RESP calculation. Atom type of opls_071 and opls_068 represent the UA model for CH_2 and CH_3 groups, respectively.

For clarity, refer Figure 3.2 (page 43) for the position of each atom name. The charge for bromide anion ($[Br^-]$) is also shown.

Ion	Atom name	OPLS atom type	Atomic charge, q
$[C_n\text{bim}]^+$	NA1	opls_557	- 0.058
	CR	opls_558	- 0.038
	HAR	opls_563	+ 0.216
	NA3	opls_559	- 0.058
	CW4	opls_560	- 0.158
	HA4	opls_564	+ 0.241
	CW5	opls_561	- 0.158
	HA5	opls_565	+ 0.241
	C1	opls_071	+ 0.386
	C2	opls_071	+ 0.000
	CS	opls_071	+ 0.000
CT	opls_068	+ 0.000	
$[Br^-]$	Br	Br	-1.000

3.6.3 Force Fields

Bonded (bonds, angles and dihedrals) and non-bonded (LJ and Coulomb) parameters for all atoms in ILs ions were obtained from OPLS FFs as published by Jorgensen *et al.* (1996) and Jorgensen, (1986). For 1-alkyl-3-butylimidazolium cations ($[C_n\text{bim}]^+$), the FFs parameters for the atoms in imidazole ring were based on the histidine imidazole, while atoms in alkyl chains were based on the parameters for organic molecules. The partial atomic charges for each atom were obtained from RESP calculation as mentioned previously. For an anion, as bromine which only contains one atom,

there are no bonded parameters except for LJ and Coulomb parameters that describe short-range interaction. The atom types for each atom in cations and anion were selected accordingly to the OPLS FFs.

Bonded and non-bonded parameters as well as partial atomic charges for all atoms in the initial crystal structure of Calf thymus DNA, nucleic acid bases (adenine, cytosine, guanine, thymine and uracil) and TIP4P model of water were also directly obtained from OPLS and used without modification. The complete functional forms of the FFs were previously discussed in Chapter 2 Section 2.11 (page 28). The topology were created using ANTECHAMBER/Gaff Force Field (Wang *et al.*, 2004) implemented in AMBER 8.0 (Case *et al.*, 2005). The topology obtained was then converted to GROMACS topology using a PERL script. The parameter details are given in Appendix A1-A3.

3.6.4 System Setup

3.6.4.1 Ionic Liquids

The starting optimized geometry structures for ILs ions were assembled in a simulation box containing an equivalent amount of cation and anion with standard PBC applied in all directions. Three simulation boxes were required for three different $[C_n\text{bim}][\text{Br}]$ ILs (where $n = 2, 4, \text{ and } 6$) systems. A total of 400 molecules with a fraction of 200 cationic molecules and 200 anionic molecules were randomly placed inside a cubic cell system with dimensions of $4.0 \times 4.0 \times 4.0$ nm, using Packmol (Martinez *et al.*, 2009). The distance between atoms from different molecules was set at 0.2 nm in order to make sure there was no significant overlap. The configuration of cations, anions and box simulation vectors were rescaled in order to begin the simulations of each ILs at a known experimental density at 298.15 K.

3.6.4.2 DNA in Ionic Liquids

The crystal structure of Calf thymus DNA was obtained from a RCSB Protein Data Bank (RCSB PDB) with a PDB ID 425D (Rozenberg *et al.*, 1998). This Calf thymus DNA was chosen in order to match the experimental condition. There were also a few studies reported the behaviour of this DNA in ILs (Wang *et al.*, 2011; Ding *et al.*, 2010). To build an initial system, a cubic box was used and the size of the box was calculated based on a cut-off distance of 1.2 nm. The crystal structure of DNA was placed at the

center of a $6.7 \times 6.7 \times 6.7$ nm box and solvated in three different neat $[C_n\text{bim}][\text{Br}]$ ILs ($n = 2, 4$ and 6). In control simulation, the DNA was simulated in an aqueous system using the TIP4P model of water. The concentration of aqueous system was set to 100 mM by replacing a selected water molecule by sodium and chloride ions. Figure 3.3 shows the initial cubic box system of Calf thymus DNA in water and neat $[C_n\text{bim}][\text{Br}]$ ILs.

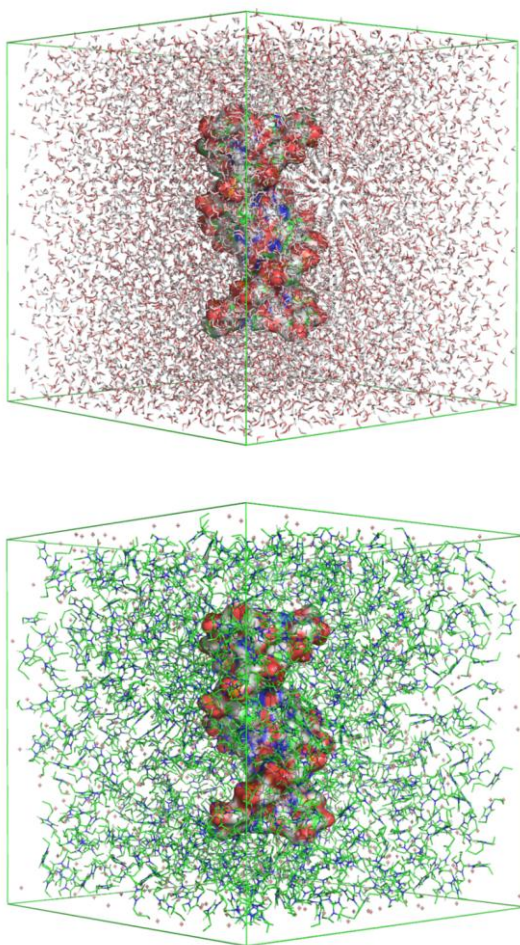


Figure 3.3. Snapshot of initial box of simulation for Calf thymus DNA in TIP4P model of water (top) and neat $[C_2\text{bim}][\text{Br}]$ (bottom).

As water activity plays a major role in the stabilization of DNA, the effect of water content in hydrated IL system was also studied. Only [C₄bim][Br] IL was selected as a model for this purpose. Subsequently, three additional simulations were performed by varying the ratio of [C₄bim][Br] and water. Figure 3.4 illustrates the initial systems of Calf thymus DNA in hydrated [C₄bim][Br]. The number of molecules required in a given simulation box were calculated based on percentage weight of IL over weight of water (% w/w).

For simulation of DNA in a mixture of [C₄bim][Br] and water systems, the equilibrated DNA structure with a layer of surrounding water molecules within 0.35 nm from DNA surface was taken from the trajectory of a MD simulation of DNA in water at 298.15 K. This DNA was placed into a center of simulation box with the size of cubic box similar as previously mentioned. The box was then filled with the requisite number of cations, anions and water molecules to reach the desired ratios. The effect of temperature on the structural stability of Calf thymus DNA was also determined. The systems of DNA in water, neat ILs and hydrated [C₄bim][Br] were simulated at temperatures of 298.15 K, 323.15 K, 343.15 K and 373.15 K. Further details of the systems used in simulation are given in Table 3.3.

Table 3.3. Number of molecules used in the simulation of DNA.

Entry	System	Ratio [IL]:H ₂ O (% w/w)	Number of molecules		
			Cation	Anion	TIP4P
1	[C ₂ bim][Br]	100 : 0	962	940	-
2	[C ₄ bim][Br]	100 : 0	826	804	-
3	[C ₆ bim][Br]	100 : 0	737	715	-
4	H ₂ O	0 : 100	40 Na ^a	18 Cl ^a	9637
5	[C ₄ bim][Br]	25 : 75	223	201	7108
6	[C ₄ bim][Br]	50 : 50	424	402	4840
7	[C ₄ bim][Br]	75 : 25	625	603	2420

^a 22 sodium atoms were used as counter ion to neutralize the DNA charges. The remaining 18 sodium and 18 chlorine atoms were used to set 100 mM concentration of aqueous system.

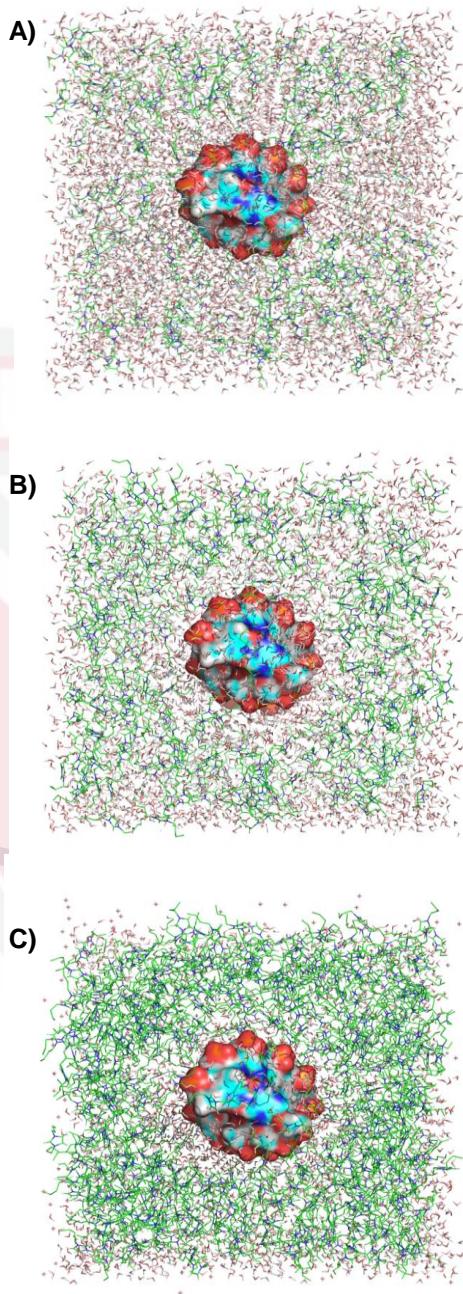


Figure 3.4. The initial box of simulation for the DNA in hydrated [C₄bim][Br] systems. A) 25%; B) 50% and C) 75% (w/w) [C₄bim][Br] in water. View from top of cubic simulation box.

3.6.4.3 Solvation Free Energy

The initial configuration of each nucleic acid bases were obtained from the RSCB Protein Data Bank (PDB) with the PDB entry code ADE (adenine), CYT (cytosine), GUN (guanine), TDR (thymine) and URA (uracil). Each base was placed at the center of a $3.0 \times 3.0 \times 3.0$ nm cubic box and solvated in ILS [C₂bim][Br], [C₄bim][Br] and [C₆bim][Br]. In a control simulation, the bases were simulated in an aqueous system using the TIP4P model of water. Details involving the number of ILS and water molecules required in a given simulation box were depicted in Table 3.4.

Table 3.4. Number of molecules used in the free energy simulation.

Bases	Number of molecules			
	[C ₂ bim][Br]	[C ₄ bim][Br]	[C ₆ bim][Br]	TIP4P
Adenine	87	74	65	879
Cytosine	87	74	65	879
Guanine	87	74	65	880
Thymine	87	74	65	877
Uracil	87	74	65	880

3.6.5 Molecular Dynamics Parameters

The integration step of 2.0 fs was used with PBC applied in all directions (x , y , z). Non-bonded (LJ and Coulomb) interactions were calculated up to 1.2 nm and long-range electrostatic interaction were treated with PME (Essmann *et al.*, 1995; Darden *et al.*, 1993) with a grid spacing of 0.12 nm and fourth-order interpolation. Neighbor searching of 1.2 nm was used and updated every 5 steps. Bond lengths were constrained with LINCS (Hess *et al.*, 1997). Temperature and pressure control were implemented using a Berendsen thermostat and Berendsen barostat, respectively (Berendsen *et al.*, 1984). The heat was separated in two heat baths with temperature coupling constants of 0.1 ps. A reference pressure of 1.0 atm and relaxation time of 2.0 ps were applied. Isothermal compressibility for pressure control was set at 4.5×10^{-5} bar⁻¹. Energies, forces, velocities and trajectories were recorded every 500 steps.

For simulation of solvation free energy systems, the MD parameters used were similar to the parameters mentioned in the previous page with the addition of some free energy parameters. The soft-core energy parameters were set to $\alpha_{LJ} = 0.5$ and soft-core sigma = 0.3, while the λ power dependency was set to 2. Free energy calculation was performed with 21 equidistant set of λ values ($\Delta\lambda = 0.05$). Coordinates, velocities, and $\delta H/\delta\lambda$ were saved to disk every five steps.

3.6.6 Simulation Details

3.6.6.1 Systems of Ionic Liquids

The initial system was relaxed by performing two energy minimizations. First, energy minimization of the ILs system was computed using the steepest descent method, followed by a conjugate gradient scheme. 5000 steps were applied for each minimization step with a time step of 0.2 fs. A NVT with a 2 ns simulation time was applied for proper and efficient pre-equilibration because of the slow dynamics of alkylimidazolium based ILs (Yan *et al.*, 2004). For production simulation, 10 ns NPT was computed and was long enough to obtain accurate properties of $[C_n\text{bim}][\text{Br}]$ ILs. The first 5 ns were dedicated for the system to achieve equilibration and the properties for analysis were taken from the last 2 ns trajectory. The energies, forces, velocities and trajectories were recorded every 500 steps (1 ps). The complete set of simulation parameters are shown in Appendix B1-B5.

3.6.6.2 Systems of DNA in Ionic Liquids

A few steps of energy minimization were performed. Each system was energy-minimized with 5000 steps of the steepest descent method followed by 5000 steps of conjugate gradient. During the energy minimization, all DNA heavy atoms (all atoms except hydrogen) were position-restrained with a constant force of 10^6 kJ mol⁻¹ nm⁻². The system was further minimized with 5000 steps of steepest descent with position restraints applied to the DNA main chain atoms, with the same force constant as previously mentioned. The main chain atom selection includes all phosphorous and oxygen atoms of the phosphate groups and the connecting atoms of the sugar residues. The system was then energy-minimized for the third time without applying any position restraints with 5000 steps of steepest descent, followed by 5000 conjugate gradients.

The simulation of Calf thymus DNA in different systems was initialized in the NVT for 500 ps. Position restraints were applied again to all DNA heavy atoms with the same force constant of 10^6 $\text{kJ mol}^{-1} \text{nm}^{-2}$. Then, a 100 ps NVT ensemble was introduced to the system with the DNA main chains harmonically restrained with the same force constant. The system was pre-equilibrated using 2 ns NVT simulation with no position restraints applied. The equilibration process was continued with 10 ns NPT. The system of DNA in ILs reached equilibrium in the first 6-8 ns due to the slow dynamics of these types of solvents. For a simulation of DNA in water, the system was fully equilibrated during the first 5 ns. The energies, forces, velocities and trajectories were recorded every 500 steps (1 ps). The trajectory for data analyses was taken from the last 2 ns. All the simulation parameters used are similar to the previous work carried out by Cardoso and Micaelo (2011). The complete set of simulation parameters is similar as shown in Appendix B.

3.6.6.3 Free Energy Systems

First, each system was energy minimized with 5000 steps of the steepest descent method followed by 5000 steps of conjugate gradient. The simulation was then pre-equilibrated in the NVT for 100 ps with no position restraints applied. The equilibration process was continued with 2 ns simulation in NPT at 298.15 K for all systems. Data collection was taken from the last 1 ns. The systems required shorter simulation time to fully equilibrate because simulation box is not too large and the number of molecules is considered small. The complete set of free energy simulation parameters are shown in Appendix C1-C4. All MD simulations were performed with the GROMACS version 4.5, which offers highly optimized and parallelized algorithms for an efficient treatment of all atoms system (Hess *et al.*, 2008; van Der Spoel *et al.*, 2005).

3.6.7 Data Analysis

3.6.7.1 Density

Density (ρ) is a good starting point for validating the FFs, although it is well understood that incorrect FFs parameters can also give rise to a correct density. Generally, it is possible to accurately reproduce density while other properties such as viscosity are only poorly reproduced. The densities of ILs at 298.15 K were calculated directly from the simulation trajectories. The average density was obtained by averaging the result from last 2 ns isobaric-isothermal NPT simulation, while the pressure was maintained at 1.0 atm.

3.6.7.2 Shear Viscosity

Shear viscosity (η) is another important property for validation of FFs. This property was calculated using non-equilibrium periodic perturbation method (Ciccotti *et al.*, 1979). The perturbation method is a more accurate method to calculate shear viscosity of model liquids and this method was reviewed by Hess (2002). The simulation was performed with the periodic acceleration profile $a_x(z)$ applied along the x-axis and A is the amplitude parameter, as shown in Equation 3.4.

$$a_x(z) = A \cos\left(\frac{2\pi}{L_z} z\right) \quad (3.4)$$

These parameters have been fine-tuned in order to achieve good statistics and also to prevent the system diverging to far from the equilibrium (Szeferczyk and Cordeiro, 2011). As shown in Equation 3.5, the accuracy of shear viscosity increases if the dimension of simulation box increase along the z-axis. Based on the equation, shear viscosity of [C_nbim][Br] ILs were calculated from the velocity profile (V), amplitude parameter (A) and density (ρ).

$$\eta = \frac{A}{V} \rho \left(\frac{lz}{2\pi}\right)^2 \quad (3.5)$$

Therefore, the new box vectors were built with a new dimension 4.0 × 4.0 × 12.0 nm (Figure 3.5) by replicating the previously equilibrated system obtained by NPT simulation. A total of 600 cation molecules and 600 anion molecules in an extended box were energy minimized using the method previously described (refer Section 3.6.6.1, page 51). A 10 ns non-equilibrium NVT was applied to the simulation by varying the amplitude parameter (nm ps⁻²) to the ILs system until the shear viscosity obtained in agreement with experimental data. The systems were simulated at 298.15 K and shear viscosity was calculated from a last 5 ns trajectory.

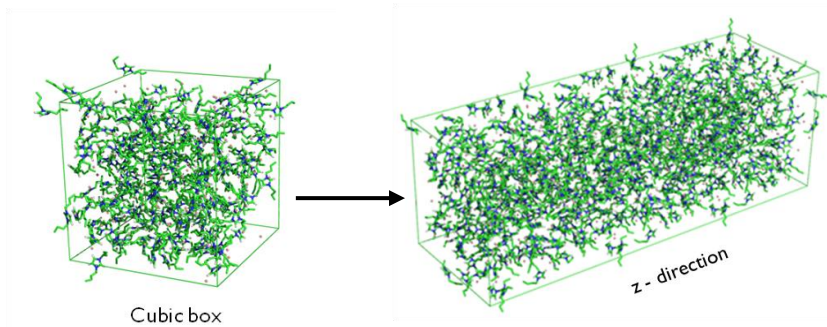


Figure 3.5. Replicating previously equilibrated system along the z-axis.

3.6.7.3 Self-diffusion Coefficient

Self-diffusion coefficient (D) is a simple property which provides quantitative information on the motion of the ions in the liquid. This property can be computed over a long enough simulation time. In this work, self-diffusion of each ILs was calculated based on equilibrium NVT simulation. A previously equilibrated system obtained by NPT simulation was used in 10 ns NVT production simulation.

The Einstein relation shows in Equation 3.6 was used to determine the self-diffusion coefficient. For molecules consist of more than one atom, \vec{r}_i can be taken as the center of mass of molecules, whereas $\vec{r}_i(t)$ is the position of atom i at specific time and $\vec{r}_i(0)$ is the position of atom i at initial time. The self-diffusion data was calculated using `g_msd` command implemented in GROMACS software.

$$D = \frac{1}{6t} \langle |\vec{r}_i(t) - \vec{r}_i(0)|^2 \rangle \quad (3.6)$$

3.6.7.4 Molecular Structure

Molecular structure of $[C_n\text{bim}][\text{Br}]$ ILs can be viewed using RDF and SDF. A function that characterizes the local structure of a fluid is known as a RDF $g(r)$. This function gives the probability of finding a pair of atoms/molecules (in this work a pair between cation and anion) at a given distance r , relative to that same probability in a completely random distribution at the same density (ρ), as shown in Equation 3.7.

$$RDF\ g(r) = \frac{\rho(r)}{\langle \rho \rangle} \quad (3.7)$$

When the distance r between the two atoms/molecules becomes large, the probability of correlation falls to that of a random isotropic liquid, $g(r)$ becomes 1 and the $g(r)$ of ILs is quite particular due to charge ordering. The pair distribution function is useful not only because due to providing insight about the liquid structure, but also because it can be related to macroscopic thermodynamic quantities such as energy, pressure and chemical potential. For simulations of DNA in ILs, the RDF was determined between the residues' centre-of-mass (RES-COM) of cation and anion around the DNA phosphate groups.

The interaction between ILs cation and anion in the three-dimensional (3D) probability distribution of anion around cation can be viewed by SDF. The SDF usually indicate which regions around the cations are more populated by the anions. The calculation of RDF and SDF were carried out using *g_rdf* and *g_spatial* programs implemented in GROMACS software, respectively.

3.6.7.5 Root Mean Square Deviation

Root mean square deviation or RMSD is used to measure an average distance of certain atoms in a molecule with respect to a reference or initial structure. A larger average distance of atoms leads to a higher RMSD value. The atomic RMSD of DNA heavy atoms (all atoms except hydrogen) with respect to an initial crystal structure of Calf thymus DNA was calculated by the program *g_rms* implemented in GROMACS software by least-square fitting both structure using Equation 3.8, where $M = \sum_{i=1}^N m_i$ and $r_i(t)$ is the position of atom i at time t .

$$RMSD(t_1, t_2) = \left[\frac{1}{M} \sum_{i=1}^N m_i \|r_i(t_1) - r_i(t_2)\|^2 \right]^{\frac{1}{2}} \quad (3.8)$$

3.6.7.6 Root Mean Square Fluctuation

Root mean square fluctuation (RMSF) is used to measure the deviation between the position of atoms (or regions) and reference or initial structure over time. It can also locate the areas with high or

low mobility. The RMSF of DNA bases was computed by taking the average position of each bases using *g_rmsf* program employed in GROMACS using Equation 3.9, where T is the time to average and \bar{y}_i is the reference/initial position of particle i .

$$RMSF = \sqrt{\frac{1}{T} \sum_{t_j=1}^T (y_i(t_j) - \bar{y}_i)^2} \quad (3.9)$$

3.6.7.7 Hydrogen Bonds

The average hydrogen bonds of Watson-Crick and hydrogen bonds between DNA bases and polar proton of ILs' cations were calculated using the command *g_hbond* command in GROMACS software. This command automatically analyzes the hydrogen bonds between all possible hydrogen-bond-donors (D) and hydrogen-bond-acceptors (A) following a geometrical criterion as shown in Equation 3.10 and 3.11.

$$r_{DA} \leq 0.35 \text{ nm} \quad (3.10)$$

$$\theta_{DA} \leq 30^\circ \quad (3.11)$$

where r_{DA} and θ_{DA} are the distance and angle between D and A . The total numbers of hydrogen bonds between two groups of atoms which must be either identical or non-overlapping were analyzed in each time frame. The bromide anion was considered a hydrogen-bond-acceptor since it has available electron pairs. Therefore hydrogen bond interaction between the bromine and DNA bases was also calculated.

3.6.7.8 Free Energy Calculation

A thermodynamic cycle such as the one shown in Figure 3.6 is usually used to calculate absolute solvation free energies (ΔG_{solv}) of a molecule A or B from gas phase (g) to aqueous system (aq). This cycle also can be used to calculate relative free energy (ΔG_{AB}) of two compound A and B. However, in this free energy simulation, we only focused on the ΔG_{solv} of five nucleic acids bases in two different solvents, water and $[\text{C}_n\text{bim}][\text{Br}]$ ILs.

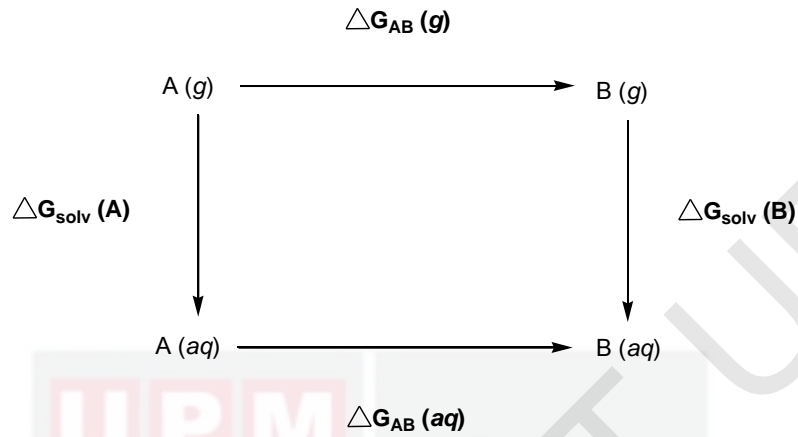


Figure 3.6. Thermodynamic cycle used to determine the absolute solvation free energy (ΔG_{solv}) of given molecules A or B.

Bennett acceptance ratio (BAR) method was applied to calculate ΔG_{solv} of nucleic acid bases. Bennett (Bennett, 1976) shows that the free energy between state i and j can be calculated according to the equation below.

$$\Delta G_{ji}^{\text{BAR}} = k_B T \left(\ln \frac{\langle f(H_i - H_j + C) \rangle_j}{\langle f(H_j - H_i - C) \rangle_i} \right) + C \quad (3.12)$$

where f is the Fermi function

$$f(x) = \frac{1}{1 + \exp\left(\frac{x}{k_B T}\right)} \quad (3.13)$$

With k_B representing the Boltzmann constant and T is temperature. H_i and H_j represent the Hamiltonians at states i and j . The value for C is determined iteratively to fulfill $\langle f(H_i - H_j + C) \rangle_j = \langle f(H_j - H_i - C) \rangle_i$. The free energy difference between states is obtained with Equation 3.14 and 3.15.

$$\Delta G_{ji}^{\text{BAR}} = -k_{\text{B}}T \ln \frac{N_j}{N_i} + C \quad (3.14)$$

and

$$\Delta G_{\text{BA}}^{\text{BAR}} = \sum_{i=1}^{n-1} \Delta G_{i+1,i}^{\text{BAR}} \quad (3.15)$$

where N_i and N_j represent the number of coordinate frames at λ_i and λ_j , respectively. Convergence of this process can only be reached if there is sufficient overlap between the forward and backward energy differences. This overlap may be monitored with the overlap integral obtained from the normalized histograms of the energy differences. It should be noted that the BAR calculation program was implemented in GROMACS version 4.5. The command `g_bar` represents the BAR calculation program in GROMACS software.

CHAPTER 4

RESULTS AND DISCUSSION

4.1 Design, Synthesis and Characterization of New Ionic Liquids

4.1.1 Screening of Ionic Liquids

The initial strategy is to design and synthesize new ILs having linear hydrocarbon chains of varying lengths attached to the alkylimidazolium-based cation. The imidazole cation was chosen due to its less toxicity as compared to thiazole and pyrrolidine. The main reason to attach linear alkyl chains is because alkyl chain provides hydrophobic groups which are crucial in the IL-DNA interaction and also play a significant role in DNA stabilization (Wang *et al.*, 2011). Since DNA is a polyanion polymer which has a negative charge on the DNA phosphate groups, thus the selection of counter anion for imidazolium-cation is not really important in DNA solvation. Many studies reported the DNA stabilization within selection of molecules/ions or buffer solutions stressed the importance of cationic molecules/atoms rather than anionic species.

Although the anion does not significantly contribute to the DNA solvation mechanism, the choice of anion would have a great influence on determining the properties of ILs. As stated in literature, a selection of halide anions will produce hydrophilic ILs while other anions for example $[\text{PF}_6]^-$ yielded a hydrophobic ILs. However, the former is preferred because DNA needs a small portion of water molecules to retain its conformation as observed in the case of proteins (Vijayaraghavan *et al.*, 2010b). Therefore, the key of synthesizing new ILs lies on three main criteria. First, a simple and straightforward method should be considered in order to get high purity ILs in moderate reaction time. Second, a new series of ILs that are going to be synthesized should have longer alkyl chain lengths tethered to the imidazole structure. Lastly, small and highly hydrophilic anions are needed in order to obtain hydrophilic ILs. Small halides anions such as bromide were chosen as they can help to increase the hydrophilicity of ILs.

Purification of ILs by conventional techniques can be a hideous process. Therefore, obtaining ILs in a pure state from the alkylation reaction is an essential and straightforward alternative. In order to avoid impurities, a simple and straightforward alkylation procedure

according to a known method published by Wang *et al.* (2007b) was used. The reaction was started with pure freshly distilled 1-butylimidazole with various bromoalkanes (Figure 4.1) as alkyl transfer reagent which gives bromide as the anionic leaving group. Bromoalkanes were chosen because they are highly reactive compared to chloroalkanes and they are inexpensive. For example, a reaction of 1-methylimidazole and chloroalkanes can take 2-3 days at 80°C whereas the reaction with bromoalkanes take about 1 day at 40–60°C (Gordon, 2003).

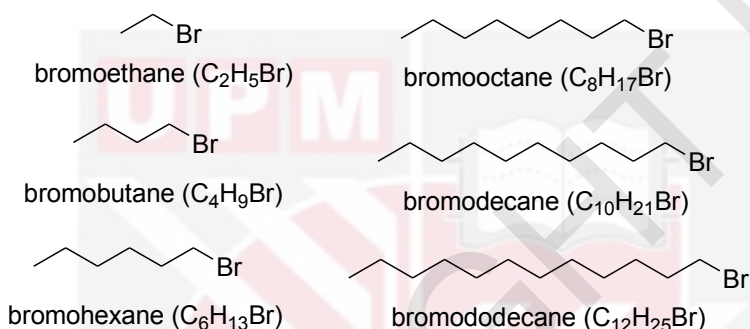
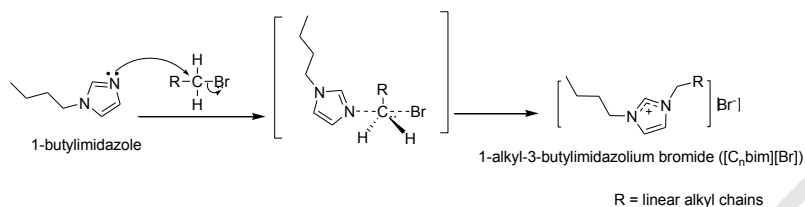


Figure 4.1. Different alkyl halides used in synthesizing of new $[C_n\text{bim}][\text{Br}]$ ILs.

This alkylation method has a major advantage since the desired ILs are produced with no by-products. The new $[C_n\text{bim}]\text{Br}$ ILs are formed by simply stirring the 1-butylimidazole with the bromoalkanes at 40°C. In the first step, the secondary amine contains an electron pair in 1-butylimidazole attacks the bromoalkanes from the backside of carbon (C) attached to the bromine atom via S_N2 reaction (Scheme 4.1). This nitrogen atom donates an electron pair to bond with C (N–C), while the C–Br bond breaks. At the transition state of the reaction, the formation and the breaking of the bonds occur simultaneously (denoted by dashed lines). The product of 1-alkyl-3-butylimidazolium is then formed when the Br is pushed off the opposite side and taking the electron pair to form $[\text{Br}]^-$ anion. The screening results are compiled in Table 4.1. Increasing the non-polar hydrocarbon group in the alkyylimidazolium cation has resulted in the increase of the hydrophobicity and reducing the hydrophilicity of ILs. The alkylation reaction of shorter alkyl halide (Table 4.1, entry 1-3) with 1-butylimidazole successfully produced the desired hydrophilic $[C_n\text{bim}][\text{Br}]$ ILs. However, the other three new ILs having longer hydrocarbon chains (Table 4.1, entry 4-6), were obtained as a semi solid and partially miscible with water.



Scheme 4.1. Mechanism of alkylation reaction of 1-butylimidazole with bromoalkanes.

Table 4.1. Physical properties and solubility of [C_nbim][Br] ILs.

Entry	ILs	Physical properties	^a Yield (%)	Solubility in water
1	[C ₂ bim][Br]	Colourless liquid	98	miscible
2	[C ₄ bim][Br]	Colourless liquid	97	miscible
3	[C ₆ bim][Br]	Yellowish liquid	97	miscible
4	[C ₈ bim][Br]	Yellowish semi solid	90	partially miscible
5	[C ₁₀ bim][Br]	Yellowish semi solid	86	partially miscible
6	[C ₁₂ bim][Br]	Yellowish semi solid	85	partially miscible

^a Yield was calculated after 24 hours of alkylation reaction.

As the duplex DNA structure contains polar bases such as adenine, cytosine, guanine and thymine, only polar and hydrophilic solvents are able to dissolve it. Hence, reducing the hydrophilicity of ILs will reduce its ability to solvate the duplex DNA molecule. Therefore, the increment of alkyl chain length of ILs was limited to hexyl group ([C₆bim][Br]) in order to restrain the hydrophilicity and polarity from being decreased. The results indicated that three out of six new [C_nbim][Br] ILs (Table 4.1, entry 1-3) were suitable as potential molecular solvent for DNA while the other three salts (Table 4.1, entry 4-6) might be useful for other applications. These three hydrophobic ILs were not used as solvent for DNA in this work due to their solubility problem with water. The properties of these hydrophobic salts were not further characterized, except for NMR, elemental analysis and thermal decomposition. Furthermore, since they exist as semi solid at room temperature, thus their density and viscosity were not determined.

4.1.2 Proton and Carbon NMR

4.1.2.1 1-ethyl-3-butylimidazolium bromide ([C₂bim][Br])

The ¹H NMR spectra of [C₂bim][Br] in *σ*-CDCl₃ is shown in Appendix D1. Two triplet signals at downfield region at 0.84 ppm and 1.49 ppm were attributed to the proton in the CH₃ groups located at the end of the alkyl chains. Each of these peaks was integrated containing three protons. Another triplet peak was detected at 4.25 ppm containing two protons which attributed to the peak N-CH₂. This was due to the protons adjacent to the nitrogen atom were deshielded and shifted upfield in the spectrum. Two set of multiplet signals at downfield region observed at 1.23–1.31 ppm and 1.77–1.83 ppm were assigned to the proton in CH₂ groups. Both of the peaks were integrate to a total of two protons for each signal. While one multiplet signal contains two protons was observed at upfield region (4.31–4.36 ppm, N-CH₂), because these protons were deshielded due to the attachment to electronegative nitrogen atom. There are three signal peaks containing one proton for each peak detected at the high upfield region. Two peaks were located at 7.46 ppm and 7.57 ppm and another at 10.17 ppm correspond to the protons on the imidazolium ring. The ¹³C NMR spectrum is shown in Appendix D2. From the spectrum, 9 carbon peaks were observed, which are in agreement with the total number of carbon in the expected structure. The assignments of the NMR spectra for [C₂bim][Br] are summarized in Table 4.2.

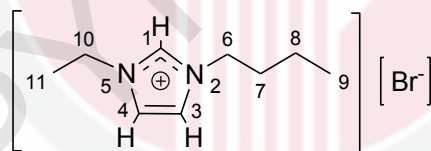


Table 4.2. ¹H and ¹³C NMR assignments of [C₂bim][Br].

Pos.	¹ H (ppm)	¹³ C (ppm)
1	10.17 (s, 1H)	136.4
2, 5	-	-
3	7.46 (s, 1H)	122.1
4	7.57 (s, 1H)	122.3
6	4.25 (t, 2H) ³ J _{HH} =7.3 Hz	45.2
7	1.77–1.83 (m, 2H)	19.4
8	1.23–1.31 (m, 2H)	15.7
9	0.84 (t, 3H) ³ J _{HH} = 7.0 Hz	13.5
10	4.31–4.36 (m, 2H)	49.8
11	1.49 (t, 3H) ³ J _{HH} = 7.0 Hz	32.2

4.1.2.2 1,3-dibutylimidazolium bromide ([C₄bim][Br])

The ¹H NMR spectra of [C₄bim][Br] in *σ*-CDCl₃ is shown in Appendix D3. Differ from others ILs, this IL has symmetrical structure. Therefore, there is only one triplet signal detected at downfield region at 0.90 ppm attributed to the proton in the CH₃ groups located at the end of the alkyl chains. This peak was integrated containing 6 protons. Another triplet peak was detected at upfield region (4.31 ppm) containing 4 protons which attributed to the peak (N-CH₂)₂. This was due to the protons adjacent to the nitrogen atom were deshielded and shifted upfield in the spectrum. Two set of multiplet signals at downfield region observed at 1.28–1.36 ppm and 1.82–1.88 ppm were assigned to the proton in CH₂ groups. Both of the peaks were integrate to a total of 4 protons for each signal. There are 2 signal peaks located at 7.49 ppm which are integrate contain 2 protons and at 10.38 ppm contains one proton correspond to the protons on the imidazolium ring. The ¹³C NMR spectrum is shown in Appendix D4. From the spectrum, 6 carbon peaks were observed, which are in agreement with the total number of carbon in the expected structure. The assignments of the NMR spectra for [C₄bim][Br] are summarized in Table 4.3.

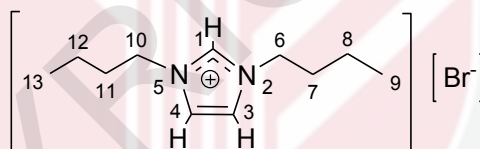


Table 4.3. ¹H and ¹³C NMR assignments of [C₄bim][Br].

Pos.	¹ H (ppm)	¹³ C (ppm)
1	10.38 (s, 1H)	137.0
2, 5	-	-
3, 4	7.49 (d, 2H)	122.2
6, 10	4.31 (t, 4H) ³ J _{HH} = 7.3 Hz	49.8
7, 11	1.82–1.88 (m, 4H)	32.2
8, 12	1.28–1.36 (m, 4H)	19.5
9, 13	0.90 (t, 6H) ³ J _{HH} = 7.0 Hz	13.5

4.1.2.3 1-hexyl-3-butylimidazolium bromide ([C₆bim][Br])

The ¹H NMR spectra of [C₆bim][Br] in *σ*-CDCl₃ is shown in Appendix D5. Two triplet signals at downfield region at 0.71 ppm and 0.81 ppm were attributed to the proton in the CH₃ groups located at the end of the alkyl chains. Each of these peaks was integrated containing three protons. Another triplet peak was detected at 4.24 ppm containing four protons which attributed to the peak (N-CH₂)₂. This was due to the protons adjacent to the nitrogen atom were deshielded and shifted upfield in the spectrum. Three set of multiplet signals at downfield region observed at 1.12–1.17 ppm, 1.19–1.27 ppm and 1.74–1.80 ppm were assigned to the proton in CH₂ groups. These multiplet signals were integrate to a total of four protons for each signal. There are three signal peaks containing one proton for each peak detected at the high upfield region. Two peaks were located at 7.47 ppm and 7.51 ppm and another at 10.19 ppm correspond to the protons on the imidazolium ring. The ¹³C NMR spectrum is shown in Appendix D6. From the spectrum, 13 carbon peaks were observed, which are in agreement with the total number of carbon in the expected structure. The assignments of the NMR spectra for [C₆bim][Br] are summarized in Table 4.4.

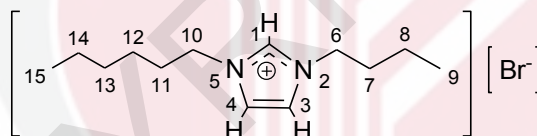


Table 4.4. ¹H and ¹³C NMR assignments of [C₆bim][Br].

Pos.	¹ H (ppm)	¹³ C (ppm)
1	10.19 (s, 1H)	136.6
2, 5	-	-
3	7.51 (s, 1H)	122.4
4	7.47 (s, 1H)	122.3
6, 10	4.24 (t, 4H) ³ J _{HH} = 7.3 Hz	49.9, 49.7
7, 8	1.74–1.80 (m, 4H)	31.0, 32.2
9	0.81 (t, 3H) ³ J _{HH} = 7.0 Hz	13.9
11, 12	1.19–1.27 (m, 4H)	25.8, 30.2
13, 14	1.12–1.17 (m, 4H)	19.4, 22.3
15	0.71 (t, 3H) ³ J _{HH} = 7.0 Hz	13.4

4.1.2.4 1-octyl-3-butylimidazolium bromide ($[C_8bim][Br]$)

The 1H NMR spectra of $[C_8bim][Br]$ in σ - $CDCl_3$ is shown in Appendix D7. Two triplet signals at downfield region at 0.70 ppm and 0.80 ppm were attributed to the proton in the CH_3 groups located at the end of the alkyl chains. Each of these peaks was integrated containing three protons. Two set of multiplet signals at downfield region observed at 1.26–1.04 ppm integrated contain 12 protons and 1.80–1.73 ppm integrated contain 4 protons were assigned to the proton in CH_2 groups. Meanwhile one multiplet signal was observed at 4.25–4.18 ppm containing four protons which attributed to the peak $(N-CH_2)_2$. This was due to the protons adjacent to the nitrogen atom were deshielded and shifted upfield in the spectrum. There are three signal peaks containing one proton for each peak detected at the high upfield region. Two peaks were located at 7.45 ppm and 7.51 ppm and another at 10.13 ppm correspond to the protons on the imidazolium ring. The ^{13}C NMR spectrum is shown in Appendix D8. From the spectrum, 15 carbon peaks were observed, which are in agreement with the total number of carbon in the expected structure. The assignments of the NMR spectra for $[C_8bim][Br]$ are summarized in Table 4.5.

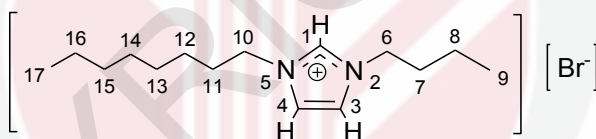


Table 4.5. 1H and ^{13}C NMR assignments of $[C_8bim][Br]$.

Pos.	1H (ppm)	^{13}C (ppm)
1	10.13 (s, 1H)	136.5
2, 5	-	-
3	7.51 (s, 1H)	122.4
4	7.45 (s, 1H)	122.3
6, 10	4.25–4.18 (m, 4H)	49.5, 49.8
7, 8	1.80–1.73 (m, 4H)	29.3, 31.7
9	0.80 (t, 3H) $^3J_{HH} = 7.0$ Hz	14.0
11-16	1.26–1.04 (m, 12H)	19.3, 22.5, 26.1, 28.9, 29.1, 29.2
17	0.70 (t, 3H) $^3J_{HH} = 7.0$ Hz	13.3

4.1.2.5 1-decyl-3-butylimidazolium bromide ([C₁₀bim][Br])

The ¹H NMR spectra of [C₁₀bim][Br] in *σ*-CDCl₃ is shown in Appendix D9. Two triplet signals at downfield region at 0.58 ppm and 0.68 ppm were attributed to the proton in the CH₃ groups located at the end of the alkyl chains. Each of these peaks was integrated containing three protons. Two set of multiplet signals at downfield region observed at 1.14–0.91 ppm integrated contain 16 protons and 1.68–1.62 ppm integrated contain 4 protons were assigned to the proton in CH₂ groups. Meanwhile one multiplet signal was observed at 4.14–4.08 ppm containing four protons which attributed to the peak (N-CH₂)₂. This was due to the protons adjacent to the nitrogen atom were deshielded and shifted upfield in the spectrum. There are three signal peaks containing one proton for each peak detected at the high upfield region. Two peaks were located at 7.40 ppm and 7.47 ppm and another at 10.06 ppm correspond to the protons on the imidazolium ring. The ¹³C NMR spectrum is shown in Appendix D10. From the spectrum, 17 carbon peaks were observed, which are in agreement with the total number of carbon in the expected structure. The assignments of the NMR spectra for [C₁₀bim][Br] are summarized in Table 4.6.

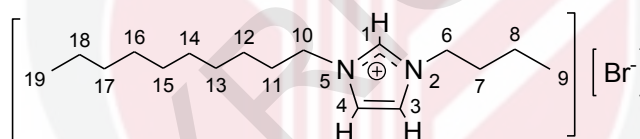


Table 4.6. ¹H and ¹³C NMR assignments of [C₁₀bim][Br].

Pos.	¹ H (ppm)	¹³ C (ppm)
1	10.06 (s, 1H)	136.4
2, 5	-	-
3	7.47 (s, 1H)	122.5
4	7.40 (s, 1H)	122.2
6, 10	4.14–4.08 (m, 4H)	49.5, 49.8
7, 8	1.68–1.62 (m, 4H)	31.6, 32.0
9	0.68 (t, 3H) ³ J _{HH} = 7.0 Hz	13.9
11-18	1.14–0.91 (m, 16H)	19.2, 22.4, 26.0, 28.8, 29.0, 29.2, 29.2, 30.2
19	0.58 (t, 3H) ³ J _{HH} = 7.0 Hz	13.3

4.1.2.6 1-dodecyl-3-butylimidazolium bromide ([C₁₂bim][Br])

The ¹H NMR spectra of [C₁₂bim][Br] in *σ*-CDCl₃ is shown in Appendix D11. Two triplet signals at downfield region at 0.71 ppm and 0.80 ppm were attributed to the proton in the CH₃ groups located at the end of the alkyl chains. Each of these peaks was integrated containing three protons. Two set of multiplet signals at downfield region observed at 1.26–1.02 ppm integrated contain 20 protons and 1.80–1.73 ppm integrated contain 4 protons were assigned to the proton in CH₂ groups. Meanwhile one multiplet signal was observed at 4.25–4.18 ppm containing four protons which attributed to the peak (N-CH₂)₂. This was due to the protons adjacent to the nitrogen atom were deshielded and shifted upfield in the spectrum. There are three signal peaks containing one proton for each peak detected at the high upfield region. Two peaks were located at 7.45 ppm and 7.53 ppm and another at 10.19 ppm correspond to the protons on the imidazolium ring. The ¹³C NMR spectrum is shown in Appendix D12. From the spectrum, 19 carbon peaks were observed, which are in agreement with the total number of carbon in the expected structure. The assignments of the NMR spectra for [C₁₂bim][Br] are summarized in Table 4.7.

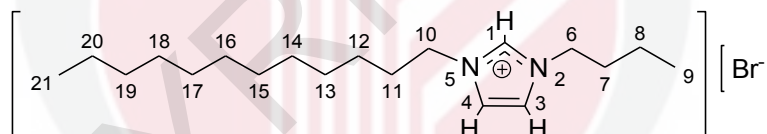


Table 4.7. ¹H and ¹³C NMR assignments of [C₁₂bim][Br].

Pos.	¹ H (ppm)	¹³ C (ppm)
1	10.19 (s, 1H)	136.7
2	-	-
3	7.53 (s, 1H)	122.5
4	7.45 (s, 1H)	122.3
5	-	-
6, 10	4.25–4.18 (m, 4H)	49.7, 50.0
7–8	1.80–1.73 (m, 4H)	31.8, 32.1
9	0.80 (t, 3H) ³ J _{HH} = 7.0 Hz	14.1
11–20	1.26–1.02 (m, 20H)	19.4, 22.6, 26.2, 28.9, 29.2, 29.3, 29.4, 29.5, 29.6, 30.3
21	0.71 (t, 3H) ³ J _{HH} = 7.0 Hz	13.4

4.1.3 Physico-Chemical Properties

4.1.3.1 Elemental Analysis (CHN) Studies

As summarized in Table 4.8, the quantitative results of each element in ILs except for bromine atom were in a good agreement with the theoretical calculations. In average, the percentage of deviations found was about $\pm 1.0\%$. This might be due to some impurities present in ILs, mostly because of the water content. Generally, ILs (either hydrophilic or hydrophobic) are well known hygroscopic compounds, which implies that they can easily absorb moisture from an open atmosphere.

Table 4.8. Quantitative analysis of carbon, hydrogen and nitrogen in $[C_n\text{bim}][\text{Br}]$ ILs compared with calculated theoretical values (shown in bracket).

Entry	ILs	Percentage of element (%)		
		Carbon	Hydrogen	Nitrogen
1	$[C_2\text{bim}][\text{Br}]$	45.74 (46.36)	8.12 (7.35)	11.65 (12.02)
2	$[C_4\text{bim}][\text{Br}]$	49.72 (50.58)	9.02 (8.10)	10.03 (10.72)
3	$[C_6\text{bim}][\text{Br}]$	52.81 (53.98)	9.43 (8.71)	9.12 (9.68)
4	$[C_8\text{bim}][\text{Br}]$	56.21 (56.78)	9.47 (9.21)	8.74 (8.83)
5	$[C_{10}\text{bim}][\text{Br}]$	58.77 (59.12)	9.85 (9.63)	7.97 (8.11)
6	$[C_{12}\text{bim}][\text{Br}]$	60.80 (61.11)	10.28 (9.99)	7.06 (7.50)

The percentage of hydrogen for three hydrophilic $[C_n\text{bim}][\text{Br}]$ ILs (Table 4.8, entry 1–3) were increased between 0.5–1.0%, while for hydrophobic (Table 4.8, entry 4–6), the slight increment below 0.3% was observed in comparison to the theoretical/calculated values, respectively. The elemental analysis results indicated that these new ILs, contained a small amount of water. This was also confirmed by ^1H NMR spectra (see Appendix D). From our previous studies, a few water molecules have been detected in the crystal structure of tetraethylammonium L-tartrate, another type of ILs and formed strong inter-hydrogen bonding with the structure of this salt (Abdul Rahman *et al.*, 2008). This shows that small amount of water molecules exists even in dried ILs and it is difficult to remove.

4.1.3.2 Thermal Analysis

The properties of each ILs including their thermal stability, studied by the TGA, are summarized in Table 4.9. The thermal stability of ILs is defined by the strength of their heteroatom-carbon and heteroatom-hydrogen bonds (Anouti *et al.*, 2008). The results indicated that the ILs salts have higher thermal stability at above 270°C with [C₂bim][Br] showing the highest stability with the decomposition temperature (T_{onset}) of 286°C. This was followed by [C₄bim][Br] and [C₆bim][Br] with a little variation on the T_{onset} at 281°C and 278°C, respectively. When the alkyl chain length is longer, the T_{onset} slightly decreased with the lowest decomposition temperature was observed for [C₁₂bim][Br]. It clearly demonstrates that the decomposition temperature follows the trend in which the weight loss decreases with an increase in number of the carbon chains.

Table 4.9. Physico-chemical properties of [C_nbim][Br] ILs.

Entry	ILs	ρ (kg m ⁻³)	η (mPa·s)	T_{onset} (°C)
1	[C ₂ bim][Br]	1.248	199	286
2	[C ₄ bim][Br]	1.190	1052	281
3	[C ₆ bim][Br]	1.143	1180	278
4	[C ₈ bim][Br]	nd	nd	277
5	[C ₁₀ bim][Br]	nd	nd	275
6	[C ₁₂ bim][Br]	nd	nd	274

nd = not detected because these ILs appear as semi solid at room temperature

The T_{onset} which is the temperature for decomposition was determined from the beginning of the experiment and the tangent of the weight versus temperature as shown in Figure 4.2. As can be seen, the entire thermograms exhibit single thermal curve with weight loss of almost 95% indicating that ILs decompose in one step. This behavior is similar to that reported previously for 1,3-dialkylimidazolium where a single temperature mass loss event was observed (Gordon *et al.*, 1998). However, the first drop, which was below 5% in weight, stopped at lower than 100°C. This may be due to the evaporation of the moisture adsorbed by these ILs.

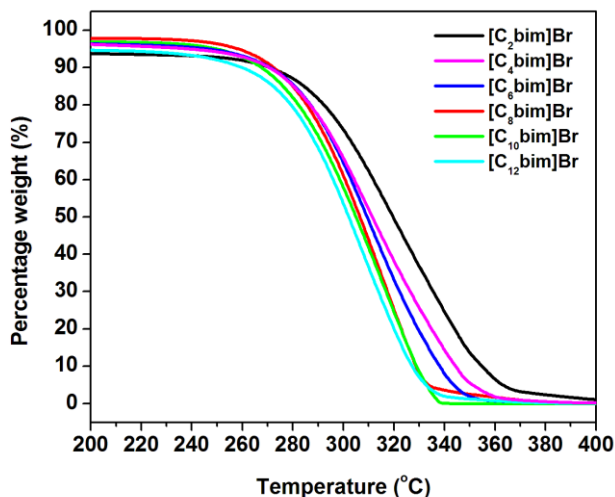
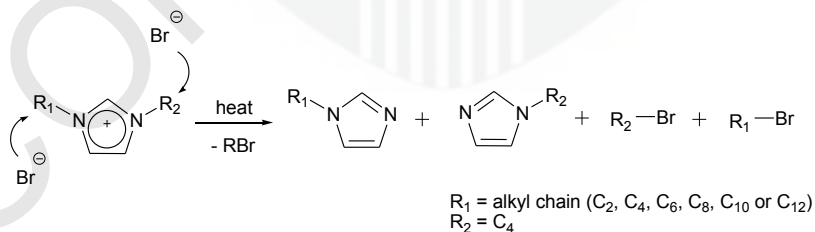


Figure 4.2. Thermograms of $[C_n \text{bim}][\text{Br}]$ ILs detected by TGA.

However, the differences in the cation size from $[C_2 \text{bim}]^+$ to $[C_{12} \text{bim}]^+$ does not produce a significant effect on the thermal stability of the $[C_n \text{bim}][\text{Br}]$ ILs. Decreasing in thermal stability can be explained by the pyrolysis of the alkylimidazolium either proceeding via S_N1 or S_N2 , depending on the basicity and/or nucleophilicity of the anions (Awad *et al.*, 2004; Fox *et al.*, 2003). Awad *et al.* (2004) reported that the pyrolysis reaction, also known as the thermochemical decomposition of organic compounds, went through S_N2 mechanism in the presence of nucleophilic halide ions, as shown in Scheme 4.2.



Scheme 4.2. Pyrolysis of alkylimidazolium with different alkyl chains length attached to nitrogen atoms via S_N2 mechanism in the presence of nucleophilic bromide (Source: Awad *et al.*, 2004).

4.1.3.3 Density

Table 4.9 (page 69) tabulated the density of $[C_n\text{bim}][\text{Br}]$ ILs at 25°C. It was observed that $[C_2\text{bim}][\text{Br}]$ has the highest density at 1.248 kg m⁻³ followed by $[C_4\text{bim}][\text{Br}]$ and $[C_6\text{bim}][\text{Br}]$ with the density of 1.190 and 1.143 kg m⁻³, respectively. The density of these ILs was relatively lower than other alkyimidazolium-based ILs and comparable with the other organic solvents. The densities for other ILs were not determined because they appeared as a semi solid at room temperature. From the data obtained, it clearly shows that the density of ILs significantly decreases with increasing the number of alkyl chain lengths, corroborated with Pereiro *et al.* (2007) and Tokuda *et al.* (2005). Increasing the hydrocarbon atoms has resulted in the increase of the formula weight and has caused a subsequent decrease in the ILs concentration, following the general formula of density:

$$\rho = \frac{m}{v} \quad (4.1)$$

where ρ is density (kg m⁻³), m is mass (kg) and v is volume (m³). Furthermore, it was also found that addition of the non-polar methylene CH_2 groups in the chains of hydrocarbon has a small contribution in decreasing the density due to the fact that CH_2 is less dense in comparison to imidazolium ring. Apart from that, the increase of more non-polar over the polar groups of imidazole ring in the structure of ILs has also resulted in the reduction of the hydrophilicity properties of $[C_n\text{bim}][\text{Br}]$. In addition, simple bromide ion also has a significant influence on density. As reported by Huddleston *et al.* (2001), by comparing the $[C_4\text{mim}][\text{Cl}]$ with $[C_4\text{mim}][\text{PF}_6]$, they found that the halide ILs have a lower density compared to the larger size of $[\text{PF}_6]^-$ anion.

4.1.3.4 Viscosity

Ionic liquids are well known as very viscous like most common solvents. Since ILs are composed of only ions, the strong electrostatic interaction formed between cationic and anionic species gives rise to different characteristic properties such as high viscosity and high ionic conductivity, and it also distinguishes them from the common organic solvents. Generally, the viscosity of ILs at room temperature ranges from around 10 mPa·s to value in excess of 1000 mPa·s, depending on the structure of cations and anions.

Table 4.9 (see page 69) shows the viscosities of $[C_n\text{bim}][\text{Br}]$ ILs at 25°C. The order of increasing viscosity with respect to the cation is as follows: $[C_2\text{bim}][\text{Br}] < [C_4\text{bim}][\text{Br}] < [C_6\text{bim}][\text{Br}]$.

As expected, longer alkyl substituents attached to the imidazole ring produced more viscous ILs. It has been shown by Dzyuba and Bartsch, (2002) and Bonhôte *et al.* (1996) that the viscosity of the imidazolium-based ILs was influenced by the strength of their *van der Waals* interactions and their ability to form hydrogen bonds. It was suggested that increasing the number of alkyl chains led to increase the *van der Waals* forces and caused the increment of the viscosity. In addition, longer side chains reduce the rotational freedom of molecules, which thus leads to a higher viscosity, in agreement with the finding of Bonhôte *et al.* (1996). The higher viscosity of these salts can also be explained in terms of steric hindrance in which adding more CH_2 group to the cation strengthened the steric hindrance, thus resulted in the increase of the viscosity.

The geometry structure also influenced the viscosity as it was reported that the symmetric ion structures have caused high viscosity of ILs (MacFarlane *et al.*, 2006). In this study, $[C_4\text{bim}]^+$ cation has a symmetrical structure with both side chains containing four hydrocarbons, as illustrated in Figure 4.3. When carbon chains of 1-alkyl-3-butylimidazolium cation were increased from C_2 to C_6 , the viscosity of $[C_n\text{bim}][\text{Br}]$ greatly increased from 199 mPa·s (viscosity of $[C_2\text{bim}][\text{Br}]$) to 1052 mPa·s (viscosity of $[C_4\text{bim}][\text{Br}]$), while further increment of the alkyl chains has shown a small change in the viscosity (1180 mPa·s for $[C_6\text{bim}][\text{Br}]$). This shows that the effect of the cation symmetry is more obvious as compared to the alkyl chains lengths.

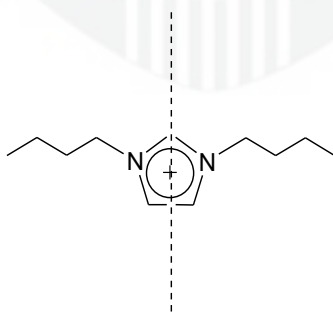


Figure 4.3. The geometry structure of $[C_4\text{bim}]^+$ cation. The dashed line shows the symmetrical point.

For example, the viscosity of the commercial ILs $[C_n\text{mim}][\text{BF}_4]$ (where $n = 2, 4, 6$) has gradually increased with the increase of the alkyl chains with the viscosity of 43, 91.4 and 177 mPa·s respectively (Seddon *et al.*, 2000). The effect of the different shear rates on the viscosity was also studied. It was found that these $[C_n\text{bim}][\text{Br}]$ ILs can be classified as the Newtonian fluid whose viscosity remained constant with increasing shear rates. This finding is parallel with the previously reported experiment which indicated that shear rates did not make any differences in the viscosity of $[C_n\text{mim}][\text{BF}_4]$ with $n = 4, 6$ and 8 alkyl chains (Seddon *et al.*, 2000).

4.2 Biophysical Properties of DNA in Ionic Liquids

4.2.1 Ionic liquid-DNA Binding

When a particular molecule binds to DNA, it is subjected to a change in the local microenvironment from being completely solvated in aqueous solution to being in the hydrophobic environment of the DNA grooves and base stack. The changes in the local microenvironment can be monitored by perturbations that occur in the UV-visible as well as the fluorescence emission when the binding event takes place. The excited state fluorescence emission spectra (both intensity and wavelength) are sensitive to the microenvironment of ions or molecules. Generally, the emission intensity of certain molecules such as ligands will increase upon the addition of DNA. The increase in the emission intensity demonstrates that molecules have an ability to bind with DNA.

The fluorescence emission enhancement during the binding of $[C_n\text{bim}][\text{Br}]$ ILs into Calf thymus DNA was illustrated in luminescence experiments. As shown in Figure 4.4, the emission intensity of $[C_4\text{bim}][\text{Br}]$ increased when DNA was added, indicating that a binding process took place between $[C_4\text{bim}][\text{Br}]$ and DNA. A similar pattern in the increase of the emission intensity was also observed during the titration of the same DNA into a solution of $[C_2\text{bim}][\text{Br}]$ and $[C_6\text{bim}][\text{Br}]$ respectively, as shown in Appendix E1 and E2.

During the addition of Calf thymus DNA, the positively charged imidazole ring of $[C_n\text{bim}]^+$ cations were positioned to interact with the negative charges of the DNA phosphate groups. Thus, the cationic-anionic attraction which is also known as electrostatic attraction was formed mostly on the DNA surface because the DNA phosphate groups were located at the backbone of DNA. This

interaction was clearly observed as evidence from ^{31}P NMR spectrum, reported by Ding *et al.* (2010) and Wang *et al.* (2007a). This indicates that the binding mode is the electrostatic attraction between $[\text{C}_n\text{bim}]^+$ cations and DNA phosphate groups.

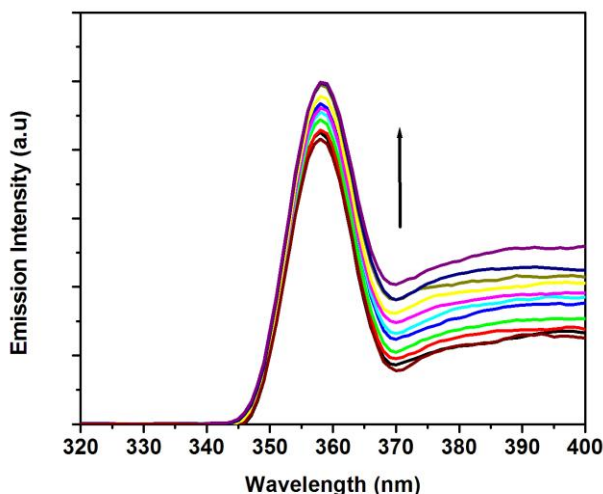


Figure 4.4. Fluorescence emission spectra of $[\text{C}_4\text{bim}][\text{Br}]$ in the absence (bottom curve) and presence of Calf thymus DNA in aqueous solution of deionized water. The arrow indicates that the emission intensity of $[\text{C}_4\text{bim}][\text{Br}]$ increases with the addition of DNA. Excitation wavelength for $[\text{C}_4\text{bim}][\text{Br}]$ was set at 320 nm.

However, as reported by Pullman and Pullman (1981), the negative charge of DNA phosphate groups can also be found in grooves in which the charge is greater in the A-T minor groove rather than in the major groove. It is believed that $[\text{C}_n\text{bim}]^+$ molecules also can enter both grooves and form non-covalent interaction to the DNA phosphate groups inside of the grooves. During the addition of DNA into $[\text{C}_4\text{bim}][\text{Br}]$ solution, the $[\text{C}_4\text{bim}]^+$ cations do not only bind to DNA phosphate groups, but also form interaction with the bases of DNA in the major and minor grooves. These bases in grooves serve as a protector for nitrogen atom in the ring of $[\text{C}_n\text{bim}]^+$ from bulk water molecules, by forming hydrogen bonds with the nitrogen.

The increases in the emission intensity of $[C_n\text{bim}][\text{Br}]$ ILs with the addition of calf thymus DNA can be explained based on the fluorescence resonance energy transfer (FRET). FRET refers to the energy transfer from a donor molecule to an acceptor molecule. The $[C_n\text{bim}][\text{Br}]$ ILs are considered as donor molecules that initially absorb the energy and DNA is acceptor to which the energy is transferred from the ILs molecules. This resulting IL-DNA that interacts in such manner is often referred to as donor-acceptor pair. When ILs were excited without the presence of DNA, its electrons jump from the ground state (S_0) to a higher vibrational level. Then, very rapidly these electrons decay to the lowest vibrational levels (S_1) and eventually decay back to the S_0 state and a photon of light is emitted. Upon excitation of the $[C_4\text{bim}][\text{Br}]$ in the presence of DNA, the photon is not emitted, but rather the energy is transferred via dipole-dipole interaction to the DNA molecule, whose electrons in turn become excited. Thus, the DNA emits light provided that the IL molecules especially the cation is bound to the DNA *via* electrostatic attraction and hydrogen bonds, which causes an enhancement in the emission intensity (Friedman *et al.*, 1990).

When a particular molecule associates either in the major or minor groove of DNA, it is said to be a groove-binding agent. The DNA bases can be accessed through both grooves because there are many hydrogen bond recognition sites of A-T and C-G base pairs that are accessible as illustrated in Figure 4.5. The A-T base pairs include the adenine N-7 and thymine C-4 carbonyl as hydrogen bond acceptors, meanwhile adenine C-6 amine act as a hydrogen bond donor and the thymine methyl group as a stabilizer for *van der Waals* interactions. For C-G base pair, guanine N-7 and the guanine C-6 carbonyl can function as hydrogen bond acceptors and the cytosine C-4 amine can act as a hydrogen bond donor. Hence, the cation molecules inside the grooves, especially the polar imidazole ring can form non-covalent complexes with DNA. The cations-DNA binding form *van der Waals* connections with the grooves and hydrogen bonding interaction between polar protons in the imidazole ring and the acceptor groups of the DNA bases.

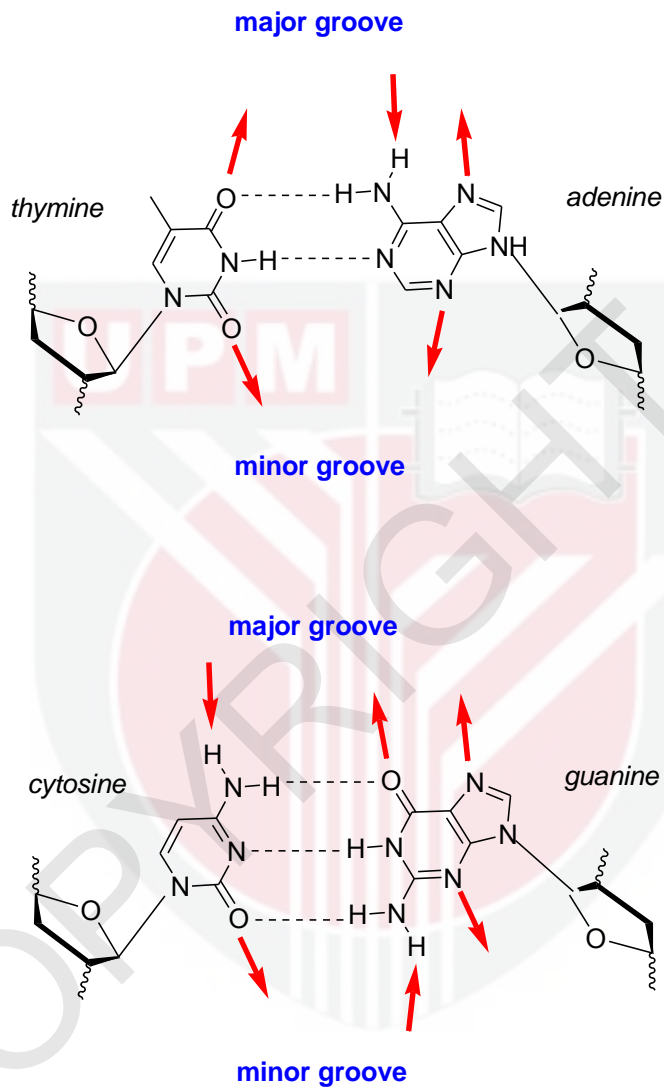


Figure 4.5. Hydrogen bond recognition sites accessible from the DNA major and minor grooves. Arrow outside the major and minor grooves represent the hydrogen bond receptors while arrow inside represents hydrogen bond donors.

Most of the ligands, molecules and/or ions can interact with DNA in three primary ways, namely electrostatic, intercalation and/or major or minor groove binding. During the binding process of $[C_n\text{bim}]$ -DNA, hypsochromic and bathochromic shifts which are a change of a spectral band positioned in the emission spectrum to a shorter and longer wavelength were not observed. In particular, large hypsochromic or bathochromic effects are the result of intercalation of molecules into DNA grooves (Sinha *et al.*, 2006). This indicates that intercalation is not the other binding mode for $[C_n\text{bim}]$ -DNA.

Based on the fluorescence emission results, it was proposed that groove binding is the second binding mode involved in the complexes of $[C_n\text{bim}]$ -DNA system, in addition to the electrostatic attraction. By examining the structure of a particular $[C_n\text{bim}]^+$, these cations can enter and fit into the grooves easily without altering the duplex major and minor grooves as well as the whole DNA structure. The edges of the DNA bases are exposed to these grooves and provide sites at which small molecules like alkylimidazolium can interact with DNA.

Most of the minor groove binders have shown an enhanced preference for A-T rich regions of DNA. Since Calf thymus DNA contains 41.9% mole C-G and 58.1% mole A-T pairs, it can be predicted that the $[C_n\text{bim}]^+$ molecules prefer to bind through the minor groove rather than major groove. This has also contributed to the steric of the C-2 amine of guanine above the floor of the minor groove along with the narrower groove in A-T rich regions, helping to maximize the hydrophobic and *van der Waals* contacts between the $[C_n\text{bim}]^+$ molecule and the groove walls (Berman, 1994).

4.2.2 Effect of Hydrocarbon Length of Ionic Liquids

The fluorescence emission spectra of EB-bound DNA quenched by three different alkyl chain lengths of $[C_n\text{bim}][\text{Br}]$ ILs were recorded. Ethidium bromide is a well-known classical intercalator. The planar ring system of EB stacks with DNA base pairs during intercalation process and forms intercalation complex with DNA. As depicted in Figure 4.6, the EB emission maxima exhibited an increase in emission intensity and hypsochromic change (shift to shorter wavelength) in λ_{max} from 618 nm to 607 nm in the presence of Calf thymus DNA. This phenomenon was also observed by Garbett *et al.* (2004).

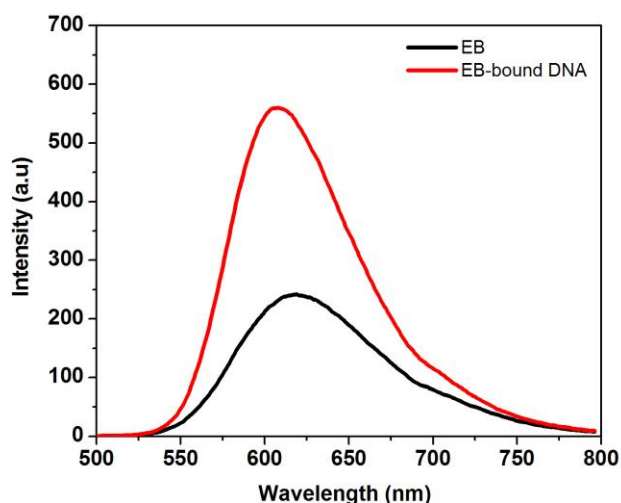


Figure 4.6. The fluorescence profile of EB exhibits both increased emission intensity and hypsochromic shift in the presence of Calf thymus DNA. Excitation wavelength of EB was set at 510 nm.

A large EB emission enhancement of almost 3 times is a clear indication of a strong intercalation because the hydrophobic microenvironment found between the base pairs protects the EB probe from water molecules and molecular oxygen that may decrease its fluorescence emission (Rodríguez-Pulido *et al.*, 2008). Considering the substantial sensitivity of photo physical properties of EB towards DNA, the present intercalator probe may be used to gain more information about the interaction properties between $[C_n\text{bim}][\text{Br}]$ ILs and DNA. Any small alterations in the DNA structure owing to its interaction with these ILs will affect the microenvironment of the EB-bound DNA and lead to a large modulation in its photophysical behavior. Therefore, in order to understand the interaction between various $[C_n\text{bim}][\text{Br}]$ ILs and DNA, fluorescence displacement studies on EB-bound DNA solution in the presence of $[C_n\text{bim}][\text{Br}]$ ILs were carried out.

The emission spectra of EB-bound DNA complex in different concentrations of $[C_n\text{bim}][\text{Br}]$ ILs was illustrated in Figure 4.7. The emission intensity of EB-bound DNA complex has decreased continuously with increasing the concentration of $[C_2\text{bim}][\text{Br}]$ (Figure 4.7A). It has also been observed that the emission spectra of EB-

bound DNA spontaneously shifted towards a longer wavelength with the further addition of $[C_2\text{bim}][\text{Br}]$. The results clearly indicate that the EB probe was released gradually from DNA to the bulk water phase due to the addition of $[C_2\text{bim}][\text{Br}]$ to the EB-bound DNA solution. Like $[C_2\text{bim}][\text{Br}]$, the emission intensity of EB-bound DNA solution was also observed to decrease with the addition of $[C_4\text{bim}][\text{Br}]$ and $[C_6\text{bim}][\text{Br}]$ as shown in Figure 4.7B and Figure 4.7C, respectively.

The decreased in emission intensity of EB-bound DNA upon the addition of $[C_n\text{bim}]\text{Br}$ ILs may arise from the exclusion of EB from the DNA base pair microenvironment toward the aqueous solution. During the addition of $[C_n\text{bim}][\text{Br}]$ ILs, the positive charge of $[C_n\text{bim}]^+$ cation molecules form electrostatic attraction with the negative charge located at the DNA phosphate groups on the surface, as well as inside of the grooves. Further addition of ILs into EB-bound DNA solution will form stronger electrostatic attraction, thus lead to the transformation of DNA conformation into compact structure. The resulting DNA compact structure left insufficient space for the EB probe and gradually released free EB from DNA.

The decreased in emission intensity indicated that there are many free EBs than EB-bound DNA in the aqueous solution. This observation also indicated that the electrostatic attraction between $[C_n\text{bim}]^+$ and DNA phosphate groups was adequately strong. This finding is similar to what has been observed by Ding *et al.* (2010). They found that when DNA is condensed or compacted by small molecule, the fluorescence intensity of the EB decreases indicated that the intercalation of EB probe is prevented. Cheng *et al.* (2007) also reported that the transformation of DNA conformation along with a decrease of base-pair interstice prohibits the intercalation of ethidium into the DNA structure. However, the resulting compacted DNA structure by ILs was able to retain the double-helical conformation, which was verified by the CD results as discussed in Section 4.2.3.2 (page 84).

The continuous decrease in the intensity and the red shift of emission peak of EB-bound DNA with addition of $[C_n\text{bim}][\text{Br}]$ ILs also show that the release of EB probe was also driven by the hydrophobic interactions between the hydrocarbon chains of $[C_n\text{bim}]^+$ cations and DNA bases (Rodríguez-Pulido *et al.*, 2008; Bhattacharya and Mandal, 1997). Comparing Figure 4.7A, 4.7B and 4.7C, it show that the emission intensity of the EB at the λ_{max} in addition of 2.0 M of $[C_6\text{bim}][\text{Br}]$ was 250.29, which was lower than that observed in $[C_4\text{bim}][\text{Br}]$ (emission intensity of 255.65) and $[C_2\text{bim}][\text{Br}]$ (emission intensity of 302.87).

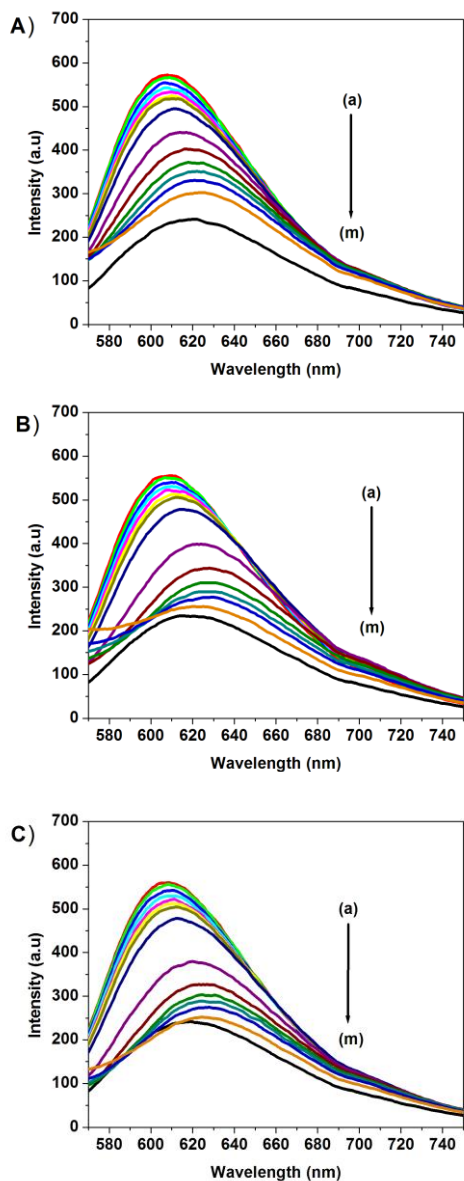


Figure 4.7. Fluorescence emission spectra of EB-bound DNA complex in the presence of different concentration of ILs: (a) 2.5×10^{-3} M, (b) 5.0×10^{-3} M, (c) 7.5×10^{-3} M, (d) 1.0×10^{-2} M, (e) 1.25×10^{-2} M, (f) 1.5×10^{-2} M, (g) 2.5×10^{-2} M, (h) 5.0×10^{-1} M, (i) 7.5×10^{-1} M, (j) 1.0 M, (k) 1.25 M, (l) 1.5 M and (m) 2.0 M. The arrow shows the decreased emission intensity of EB-bound DNA upon the addition of (A) $[C_2bim][Br]$; (B) $[C_4bim][Br]$ and (C) $[C_6bim][Br]$. Excitation wavelength of EB was set at 510 nm.

This reveals that the different length of linear alkyl chains in the structure of $[C_n\text{bim}][\text{Br}]$ ILs have their own capability to release EB from DNA. At the same concentration of 2.0 M, $[C_6\text{bim}][\text{Br}]$ released more EB molecules from EB-bound DNA complex compared to the two other ILs. Figure 4.8 represents the normalized emission intensity for the variation in the emission intensity of EB-bound DNA solution against various concentrations of $[C_n\text{bim}][\text{Br}]$ ILs. It is obvious that the pattern of decreasing the intensity of EB-bound DNA solution with the continuous addition of different $[C_n\text{bim}][\text{Br}]$ ILs was observed.

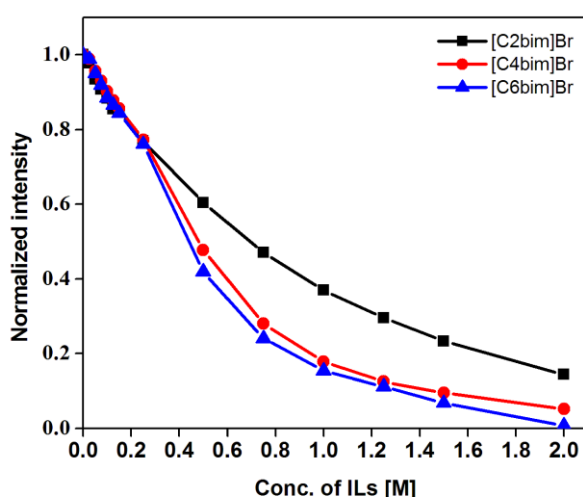


Figure 4.8. Normalized emission intensity of EB-bound DNA complex with the continuous addition of different concentration of $[C_n\text{bim}][\text{Br}]$ ILs. The excitation wavelength of EB was set at 510 nm while the emission intensity was observed at λ_{max} 618 nm.

At concentration of $[C_n\text{bim}][\text{Br}]$ ILs below 0.25 M, the observed emission intensity of EB-bound DNA at λ_{max} 618 nm in three of these ILs were almost similar. This implies that the hydrocarbon chains of $[C_n\text{bim}]^+$ cations did not play any role in releasing EB from the EB-bound DNA complexes. This suggests that at low concentrations, the release of EB from EB-bound DNA is mainly due to the electrostatic attraction between $[C_n\text{bim}]^+$ and phosphate groups of DNA. When the concentration of $[C_n\text{bim}][\text{Br}]$ was further increased above 0.25 M, the hydrocarbon chains showed a

significant contribution. At 2.0 M of $[C_n\text{bim}][\text{Br}]$ solution, the observed emission intensity of EB-bound DNA solution was reduced by 99.3% from the initial emission intensity in the presence of $[C_6\text{bim}][\text{Br}]$, whereas a reduction of 94.82% and 85.65% was observed in the solution of $[C_4\text{bim}][\text{Br}]$ and $[C_2\text{bim}][\text{Br}]$, respectively.

There was a substantial difference in decreasing emission intensity of EB-bound DNA by $[C_2\text{bim}][\text{Br}]$ in comparison to $[C_4\text{bim}][\text{Br}]$, but it was found to be relatively small when comparing $[C_4\text{bim}][\text{Br}]$ with $[C_6\text{bim}][\text{Br}]$. This shows that the binding of $[C_6\text{bim}][\text{Br}]$ with Calf thymus DNA was slightly stronger than $[C_4\text{bim}][\text{Br}]$, and much stronger than $[C_2\text{bim}][\text{Br}]$. The stronger interaction of $[C_6\text{bim}][\text{Br}]$ with Calf thymus DNA could be explained in terms of alkyl chain lengths attached to the imidazolium cations.

Due to longer alkyl chains, there are more hydrophobic groups in $[C_6\text{bim}][\text{Br}]$. Such hydrophobic interactions cause a stronger DNA condensation in $[C_6\text{bim}][\text{Br}]$ followed by $[C_4\text{bim}][\text{Br}]$ and $[C_2\text{bim}][\text{Br}]$ ILs. This condensation yields a very compact structure of an EB-bound DNA, thus disrupting the controlling forces responsible for non-covalent binding (Barreleiro and Lindman, 2003). The fluorescence displacement result clearly indicated that although the electrostatic attraction was the major interaction, the strong hydrophobic interactions between the alkyl chains of $[C_n\text{bim}]^+$ and the DNA bases also provided a significant contribution for the IL-DNA binding.

4.2.3 Structural Stability of DNA

4.2.3.1 DNA in Aqueous Solution

The stability of double-helix Calf thymus DNA is best analyzed using circular dichroism (CD) spectroscopy. From the CD spectra, the secondary structure of Calf thymus can be detected. The secondary structure of DNA in deionized water at selected temperatures was first measured as shown in Figure 4.9. The characteristic positive band at around 278 nm corresponding to π - π base packing and a shortwave negative band at almost 248 nm corresponding to helicity were presented for DNA in deionized water at different temperatures. Both positive and negative bands confirmed the presence of a helical structure of B-DNA (Cao *et al.*, 2008).

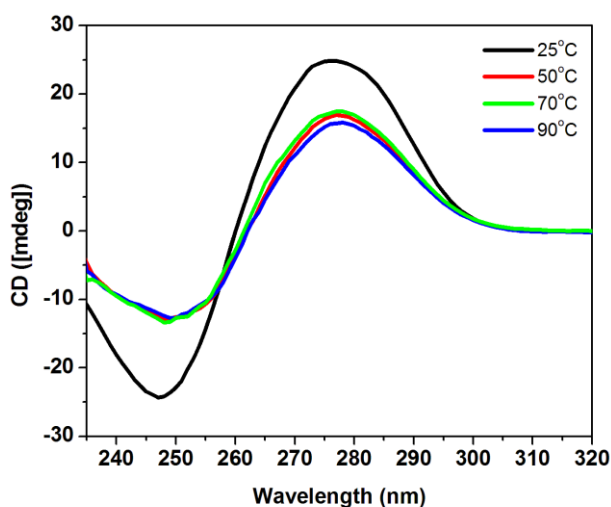


Figure 4.9. Circular dichroism spectra of Calf thymus DNA (300 μM) in deionized water at different temperatures.

However, the observed DNA spectra at 25°C was different from the DNA spectra detected at temperature 50°C, 70°C and 90°C. As illustrated, the peak of Calf thymus DNA at 50°C shows that the magnitude of positive band was greatly decreased and the magnitude of negative band was largely increased, almost $\sim\pm 10$ mdeg, in comparison to the spectrum of DNA at 25°C. When the DNA was exposed at high temperatures of 70°C and 90°C, a comparable spectrum like a spectrum of DNA at 50°C was observed, with the magnitude of both positive and negative bands remaining almost unchanged.

The result shows that the CD spectra of the high molecular weight natural Calf thymus DNA in aqueous system at 25°C clearly suggest the B-form double helical DNA conformation. This indicated that the DNA was able to maintain its native structure at 25°C, matching the results found by Vijayaraghavan *et al.* (2010a). They reported that DNA from Salmon testes dissolved in aqueous solution without any buffer solution was found to be stable for a short period (1 week) at 25°C. Therefore, the Calf thymus DNA in deionized water at 25°C was used as a control throughout this experiment.

When DNA molecule undergoes denaturation transition, the double-helix structure transforms into a single-stranded molecule or open coil (Hammouda, 2009). Thus, it can be said that denature transition occurred when the Calf thymus DNA solution was heated at 50, 70 and 90°C. The huge decrease in the magnitude of the positive band and the huge increase in the magnitude of the negative band both confirmed the characteristics of the single-stranded DNA (Johnson, 2000). In order to further strengthen the CD spectra result, UV-absorbance of Calf thymus DNA was also measured during the heating process, as shown in Figure 4.10. It clearly shows that the absorbance of Calf thymus DNA increased with increasing temperature due to unstacking of the nucleotide DNA bases when presented with the formation of single-stranded DNA in the aqueous solution at 50°C, 70°C and 90°C.

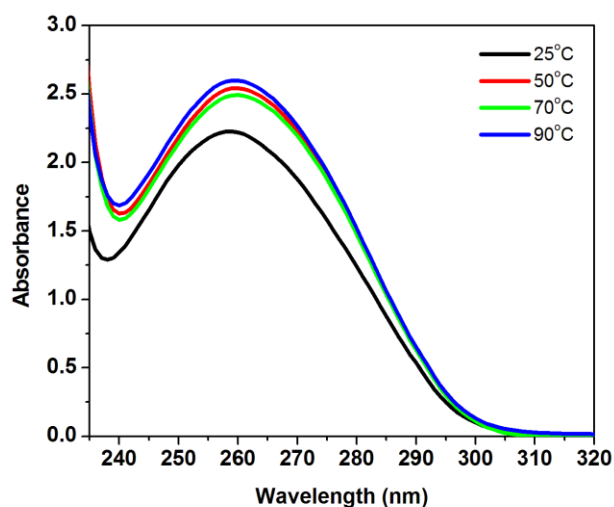


Figure 4.10. UV-absorbance spectra of Calf thymus DNA (300 μ M) in deionized water at different temperatures.

4.2.3.2 DNA in Ionic Liquids

The effects of ILs on the binding process and the stability of Calf thymus DNA are our main focus. The spectra of DNA in the presence of different percentages of $[C_n\text{bim}][\text{Br}]$ ILs in aqueous solution (12.5%, 25.0%, 37.5%, 50.0% and 75.0% w/w) at 25°C were also detected using circular dichroism. As shown in Figure 4.11, the characteristic positive band at around 278 nm corresponding to π - π base packing and a shortwave, negative band at 243 nm corresponding to helicity were also present in all

systems. The CD spectra of DNA in different percentages of $[C_4bim][Br]$ solution shows a shape almost similar to that of DNA in deionized water at 25°C. This indicated that the duplex B-conformation of Calf thymus DNA retains its structure in hydrated $[C_4bim][Br]$, despite high salt concentration up to 75%.

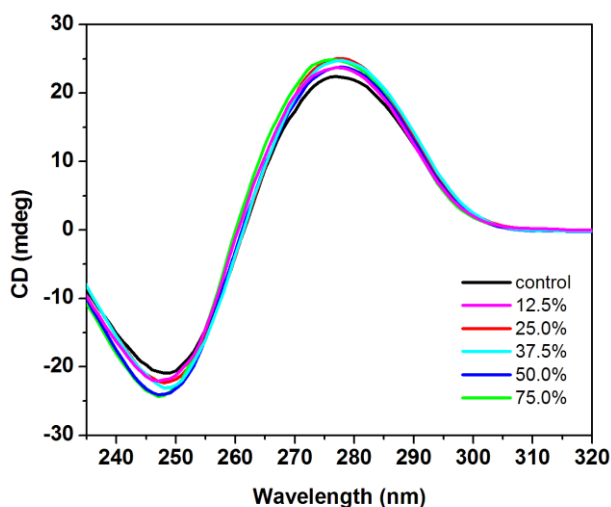


Figure 4.11. Circular dichroism spectra of Calf thymus DNA (300 μ M) in deionized water and in different percentages of hydrated $[C_4bim][Br]$ at 25°C. Control was Calf thymus DNA (300 μ M) in aqueous solution at 25°C.

Upon the addition of $[C_4bim][Br]$, the magnitude of positive and negative bands of Calf thymus DNA were slightly increased and decreased, respectively. It was observed that the magnitude of negative band slightly decreased with increasing salt concentration follow the order of 12.5% < 25.0% < 37.5% < 50.0% < 75.0%. Increasing concentration of ILs will increase the number of $[C_4bim][Br]$ molecules in the solution and thus increase the population of $[C_4bim]^+$ cations on the DNA phosphate groups. This has resulted in increasing electrostatic interaction between the $[C_4bim]^+$ and the DNA phosphate groups, as well as the hydrophobic interaction between the DNA bases and hydrocarbon chains of $[C_4bim]^+$ cations. The CD spectrum results were also supported by the absorbance evidence of the DNA at different temperatures, as depicted in Figure 4.12.

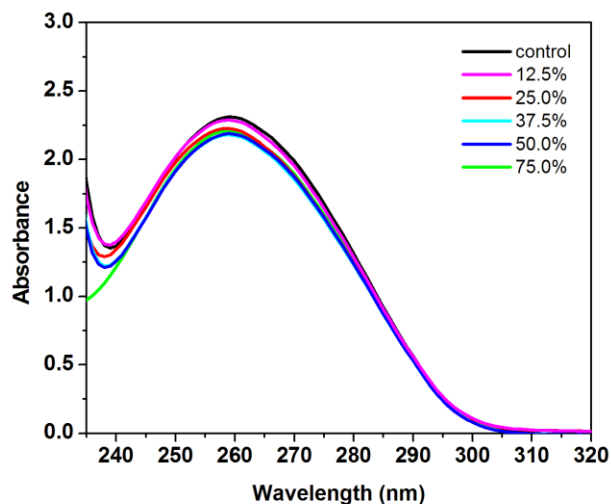


Figure 4.12. Absorbance of Calf thymus DNA (300 μM) in deionized water (control, black line) and in different percentages of hydrated $[\text{C}_4\text{bim}][\text{Br}]$ at 25°C. Control was calf thymus DNA (300 μM) in aqueous solution at 25°C.

It was observed that the absorbance of DNA did not increase with increasing concentration of $[\text{C}_4\text{bim}][\text{Br}]$. This confirmed that Calf thymus DNA did not undergo a denature transition and maintained its native structure in the $[\text{C}_4\text{bim}][\text{Br}]$ solution. Interestingly, the observed absorbance of DNA slightly decreased with increasing percentage of the salt. This may be due to the strong electrostatic attraction that could alter the base packing and helical structure of Calf thymus DNA, which could lead to a transition from the extended double helical structure to the more compact conformation known as the Ψ structure (Cao *et al.*, 2008). In fact, the compact helical structure usually decreases the absorbance of DNA.

In addition to electrostatic attraction, hydrophobic interaction also caused a DNA condensation and yielding a compact structure (Barreleiro and Lindman, 2003). Referring back to the previous Figure 4.11 (page 85) the absence of any large induced signals in the CD spectra of DNA with the addition of $[\text{C}_4\text{bim}][\text{Br}]$ strengthen the fluorescence results presented earlier (Section 4.2.1, page 73) that $[\text{C}_n\text{bim}][\text{Br}]$ ILs are not intercalator. The intercalation usually greatly induces the magnitude of positive and negative bands of CD spectra of DNA (Jordan *et al.*, 1972).

According to the obtained results, it was concluded that ILs, especially those based on alkyimidazolium cations do not intercalate with the DNA bases but rather bind to DNA bases through groove binding and hydrophobic interactions. These bindings and major electrostatic attractions help to stabilize DNA and retain its duplex B-conformation in ILs. This explanation was also true for Calf thymus DNA in various percentages of $[C_2\text{bim}][\text{Br}]$ and $[C_6\text{bim}][\text{Br}]$ because the spectra observed was almost the same as the CD spectra of Calf thymus DNA in hydrated $[C_4\text{bim}][\text{Br}]$ as shown in Figure 4.11 and absorbance spectra in Figure 4.12.

The thermal stability of the duplex Calf thymus DNA ($300\ \mu\text{M}$) in the presence of 25% $[C_4\text{bim}][\text{Br}]$ in aqueous solution was observed at different temperatures as shown by CD spectrum in Figure 4.13. Interestingly, the spectrum of DNA at 25 and 50°C showed a similar shape with the controlled DNA spectra in deionized water at 25°C . At 50°C , the observed magnitude of negative band slightly increased about ~ 3.0 mdeg compared to the control DNA system, but the magnitude of positive band remained unchanged. Meanwhile, at 70°C and 90°C , the magnitude of both positive and negative bands were greatly induced, somewhat similar to a CD spectrum of DNA in aqueous solution at the same temperature as previously shown in Figure 4.9 (page 83).

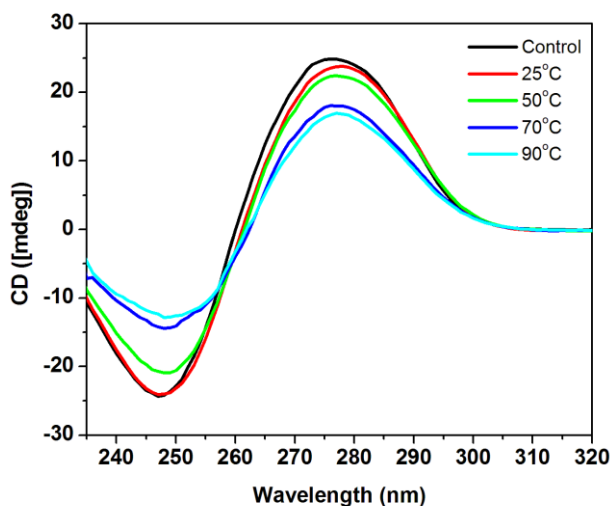


Figure 4.13. Circular dichroism spectra of Calf thymus DNA ($300\ \mu\text{M}$) in the presence of 25% $[C_4\text{bim}][\text{Br}]$ solution at different temperatures. Control DNA spectrum was Calf thymus DNA ($300\ \mu\text{M}$) in deionized water at 25°C .

Looking closely at the absorbance of DNA at λ_{\max} 260 nm as illustrated in Figure 4.14, it was found that small changes in absorbance was observed for DNA at 25°C and 50°C relative to the absorbance of Calf thymus DNA in deionized water at 25°C. However, a large increase in absorbance was detected for DNA at 70°C and 90°C, respectively. Based on the CD results and with the support of UV-absorbance spectra, it can be concluded that Calf thymus DNA retains its native-like B-conformation in 25% [C₄bim][Br] solution at 25°C and 50°C. While at high temperature of 70°C and 90°C, the double helical DNA structure was less stable and lost its double helical conformation. The similar results were also observed for Calf thymus DNA in hydrated [C₂bim][Br] and [C₆bim][Br] as shown in Appendix F1 and Appendix F2.

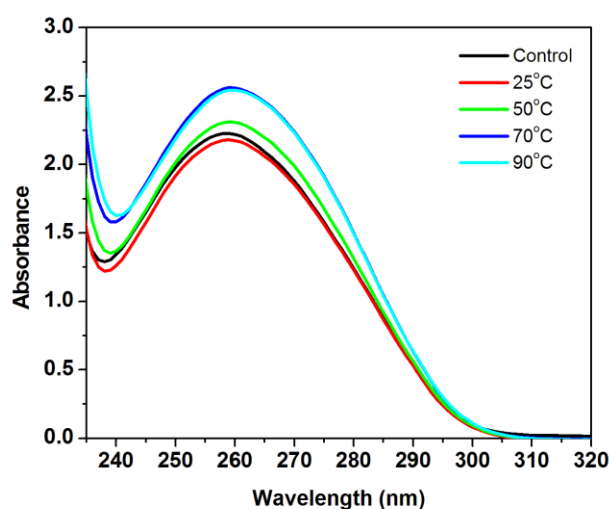


Figure 4.14. UV-absorbance spectra of Calf thymus DNA (300 μ M) in the presence of 25% [C₄bim][Br] solution at different temperatures.

4.2.4 Melting Temperature of DNA

In the previous section, the effect of alkyl chain length of [C_nbim][Br] ILs towards the thermal stability of Calf thymus DNA was observed by CD spectra. Although all of the three [C_nbim][Br] ILs were able to stabilize the duplex Calf thymus DNA conformation up to the temperature between 50°C and 70°C, effect of the length of alkyl chains [C_nbim][Br] ILs was not really clear. Therefore, to better

understand the effect of alkyl chain lengths of $[C_n\text{bim}][\text{Br}]$ ILs towards the thermal stability of DNA, the melting temperature of DNA in these ILs was detected. A number of publications have addressed the melting temperature of DNA in various non-aqueous and mixed solvents (Hammouda and Worcester, 2006; Bonner and Klibanov, 2000), but so far none has reported on the melting temperature of double helical DNA in ILs.

Based on UV absorbance, the melting temperature of Calf thymus DNA in the presence of $[C_n\text{bim}][\text{Br}]$ ILs was recorded as a function of temperature up to 90°C . As depicted in Figure 4.15, the shape of the sigmoidal curve shows a typical melting curve of DNA. This indicates the conformational transition from double-stranded into single-stranded DNA involving the unstacking of the DNA base pairs which increases absorbance at wavelength of 260 nm (A_{260}). As illustrated, the melting temperature of the duplex DNA constantly increases with increasing carbon chain of $[C_n\text{bim}][\text{Br}]$ ILs according to the following order $[C_2\text{bim}][\text{Br}]$ ($56.1 \pm 1.0^\circ\text{C}$) < $[C_4\text{bim}][\text{Br}]$ ($57.5 \pm 1.0^\circ\text{C}$) < $[C_6\text{bim}][\text{Br}]$ ($58.1 \pm 1.0^\circ\text{C}$). This trend was similar to the results obtained by Hammouda, (2009) showing that the melting temperature of DNA increases in the presence of long alkyl chain alcohols.

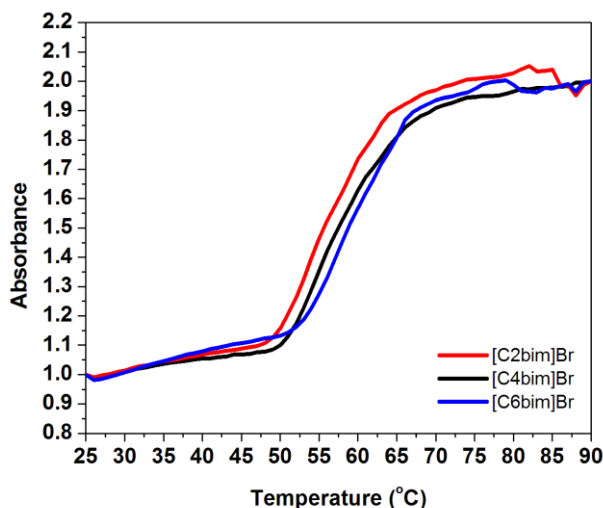


Figure 4.15. Effects of alkyl chain lengths of $[C_n\text{bim}][\text{Br}]$ ILs towards the thermal stability of Calf thymus DNA. The Calf thymus DNA ($60 \mu\text{M}$) was dissolved in 25% $[C_n\text{bim}][\text{Br}]$ ILs in aqueous solution.

The results have shown the importance of the length of alkyl chain in addition to the electrostatic interaction towards the thermal stability of Calf thymus DNA. It has been reported that the stability of double helical DNA is controlled by the ability of the solvent especially water molecules to cross the hydrophobic sugar-rich region (Hammouda, 2009). In the duplex DNA structure, DNA contains partly hydrophobic (sugar) and hydrophilic (phosphate backbone) regions (Figure 4.16). Both of the regions play important role in stabilizing the DNA conformation in a solution. Since water is well-known to hydrate the phosphate groups on the DNA surface and the amine bases inside of the helix structure, therefore, the DNA helical structure is formed in order to shield the hydrophobic groups from making contact with water molecules (Hammouda, 2009).

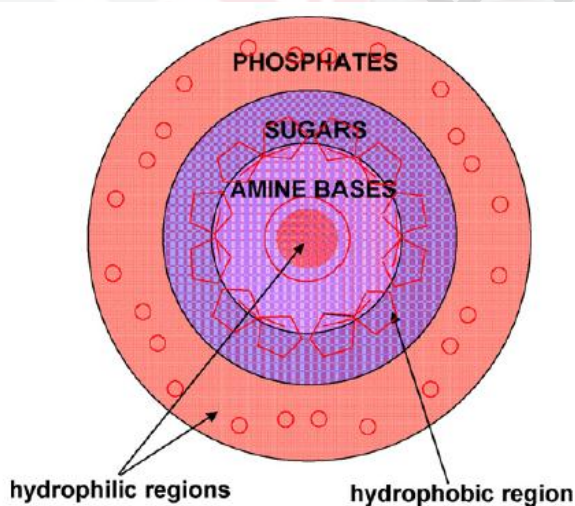


Figure 4.16. Schematic representation of duplex DNA view from the top showing the cylindrical model of DNA. DNA phosphate groups on the outside and amine groups on the inside show the hydrophilic regions, whereas the sugar groups in between phosphate and amine groups form a partly hydrophobic region (Source: Hammouda, 2009).

One way to enhance the protection of DNA hydrophobic groups from water is by increasing the hydrophobic groups of molecules or ions. In this study, increasing the length of alkyl chains in $[C_n\text{bim}][\text{Br}]$ ILs by adding non-polar CH_2 has resulted in gradually increasing the hydrophobicity of $[C_n\text{bim}][\text{Br}]$. When alkyl chain lengths got even longer in the case of $[C_6\text{bim}][\text{Br}]$, the tail of the alkylimidazolium cation became more hydrophobic. This fact is consistent with the MD simulation results, showing that the non-polar regions (hydrophobic groups) increased with increasing hydrocarbon chains of $[C_n\text{bim}][\text{Br}]$ ILs (Refer Section 4.3.5 in page 104). As discussed previously, upon the addition of DNA the long hydrophobic chains were trapped in the partly hydrophobic region (sugar-rich region) through both major and minor grooves and formed hydrophobic interaction with the non-polar sugar region. The trapped and stacked long hydrocarbon tails thereby increase its ability to block the water routes across to the amine bases.

Based on Figure 4.15, the ability of $[C_n\text{bim}][\text{Br}]$ to block the water routes increased with increasing the length of alkyl chains with the following order of $[C_2\text{bim}][\text{Br}] < [C_4\text{bim}][\text{Br}] < [C_6\text{bim}][\text{Br}]$. As a result, it was more difficult for water inside the helical structure to diffuse in the presence of $[C_6\text{bim}][\text{Br}]$, compared to $[C_4\text{bim}][\text{Br}]$ and $[C_2\text{bim}][\text{Br}]$. This has helped reducing the disturbance of amine stacking by water molecules thus enhanced the thermal stability as observed by increasing the melting temperature of Calf thymus DNA. This finding underscores the importance of hydrophobic interactions in the stabilization of DNA. To the best of our knowledge, this is the first work carried out to study the melting temperature of DNA in ILs.

4.3 Molecular Dynamics Simulation of Ionic Liquids

In this first part of computational section, the MD simulations were performed on these new $[C_n\text{bim}][\text{Br}]$ ILs (where $n = 2, 4, 6$, only liquid form at room temperature) in order to validate the OPLS-UA FFs used. The FFs validation is based on the agreement between experimental results density and viscosity with simulation data obtained. The correct FFs parameters are critically important criteria for obtaining reliable properties about the structure and interactions of these salts at the molecular level and may also be useful for future design of ILs. By analyzing the mean-square displacement (MSD) profiles as a function of time, the self-diffusion coefficients (D) for the ions in the ionic compounds were determined and related with their molecular structure. The effect of alkyl chain lengths on the liquid structure was observed with the aid of RDF and SDF. Polar and non-polar regions were also discussed.

4.3.1 Density

In order to optimize the simulation conditions and to validate the FFs parameters, the densities (ρ) of each ILs at 1.0 atm and 298.15 K were computed as shown in Table 4.10. Liquid density can be directly calculated from the MD simulation data. As reported by (Liu *et al.*, 2004), density is one of the main useful criteria used to validate the FFs rather than viscosity. Initially, the predicted simulation density obtained for these [C_nbim][Br] liquids using OPLS-UA FFs (Jorgensen *et al.*, 1996) were underestimated compared to experimental values by about 5–10% (Table 4.10, entry 1, 5 and 7). This implies that the UA model using original OPLS FFs does not accurately predict the properties of ILs in MD simulations. As reported in many MD simulation studies of ILs, FFs parameters are well parameterized if one of the properties, which is density shows a percentage error relative to experimental results is less than 5%.

Table 4.10. Predicted density obtained from MD simulation using different collision parameter (σ) in comparison to the experimental density of [C_nbim][Br] ILs at 298.15 K.

Entry	System	Collision diameter (σ) (10 ⁻¹ nm)	Modify (%)	Average density (ρ , kg m ⁻³)		Deviation (%)
				Sim.	Exp. ^b	
1	[C ₂ bim][Br]	4.62 ^a	0	1129 ± 3.8		- 9.45
2		4.16	10	1205 (2.6)		- 3.41
3		3.69	20	1229 (4.9)	1248	- 1.52
4		3.23	30	1324 (3.3)		+ 6.15
5	[C ₄ bim][Br]	4.62 ^a	0	1112 (5.1)		- 6.55
6		3.69	20	1173 (4.2)	1190	- 1.42
7	[C ₆ bim][Br]	4.62 ^a	0	1080 (2.9)		- 5.50
8		3.69	20	1135 (3.7)	1143	- 0.70

^a Original collision parameter obtained from OPLS FFs. ^b Experimental density obtained from our work as previously discussed in experimental section. Errors in parentheses are the standard deviation.

Many FFs parameters for ILs have been modified in order to improve predicted properties. For example, Liu *et al.* refined and developed a series of FFs for alkylimidazolium based ILs in order to obtain simulation properties in agreement with experimental results (Liu *et al.*, 2010; Liu *et al.*, 2006; Liu *et al.*, 2004). They also adjusted several parameters such as LJ potential and re-fitted partial atomic charge to get better agreement than other reported simulations.

In order to obtain correct FFs parameters for these $[C_n\text{bim}][\text{Br}]$ ILs, the modification of the FFs parameter was carried out. The parameter for anion bromide was refined, as it has been reported that the dynamics properties of ILs such as density are strongly dependent on the molecular geometry of molecules such as bond lengths, angles and LJ collision diameter (Kulschewski and Pleiss, 2013). More importantly, the ILs properties are also dependent on hydrogen bonding of anions and the *van der Waals* interactions (Bonhôte *et al.*, 1996). Therefore, the LJ collision diameter (σ) (see Equation 2.10 in page 31 under Section 2.11.2 for detail about LJ) of the bromine atom was refined by decreasing the value by 10% and the densities of ILs systems were recomputed. If the percentage deviation were still higher than 5%, then the refinement was repeated by decreasing another 10% until an acceptable percentage error was accomplished.

The average predicted density of our model system was calculated based on the equilibrium trajectories over the last 2 ns and compared with experimental data. The new density results using new LJ collision diameter (σ) were also tabulated in Table 4.10. The average simulation density gradually increased with reducing the value of collision diameter. It shows that, by reducing 20% from the original collision diameter value, the percentage error relative to the experimental results for the three $[C_n\text{bim}][\text{Br}]$ ILs under study were less than 2%. Figure 4.17 shows a representative graph of density using a new collision diameter of 0.369 nm for each ILs.

The simulation densities using a new collision diameter were found slightly underestimated, with the averaged liquid densities showing more accurate prediction for longer alkyl chains in $[C_6\text{bim}][\text{Br}]$ with a relatively small percentage error of 0.7% (Entry 8) as compared to $[C_4\text{bim}][\text{Br}]$ (1.42%, Entry 6) and $[C_2\text{bim}][\text{Br}]$ (1.52%, Entry 3). The $[C_6\text{bim}][\text{Br}]$ has a significantly lower density than the other two salts, suggesting that the extra CH_2 group on the $[C_6\text{bim}]^+$ cation reduces the packing efficiency of the fluid, thereby decreasing the density. Based on the results, a refined collision diameter of anion gives an overall good agreement with experimental data, indicating that the correct parameters for these salts have been obtained.

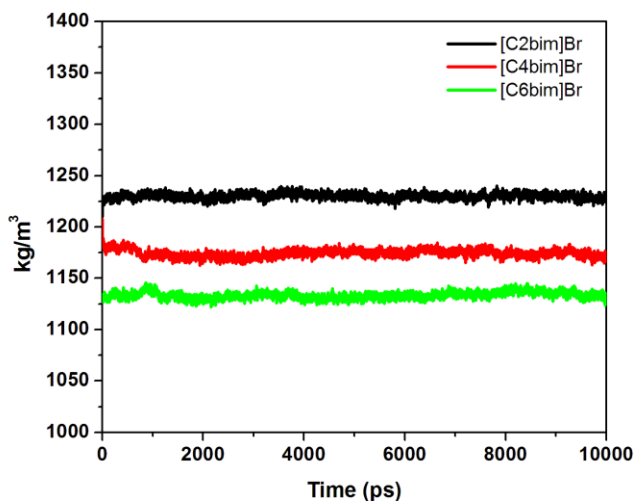


Figure 4.17. A representative 10 ns graph of density of $[C_n \text{bim}][\text{Br}]$ ILs using new collision diameter (σ) of 0.369 nm at 298.15 K.

4.3.2 Shear Viscosity

Differing from the dynamics property, kinetic properties such as shear viscosity (η) are governed by contributions from intermolecular interactions. The LJ parameter of well depth or maximum attractive energy (known as ϵ) and the partial atomic charges are the parameters that dominate the interaction energy of molecules. Therefore, viscosity of liquid system is another important criterion for validating the FFs parameters of ILs (Micaelo *et al.*, 2006). Based on the periodic perturbation method displayed in Equation 3.4 (Chapter 3, page 53), the shear viscosities of ILs are dependent on the external amplitude parameter (A) values. Therefore, three different amplitude parameters were first tested in non-equilibrium MD simulation (NEMD) to determine which parameter gives a predicted viscosity close to experimental results.

The predicted shear viscosities were summarized in Table 4.11. The shear viscosity results show that the external acceleration amplitude of 0.02 nm ps^{-2} gave a predicted shear viscosity close to the experimental results for three of $[C_n \text{bim}][\text{Br}]$ ILs. However, the calculated shear viscosities were overestimated for $[C_2 \text{bim}][\text{Br}]$.

Although the equilibrium density was perfectly near predicted for [C₂bim][Br], the calculated shear viscosity experienced a larger error in comparison with the experimental data (15.6% higher than experimental viscosity). For [C₄bim][Br] and [C₆bim][Br], the shear viscosities were slightly overestimated, with a percentage error of 3.0% (Table 4.11, entry 4) and 9.6% (Table 4.11, entry 5), respectively.

Table 4.11. Calculated viscosities with different amplitude parameter.

Entry	System	Amplitude parameter (nm ps ⁻²)	Shear viscosity (mPa·s)		Deviation (%)
			Sim. ^a	Exp. ^b	
1		0.01	> 1000		
2	[C ₂ bim][Br]	0.02	250 (26)	199	+ 15.6
3		0.03	787 (72)		
4		[C ₄ bim][Br]	0.02	1084 (177)	
5	[C ₆ bim][Br]	0.02	1294 (229)	1180	+ 9.6

^a Errors (in parentheses) from simulations are calculated using Equation 25 from Hess (2002).

^b Experimental viscosity obtained from our experimental work.

These results implied that the FFs parameters seem to have a small problem when it was used to treat shorter alkyl chain structure. However, the predicted viscosities for [C₄bim][Br] and [C₆bim][Br] show good agreement with experimental results, indicating that the refined FFs have been successfully validated, especially for longer alkyl chains of these salts. Figure 4.18 illustrates the graph of viscosities with respect to the external acceleration amplitude applied in the simulations at 298.15 K.

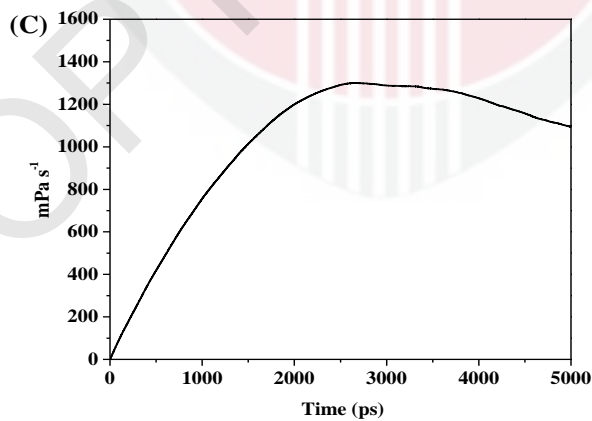
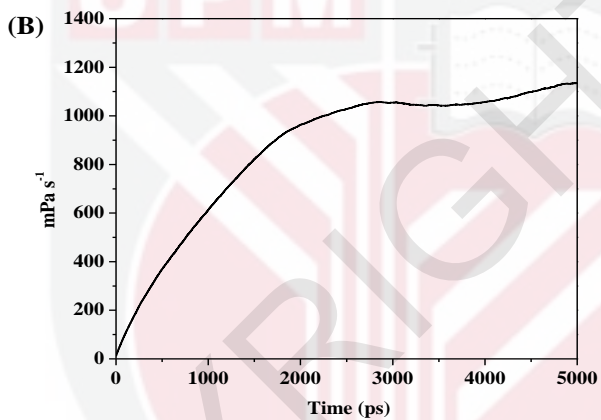
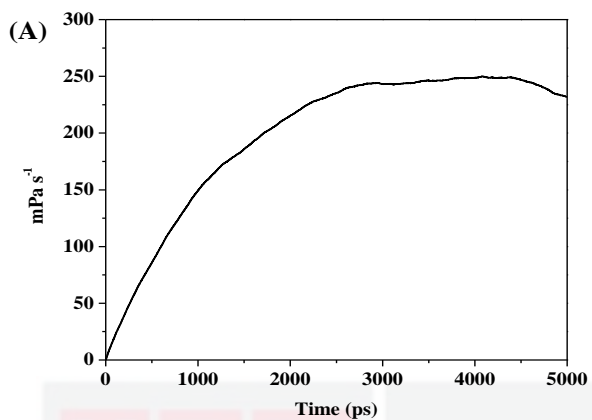


Figure 4.18. Graph of shear viscosities for A) $[C_2\text{bim}][\text{Br}]$, B) $[C_4\text{bim}][\text{Br}]$ and C) $[C_6\text{bim}][\text{Br}]$ obtained using acceleration amplitude 0.02 nm ps^{-2} .

4.3.3 Self-diffusion Coefficient

The microscopic dynamics properties of ILs play an important role in determining the rheological properties of these salts. MSD and self-diffusion coefficient (D) are considered as two particularly reliable methods to measure a liquid dynamics in a dense fluid (Liu *et al.*, 2008). There are two aspects which must be considered. First, the shorter the run length used for linear fitting, the greater overestimation of self-diffusion. Second, fitting the initial and final regions run length should be avoided (Micaelo *et al.*, 2006; Fioroni *et al.*, 2000). Therefore, the results from MD simulation are more reliable for shorter times (Morrow and Maginn, 2002). Figure 4.19 shows the MSD of three $[C_n\text{bim}][\text{Br}]$ ILs as a function of time, averaged over 5 ns of production simulation.

The self-diffusion coefficient for each cation and anion from the linear fitting of the slope of MSD was calculated using data in the range of 1–2 ns. The computed self-diffusion coefficient of the three $[C_n\text{bim}][\text{Br}]$ ILs at 298.15 K was summarized in Table 4.12. The self-diffusion coefficient is difficult to evaluate for this type of system due to the high rotational and translation motion correlation times expected for ILs (Micaelo *et al.*, 2006). Also, there were no experimental result for self-diffusion coefficient of these new $[C_n\text{bim}][\text{Br}]$ ILs due to some difficulty in performing NMR experiments. However, the predicted diffusion coefficients of these ions in the range of $10^{-11} \text{ m}^2 \text{ s}^{-1}$ at 298.15 K, are consistent with others computational studies of alkylimidazolium based ILs (Urahata and Ribeiro, 2005; Hanke *et al.*, 2001).

Table 4.12. The self-diffusion coefficient (D) from the slope of MSD plots (with standard deviation values in parentheses) and cationic (t_+) and anionic (t_-) anionic transference numbers for cations and anion in $[C_n\text{bim}][\text{Br}]$ ILs. The collision parameter (σ) of 0.369 for bromine atom was used.

System	Self-diffusion coefficient (D) ^a			
	(x $10^{-11} \text{ m}^2 \text{ s}^{-1}$)		t_+	t_-
	D_{cation}	D_{anion}		
$[\text{C}_2\text{bim}][\text{Br}]$	1.83 ± 0.1	1.31 ± 0.5	0.58	0.42
$[\text{C}_4\text{bim}][\text{Br}]$	1.65 ± 1.0	1.81 ± 0.2	0.48	0.52
$[\text{C}_6\text{bim}][\text{Br}]$	1.47 ± 0.1	1.07 ± 1.0	0.57	0.42

^a The difference of the self-diffusion coefficients obtained from fits over the two halves of the fit interval for the self-diffusion coefficient.

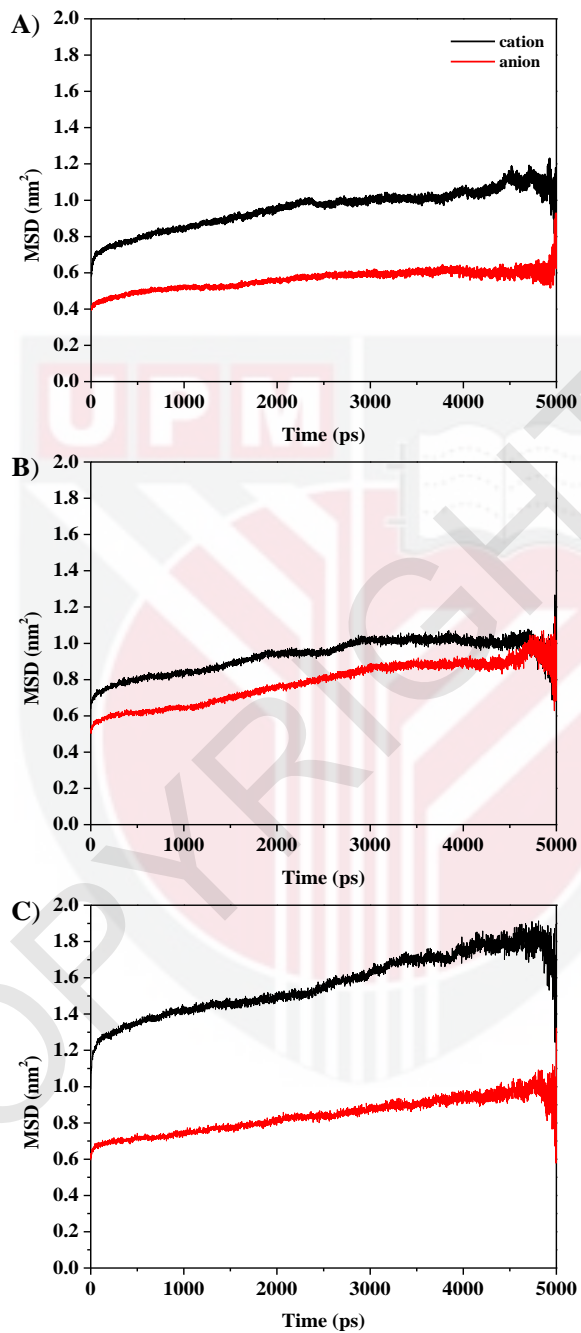


Figure 4.19. MSD as a function of time for A) [C₂bim][Br]; B) [C₄bim][Br] and C) [C₆bim][Br].

It was observed that the trends in the diffusion coefficients for different alkyl chain lengths of cations are $D [\text{C}_2\text{bim}]^+ > D [\text{C}_4\text{bim}]^+ > D [\text{C}_6\text{bim}]^+$. The bulky $[\text{C}_6\text{bim}]^+$ cation has the lowest diffusion coefficient of $1.47 \times 10^{-11} \text{ m}^2 \text{ s}^{-1}$ while $[\text{C}_4\text{bim}]^+$ has a diffusion coefficient midway between $[\text{C}_2\text{bim}]^+$ and $[\text{C}_6\text{bim}]^+$ molecules. The structure of $[\text{C}_2\text{bim}]^+$ cation is practically quite smaller compared to the other two cations. Therefore, the $[\text{C}_2\text{bim}]^+$ cation was expected to diffuse more quickly than the large $[\text{C}_6\text{bim}]^+$ cation. While, the long alkyl chain of $[\text{C}_6\text{bim}]^+$ restricts its mobility and reduces free space among the ions (Kowsari *et al.*, 2008).

Decreasing the diffusion with increasing the length of alkyl chains was in agreement with the previous experimental findings on the alkylimidazolium-based ILs (Tokuda *et al.*, 2006a; Tokuda *et al.*, 2006b; Tokuda *et al.*, 2005; Tokuda *et al.*, 2004; Every *et al.*, 2004). Except for $[\text{C}_4\text{bim}][\text{Br}]$, the diffusion coefficients of cations were slightly higher than the smaller anion despite a larger size, confirming with the NMR studies of alkylimidazolium based ILs by Umecky *et al.*, (2005b). In the case of $[\text{C}_4\text{bim}][\text{Br}]$, it was observed that the anion has a slightly higher diffusion coefficient than cation. One explanation for this phenomena may be due to the symmetrical structure of the $[\text{C}_4\text{bim}]^+$ cation. The present results correlated well with the inverse of the viscosity, which is the lower viscosity of the salts, the higher the self-diffusion coefficient. For equimolar solutions, the relative contributions of the cations and anions to the total conductivity of the solution were characterized by transport numbers of the cation and anion. The transference numbers in the range between 0 and 1, were calculated using Equation 4.2 and Equation 4.3.

$$t_+ = \frac{D_{\text{cation}}}{D_{\text{cation}} + D_{\text{anion}}} \quad (4.2)$$

$$t_- = \frac{D_{\text{anion}}}{D_{\text{cation}} + D_{\text{anion}}} \quad (4.3)$$

The transport numbers are important in determining the behavior of the ILs as electrolytes (Sirjoosingh *et al.*, 2009). As tabulated in Table 4.12 (page 97), the transport numbers for the cations in $[\text{C}_n\text{bim}][\text{Br}]$ were higher than the ones for the anions, except for $[\text{C}_4\text{bim}][\text{Br}]$. On the contrary, the anion in $[\text{C}_4\text{bim}][\text{Br}]$ has a higher transport number than the cation species. A higher transport number indicates the ability of the ion to diffuse faster and stronger contribution to the ionic conductivity of the electrolyte.

4.3.4 Molecular Structure

To investigate the influence of the cation size on the structural properties of ILs, the RDF and SDF of each ILs have been computed from the last 5 ns from the NPT simulation trajectories. A RDF is usually used to describe the probability distribution of molecules around a given set of the other molecules up to a certain distance (Sun *et al.*, 2010). All atoms in $[C_n\text{bim}]^+$ structures and the adjacent proton atoms were considered as the representative of the center-of-mass (COM) of the cations. As shown in Figure 4.20, all ILs exhibited the first solvation shell for cation-anion (ca) pair forms at a smallest distance of about 0.45 nm. The first solvation peaks were well defined, sharper and located at shorter distance as compared to cation-cation (cc) and anion-anion (aa) first peaks.

Despite the first peaks of each ILs being located at the same solvation shell, the second cation-anion (ca) solvation peak occurs at a slightly different distance. For $[C_2\text{bim}][\text{Br}]$, the second solvation shell was observed at ~ 0.85 nm (Figure 4.20A), while for $[C_4\text{bim}][\text{Br}]$ and $[C_6\text{bim}][\text{Br}]$, the second peak occurred at ~ 0.80 (Figure 4.20B) and ~ 1.05 nm (Figure 4.20C), respectively. These findings show that $[C_6\text{bim}][\text{Br}]$ has a higher distance of the cation-anion second solvation peak. This can be explained due to the steric hindrance of the long alkyl chains $[C_n\text{bim}]^+$ cation. When the cationic alkyl chain length becomes longer, the steric hindrance effect increases and the mobility of anions to move to the second solvation shell around the polar region in alkylimidazolium ring will be limited.

The anion-anion (aa) first solvation shell was computed at ~ 0.75 nm and cation-cation (cc) maxima peak occurs at distance near to 0.80 nm for each ILs. This split peak is the result of sequential ordering as induced by the cation-anion pairs. It can be seen that the oscillations of cation-cation (cc) and anion-anion (aa) were out of phase with those of cation-anion (ca). The solvation peak of cation-anion (ca) shows an intensity indicating charge ordering effect, in which anions and cations were preferentially surrounded by their corresponding counter-ions via electrostatic attraction. Given the long-range Coulombic interactions, it was observed that all $[C_n\text{bim}][\text{Br}]$ ILs systems displayed long-range spatial correlations which extend beyond 1.5 nm showing a characteristic of ILs. The RDF were in agreement with those of Shah *et al.* (2002) and Micaelo *et al.* (2006) who used a simple UA model for ILs system.

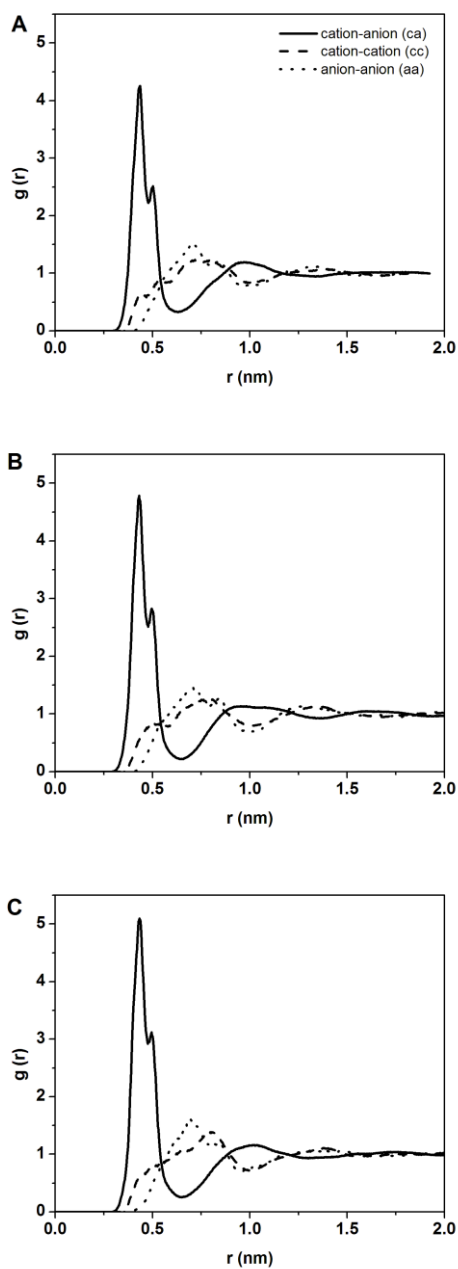


Figure 4.20. RDF for the cation-anion (ca), cation-cation (cc) and anion-anion (aa) interactions in A) $[C_2bim][Br]$, B) $[C_4bim][Br]$ and C) $[C_6bim][Br]$.

The existence of the highest intensity regions cation-anion (ca) first solvation peak for $[\text{C}_6\text{bim}][\text{Br}]$ (Figure 4.20C) compared to RDF of $[\text{C}_4\text{bim}][\text{Br}]$ (Figure 4.20B) and $[\text{C}_2\text{bim}][\text{Br}]$ (Figure 4.20A) might be interesting to observe. For clarity, Figure 4.21 illustrated the combination of RDF cation-anion (ca) for each ILs. Increasing of alkyl side chain in alkylimidazolium cation has affected the distribution of the anions. As alkyl side chains increased, the intensity of the RDF cation-anion (ca) first solvation peak also increased due to the enriched concentration of anions in the surrounded area of the imidazolium ring. This occurs because the side chains become less favorable location for anions. The hydrocarbon is able to rotate freely in a space, thus the flexibility of side chains will create an excluded volume for anions. Thus, the anions were pushed near to the imidazolium ring. Similar phenomena have also been observed by Raabe and Köhler, (2008) and Urahata and Ribeiro, (2004).

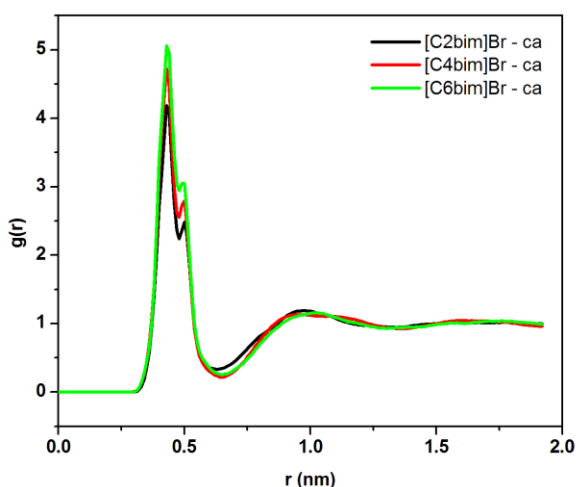


Figure 4.21. RDF of cation-anion (ca) of each $[\text{C}_n\text{bim}][\text{Br}]$ ILs.

The preferred distribution of the anions around the cations was best analyzed through the depictions of their SDF. The SDF localizes the regions around the cations that are more populated by the anions (Micaelo *et al.*, 2006). Figure 4.22 illustrates three high-probability regions where the anions can be found, which contribute to the first shell solvation in RDF. As expected and also as shown by other simulation studies (Raabe and Köhler, 2008; Liu *et al.*, 2004; Del Pópolo and Voth, 2004; Urahata and Ribeiro, 2004), the regions with a high probability of finding anions are located around the alkylimidazolium ring, specifically at HAR, HA4 and HA5 atoms (refer Figure 3.2 page 43 for clarity).

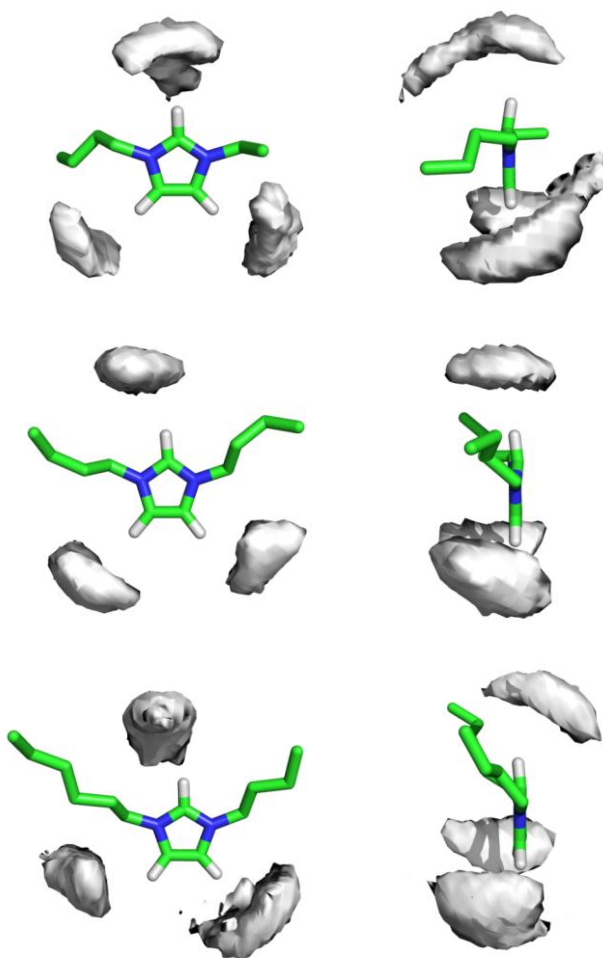


Figure 4.22. Spatial distribution probability density of anions around cations in [C₂bim][Br] (top), [C₄bim][Br] (mid) and [C₆bim][Br] (bottom) at 298.15 K. Anions at a maximum distance of 0.45 nm from the imidazole geometric center were selected.

It is not surprising to see that the distribution density of anions was dominant in these regions due to a high positive charge. The distribution of anions was almost the same in the regions due to the fact that the deviation of charge for each proton was relatively small. This also indicates that the stronger Coulombic interactions in [C_nbim][Br] ILs, as the negative charge is dispersed to only one bromine atom that strengthens the electrostatic forces (Dong *et al.*, 2006).

4.3.5 Polar and Non-Polar Regions

A simple way to visualize the polar and non-polar regions in the bulk $[C_n\text{bim}][\text{Br}]$ ILs is to use color-schemed snapshots of the simulation boxes. As shown in Figure 4.23, polar and non-polar atoms were colored red and green, respectively. Polar domains included all atoms in the ring of alkylimidazolium from the cation and atom bromine from the anion part whereas UA for the alkyl chains are part of the non-polar domain. By observing the colored boxes, it has clearly shown that the regions indicated in green color, representing the non-polar regions, were increased by increasing the alkyl side chain from $[C_2\text{bim}][\text{Br}]$ to $[C_6\text{bim}][\text{Br}]$. The results obtained were in agreement with those observed by Wang and Voth, (2005) and Lopes and Pádua, (2006b) who used an AA model to represent their system.

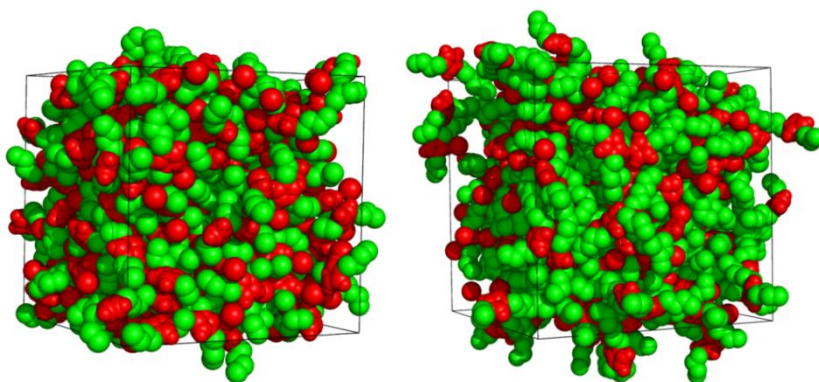


Figure 4.23. Snapshots of simulation boxes of $[C_2\text{bim}][\text{Br}]$ (left) and $[C_6\text{bim}][\text{Br}]$ (right) in which atoms belonging to the polar domains of the cation (imidazolium ring) and to the anion were colored in red and atoms belonging to the non-polar domains (alkyl side chain) were colored in green.

The red colored domains showed that the distribution of the charged (polar) domains was not homogeneous and randomly placed in the simulation boxes. The polar domains were more permeated by non-polar (green) regions in the simulation box of $[C_6\text{bim}][\text{Br}]$ compared to $[C_2\text{bim}][\text{Br}]$. The alkyl chains form continuous non-polar domains. Nevertheless, the polar region managed to preserve their continuity even though alkyl chains

increased. Therefore, it may be interesting to check the correlation between polar and non-polar domains by observing RDF. The perseverance of the polar groups as the length of alkyl chains increases was observed by computing the RDF of anion-anion (aa), as shown in Figure 4.24. Obviously, the distance of anion-anion (aa) remained almost similar in these three $[\text{C}_n\text{bim}][\text{Br}]$ ILs at about 0.75 nm. This indicated that the presence of longer alkyl chains must be accommodated in the system without disturbing the cation-anion (ca) network and their characteristic distances.

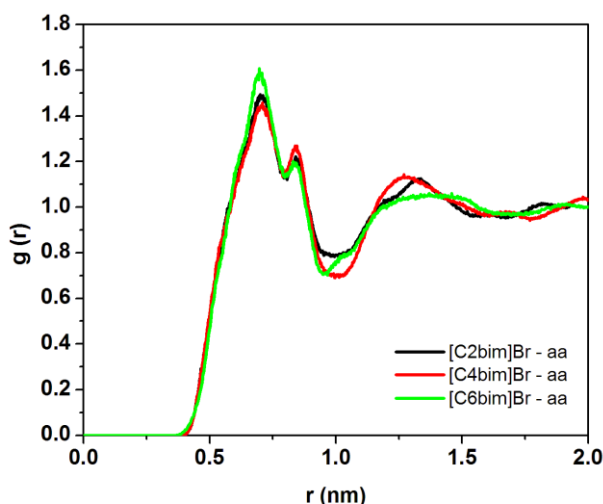


Figure 4.24. RDF of anion-anion (aa) correlation for each of $[\text{C}_n\text{bim}][\text{Br}]$ ILs.

To obtain more information about the polar and non-polar domains in these liquids, the combined RDF of cation-anion (ca) (polar-polar interaction) for each $[\text{C}_n\text{bim}][\text{Br}]$ ILs were further analyzed (refer back Figure 4.21, page 102). As observed previously, the intensity of the peaks gradually increases when the number of carbons in the alkyl side chain cations increases from $[\text{C}_2\text{bim}]^+$ to $[\text{C}_6\text{bim}]^+$. This implies that the tendency to form non-polar domains increases as the size of the non-polar moieties (alkyl side chain) becomes larger (Lopes and Pádua, 2006b). These results are in agreement with other MD simulations studies with alkylimidazolium-based ILs (Lopes *et al.*, 2006) and ammonium based ILs (Shimizu *et al.*, 2010).

4.4 DNA Molecular Solvation in Ionic Liquids

4.4.1 Structural Modeling of DNA in Ionic Liquids

The structural stability of B-conformation Calf thymus DNA was investigated by comparing the atomic RMSD of DNA (all heavy atoms) solvated in neat $[C_n\text{bim}][\text{Br}]$ ILs (using the validated FFs parameters) relative to the initial position in the crystal structure, as shown in Figure 4.25. On average over the last 2 ns, all RMSD values calculated for DNA in each ILs were found to be lower than those observed in an aqueous system (averaged $\text{RMSD}_{\text{in neat ILs}} = 0.143$ nm and $\text{RMSD}_{\text{in water}} = 0.290$ nm). Increasing carbon chain cations from C_2 to C_6 seems to slightly decrease the RMSD of DNA. This indicates that alkyl chain lengths of cations have a small influence on the stability of B-DNA which is in agreement with experimental results obtained in Section 4.2.4 (page 88).

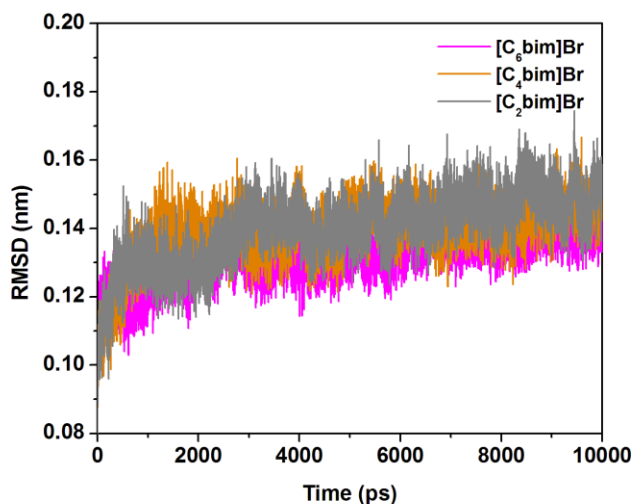


Figure 4.25. RMSD (nm) of duplex Calf thymus B-DNA conformation (all heavy atoms) solvated by three $[C_n\text{bim}][\text{Br}]$ ILs at 298.15 K.

For an inspection, the structure of duplex DNA solvated in different neat ILs was also taken from final conformations of a 10 ns MD simulation trajectories and its conformation was compared with the crystal structure as shown in Figure 4.26. The figure shows that the structures were stable and the final configurations were similar to the initial structure. Both findings demonstrate that DNA maintains

its B-native structure in neat ILs and corroborates with previous simulation finding, where the authors have noted the existence of native DNA conformation in a variety of neat ILs at 298.15 K (Cardoso and Micaelo, 2011).

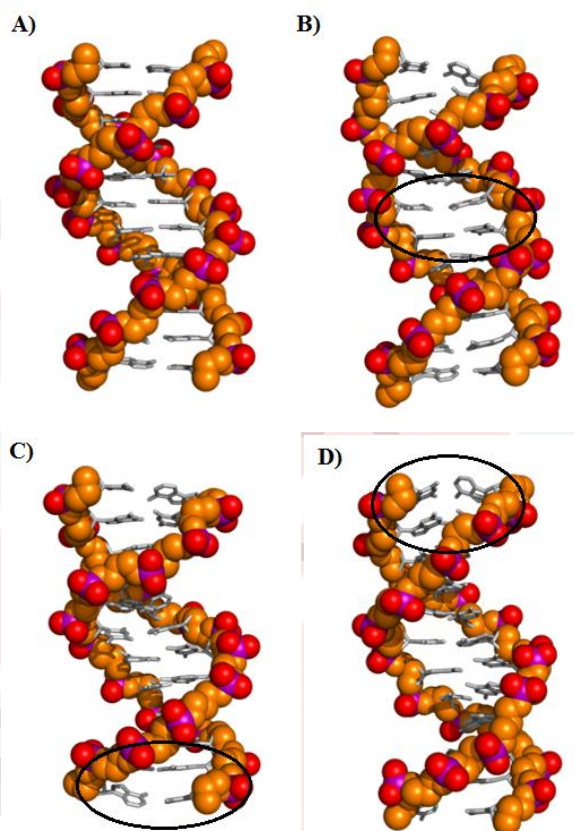


Figure 4.26. Comparison of calf thymus B-DNA structures after solvation in different neat ILs at 298.15 K. Initial crystal structure of DNA (A), structure of DNA in neat $[C_2\text{bim}][\text{Br}]$ (B), $[C_4\text{bim}][\text{Br}]$ (C) and $[C_6\text{bim}][\text{Br}]$ (D). The circles show that the bases in DNA strands located at head and tail were most disturbed by ILs molecules in comparison to the bases in the middle of DNA strands. The backbone of DNA consists of phosphate groups is able to maintain its helical shape due to the strong electrostatic attraction formed between ILs' cation and DNA phosphate groups. Colour schemes are as follow: red, oxygen; magenta, phosphorus; orange, backbone of DNA and gray, DNA bases. The structure of DNA in each ILs was taken from the final conformations of a 10 ns MD simulation trajectory.

Since ILs are well known to be thermally stable, the simulation of DNA in neat IL $[C_4\text{bim}][\text{Br}]$ was also performed at different temperatures. Interestingly, it was observed that the average RMSD of DNA slightly increases with increasing temperature as shown in Figure 4.27, indicating that ILs are able to stabilize DNA and maintain its native B-conformation at temperature up to 373.15 K. MD simulation of DNA in hydrated ILs was also performed. For this purpose, only $[C_4\text{bim}][\text{Br}]$ was selected as a model in order to further study the structural stability and dynamics of double helical DNA structure in a mixture of this IL and water. The average RMSD of DNA (all heavy atoms) solvated in different percentages of $[C_4\text{bim}][\text{Br}]$ (25%, 50% and 75% w/w which are similar to experimental conditions) at various temperatures is depicted in Figure 4.28.

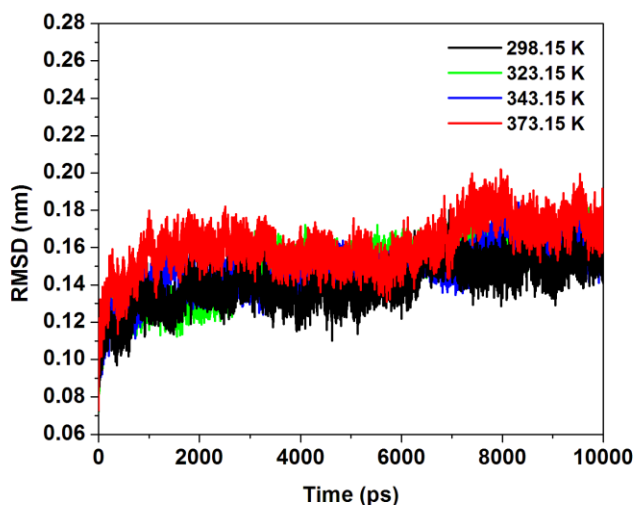


Figure 4.27. RMSD (nm) of duplex DNA (all heavy atoms) simulated in neat $[C_4\text{bim}][\text{Br}]$ at various temperatures.

At 298.15 K, the average RMSD of DNA in 75% (w/w) $[C_4\text{bim}][\text{Br}]$ solution was found to be only 0.169 nm. Even in 25% and 50% dilute solutions, the average RMSD of DNA was lower, 0.232 and 0.222 nm respectively. The results imply that increasing percentages of $[C_4\text{bim}][\text{Br}]$ result in a more native-like DNA structure. It shows that DNA in all percentages of $[C_4\text{bim}][\text{Br}]$ solution has RMSD smaller than the average RMSD of DNA in an aqueous system (0.290 nm), suggesting that DNA retains its native conformation at 298.15 K, which is in good agreement with the spectroscopic findings.

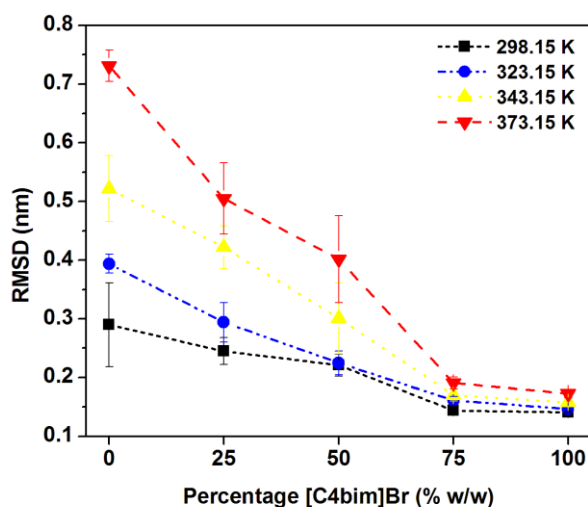


Figure 4.28. Average RMSD (nm) of DNA (all heavy atoms) solvated in different percentages of hydrated [C₄bim][Br] solution (25%, 50% and 75% w/w) at various temperatures. For comparison, simulation of DNA in aqueous system is shown at zero percentage of [C₄bim][Br]. Values are averages over the last 2 ns of MD simulation.

Although the average RMSD of DNA increases with increasing the temperature, DNA in 75% IL solution shows RMSD of DNA at 373.15 K which is even lower than the RMSD of DNA in an aqueous system at 298.15 K. This result indicates that DNA maintains its native conformation even at high temperatures in the presence of a small amount of water, as observed in proteins (Vijayaraghavan *et al.*, 2010b; Fujita *et al.*, 2007; Fujita *et al.*, 2005). The data corroborated well with the experimental evidence from Vijayaraghavan *et al.* (2010a) who reported that DNA is stable and retains its B-conformation in hydrated choline-based ILs. Meanwhile, DNA in 50% (w/w) [C₄bim][Br] solution at 323.15 K shows that RMSD of DNA was lower than RMSD of DNA in water at 298.15 K.

As observed, it is clear that the stability of DNA is mainly dependent on the water content, or more specifically the properties of hydration shells around DNA. To understand this hypothesis, the distribution of cations on DNA surface picked up at 10 ns was investigated as illustrated in Figure 4.29. It is evident that, the populations of cations were not only located near the DNA

phosphate groups due to the charge attraction, but also associate with the major groove of DNA. Interestingly, few $[C_4bim]^+$ ions were also observed in the minor groove as well. This implies that the surrounding cations around DNA surface entered the major and minor grooves by disrupting the hydration shells and remained bound to the grooves without disturbing the DNA helical structure. Not surprisingly, the population of $[C_4bim]^+$ was found to be slightly higher in the wider major groove than the narrower minor groove. This finding confirmed the experimental evidence obtained in Section 4.2 (page 73).

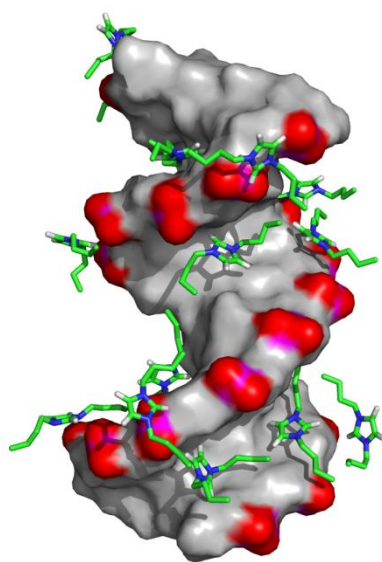


Figure 4.29. Representative distribution of $[C_4bim]^+$ molecules showing their association with the DNA phosphate groups, major and minor grooves. The distribution of anion ($[Br^-]$) molecules was not shown here. Colour schemes are as follow: red, oxygen; magenta, phosphorus; gray, DNA structure; green, carbon; blue; nitrogen and white; proton. Figure made from the final conformations of a 10 ns MD simulation trajectory.

It was detected that the hydrocarbon chains of cation were perpendicular to the surface of DNA and formed hydrophobic interactions with the DNA bases. This observation was supported by the experimental results obtained earlier and the evidences from Wang *et al.* (2011) and Ding *et al.* (2010) who pointed out that hydrophobic interactions formed between hydrocarbon chains of

the ILs and the DNA bases. Since cations were also detected in both grooves, the hydrogen bonding together with contribution of hydrophobic interactions between cation-grooves might also assist in stabilizing the DNA.

4.4.2 Role of Hydration Shells

Based on the current work, it is obvious that the hydration shells play a vital role in stabilizing or destabilizing DNA and their conformational dynamics. Figure 4.30 shows representative distribution of cation and water molecules in the solvation layers of DNA, defined as a shell of 0.35 nm. The figure clearly illustrates that at 25% and 50% $[C_4bim][Br]$ solution, accumulation of water surrounding the DNA surface is high as compared to cations, thus the arrangement of water molecules forms strong hydration shell (Figure 4.30A and 4.30B). In 75% IL solution, $[C_4bim]^+$ cations were able to enter the water hydration layer and take part in solvation mechanism (Figure 4.30C).

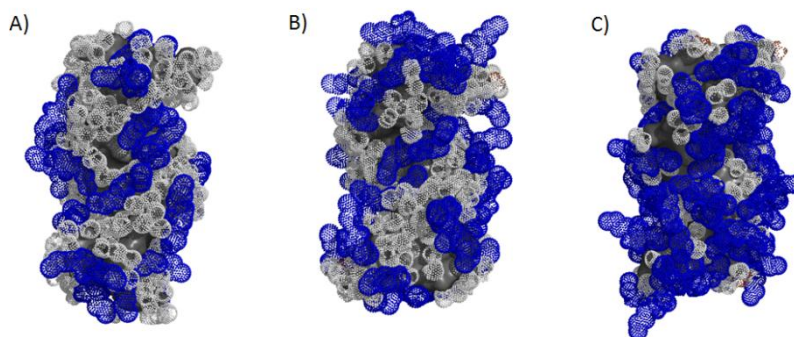


Figure 4.30. Representative populations of cations and water molecules within 0.35 nm from DNA surface. A) 25%, B) 50% and C) 75% (w/w) $[C_4bim][Br]$ solutions at 298.15 K. Colour scheme are as follow: white, water; blue, cation. Figures were taken from the final conformations of a 10 ns MD simulation trajectory.

At low relative humidity, water does not diffuse freely and mostly located around DNA phosphate groups (Schneider *et al.*, 1998; Edwards *et al.*, 1984). In the presence of bulk $[C_4bim][Br]$ molecules, many hydrophobic tail of $[C_4bim]^+$ cation stacked in the hydrophobic sugar-rich region via hydrophobic interaction. This

interaction thereby blocks the water pathway to the bases of amine. Thus, it causes water to have more difficulty diffused inside the DNA helical structure and less disturbs the amine stacking (Hammouda, 2009). Therefore, the disturbing of DNA conformation by water diffusion is reduced. Such the so-called partial dehydration of DNA by $[C_4\text{bim}][\text{Br}]$ IL also could prevent hydrolytic reactions such as deamination and depurination.

However, with increasing the water percentages, many water molecules can cross the hydrophobic sugar-rich region and form “spine of hydration”, especially in the minor groove of DNA (Arai *et al.*, 2005; Drew and Dickerson, 1981). This will cause the diffusion of water molecules inside the helical DNA structure to be increased and disturbs the amine stacking more. As a result, the double helical B-DNA structure is changed with increasing the percentage of water but still retains its native B-conformation as shown in Figure 4.31.

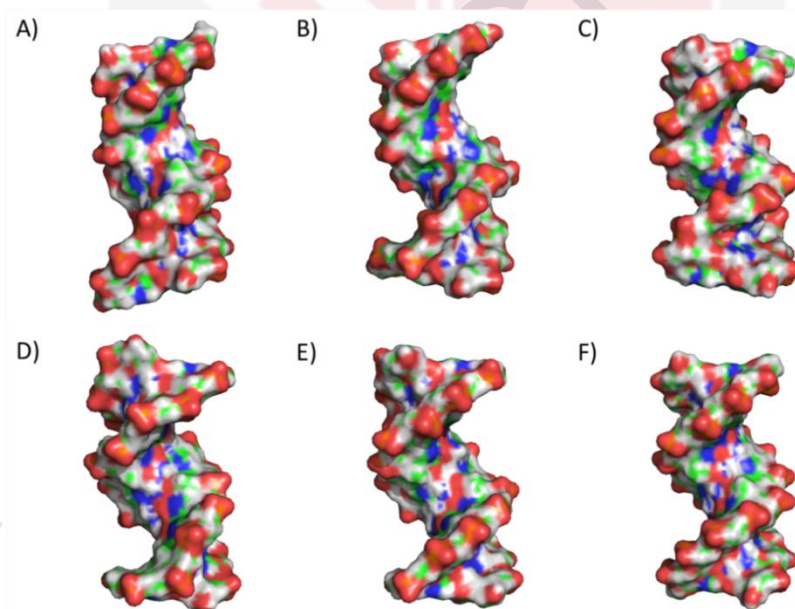


Figure 4.31. DNA conformations obtained from last 10 ns simulation trajectories. A) Structure of DNA in pure water system; B) 25%; C) 50%; D) 75%; E) Neat (100%) $[C_4\text{bim}][\text{Br}]$ and F) Initial crystal structure of DNA.

To further understand the role of hydration shells in DNA stability, the distribution of [C₄bim][Br] and water molecules around DNA surface was calculated (Table 4.13). In 25%, 50% and 75% [C₄bim][Br] solutions, on average, 6.6, 9.4 and 13.9 molecules of cations were observed entering the hydration layers and getting involved in DNA solvation, respectively. Anions were virtually absent in the hydration layers with the average of 0.5 in 25% [C₄bim][Br] solution at any temperature. As the temperature is increased from 298.15 to 373.15 K, it was found that 16 and 30 water molecules were removed from the hydration layers by 25 and 50% IL solutions.

Table 4.13. Average number of [C₄bim][Br] ions and water molecules within 0.35 nm from the DNA surface at different temperatures. Data averaged from the last 2 ns of MD simulations.

[C ₄ bim][Br]:H ₂ O (% w/w)	Temp. (K)	Average Number of Molecules		
		Cation	Anion	H ₂ O
0 : 100	298.15	-	-	356.7 ± 7.3
	323.15	-	-	347.8 ± 8.1
	343.15	-	-	336.0 ± 9.7
	373.15	-	-	310.9 ± 9.7
25 : 75	298.15	6.4 ± 1.9	0.4 ± 0.1	250.1 ± 9.8
	323.15	6.0 ± 2.6	0.5 ± 0.1	234.6 ± 10.6
	343.15	7.5 ± 1.8	0.5 ± 0.1	246.5 ± 9.0
	373.15	6.6 ± 2.0	0.5 ± 0.1	233.5 ± 11.2
50 : 50	298.15	9.7 ± 2.3	1.6 ± 0.8	205.5 ± 5.9
	323.15	8.9 ± 2.2	2.9 ± 1.4	196.1 ± 8.8
	343.15	10.6 ± 2.1	2.3 ± 1.3	185.9 ± 8.8
	373.15	8.3 ± 2.2	2.9 ± 1.4	175.0 ± 7.5
75 : 25	298.15	12.6 ± 2.2	5.1 ± 0.8	128.5 ± 4.1
	323.15	13.1 ± 1.9	4.7 ± 0.6	101.3 ± 3.1
	343.15	13.4 ± 2.2	7.2 ± 1.3	100.6 ± 3.1
	373.15	16.5 ± 2.8	7.2 ± 1.2	94.5 ± 3.8
100 : 0	298.15	14.9 ± 1.9	6.3 ± 0.6	-
	323.15	15.6 ± 2.0	8.5 ± 1.0	-
	343.15	15.6 ± 1.9	10.4 ± 0.9	-
	373.15	17.4 ± 2.6	14.3 ± 0.9	-

However, the average numbers of $[C_4\text{bim}][\text{Br}]$ ions in the hydration layers remained unchanged with increasing temperature in 25% and 50%, suggesting three possible explanations. First, this implies that incrementing the simulation temperature does not seem to affect the localization of cations round DNA surface. Second, any interactions between cations and DNA are not broken and are maintained in the hydration layers. Third, the remaining water molecules still formed strong hydration shells, thus prevented other cations to enter and disrupted the well-coordinated hydration layers.

With the increase in IL concentration, the population of $[C_4\text{bim}][\text{Br}]$ rises significantly. At high concentration (75% w/w), the average number of $[C_4\text{bim}][\text{Br}]$ molecules in the DNA solvation layers increases significantly with increasing temperature while the average number of water molecules greatly reduces from 128.5 to 94.5. At 75% IL solution, the hydration shells become weaker. The arrangement of water molecules or the so-called "cone of hydration", the tetrahedral arrangement in the hydration layers especially on the surface of DNA phosphate groups (Schneider *et al.*, 1998) was greatly disturbed by the penetration of ILs' cations. Many $[C_4\text{bim}]^+$ cations can compete for binding to the DNA phosphate groups and forming strong electrostatic attractions. The competition might also take place in the major and minor grooves of DNA, which are rich with hydrogen donors/acceptors. Figure 4.32 shows the penetration of cation molecules into DNA minor groove in different percentages of $[C_4\text{bim}][\text{Br}]$ solution.

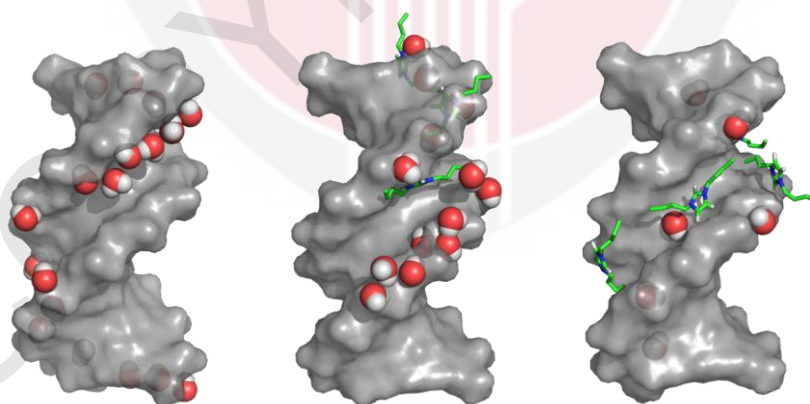


Figure 4.32. Spin of hydration layers of water in the minor groove of DNA from control simulation (left). Penetration of hydration layers by $[C_4\text{bim}]^+$ cations at the minor groove in 25% (mid) and 75% (right) of $[C_4\text{bim}][\text{Br}]$ solutions.

It can be said that electrostatic attraction in combination with hydrogen bonds helps to stabilize duplex DNA. This finding is in agreement with Korolev *et al.* (2003) that the hydration shells were the main factor for ionic binding to the phosphate groups of DNA, as well with X-ray studies (Egli *et al.*, 1998). Overall, it shows that from the data in Table 4.13 (page 113), the higher accumulation of cations over anions was observed due to less available space filled by cation molecules and neighbouring cation layers.

4.4.3 Water Stripped from DNA Surface

The percentage of water molecules stripped from the DNA hydration layers was calculated as a function of time and temperature. As depicted in Figure 4.33, at 298.15 K, cations stripped about 60% of water molecules from the surface of DNA in 75% [C₄bim][Br] solution, averaged over the last 2 ns of the simulations. The percentage of water stripped increased up to 70% when the temperature was increased to 323.15 K. This indicates that increasing the temperature leads to increasing the penetration of [C₄bim][Br] molecules into the hydration shells, which replaced the water molecules.

However, the percentage of water stripped remained constant at 343.15 K and 373.15 K, possibly due to the remaining water molecules that are retained in the deep hydration layers. At 25% and 50% IL solutions, about 30% and 45% of the water molecules were stripped from the hydration shells at any temperature, demonstrating that at low and medium percentages of IL solutions, the hydration shells are strong even at high temperatures.

It is well known that the double-helical DNA structure melts into an open coil at high temperatures. Prior MD simulations have revealed that the thermal stability of DNA is mainly due to the hydration shells on DNA surface. Specifically, it is related to the solvent thermodynamics, especially entropy and enthalpy of water. As reported by Auffinger and Westhof, (2002) increasing the entropy of water will overcome enthalpy stabilization, leading to pre-melting of the solvent that facilitates duplex disruption. Generally, entropy of water rapidly increases with increasing temperature. When the water content is high (in solution of 25% [C₄bim][Br] solution), the entropy of water molecules surrounding the duplex DNA especially the DNA phosphate groups increases with temperature, by reducing the number and strength of the solvent-solute (H₂O-DNA) interactions.

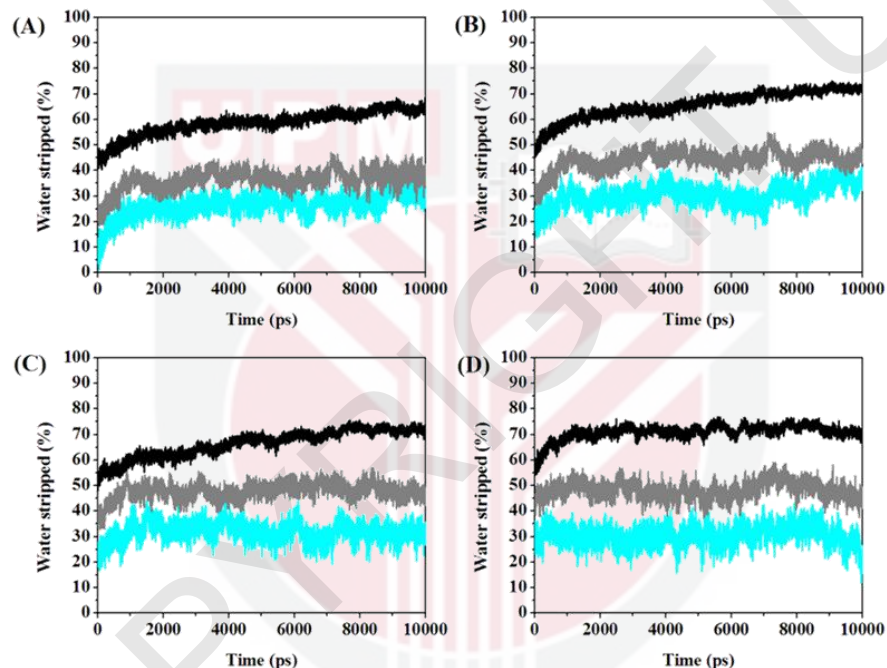


Figure 4.33. Percentage of water stripped from the DNA surface at different percentages of $[C_4bim][Br]$ in solution and at different temperatures. A) 298.15 K, B) 323.15 K, C) 343.15 K and D) 373.15 K. Colour scheme: black, 75%; gray, 50% and cyan, 25% (w/w) $[C_4bim][Br]$ solution. The percentage of water molecules stripped from DNA surface was calculated from the fraction of water present within 0.35 nm located from DNA surface divided with the initial water count in the same distance. Data for analysis was taken from the last 2 ns simulation trajectories.

With further temperature increases, water molecules lose their cohesion where the solvent-solute is no longer sufficiently strong to stabilize the interactions and thus destabilizing the DNA structure. Referring back to Figure 4.28 (109) the RMSD of DNA in hydrated 25% [C₄bim][Br] solution increases dramatically with temperature, indicating that the duplex DNA was not stable and the weakest structural elements of DNA system start to melt or undergo a helix-to-coil transition upon heating. Conversely, at low water content in 75% [C₄bim][Br] solution, the DNA phosphate group was surrounded and occupied by [C₄bim]⁺ cations rather than water.

Therefore, the increasing entropy of water does not affect the interaction between solvent-solute (in this case, the population of cations around the DNA surface were higher than water, thus the major interaction is between [C₄bim]⁺ cations and DNA) as the ILs have high thermal stability. The cation-DNA interaction was said stable and maintained even at higher temperature. Based on the MD data, it was found that 75% IL solution was a suitable media for stabilizing the duplex DNA structure. This finding is in agreement with experimental work carried out by Vijayaraghavan *et al.*, (2010a).

4.4.4 Binding Characteristics of Ionic Liquid-DNA

The characteristics of binding pattern between ILs and DNA were computed using RDF of cation and anion around DNA surface. Centre of mass RDF (COM-RDFs) shows that alkylimidazolium cations in neat ILs interact most frequently with the DNA phosphate backbone groups. The distributions show a favored localization of the [C_nbim]⁺ cations located at a distance of 0.5 nm from the DNA phosphate groups (Figure 4.34A) and the exclusion of anion at the same region (Figure 4.34B). The average coordination number indicated that there was no significant difference in the cumulative number of each cation around DNA phosphate groups. On average, only one cation was observed in each simulation systems within a distance of 0.5 nm from negative charges of DNA phosphate groups.

The calculated interaction energies between different parts of the simulation systems showed that the electrostatic attraction between [C₄bim]⁺ cation and DNA phosphate groups is more negative compared to the interaction between water and DNA (Table 4.14). This confirmed that the electrostatic attraction formed between ILs and DNA has a major contribution to the DNA stability. This discovery confirmed the lab-work evidence that electrostatic attraction between [C_nbim]⁺ cations and DNA phosphate groups

was the main attraction in stabilizing duplex DNA conformation. This finding also correlates well with the ^{31}P NMR and FT-IR spectra studies of Ding *et al.* (2010) and Wang *et al.* (2007b). Further research by Wang *et al.* (2011) reveals that the strong electrostatic interactions also caused a major contribution to the binding Gibbs energy of the ILs to DNA.

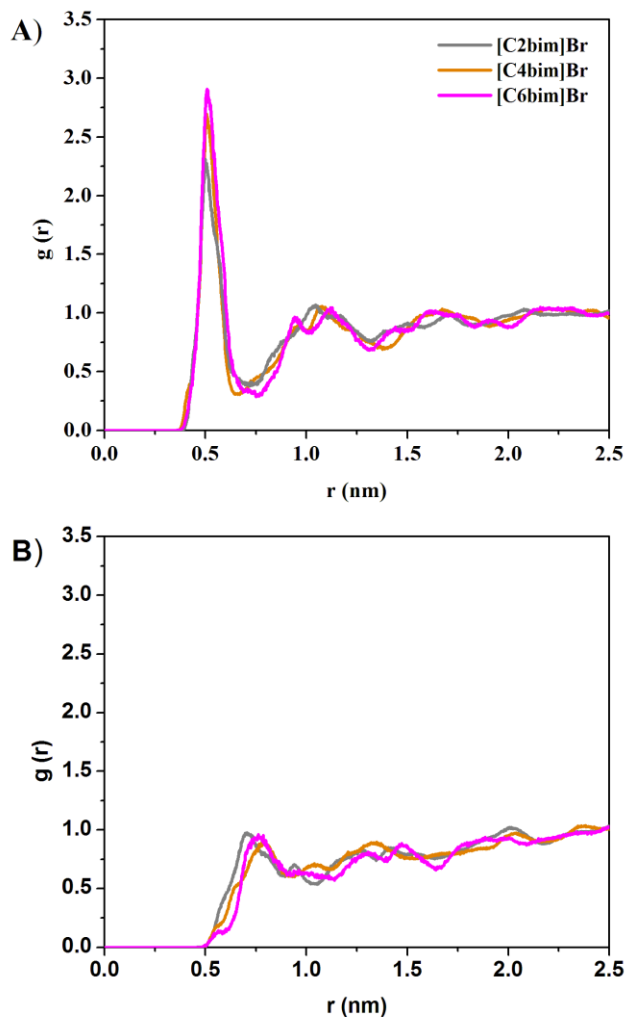


Figure 4.34 (A) ILs' cations (head charge group) COM-RDF around DNA phosphate groups. **(B)** Exclusion of ILs' anions COM-RDF in the same region. Colour scheme: gray, [C₂bim][Br]; orange, [C₄bim][Br] and magenta, [C₆bim][Br].

Table 4.14. The calculated of interaction energies between different parts in the simulation systems. The contribution of electrostatic and *van der Waals* interactions are shown.

Interaction	Electrostatic energy (kcal mol ⁻¹)	<i>van der Waals</i> energy (kcal mol ⁻¹)
Water – [PO ₄] ⁻	-12.78 ± 2.12	+ 1.79 ± 0.87
[C ₄ bim] ⁺ – [PO ₄] ⁻	- 46.55 ± 4.75	- 2.31 ± 2.49
[Br] ⁻ – [PO ₄] ⁻	+ 0.41 ± 0.17	+ 0.64 ± 0.36

4.4.5 Flexibility of DNA in Ionic Liquids

Root mean square fluctuations (RMSF) of DNA bases in a series of hydrated [C₄bim][Br] solutions were also calculated. RMSF also can locate the regions with high or low mobility based on the fluctuation of the position each DNA base relative to the average structure. RMSF of each DNA bases in neat and hydrated [C₄bim][Br] solutions are shown in Figure 4.35. Duplex DNA was observed to have lower flexibility in hydrated [C₄bim][Br] at low water percentage and neat [C₄bim][Br]. The fluctuation of DNA bases decreases with increasing the percentage of [C₄bim][Br] solution. At 25% (w/w), higher fluctuations occur, for the most part, in the heads and tails of DNA strands. Increasing temperatures from 298.15 K to 373.15 K results in significant increments in fluctuations (Figure 4.35A).

At 50%, high fluctuations were still observed (Figure 4.35B). However, the fluctuations of DNA bases in the heads and tails of DNA strands at 343.15 K and 373.15 K were found to be slightly lower than in 25% [C₄bim][Br], indicating that the opening of base pairs might occur at high temperatures in both solution (25% and 50%). In 75% and neat [C₄bim][Br] (Figure 4.35C and 4.35D), despite temperature increases, low fluctuations of DNA bases were still observed, demonstrating the rigidity of duplex DNA, leading to the assumption that 75% and 100% [C₄bim][Br] solutions might be able to prevent the opening of DNA strands at high temperatures.

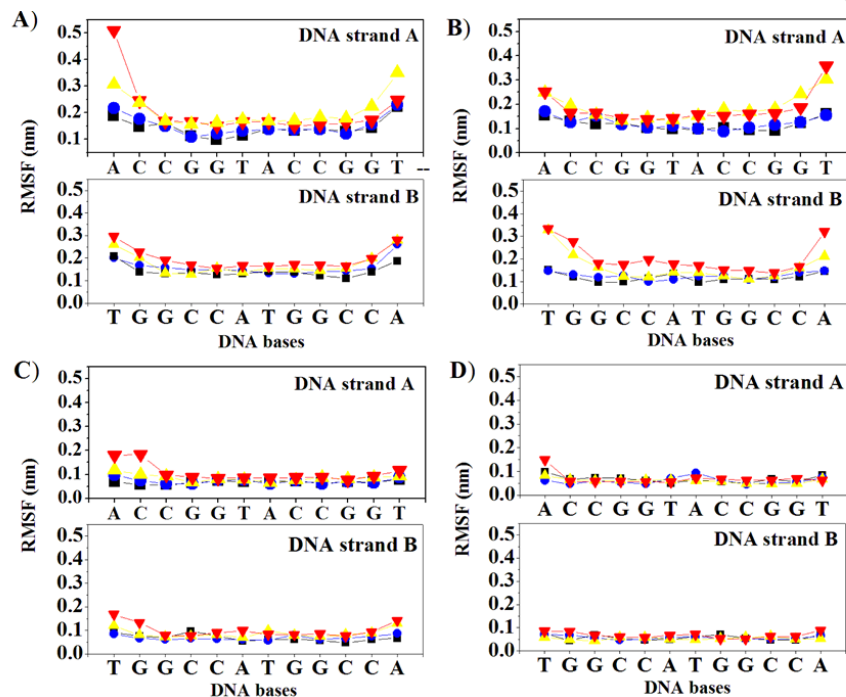


Figure 4.35. RMSF of DNA bases (all heavy atoms) in different hydrated $[C_4bim][Br]$ systems including DNA in neat $[C_4bim][Br]$ at various temperatures. DNA in 25% (w/w) $[C_4bim][Br]$, (A); 50%, (B); 75%, (C) and neat $[C_4bim][Br]$ (D). Colour scheme are as follow: black, 298.15 K; blue, 323.15 K; yellow, 343.15 K and red, 373.15 K. Bases of DNA strand A pair with bases of DNA strand B with the following combination A-T and C-G pairs. RMSF averaged over the last 2 ns of MD simulation.

4.4.6 Hydrogen Bonding Interaction

To prove the opening of DNA strands, the average of Watson-Crick hydrogen bonds between base pairs was calculated (Table 4.15). The average number of hydrogen bonds decreases when the temperature increases from 298.15 K to 373.15 K. The average number of hydrogen bonds between DNA strands in 75% [C₄bim][Br] solution slightly reduced as compared to DNA in 50% and 25% of [C₄bim][Br], showing that increasing in concentrations of [C₄bim][Br] helps to maintain the Watson-Crick hydrogen bonds and prevent the opening of base pairs. This fact can be correlated well with the low RMSD value (refer back Figure 4.28, page 109), which indicated that the unfolding/denaturation of DNA in ILs are avoided at high temperatures. For DNA in aqueous solution, the average number of hydrogen bonds greatly decreased as the temperature increased, indicating the separation of some of the base pairs.

Table 4.15. Average number of Watson-Crick hydrogen bonds of DNA strands at different percentages of [C₄bim][Br] (% w/w) and various temperatures. Hydrogen bonds are considered when the distances between the donor and the acceptor less than 0.35 nm and the angle hydrogen-donor-acceptor are lower than 30°. Average hydrogen bonds of DNA strands in aqueous system were also calculated for the purpose of comparison. Data averaged over the last 2 ns of MD simulations.

^a System	[C ₄ bim][Br]:H ₂ O (% w/w)	Temperature (K)			
		298.15	323.15	343.15	373.15
H ₂ O	0 : 100	31.9 (1.9)	27.6 (1.5)	28.1 (1.6)	24.7 (1.8)
[C ₄ bim][Br]	25 : 75	32.0 (1.8)	29.0 (1.2)	28.5 (1.4)	27.3 (1.7)
[C ₄ bim][Br]	50 : 50	32.0 (0.9)	31.0 (1.3)	29.1 (1.3)	28.4 (1.4)
[C ₄ bim][Br]	75 : 25	32.0 (1.1)	30.6 (1.3)	30.4 (1.5)	30.0 (1.8)
[C ₄ bim][Br]	100 : 0	32.0 (1.3)	31.5 (1.6)	31.3 (1.4)	31.2 (1.8)

^a The number of Watson-Crick hydrogen bonds between the two strands in the initial crystal structure is 32. Errors in parentheses are the standard error.

As molecules of ILs have hydrogen bond donors/acceptors, they may be able to engage in inter-hydrogen bonding with the bases of the DNA helix, thus help to maintain its double-helix structure. Increasing simulation temperatures from 298.15 K to 373.15 K slightly increases the average number of hydrogen bonds for both cations and anions (Table 4.16). For DNA in hydrated IL system, increasing the percentage of $[C_4bim][Br]$ leads to an increase in the number of hydrogen bonds. The average number of hydrogen bonds is almost unchanged for the system containing 25% and 50% and slightly increases for the system 75% and neat $[C_4bim][Br]$ when the temperature increases from 298.15 K to 373.15 K.

Table 4.16. Average hydrogen bonds formed between DNA bases and $[C_4bim]^+$ cations and $[Br]^-$ anion at different temperatures. Hydrogen bond is considered to occur when the distances between the donor and the acceptor are less than 0.35 nm is and the angle hydrogen-donor-acceptor is lower than 30° . The average hydrogen bond is considered between a proton in an $[C_4bim]^+$ ring and DNA bases. Data is averaged over the last 2 ns of MD simulations.

System	$[C_4bim][Br]:H_2O$ (% w/w)	Temp. (K)	Average H-bonds	
			Cation	Anion
$[C_4bim][Br]$	25 : 75	298.15	3.7 ± 1.7	0.1 ± 0.04
		323.15	3.9 ± 1.9	0.2 ± 0.04
		343.15	3.5 ± 1.8	0.2 ± 0.06
		373.15	3.9 ± 1.9	0.2 ± 0.07
	50 : 50	298.15	6.1 ± 2.2	0.8 ± 0.17
		323.15	6.1 ± 2.4	1.5 ± 0.16
		343.15	6.1 ± 2.4	1.2 ± 0.13
		373.15	6.7 ± 2.4	1.7 ± 0.12
	75 : 25	298.15	8.8 ± 2.5	3.9 ± 0.95
		323.15	9.5 ± 2.8	4.3 ± 1.03
		343.15	12.5 ± 3.0	6.2 ± 0.85
		373.15	11.8 ± 3.1	6.0 ± 1.26
	100 : 0	298.15	16.6 ± 3.3	6.9 ± 0.28
		323.15	16.5 ± 3.1	5.9 ± 0.12
		343.15	16.4 ± 3.3	8.7 ± 0.45
		373.15	17.4 ± 3.6	12.3 ± 1.18

This proved that temperature does not affect the formation of inter-hydrogen bonds between DNA bases and IL's ions. The hydrogen bonds were well preserved at higher temperatures, perhaps due to the thermal stability of ILs. The number of hydrogen bonds formed was found to be two or three times higher for DNA bases and cations than anions. DNA is well known as a poly-anion polymer, thus it is not surprising that the cations are well-distributed than anions on the surface of DNA, thus form more hydrogen bonding interaction.

4.5 Free Energies Solvation

4.5.1 Nucleic Acids Bases in Aqueous System

Most of the solvent influences the structural, topological and reactivity properties of the solutes. The extent of such effects depends on the nature of solvent and the polarity of the solute. Polar solvents such as water lead to the largest changes in the nuclear and electronic distribution of solutes; these changes are maximized by large polarity in the solutes (Mestres *et al.*, 1996; Luque *et al.*, 1995a; Luque *et al.*, 1994). Accordingly, it is expected that water would dramatically affect the properties of highly polar and polarizable molecules such as nucleic acid bases (Orozco and Luque, 1993).

Therefore, to understand the effect of water on the properties of polar molecules, free solvation energy of nucleic acids bases in water was computed by using TIP4P water model and the results were tabulated in Table 4.17. In order to obtain reliable results from BAR method, the results from other methods are also listed for comparison, including similar models (Table 4.17, row 2-5), the *ab initio* method (Table 4.17, row 6-7), semi empirical (Table 4.17, row 8-10), combined (QM/MM) (Table 4.17, row 11) and FDPB models (Table 4.17, row 12). Except for our work (Table 4.17, row 1) and the QM/MM method (Table 4.17, row 11), the values shown were for methylated nucleic acids bases as no experimental data were available for non-methylated bases because of low volatility of nucleic acids bases (Cullis and Wolfenden, 1981). Methylation typically decreases the solvation free energy of the bases to 1-2 kcal mol⁻¹ (Cramer and Truhlar, 1992).

Table 4.17 Solvation free energy (kcal mol⁻¹) of nucleic acids bases in water.

Entry	FFs / Method	Adenine	Cytosine	Guanine	Thymine	Uracil	Ref
1	OPLS / BAR	-16.5	-22.5	-25.9	-17.4	-17.0	this work
2	OPLS / FEP	-11.6	-20.1	-21.7	-13.1	-12.8	a
3	OPLS / MC	-39.2	-40.5	-47.9	-40.6	-	b
4	AMBER / TI	-12.0	-18.4	-22.4	-12.4	-14.0	c
5	AMBER / FEP	-12.6	-12.7	-19.6	-7.5	-	d
6	6-31*-MST	-8.5	-15.1	-18.1	-10.3	-10.9	e
7	SCRF(6-31G*)	-6.5	-13.0	-16.1	-8.9	-10.0	f
8	AM1 / SM2	-20.9	-18.7	-24.3	-13.3	-14.8	g
9	SCRF(AM1)	-11.3	-14.4	-18.1	-8.6	-	h
10	AM1-MST	-10.8	-16.1	-21.1	-10.1	-10.4	e
11	QM / MM	-5.1	-16.3	-13.5	-8.5	-9.9	i
12	FDPB	-10.4	-16.8	-19.7	-10.4	-	j

(a) Elcock and Richards (1993); (b) Monajjemi *et al.*, (2006); (c) Miller and Kollman (1996); (d) Bash *et al.*, (1987); (e) Orozco *et al.*, (1996); (f) Young and Hillier (1993); (g) Cramer and Truhlar (1992); (h) Orozco and Luque (1993); (i) Gao (1994); (j) Mohan *et al.*, (1992).

Our computed results (Table 4.17, row 1) show much large and negative free energies. As many authors have noted, nucleic acid bases have large and negative free energies of solvation, showing that the nucleic acid bases are very polar and can interact well with water. Our results indicate that guanine has the more negative free energy of solvation ($-26.4 \text{ kcal mol}^{-1}$), while adenine has the smaller free energies of solvation ($-16.9 \text{ kcal mol}^{-1}$). DNA base thymine and RNA base uracil both have almost similar free energies of -17.6 and $-17.2 \text{ kcal mol}^{-1}$, respectively. When comparing the numerical values of solvation energy of DNA bases with similar models, our results also show a similar trend, in that guanine > cytosine > thymine > adenine, except for results derived from AMBER/FEP (Table 4.17, row 5). This indicates that guanine is more likely solvated in water compared to adenine. Based on the results, a clear identification was made. The polarity of nucleic acids decreases from guanine > cytosine > thymine~uracil > adenine.

Although our results are slightly higher compared to the data obtained using same OPLS FFs but by different method (FEP, Table 4.17, row 2), the approach of the data is the same. It is difficult to compare these results directly to the other results for many reasons. The usage of molecular mechanics FFs by the methods was different. Other differences might be due to the improvement of the FFs used as well as the version of programming software used. Molecular dynamics (MD) (Table 4.17, row 1, 2, 4 and 5) or Monte Carlo (MC) (Table 4.17, row 3) simulations also affect the SFE results. Different water models also significantly affect the free energy results, even though the difference is small. Again, as stressed earlier, there were no experimental data to validate those theoretical estimates, but the agreement between the different theoretical estimates gives confidence in our results.

4.5.2 Nucleic Acids Bases in Ionic Liquids

The SFE of nucleic acids bases in ILs was also estimated as presented in Table 4.18. To the best of our knowledge, this was the first study reporting the solvation free energy of nucleic acids bases in ILs. A huge difference was observed for solvation energy of the bases in ILs and water. The predicted free energy in ILs shows much large and negative energy compared to the free energy of nucleic acid bases in water. This indicates that in general, the nucleic acid bases were better solvated in ILs than in water. Since there has been no experimental work carried out to support the data, we suggest that based on the polarity, these nucleobases are

easily dissolved in ILs. This observation was expected given that ILs are well-known polar compounds and are even more polar than water. In generally, polar molecules are soluble in polar solvents and non-polar molecules dissolve readily in non-polar solvents.

The same decreasing trend which are guanine > cytosine > thymine~adenine, was also observed for DNA bases in ILs. Guanine is expected to be the most hydrophilic molecule due to the presence of several small polar substituents on the purine ring, while adenine and thymine as well as uracil are expected to be the least hydrophilic and least polar nucleobases. Therefore, it was observed that in all ILs, guanine show the highest solvation energy (an average $-38.0 \text{ kcal mol}^{-1}$) in comparison to other nucleobases. The solvation free energy for adenine, thymine and uracil were quite similar. The effects of alkyl chain of ILs cations on the solvation energy were also observed. However, the SFE results in different alkyl chains of ILs cation were not very much different and only slightly changes were observed. It shows that polar guanine and cytosine are preferred to solvate in short alkyl chain of $[\text{C}_2\text{bim}][\text{Br}]$, while non-polar adenine, thymine and uracil are better solvated in $[\text{C}_6\text{bim}][\text{Br}]$.

Table 4.18. Solvation free energy (kcal mol⁻¹) of nucleic acids bases in [C_nbim]Br ILs from this work. Solvation free energy of nucleic acids in water was also depicted for comparison.

No	System	FFs / Method	Adenine	Cytosine	Guanine	Thymine	Uracil
1	[C ₂ bim][Br]		-22.2	-29.7	-38.5	-21.8	-22.9
2	[C ₄ bim][Br]	OPLS / BAR	-24.5	-29.6	-38.3	-23.3	-23.1
3	[C ₆ bim][Br]		-24.2	-28.2	-36.8	-24.5	-23.1
4	TIP4P		-16.5	-22.5	-25.9	-17.4	-17.0

CHAPTER 5

SUMMARY, CONCLUSION AND RECOMMENDATION FOR FUTURE RESEARCH

5.1 Summary and Conclusion

The research carried out in this study focused on the behavior and properties of DNA in new ILs. This was achieved through combined experimental methods and computer simulations. The usage of ILs as a new media for DNA solvation was aimed to solve the problems encountered using aqueous solution and volatile organic solvents such as chloroform/phenol. These problems include toxicity of organic solvents, low DNA thermal stability, hydrolytic reaction and contamination of DNA.

In the present study, a series of new 1-alkyl-3-butylimidazolium bromide ILs ($[C_n\text{bim}][\text{Br}]$ where $n = 2, 4, 6, 8, 10$ and 12) were synthesized using simple alkylation reaction. The linear hydrocarbon chain lengths of these ILs were found to significantly affect their density, viscosity and thermal stability. Three of these new ILs ($[C_2\text{bim}][\text{Br}]$, $[C_4\text{bim}][\text{Br}]$ and $[C_6\text{bim}][\text{Br}]$) existing in a liquid form and completely miscible with water were successfully used in DNA solvation. This finding shows that many possible combinations of cations-anions to form ILs can be synthesized via simple alkylation reaction. Considering that this one-step reaction does not produce any side product, the synthesized ILs can be obtained with high yield and purity in a moderate reaction time.

The behaviour of Calf thymus DNA in three hydrated $[C_n\text{bim}][\text{Br}]$ ILs (where $n = 2, 4, 6$) at different water percentages of 25%, 50% and 75% w/w was biophysically studied. The DNA maintained its native B-conformation in all hydrated ILs at 25°C due to the electrostatic attraction between $[C_n\text{bim}]^+$ cations and phosphate groups of DNA. In fact, strong hydrophobic interactions between alkyl chains of $[C_n\text{bim}]^+$ and the bases of DNA also played a significant role in IL-DNA binding. The strong electrostatic and hydrophobic interactions lead to compact DNA structure, which then excludes the intercalation of ethidium from DNA base pairs. Furthermore, a comprehensive study showed that the DNA melting temperature significantly increased from $56 \pm 1.0^\circ\text{C}$ (in $[C_2\text{bim}][\text{Br}]$) to $58 \pm 1.0^\circ\text{C}$ (in $[C_6\text{bim}][\text{Br}]$). Overall, the electrostatic attractions, hydrogen and hydrophobic interactions were all contributed to the DNA stability. This shows that ILs have an excellent characteristics as a potential media for DNA. It is also believed that the ILs are able to mimic the

functions of buffer due to the molecules of ILs being totally comprised of ions. This may open up a new era for use of ILs as a buffer and solvent simultaneously. Prior to this research, it has been shown that biophysical analyses are important tools for DNA studies.

In the first part of computer simulation, the FFs parameters for the UA models of these three new liquid $[C_n\text{bim}][\text{Br}]$ ILs (where $n = 2, 4, 6$) were successfully validated via MD simulation. The refined collision parameter (σ) of 0.369 nm for the anion was found to give a good agreement with the experimental density and viscosity, respectively. The molecular distributions showed that they were in liquid form in correlation with experimental evidences. In fact, the centre-of-mass RDFs showed that the anion tends to orient near the C^2 carbon of the cation. This observation was further visualized using three dimensional pictures of the SDF confirming the charge ordering effect of bromide around $[C_n\text{bim}]^+$ cation. The outcome of these results implies that MD simulation technique can assist in the description of the interfacial structure and help to gain molecular insights about the behavior of molecules. Furthermore, by using this technique, time-consuming processes in understanding and designing specific molecules may be reduced.

MD simulations of DNA in hydrated ILs were also performed using the validated FFs of these $[C_n\text{bim}][\text{Br}]$ great ILs. Care was taken to ensure that simulation conditions were as similar to experiments as possible. The molecular structure of DNA revealed that DNA conformation was closer to its native structure in neat and hydrated ILs (25%, 50% and 75% w/w) at 25°C. The stability of DNA was found dependent on the hydration shells around DNA surface. The binding ability of $[C_4\text{bim}]^+$ to DNA phosphate groups reduced in the presence of strong hydration shells in the system of 25% $[C_4\text{bim}][\text{Br}]$ (75% water w/w), while increased in the system of 75% $[C_4\text{bim}][\text{Br}]$. The computed interaction energy revealed that the electrostatic energy of $[C_4\text{bim}]^+ - [\text{PO}_4]^-$ ($-46.55 \pm 4.75 \text{ kcal mol}^{-1}$) was lower than water- $[\text{PO}_4]^-$ ($-12.78 \pm 2.12 \text{ kcal mol}^{-1}$). The temperature effect showed that DNA in 75% $[C_4\text{bim}][\text{Br}]$ system was able to preserve DNA's native conformation up to 373.15 K (100°C). Successful simulation of these works agreed with experimental achievements. This suggests that computer simulations were able to predict the molecular properties close to wet-lab experiments. Moreover, the data obtained can be beneficially used to aid the experimental approach as it offers insight information about the physical and dynamic properties. With the freely available FFs and programming software, these would help to avoid chemical toxicity, waste management and other related problems involved in experimental work.

The calculated solvation free energy of various nucleic acids bases in ILs was computed using Bennett's acceptance ratio (BAR) method employing the MD simulation in the last part of computer simulation. The results indicated that the bases were better solvated in $[C_n\text{bim}][\text{Br}]$ ILs (where $n = 2, 4, 6$) rather than in aqueous solution. Hydrophobicity of alkyl chain length of ILs does not play a major role due to the solute-solvent interaction which was only involved polar atoms/groups. The evidences from the computed data indicated that BAR method sufficiently described the interactions of the nucleic acids bases with solvent molecules as well as solvent-solvent interactions. This free energy of the bases in ILs has previously never been accomplished in any computer simulation studies.

5.2 Recommendations for Future Research

The outcomes of the present work are leading to several areas which virtue further study as follows. Some of these can be instantly performed, while the others depend on the time setting and resources availability.

1. New ILs could be further designed by attaching some polar groups such as hydroxyl (OH) or amine (NH_2) in the alkyl chains lengths of imidazolium ring. This may help enhancing the stability of duplex DNA by adding more possible interactions between ILs and DNA bases, given that the bases have many recognition sites.
2. Thermodynamics properties such as binding constants (K_b) and binding Gibbs energies (ΔG) of ILs to DNA may be interesting to determine. Such results may be useful in understanding the contribution of electrostatic and non-electrostatic interactions to the binding energies.
3. Considering the advances in computational chemistry and current methodology, the simulation can be extended to longer time scales and larger systems. This means that conformational changes and motions of system can be further investigated, thus provide information that cannot be obtained via experiments.

REFERENCES

- Abdul Rahman, M.B., Jumbri, K., Sirat, K., Kia, R. and Fun, H.-K. Tetra-ethylammonium L-malate 1.36-hydrate. *Acta Crystallographica Section E: Structure Reports Online* 2009; 65: 49–50.
- Abdul Rahman, M.B., Jumbri, K., Basri, M., Abdulmalek, E., Sirat, K. and Salleh, A.B. Synthesis and physico-chemical properties of new tetraethylammonium-based amino acid chiral ionic liquids. *Molecules* 2010; 15: 2388–2397.
- Abdul Rahman, M.B., Jumbri, K., Sirat, K., Kia, R. and Fun, H.-K. Tetraethylammonium L-tartrate dihydrate. *Acta Crystallographica Section E: Structure Reports Online* 2008; 64: 2343.
- Ajam, M. Methathesis and hydroformylation reactions in ionic liquids. MSc Thesis, 2005, University of Johannesburg, Auckland Park, South Africa.
- Albarino, C.G. and Romanowski, V. Phenol extraction revisited: A rapid method for the isolation and preservation of human genomic DNA from whole blood. *Molecular and Cellular Probes* 1994; 8: 423–427.
- Anouti, M., Caillon-Caravanier, M., Le Floch, C. and Lemordant, D. Alkylammonium-based protic ionic liquids part I: Preparation and physicochemical characterization. *Journal of Physical Chemistry B* 2008; 112: 9406–9411.
- Antony, J.H., Mertens, D., Dölle, A., Wasserscheid, P. and Carper, W.R. Molecular reorientational dynamics of the neat ionic liquid 1-butyl-3-methylimidazolium hexafluorophosphate by measurement of ^{13}C nuclear magnetic relaxation data. *ChemPhysChem* 2003; 4: 588–594.
- Arai, S., Chatake, T., Ohhara, T., Kurihara, K., Tanaka, I., Suzuki, N., Fujimoto, Z., Mizuno, H. and Niimura, N. Complicated water orientations in the minor groove of the B-DNA decamer d(CCATTAAATGG)₂ observed by neutron diffraction measurements. *Nucleic Acids Research* 2005; 33: 3017–3024.

- Auffinger, P. and Westhof, E. Melting of the solvent structure around a RNA duplex: A molecular dynamics simulation study. *Biophysical Chemistry* 2002; 95: 203–210.
- Awad, W.H., Gilman, J.W., Nyden, M., Harris Jr., R.H., Sutto, T.E., Callahan, J., Trulove, P.C., DeLong, H.C. and Fox, D.M. Thermal degradation studies of alkylimidazolium salts and their application in nanocomposites. *Thermochimica Acta* 2004; 409: 3–11.
- Barreireiro, P.C.A. and Lindman, B. The kinetics of DNA–cationic vesicle complex formation. *Journal of Physical Chemistry B* 2003; 107: 6208–6213.
- Bash, P.A., Singh, U.C., Langridge, R. and Kollman, P.A. Free energy calculations by computer simulation. *Science* 1987; 236: 564–568.
- Bayly, C.I., Cieplak, P., Cornell, W.D. and Kollman, P.A. A well-behaved electrostatic potential based method using charge restraints for deriving atomic charges: the RESP model. *Journal of Physical Chemistry* 1993; 97: 10269–10280.
- Becke, A.D. Density functional thermochemistry. III. The role of exact exchange. *The Journal of Chemical Physics* 1993; 98: 5648–5652.
- Bennett, C.H. Efficient estimation of free energy differences from Monte Carlo data. *Journal of Computational Physics* 1976; 22: 245–268.
- Berendsen, H.J.C., Postma, J.P.M., Van Gunsteren, W.F., Dinola, A. and Haak, J.R. Molecular dynamics with coupling to an external bath. *The Journal of Chemical Physics* 1984; 81: 3684–3690.
- Berendsen, H.J.C., van der Spoel, D. and van Drunen, R. GROMACS: A message-passing parallel molecular dynamics implementation. *Computer Physics Communications* 1995; 91: 43–56.
- Berman, H.M. Hydration of DNA: Take 2. *Current Opinion in Structural Biology* 1994; 4: 345–350.

- Berman, H.M., Westbrook, J., Feng, Z., Gilliland, G., Bhat, T.N., Weissig, H., Shindyalov, I.N. and Bourne, P.E. The Protein Data Bank. *Nucleic Acids Research* 2000, 28: 235–42.
- Bhattacharya, S. and Chaudhuri, P. Medical implications of benzimidazole derivatives as drugs designed for targeting DNA and DNA associated processes. *Current Medicinal Chemistry* 2008; 15: 1762–1777.
- Bhattacharya, S. and Mandal, S.S. Interaction of surfactants with DNA. Role of hydrophobicity and surface charge on intercalation and DNA melting. *Biochimica et Biophysica Acta (BBA) – Biomembranes* 1997; 1323: 29–44.
- Bonhôte, P., Dias, A.-P., Papageorgiou, N., Kalyanasundaram, K. and Grätzel, M. Hydrophobic, highly conductive ambient-temperature molten salts. *Inorganic Chemistry* 1996; 35: 1168–1178.
- Bonner, G. and Klibanov, A.M. Structural stability of DNA in nonaqueous solvents. *Biotechnology and Bioengineering* 2000; 68: 339–344.
- Bonnet, J., Colotte, M., Coudy, D., Couallier, V., Portier, J., Morin, B. and Tuffet, S. Chain and conformation stability of solid-state DNA: Implications for room temperature storage. *Nucleic Acids Research* 2009; 38: 1531–1546.
- Boon, J.A., Levisky, J.A., Pflug, J.L. and Wilkes, J.S. Friedel-Crafts reactions in ambient-temperature molten salts. *Journal of Organic Chemistry* 1986; 51: 480–483.
- Cadena, C., Anthony, J.L., Shah, J.K., Morrow, T.I., Brennecke, J.F. and Maginn, E.J. Why is CO₂ so soluble in imidazolium-based ionic liquids? *Journal of the American Chemical Society* 2004; 126: 5300–5308.
- Cadena, C., Zhao, Q., Snurr, R.Q. and Maginn, E.J. Molecular modeling and experimental studies of the thermodynamic and transport properties of pyridinium-based ionic liquids. *Journal of Physical Chemistry B* 2006; 110: 2821–2832.
- Cao, M., Deng, M., Wang, X.-L. and Wang, Y. Decompaction of cationic gemini surfactant-induced DNA condensates by β -cyclodextrin or anionic surfactant. *Journal of Physical Chemistry B* 2008; 112: 13648–13654.

- Cardoso, L. and Micaelo, N.M. DNA molecular solvation in neat ionic liquids. *ChemPhysChem* 2011; 12: 275–277.
- Case, D.A., Cheatham III, T.E., Darden, T., Gohlke, H., Luo, R., Merz Jr., K.M., Onufriev, A. and Woods, R.J. The AMBER biomolecular simulation programs. *Journal of Computational Chemistry* 2005; 26: 1668–1688.
- Chaires, J.B. and Dongchul, S. Criteria for the mode of binding of DNA binding agents. *Bioorganic and Medicinal Chemistry* 1995; 3: 723–728.
- Chaires, J.B. Equilibrium studies on the interaction of daunomycin with deoxypolynucleotides. *Biochemistry* 1983; 22: 4204–4211.
- Chandran, A., Ghoshdastidar, D. and Senapati, S. Groove binding mechanism of ionic liquids: A key factor in long-term stability of DNA in hydrated ionic liquids? *Journal of the American Chemical Society* 2012; 134: 20330–20339.
- Chaudhary, G.R., Bansal, S., Saharan, P., Bansal, P. and Mehta, S.K. Applications of surface modified ionic liquid/nanomaterial composite in electrochemical sensors and biosensors. *BioNanoScience* 2013; 3: 241–253.
- Cheng, D.-H., Chen, X.-W., Wang, J.-H. and Fang, Z.-L. An abnormal resonance light scattering arising from ionic-liquid/DNA/ethidium interactions. *Chemistry - A European Journal* 2007; 13: 4833–4839.
- Cheng, Y.-K. and Pettitt, B.M. Stabilities of double- and triple-strand helical nucleic acids. *Progress in Biophysics and Molecular Biology* 1992; 58: 225–257.
- Chiappe, C. and Pieraccini, D. Ionic liquids: Solvent properties and organic reactivity. *Journal of Physical Organic Chemistry* 2005; 18: 275–297.
- Ciccotti, G., Jacucci, G. and McDonald, I.R. "Thought-experiments" by molecular dynamics. *Journal of Statistical Physics* 1979; 21: 1–22.
- Cornell, W.D., Cieplak, P., Bayly, C.I., Gould, I.R., Merz Jr., K.M., Ferguson, D.M., Spellmeyer, D.C., Fox, T., Caldwell, J.W. and Kollman, P.A. A second generation force field for the simulation of proteins, nucleic acids, and organic

- molecules. *Journal of the American Chemical Society* 1995; 117: 5179–5197.
- Cramer, C.J. and Truhlar, D.G. Polarization of the nucleic acid bases in aqueous solution. *Chemical Physics Letters* 1992; 198: 74–80.
- Cullis, P.M. and Wolfenden, R. Affinities of nucleic acid bases for solvent water. *Biochemistry* 1981; 20: 3024–3028.
- Darden, T., York, D. and Pedersen, L. Particle mesh Ewald: An $N \cdot \log(N)$ method for Ewald sums in large systems. *The Journal of Chemical Physics* 1993; 98: 10089–10092.
- de Andrade, J., Böes, E.S. and Stassen, H. A force field for liquid state simulations on room temperature molten salts: 1-ethyl-3-methylimidazolium tetrachloroaluminate. *Journal of Physical Chemistry B* 2002a; 106: 3546–3548.
- de Andrade, J., Böes, E.S. and Stassen, H. Computational study of room temperature molten salts composed by 1-alkyl-3-methylimidazolium cations - force field proposal and validation. *Journal of Physical Chemistry B* 2002b; 106: 13344–13351.
- Del Pópolo, M.G. and Voth, G.A. On the structure and dynamics of ionic liquids. *Journal of Physical Chemistry B* 2004; 108: 1744–1752.
- Del Pópolo, M.G., Lynden-Bell, R.M. and Kohanoff, J. *ab initio* molecular dynamics simulation of a room temperature ionic liquid. *Journal of Physical Chemistry B* 2005; 109: 5895–5902.
- DeLano, W.L. The PyMOL Molecular Graphics System. DeLano Scientific LLC, Palo Alto, CA, USA, 2008.
- Dickerson, R.E., Drew, H.R., Conner, B.N., Wing, R.M., Fratini, A.V. and Kopka, M.L. The anatomy of A-, B-, and Z-DNA. *Science* 1982; 216: 475–485.
- Ding, Y., Zhang, L., Xie, J. and Guo, R. Binding characteristics and molecular mechanism of interaction between ionic liquid and DNA. *Journal of Physical Chemistry B* 2010; 114: 2033–2043.

- Docherty, K.M. and Kulpa Jr., C.F. Toxicity and antimicrobial activity of imidazolium and pyridinium ionic liquids. *Green Chemistry* 2005; 7: 185–189.
- Dong, K., Zhang, S., Wang, D. and Yao, X. Hydrogen bonds in imidazolium ionic liquids. *Journal of Physical Chemistry A* 2006; 110: 9775–9782.
- Drew, H.R. and Dickerson, R.E. Structure of a B-DNA dodecamer. III. Geometry of hydration. *Journal of Molecular Biology* 1981; 151: 535–556.
- Dupont, J., Consorti, C.S., Suarez, P.A.Z. and de Souza, R.F. Preparation of 1-butyl-3-methylimidazolium-based room temperature ionic liquids. *Organic Syntheses* 2004; 10: 184–189.
- Dzyuba, S.V. and Bartsch, R.A. Influence of structural variations in 1-alkyl(aralkyl)-3-methylimidazolium hexafluorophosphates and bis(trifluoromethylsulfonyl)imides on physical properties of the ionic liquids. *ChemPhysChem* 2002; 3: 161–166.
- Edwards, G.S., Davis, C.C., Saffer, J.D. and Swicord, M.L. Resonant microwave absorption of selected DNA molecules. *Physical Review Letters* 1984; 53: 1284–1287.
- Egli, M., Tereshko, V., Teplova, M., Minasov, G., Joachimiak, A., Sanishvili, R., Weeks, C.M., Miller, R., Maier, M.A. and An, H. X-ray crystallographic analysis of the hydration of A- and B-form DNA at atomic resolution. *Biopolymers* 1998; 48: 234–252.
- Elcock, A.H. and Richards, W.G. Relative hydration free energies of nucleic acid bases. *Journal of the American Chemical Society* 1993; 115: 7930–7931.
- Ellis, B., Keim, W. and Wasserscheid, P. Linear dimerisation of but-1-ene in biphasic mode using buffered chloroaluminate ionic liquid solvents. *Chemical Communications* 1999; 337–338.
- Erkkila, K.E., Odom, D.T. and Barton, J.K. Recognition and reaction of metallointercalators with DNA. *Chemical Reviews* 1999; 99: 2777–2795.

- Essmann, U., Perera, L., Berkowitz, M.L., Darden, T., Lee, H. and Pedersen, L.G. A smooth particle mesh Ewald method. *The Journal of Chemical Physics* 1995; 103: 8577–8593.
- Every, H.A., Bishop, A.G., MacFarlane, D.R., Orädd, G. and Forsyth, M. Transport properties in a family of dialkylimidazolium ionic liquids. *Physical Chemistry Chemical Physics* 2004; 6: 1758–1765.
- Fioroni, M., Burger, K., Mark, A.E. and Roccatano, D. A new 2,2,2-trifluoroethanol model for molecular dynamics simulations. *Journal of Physical Chemistry B* 2000; 104: 12347–12354.
- Foloppe, N. and MacKerell Jr., A.D. All-atom empirical force field for nucleic acids: I. Parameter optimization based on small molecule and condensed phase macromolecular target data. *Journal of Computational Chemistry* 2000; 21: 86–104.
- Fox, D.M., Awad, W.H., Gilman, J.W., Maupin, P.H., De Long, H.C. and Trulove, P.C. Flammability, thermal stability, and phase change characteristics of several trialkylimidazolium salts. *Green Chemistry* 2003; 5: 724–727.
- Fredlake, C.P., Crosthwaite, J.M., Hert, D.G., Aki, S.N.V.K. and Brennecke, J.F. Thermophysical properties of imidazolium-based ionic liquids. *Journal of Chemical & Engineering Data* 2004; 49: 954–964.
- Friedman, A.E., Chambron, J.-C., Sauvage, J.-P., Turro, N.J. and Barton, J.K. Molecular "light switch" for DNA: $\text{Ru}(\text{bpy})_2(\text{dppz})^{2+}$. *Journal of the American Chemical Society* 1990; 112: 4960–4962.
- Fujita, K., MacFarlane, D.R. and Forsyth, M. Protein solubilising and stabilising ionic liquids. *Chemical Communications* 2005; 4804–4806.
- Fujita, K., MacFarlane, D.R., Forsyth, M., Yoshizawa-Fujita, M., Murata, K., Nakamura, N. and Ohno, H. Solubility and stability of cytochrome in hydrated ionic liquids: Effect of oxo acid residues and kosmotropicity. *Biomacromolecules* 2007; 8: 2080–2086.

- Fuller, J., Carlin, R.T., De Long, H.C. and Haworth, D. Structure of 1-ethyl-3-methylimidazolium hexafluorophosphate: Model for room temperature molten salts. *Journal of the Chemical Society, Chemical Communications* 1994; 299–300.
- Gao, J. The hydration and solvent polarization effects of nucleotide bases. *Biophysical Chemistry* 1994; 51: 253–261.
- Garbett, N.C., Hammond, N.B. and Graves, D.E. Influence of the amino substituents in the interaction of ethidium bromide with DNA. *Biophysical Journal* 2004; 87: 3974–3981.
- Goodsell, D.S. Refinement of Netropsin bound to DNA: Bias and feedback in electron density map interpretation. *Biochemistry* 1995; 34: 4983–4993.
- Gordon, C.M., Holbrey, J.D., Kennedy, A.R. and Seddon, K.R. Ionic liquid crystals: Hexafluorophosphate salts. *Journal of Materials Chemistry* 1998; 8: 2627–2636.
- Gordon, C.M., in ionic liquids in synthesis; Wasserscheid, P. and Welton, T., eds.; Wiley-VCH, Weinheim, Germany, 2003.
- Gorke, J., Srienc, F. and Kazlauskas, R. Toward advanced ionic liquids. Polar, enzyme-friendly solvents for biocatalysis. *Biotechnology and Bioprocess Engineering* 2010; 15: 40–53.
- Gundertofte, K., Liljefors, T., Norrby, P.-O. and Pettersson, I. A comparison of conformational energies calculated by several molecular mechanics methods. *Journal of Computational Chemistry* 1996; 17: 429–449.
- Guo, C., Song, Y., Wei, H., Li, P., Wang, L., Sun, L., Sun, Y. and Li, Z. Room temperature ionic liquid doped DNA network immobilized horseradish peroxidase biosensor for amperometric determination of hydrogen peroxide. *Analytical and Bioanalytical Chemistry* 2007; 389: 527–532.
- Hammouda, B. and Worcester, D. The denaturation transition of DNA in mixed solvents. *Biophysical Journal* 2006; 91: 2237–2242.

- Hammouda, B. Insight into the denaturation transition of DNA. *International Journal of Biological Macromolecules* 2009; 45: 532–534.
- Han, X. and Armstrong, D.W. Ionic liquids in separations. *Accounts of Chemical Research* 2007; 40: 1079–1086.
- Hanke, C.G., Price, S.L. and Lynden-Bell, R.M. Intermolecular potentials for simulations of liquid imidazolium salts. *Molecular Physics* 2001; 99: 801–809.
- Hardacre, C., Holbrey, J.D., McMath, S.E.J., Bowron, D.T. and Soper, A.K. Structure of molten 1,3-dimethylimidazolium chloride using neutron diffraction. *Journal of Chemical Physics* 2003a; 118: 273–278.
- Hardacre, C., Hunt, P. A., Maginn, E. J., Lynden-Bell, R. M., Richter, J., Leuchter, A., Palmer, G., Dölle, A., Wahlbeck, P. G. and Carper, W. R. Molecular structure and dynamics, in *Ionic Liquids in Synthesis, Second Edition* (eds P. Wasserscheid and T. Welton), 2008, Wiley-VCH Verlag GmbH & Co. KGaA, Weinheim, Germany. DOI: 10.1002/9783527621194.ch4
- Hardacre, C., McMath, S.E.J., Nieuwenhuyzen, M., Bowron, D.T. and Soper, A.K. Liquid structure of 1,3-dimethylimidazolium salts. *Journal of Physics Condensed Matter* 2003b; 15: S159–S166.
- He, Y., Li, Z., Simone, P. and Lodge, T.P. Self-assembly of block copolymer micelles in an ionic liquid. *Journal of the American Chemical Society* 2006; 128: 2745–2750.
- Headley, A.D. and Jackson, N.M. The effect of the anion on the chemical shifts of the aromatic hydrogen atoms of liquid 1-butyl-3-methylimidazolium salts. *Journal of Physical Organic Chemistry* 2002; 15: 52–55.
- Herfort, M. and Schneider, H. Spectroscopic studies of the solvent polarities of room-temperature liquid ethylammonium nitrate and its mixtures with polar solvents. *Liebigs Annalen der Chemie* 1991; 1: 27–31.
- Herskovits, T.T and Harrington, J.P. Solution studies of the nucleic acid bases and related model compounds. Solubility in aqueous alcohol and glycol solutions. *Biochemistry* 1972; 11: 4800–4811.

- Hess, B. Determining the shear viscosity of model liquids from molecular dynamics simulations. *The Journal of Chemical Physics* 2002; 116: 209–217.
- Hess, B., Bekker, H., Berendsen, H.J.C. and Fraaije, J.G.E.M. LINCS: A linear constraint solver for molecular simulations. *Journal of Computational Chemistry* 1997; 18: 1463–1472.
- Hess, B., Kutzner, C., van Der Spoel, D. and Lindahl, E. GRGMACS 4: Algorithms for highly efficient, load-balanced, and scalable molecular simulation. *Journal of Chemical Theory and Computation* 2008; 4: 435–447.
- Holbrey, J.D. and Seddon, K.R. The phase behaviour of 1-alkyl-3-methylimidazolium tetrafluoroborates: Ionic liquids and ionic liquid crystals. *Journal of the Chemical Society - Dalton Transactions* 1999: 2133–2139.
- Huddleston, J.G., Visser, A.E., Reichert, W.M., Willauer, H.D., Broker, G.A. and Rogers, R.D. Characterization and comparison of hydrophilic and hydrophobic room temperature ionic liquids incorporating the imidazolium cation. *Green Chemistry* 2001; 3: 156–164.
- Jiang, Y-Y., Wang, G-N., Zhou, Z., Wu, Y-T., Geng, J. and Zhang, Z-B. Tetraalkylammonium amino acids as functionalized ionic liquids of low viscosity. *Chemical Communications* 2008: 505–507.
- Jobling, M.A and Gill, P. Encoded evidence: DNA in forensic analysis. *Nature Reviews Genetics* 2004; 5: 739–751.
- Johnson, W.C. Circular dichroism: Principles and applications, 2nd ed. (Eds.: N. Berova, K. Nakanishi, R. W. Woody), Wiley, New York, 2000.
- Jordan, C.F., Lerman, L.S. and Venable, J.H. Structure and circular dichroism of DNA in concentrated polymer solutions. *Nature: New Biology* 1972; 236: 67–70.
- Jorgensen, W.L. Optimized intermolecular potential functions for liquid alcohols. *Journal of Physical Chemistry* 1986; 90: 1276–1284.

- Jorgensen, W.L., Maxwell, D.S. and Tirado-Rives, J. Development and testing of the OPLS all-atom force field on conformational energetics and properties of organic liquids. *Journal of the American Chemical Society* 1996; 118: 11225–11236.
- Ke, F. Luu, Y.K. Hadjiargyrou, M. and Liang, D. Characterizing DNA condensation and conformational changes in organic solvents. *PLoS One* 2010, 11, No. e13308.
- Kioupis, L.I., Arya, G. and Maginn, E.J. Pressure-enthalpy driven molecular dynamics for thermodynamic property calculation II: Applications. *Fluid Phase Equilibria* 2002; 200: 93–110.
- Korolev, N., Lyubartsev, A.P., Laaksonen, A. and Nordenskiöld, L. A molecular dynamics simulation study of oriented DNA with polyamine and sodium counterions: diffusion and averaged binding of water and cations. *Nucleic Acids Research* 2003; 31: 5971–5981.
- Kowsari, M.H., Alavi, S., Ashrafizaadeh, M. and Najafi, B. Molecular dynamics simulation of imidazolium-based ionic liquids. I. Dynamics and diffusion. *Journal of Chemical Physics* 2008; 129: 224508.
- Krishnan, Y. and Simmel, F.C. Nucleic Acid Based Molecular Devices. *Angewandte Chemie International Edition* 2011; 50: 3124–3156.
- Kulschewski, T. and Pleiss, J. A molecular dynamics study of liquid aliphatic alcohols: Simulation of density and self-diffusion coefficient using a modified OPLS force field. *Molecular Simulation* 2013; 39: 754–767.
- Kutzler, M.A. and Weiner, D.B. DNA vaccines: ready for prime time?. *Nature Reviews Genetics* 2008; 9: 776–788.
- Leach, A.R. *Molecular Modelling: Principles and Applications*, 2nd Ed., Prentice Hall, New York, 2001.
- Lee, C., Yang, W. and Parr, R.G. Development of the Colle-Salvetti correlation-energy formula into a functional of the electron density. *Physical Review B* 1988; 37: 785–789.

- Leone, A.M., Weatherly, S.C., Williams, M.E., Thorp, H.H. and Murray, R.W. An ionic liquid form of DNA: Redox-active molten salts of nucleic acids. *Journal of the American Chemical Society* 2001; 123: 218–222.
- Lerman, L.S. Structural considerations in the interaction of DNA and acridines. *Journal of Molecular Biology* 1961; 3: 18–30.
- Lerman, L.S. The structure of the DNA-acridine complex. *Proceedings of the National Academy of Sciences of the United States of America* 1963; 49: 94–102.
- Lide, D.R. CRC Handbook of Chemistry and Physics, 73th Ed, CRC Press, 1992, Boca Raton.
- Lindahl, T. and Nyberg, B. Rate of depurination of native deoxyribonucleic acid. *Biochemistry* 1972; 11: 3610–3618.
- Liu, X., Zhang, S., Zhou, G., Wu, G. Yuan, X. and Yao, X. New force field for molecular simulation of guanidinium-based ionic liquids. *Journal of Physical Chemistry B* 2006; 110: 12062–12071.
- Liu, X., Zhou, G. and Zhang, S. Molecular dynamics simulation of acyclic guanidinium-based ionic liquids. *Fluid Phase Equilibria* 2008; 272: 1–7.
- Liu, Z., Chen, T., Bell, A. and Smit, B. Improved united-atom force field for 1-alkyl-3-methylimidazolium chloride. *Journal of Physical Chemistry B* 2010; 114: 4572–4582.
- Liu, Z., Huang, S. and Wang, W. A refined force field for molecular simulation of imidazolium-based ionic liquids. *Journal of Physical Chemistry B* 2004; 108: 12978–12989.
- Long, E.C. and Barton, J.K. On demonstrating DNA intercalation. *Accounts of Chemical Research* 1990; 23: 271–273.
- Lopes, J.N.C, Costa Gomes, M.F. and Pádua, A.A.H. Nonpolar, polar, and associating solutes in ionic liquids. *Journal of Physical Chemistry B* 2006; 110: 16816–16818.
- Lopes, J.N.C, Deschamps, J. and Pádua, A.A.H. Modeling ionic liquids using a systematic all-atom force field. *Journal of Physical Chemistry B* 2004; 108: 2038–2047.

- Lopes, J.N.C. and Pádua, A.A.H. Molecular force field for ionic liquids III: Imidazolium, pyridinium, and phosphonium cations; chloride, bromide, and dicyanamide anions. *Journal of Physical Chemistry B* 2006a; 110: 19586–19592.
- Lopes, J.N.C. and Pádua, A.A.H. Molecular force field for ionic liquids composed of triflate or bistriflylimide anions. *Journal of Physical Chemistry B* 2004; 108: 16893–16898.
- Lopes, J.N.C. and Pádua, A.A.H. Nanostructural organization in ionic liquids. *Journal of Physical Chemistry B* 2006b; 110: 3330–3335.
- Lukin, M. and de los Santos, C. NMR structures of damaged DNA. *Chemical Reviews* 2006; 106: 607–686.
- Luque, F.J., Alhambra, C. and Orozco, M. Effect of solvent polarization on bimolecular interactions. *Journal of Physical Chemistry* 1995a; 99: 11344–11349.
- Luque, F.J., Gadre, S.R., Bhadane, P.K. and Orozco, M. The effect of hydration on the molecular charge distribution of cations. An *ab initio* SCRF study. *Chemical Physics Letters* 1995b; 232: 509–517.
- Luque, F.J., Orozco, M., Bhadane, P.K. and Gadre, S.R. Effect of solvation on the shapes, sizes, and anisotropies of polyatomic anions via molecular electrostatic potential topography: An *ab initio* self-consistent reaction field approach. *Journal of Chemical Physics* 1994; 100: 6718–6728.
- MacFarlane, D.R., Pringle, J.M., Johanson, K.M., Forsyth, S.A. and Forsyth, M. Lewis base ionic liquids. *Chemical Communications* 2006: 1905–1917.
- MacKerell Jr., A.D., Bashford, D., Bellott, M., Dunbrack Jr., R.L., Evanseck, J.D., Field, M.J., Fischer, S., Gao, J., Guo, H., Ha, S., Joseph-McCarthy, D., Kuchnir, L., Kuczera, K., Lau, F.T.K., Mattos, C., Michnick, S., Ngo, T., Nguyen, D.T., Prodhom, B., Reiher III, W.E., Roux, B., Schlenkrich, M., Smith, J.C., Stote, R., Straub, J., Watanabe, M., Wiórkiewicz-Kuczera, J., Yin, D. and Karplus, M. All-atom empirical potential for molecular modeling and dynamics studies of proteins. *Journal of Physical Chemistry B* 1998; 102: 3586–3616.

- Margulis, C.J. Computational study of imidazolium-based ionic solvents with alkyl substituents of different lengths. *Molecular Physics* 2004; 102: 829–838.
- Margulis, C.J., Stern, H.A. and Berne, B.J. Computer simulation of a "green chemistry" room-temperature ionic solvent. *Journal of Physical Chemistry B* 2002; 106: 12017–12021.
- Marmur, J. and Doty, P. Determination of the base composition of deoxyribonucleic acid from its thermal denaturation temperature. *Journal of Molecular Biology* 1962; 5: 109–118.
- Martinez, L., Andrade, R., Birgin, E.G. and Martínez, J.M. PACKMOL: A package for building initial configurations for molecular dynamics simulations. *Journal of Computational Chemistry* 2009; 30: 2157–2164.
- Matsumoto, M., Mochiduki, K. and Kondo, K. Toxicity of ionic liquids and organic solvents to lactic acid-producing bacteria. *Journal of Bioscience and Bioengineering* 2004; 98: 344–347.
- Meng, Z., Dolle, A. and Carper, W.R. Gas phase model of an ionic liquid: semi-empirical and *ab initio* bonding and molecular structure. *Journal Molecular Structure - Thermochem* 2002; 585:119–128.
- Mestres, J., Solà, M., Carbó, R., Luque, F.J. and Orozco, M. Effect of solvation on the charge distribution of a series of anionic, neutral, and cationic species. A quantum molecular similarity study. *Journal of Physical Chemistry* 1996; 100: 606–610.
- Micaelo, N.M., Baptists, A.M. and Soares, C.M. Parameterization of 1-butyl-3-methylimidazolium hexafluorophosphate/nitrate ionic liquid for the GROMOS force field. *Journal of Physical Chemistry B* 2006; 110: 14444–14451.
- Miller, J.L. and Kollman, P.A. Solvation free energies of the nucleic acid bases. *Journal of Physical Chemistry* 1996; 100: 8587–8594.
- Mohan, V., Davis, M.E., McCammon, J.A. and Pettitt, B.M. Continuum model calculations of solvation free energies: Accurate evaluation of electrostatic contributions. *Journal of Physical Chemistry* 1992; 96: 6428–431.

- Monajjemi, M., Ketabi, S., Hashemian Zadeh, M. and Amiri, A. Simulation of DNA bases in water: Comparison of the Monte Carlo algorithm with molecular mechanics force fields. *Biochemistry (Moscow)* 2006; 71: S1–S8.
- Montesi, A. Pasquali, M. and MacKintosh, F.C. Collapse of a semiflexible polymer in poor solvent. *Physical Review E* 2004, 69, 021916-1-021916-10.
- Morrow, T.I. and Maginn, E.J. Erratum: Molecular dynamics study of the ionic liquid 1-n-butyl-3-methylimidazolium hexafluorophosphate (*Journal of Physical Chemistry B* 2002; 106: 12807-12813). *Journal of Physical Chemistry B* 2003; 107: 9160.
- Morrow, T.I. and Maginn, E.J. Molecular dynamics study of the ionic liquid 1-n-butyl-3-methylimidazolium hexafluorophosphate. *Journal of Physical Chemistry B* 2002; 106: 12807–12813.
- Mou, Z., Li, P., Bu, Y., Wang, W., Shi, J. and Song, R. Investigations of coupling characters in ionic liquids formed between the 1-ethyl-3-methylimidazolium cation and the glycine anion. *Journal of Physical Chemistry B* 2008; 112: 5088–5097.
- Muller, D. Hofer, B. Koch, A. and Koester, H. Aspects of the mechanism of acid-phenol extraction of nucleic acids. *BBA - Gene Structure and Expression* 1983; 740: 1–7.
- Muldoon, M.J., Gordon, C.M. and Dunkin, I.R. Investigations of solvent–solute interactions in room temperature ionic liquids using solvatochromic dyes. *Journal of the Chemical Society, Perkin Transactions 2* 2001; 433–435.
- Ngo, H.L., Le Compte, K., Hargens, L. and McEwen, A.B. Thermal properties of imidazolium ionic liquids. *Thermochimica Acta* 2000; 357-358: 97–102.
- Nishimura, N. and Ohno, H. Design of successive ion conduction paths in DNA films with ionic liquids. *Journal of Materials Chemistry* 2002; 12: 2299–2304.
- Nishimura, N., Nomura, Y., Nakamura, N. and Ohno, H. DNA strands robed with ionic liquid moiety. *Biomaterials* 2005; 26: 5558–5563.

- Ohno, H. and Nishimura, N. Ion conductive characteristics of DNA film containing ionic liquids. *Journal of the Electrochemical Society* 2001; 148: E168–E170.
- Oostenbrink, C., Villa, A., Mark, A.E. and Van Gunsteren, W.F. A biomolecular force field based on the free enthalpy of hydration and solvation: The GROMOS force-field parameter sets 53A5 and 53A6. *Journal of Computational Chemistry* 2004; 25: 1656–1676.
- Orozco, M. and Luque, F.J. Self-consistent reaction field computation of the reactive characteristics of DNA bases in water. *Biopolymers* 1993; 33: 1851–1869.
- Orozco, M., Colominas, C. and Luque, F.J. Theoretical determination of the solvation free energy in water and chloroform of the nucleic acid bases. *Chemical Physics* 1996; 209: 19–29.
- Perdew, J.P., Chevary, J.A., Vosko, S.H., Jackson, K.A., Pederson, M.R., Singh, D.J. and Fiolhais, C. Atoms, molecules, solids, and surfaces: Applications of the generalized gradient approximation for exchange and correlation. *Physical Review B* 1992; 46: 6671–6687.
- Pereiro, A.B., Legido, J.L. and Rodríguez, A. Physical properties of ionic liquids based on 1-alkyl-3-methylimidazolium cation and hexafluorophosphate as anion and temperature dependence. *Journal of Chemical Thermodynamics* 2007; 39: 1168–1175.
- Pérez, A., Marchán, I., Svozil, D., Spöner, J., Cheatham III, T.E., Loughton, C.A. and Orozco, M. Refinement of the AMBER force field for nucleic acids: Improving the description of α/γ conformers. *Biophysical Journal* 2007; 92: 3817–3829.
- Pomaville, R.M. and Poole, C.F. Gas chromatographic study of the solution thermodynamics of organic solutes in tetraalkylammonium alkanesulfonate and perfluoroalkanesulfonate solvents. *Journal of Chromatography A* 1990; 499: 749–759.
- Pringle, J.M., Golding, J., Baranyai, K., Forsyth, C.M., Deacon, G.B., Scott, J.L. and MacFarlane, D.R. The effect of anion fluorination in ionic liquids - physical properties of a range

- of bis(methanesulfonyl)amide salts. *New Journal of Chemistry* 2003; 27: 1504–1510.
- Pullman, A. and Pullman, B. Molecular electrostatic potential of the nucleic acids. *Quarterly Reviews of Biophysics* 1981; 14: 289–380.
- Qin, W. and Li, S.F.Y. Electrophoresis of DNA in ionic liquid coated capillary. *Analyst* 2003; 128: 37–41.
- Raabe, G. and Köhler, J. Thermodynamical and structural properties of imidazolium based ionic liquids from molecular simulation. *Journal of Chemical Physics* 2008; 128: art. no. 154509.
- Reichmann, M.E., Rice, S.A., Thomas, C.A. and Doty, P. A further examination of the molecular weight and size of desoxyribose nucleic acid. *Journal of the American Chemical Society* 1954; 76: 3047–3053.
- Rodríguez-Pulido, A., Ortega, F., Llorca, O., Aicart, E. and Junquera, E. A physicochemical characterization of the interaction between DC-Chol/DOPE cationic liposomes and pDNA. *Journal of Physical Chemistry B* 2008; 112: 12555–12565.
- Rozenberg, H., Rabinovich, D., Frolow, F., Hegde, R.S. and Shakked, Z. Structural code for DNA recognition revealed in crystal structures of papillomavirus E2-DNA targets. *Proceedings of the National Academy of Sciences of the United States of America* 1998; 95: 15194–15199.
- Saenger, W. Structure and dynamics of water surrounding biomolecules. *Annual Review of Biophysics and Biophysical Chemistry* 1987; 16: 93–114.
- Sasaki, Y., Miyoshi, D. and Sugimoto, N. Regulation of DNA nucleases by molecular crowding. *Nucleic Acids Research* 2007, 35, 4086–4093.
- Satyanarayana, S., Dabrowiak, J.C. and Chaires, J.B. Tris(phenanthroline)ruthenium(II) enantiomer interactions with DNA: mode and specificity of binding. *Biochemistry* 1993; 32: 2573–2584.

- Schmidt, M.W., Baldrige, K.K., Boatz, J.A., Elbert, S.T., Gordon, M.S., Jensen, J.H., Koseki, S., Matsunaga, N., Nguyen, K.A., Su, S.J., Windus, T.L., Dupuis, M. and Montgomery, J.A. General atomic and molecular electronic structure system. *Journal of Computational Chemistry* 1993; 14: 1347–1363.
- Schneider, B., Patel, K. and Berman, H.M. Hydration of the phosphate group in double-helical DNA. *Biophysical Journal* 1998; 75: 2422–2434.
- Seddon, K.R., Stark, A. and Torres, M.-J. Influence of chloride, water, and organic solvents on the physical properties of ionic liquids. *Pure and Applied Chemistry* 2000; 72: 2275–2287.
- Shah, J.K., Brennecke, J.F. and Maginn, E.J. Thermodynamic properties of the ionic liquid 1-n-butyl-3-methylimidazolium hexafluorophosphate from Monte Carlo simulations. *Green Chemistry* 2002; 4: 112–118.
- Shimizu, K., Pádua, A.A.H. and Lopes, J.N.C. Nanostructure of trialkylmethylammonium bistriflamide ionic liquids studied by molecular dynamics. *Journal of Physical Chemistry B* 2010; 114: 15635–15641.
- Sines, C.C., McFail-Isom, L., Howerton, S.B., VanDerveer, D. and Williams, L.D. Cations mediate B-DNA conformational heterogeneity. *Journal of the American Chemical Society* 2000; 122: 11048–11056.
- Sinha, R., Islam, Md. M., Bhadra, K., Kumar, G.S., Banerjee, A. and Maiti, M. The binding of DNA intercalating and non-intercalating compounds to A-form and protonated form of poly(rC)-poly(rG): Spectroscopic and viscometric study. *Bioorganic and Medicinal Chemistry* 2006; 14: 800–814.
- Sirjoosingh, A., Alavi, S. and Woo, T.K. Molecular dynamics simulations of equilibrium and transport properties of amino acid-based room temperature ionic liquids. *Journal of Physical Chemistry B* 2009; 113: 8103–8113.
- Sun, H., Qiao, B., Zhang, D., Liu, C. Structure of 1-butylpyridinium tetrafluoroborate ionic liquid: Quantum chemistry and molecular dynamic simulation studies. *Journal of Physical Chemistry A* 2010; 114: 3990–3996.

- Sun, W., Li, Y., Duan, Y. and Jiao, K. Direct electrocatalytic oxidation of adenine and guanine on carbon ionic liquid electrode and the simultaneous determination. *Biosensors and Bioelectronics* 2008a; 24: 988–993.
- Sun, W., Li, Y., Yang, M., Liu, S. and Jiao, K. Direct electrochemistry of single-stranded DNA on an ionic liquid modified carbon paste electrode. *Electrochemistry Communications* 2008b; 10: 298–301.
- Swartling, D., Ray, L., Compton, S. and Ensor, D. Temperature dependence of viscosity for room temperature ionic liquids. *Bulletin Biochemistry and Biotechnology* 2000; 13: 145–151.
- Szefczyk, B. and Cordeiro, M.N.D.S. Physical properties at the base for the development of an all-atom force field for ethylene glycol. *Journal of Physical Chemistry B* 2011; 115: 3013–3019.
- Takahashi, S., Suzuya, K., Kohara, S., Koura, N., Curtiss, L.A. and Saboungi, M.-L. Structure of 1-ethyl-3-methylimidazolium chloroaluminates: Neutron diffraction measurements and *ab initio* calculations. *Zeitschrift fur Physikalische Chemie* 1999; 209: 209–221.
- Texter, J. Nucleic acid-water interactions. *Progress in Biophysics and Molecular Biology* 1978; 33: 83–97.
- Tokuda, H., Hayamizu, K., Ishii, K., Susan, M.A.B.H. and Watanabe, M. Physicochemical properties and structures of room temperature ionic liquids. 2. Variation of alkyl chain length in imidazolium cation. *Journal of Physical Chemistry B* 2005; 109: 6103–6110.
- Tokuda, H., Hayamizu, K., Ishii, K., Susan, Md.A.B.H. and Watanabe, M. Physicochemical properties and structures of room temperature ionic liquids. 1. Variation of anionic species. *Journal of Physical Chemistry B* 2004; 108: 16593–16600.
- Tokuda, H., Ishii, K., Susan, M.A.B.H., Tsuzuki, S., Hayamizu, K. and Watanabe, M. Physicochemical properties and structures of room-temperature ionic liquids. 3. Variation of cationic structures. *Journal of Physical Chemistry B* 2006a; 110: 2833–2839.

- Tokuda, H., Tsuzuki, S., Susan, Md.A.B.H., Hayamizu, K. and Watanabe, M. How ionic are room-temperature ionic liquids? An indicator of the physicochemical properties. *Journal of Physical Chemistry B* 2006b; 110: 19593–19600.
- Umecky, T., Kanakubo, M. and Ikushima, Y. Effects of alkyl chain on transport properties in 1-alkyl-3-methylimidazolium hexafluorophosphates. *Journal of Molecular Liquids* 2005a; 119: 77–81.
- Umecky, T., Kanakubo, M. and Ikushima, Y. Self-diffusion coefficients of 1-butyl-3-methylimidazolium hexafluorophosphate with pulsed-field gradient spin-echo nmr technique. *Fluid Phase Equilibria* 2005b; 228-229: 329–333.
- Urahata, S.M. and Ribeiro, M.C.C. Single particle dynamics in ionic liquids of 1-alkyl-3-methylimidazolium cations. *Journal of Chemical Physics* 2005; 122: art. no. 024511.
- Urahata, S.M. and Ribeiro, M.C.C. Structure of ionic liquids of 1-alkyl-3-methylimidazolium cations: A systematic computer simulation study. *Journal of Chemical Physics* 2004; 120: 1855–1863.
- van Der Spoel, D., Lindahl, E., Hess, B., Groenhof, G., Mark, A.E. and Berendsen, H.J.C. GROMACS: Fast, flexible, and free. *Journal of Computational Chemistry* 2005; 26: 1701–1718.
- Vijayaraghavan, R., Izgorodin, A., Ganesh, V., Surianarayanan, M. and MacFarlane, D.R. Long-term structural and chemical stability of DNA in hydrated ionic liquids. *Angewandte Chemie - International Edition* 2010a; 49: 1631–1633.
- Vijayaraghavan, R., Thompson, B.C., MacFarlane, D.R., Kumar, R., Surianarayanan, M., Aishwarya, S. and Sehgal, P.K. Biocompatibility of choline salts as cross linking agents for collagen based biomaterials. *Chemical Communications* 2010b; 46: 294–296.
- Viswamitra, M.A., Kennard, O., Jones, P.G., Sheldrick, G.M., Salisbury, S., Favello, L., Shakked, Z. DNA double helical fragment at atomic resolution. *Nature* 1978, 273: 687–688.

- Walden, P. Molecular weights and electrical conductivity of several fused salts. *Bulletin of the Imperial Academy of Sciences (Saint Petersburg)* 1914; 1800: 405–422.
- Wang, H., Wang, J. and Zhang, S. Binding Gibbs energy of ionic liquids to calf thymus DNA: A fluorescence spectroscopy study. *Physical Chemistry Chemical Physics* 2011; 13: 3906–3910.
- Wang, J., Wang, H., Zhang, S., Zhang, H. and Zhao, Y. Conductivities, volumes, fluorescence, and aggregation behavior of ionic liquids [C₄mim][BF₄] and [C_nmim][Br] (*n* = 4, 6, 8, 10, 12) in aqueous solutions. *Journal of Physical Chemistry B* 2007b; 111: 6181–6188.
- Wang, J., Wolf, R.M., Caldwell, J.W., Kollman, P.A. and Case, D.A. Development and testing of a general AMBER force field. *Journal of Computational Chemistry* 2004; 25: 1157–1174.
- Wang, J.-H., Cheng, D.-H., Chen, X.-W., Du, Z. and Fang, Z.-L. Direct extraction of double-stranded DNA into ionic liquid 1-butyl-3-methylimidazolium hexafluorophosphate and its quantification. *Analytical Chemistry* 2007a; 79: 620–625.
- Wang, Y. and Voth, G.A. Unique spatial heterogeneity in ionic liquids. *Journal of the American Chemical Society* 2005; 127: 12192–12193.
- Wartell, R.M., Larson, J.E. and Wells, R.D. Netropsin. A specific probe for AT regions of duplex deoxyribonucleic acid. *Journal of Biological Chemistry* 1974; 249: 6719–6731.
- Wasserscheid, P. and Keim, W. Ionic liquids - New 'solutions' for transition metal catalysis. *Angewandte Chemie - International Edition* 2000; 39: 3773–3789.
- Wasserscheid, P. and Welton, T. *Ionic Liquids in Synthesis*, eds. Weinheim, Germany: Wiley-VCH, 2003.
- Westhof, E. Water: An Integral Part of Nucleic Acid Structure. *Annual Review of Biophysics and Biophysical Chemistry* 1988; 7: 125–144.
- Wilkes, J.S. and Zaworotko, M.J. Air and water stable 1-ethyl-3-methylimidazolium based ionic liquids. *Chemical Communications* 1992: 965–967.

- Wilkes, J.S., Levisky, J.A., Wilson, R.A. and Hussey, C.L. Dialkylimidazolium chloroaluminate melts: A new class of room-temperature ionic liquids for electrochemistry, spectroscopy and synthesis. *Inorganic Chemistry* 1982; 21: 1263–1264.
- Wu, Y. and Zhang, T. Structural and electronic properties of amino acid based ionic liquids: A theoretical study. *Journal of Physical Chemistry A* 2009; 113: 12995–13003.
- Xie, Y.N., Wang, S.F., Zhang, Z.L. and Pang, D.W. Interaction between room temperature ionic liquid [bmim]BF₄ and DNA investigated by electrochemical micromethod. *The Journal of Physical Chemistry B* 2008; 112: 9864–9868.
- Yan, T., Burnham, C.J., Del Pópolo, M.G. and Voth, G.A. Molecular dynamics simulation of ionic liquids: The effect of electronic polarizability. *Journal of Physical Chemistry B* 2004; 108: 11877–11881.
- Yi-Gui, G., Robinson, H. and Wang, A.H.-J. High-resolution A-DNA crystal structures of d(AGGGGCCCT) an A-DNA model of poly(dG) · poly(dC). *European Journal of Biochemistry* 1999; 261: 413–420.
- Young, P.E. and Hillier, I.H. Hydration free energies of nucleic acid bases using an *ab initio* continuum model. *Chemical Physics Letters* 1993; 215: 405–408.
- Zhang, W., Yang, T., Zhuang, X., Guo, Z. and Jiao, K. An ionic liquid supported CeO₂/nanoshuttles-carbon nanotubes composite as a platform for impedance DNA hybridization sensing. *Biosensors and Bioelectronics* 2009a; 24: 2417–2422.
- Zhang, Y., Chen, X., Lan, J., You, J. and Chen, L. Synthesis and biological applications of imidazolium-based polymerized ionic liquid as a gene delivery vector. *Chemical Biology and Drug Design* 2009b; 74: 282–288.

APPENDIX A1

Table A1. Non-bonded Parameters.

i	m/amu	q	σ (Å)	E (kJ mol ⁻¹)	Source
C1	14.027	0.386	3.50	0.27614	this work (q), OPLS (alkane ^a)
C2	14.027	0.000	3.50	0.27614	this work (q), OPLS (alkane ^a)
CS	14.027	0.000	3.50	0.27614	this work (q), OPLS (alkane ^a)
CT	15.035	0.000	3.50	0.27614	this work (q), OPLS (alkane ^a)
CR	12.011	-0.038	3.55	0.29288	this work (q), OPLS (HIP ^c) ^b
CW4	12.011	-0.158	3.55	0.29288	this work (q), OPLS (HIP ^c) ^b
CW5	12.011	-0.158	3.55	0.29288	this work (q), OPLS (HIP ^c) ^b
HAW4	1.008	0.241	2.42	0.12552	this work (q), OPLS (HIP ^c) ^b
HAW5	1.008	0.241	2.42	0.12552	this work (q), OPLS (HIP ^c) ^b
HAR	1.008	0.216	2.42	0.12552	this work (q), OPLS (HIP ^c) ^b
NA1	14.007	-0.058	3.25	0.71128	this work (q), OPLS (HIP ^c) ^b
NA3	14.007	-0.058	3.25	0.71128	this work (q), OPLS (HIP ^c) ^b
Br	79.904	-1.000	3.69	0.86000	this work (q) and σ

a) Jorgensen *et al.*, (1996); (b) Rizzo and Jorgensen, (1999); (c) HIP is the protonated histidine cation.

APPENDIX A2

Table A2. Bonds and angles parameters.

Bonds	r_{eq} (Å)	K_a (kJ mol ⁻¹)	Source
CR/CW-HA	1.080	constrained	OPLS imidazole ^e
CR-NA	1.315	3992	r_{eq}^d ; K_a from OPLS imidazole ^e
CW-NA	1.378	3574	r_{eq}^d ; K_a from OPLS imidazole ^e
CW-CW	1.341	4352	r_{eq}^d ; K_a from OPLS imidazole ^e
NA-C1	1.466	2820	r_{eq}^d ; K_a from OPLS imidazole ^e
C*-C*	1.529	2242	OPLS alkane ^a

Angles	θ_{eq} (deg)	K_a (kJ mol ⁻¹)	Source
CW-NA-CR	108.0	585.8	θ_{eq}^d ; K_a from OPLS imidazole ^e
CR-NA-C1	125.6	585.8	θ_{eq}^d ; K_a from OPLS imidazole ^e
CR-NA-C1	126.4	585.8	θ_{eq}^d ; K_a from OPLS imidazole ^e
NA-CR-HA	125.1	292.9	θ_{eq}^d ; K_a from OPLS imidazole ^e
NA-CR-NA	109.8	585.8	θ_{eq}^d ; K_a from OPLS imidazole ^e
NA-CW-CW	107.1	585.8	θ_{eq}^d ; K_a from OPLS imidazole ^e
NA-CW-HA	122.0	292.9	θ_{eq}^d ; K_a from OPLS imidazole ^e
CW-CW-HA	130.9	292.9	θ_{eq}^d ; K_a from OPLS imidazole ^e
NA/C*-C*-C*	112.7	488.3	OPLS alkane ^a

(a) Jorgensen *et al.*, (1996); (d) Lopes *et al.*, (2004); (e) McDonald and Jorgensen, (1998); C* represents a generic aliphatic carbon, C1, C2, CS, or CT.

APPENDIX A3

Table A3. Dihedral and improper dihedral parameters.

Dihedrals	Type	V1	V2	V3	V4	Source
CW-NA-CR-NA	cos3	0.0000	19.4600	0.0000	0.0000	d
CW-NA-CR-HA	cos3	0.0000	19.4600	0.0000	0.0000	d
CT-NA-CR-NA	cos3	0.0000	19.4600	0.0000	0.0000	d
CT-NA-CR-HA	cos3	0.0000	19.4600	0.0000	0.0000	d
CR-NA-CW-CW	cos3	0.0000	12.5500	0.0000	0.0000	d
CR-NA-CW-HA	cos3	0.0000	12.5500	0.0000	0.0000	d
C1-NA-CW-CW	cos3	0.0000	12.5500	0.0000	0.0000	d
C1-NA-CW-HA	cos3	0.0000	12.5500	0.0000	0.0000	d
NA-CW-CW-NA	cos3	0.0000	44.9800	0.0000	0.0000	d
NA-CW-CW-HA	cos3	0.0000	44.9800	0.0000	0.0000	d
HA-CW-CW-HA	cos3	0.0000	44.9800	0.0000	0.0000	d
CR-NA-C1-C2	cos3	-5.2691	0.0000	0.0000	0.0000	d
NA-C1-C2-CS	cos3	-7.4797	3.1642	-1.2026	0.0000	d
C*-C*-C*-C*	cos3	7.2800	-0.6569	1.1673	0.0000	d
^f CR-CW-NA-C1	cos3	0.0000	8.3700	0.0000	0.0000	d
^f NA-NA-CR-HA	cos3	0.0000	9.2000	0.0000	0.0000	d
^f NA-CW-CW-HA	cos3	0.0000	9.2000	0.0000	0.0000	d

(d) Lopes *et al.*, (2004); (f)improper parameters; C* represents a generic aliphatic carbon, C1, C2, CS, or CT.

APPENDIX B1

```
; Energy Minimization
; Steepest Descent Method
;
integrator          = steep
emtol              = 50.0
emstep            = 0.002
nstcgsteep        = 500
nsteps            = 5000
nstenergy         = 10
;
; Electrostatics and van der Waals
;
nstlist           = 5
ns_type          = grid
pbc              = xyz
rlist            = 1.2
coulombtype      = PME
rcoulomb         = 1.2
vdwtype         = cut-off
rvdw            = 1.2
constraints      = none
```

APPENDIX B2

```
; Energy minimization
; Conjugate Gradient Method
;
integrator          = cg
emtol              = 50.0
emstep            = 0.002
nstcgsteep        = 500
nsteps            = 5000
nstenergy         = 10
;
; Electrostatics and van der Waals
;
nstlist           = 5
ns_type          = grid
pbc              = xyz
rlist            = 1.2
coulombtype      = PME
rcoulomb         = 1.2
vdwtype         = cut-off
rvdw            = 1.2
constraints      = none
```

APPENDIX B3

```

integrator          = md          ; (NVT pre-equilibration)
dt                 = 0.002       ; ps integration time steps
nsteps             = 1000000
nstcomm           = 1
nstxtcout         = 500
xtc-precision     = 1000
nstxout           = 500
nstvout           = 100
nstfout           = 0
nstlog            = 500
nstenergy         = 500
nstlist           = 5           ; update every steps
ns_type           = grid
pbc               = xyz
rlist             = 1.2        ; neighbor searching
coulombtype       = PME        ; long-range electrostatic interaction
rcoulomb          = 1.2
vdwtype           = cut-off
rvdw              = 1.2
Tcoupl            = Berendsen
tc-grps           = system
tau_t             = 0.1        ; temperature coupling constant
ref_t             = 298.15     ; ref temperature
energygrps        = system
Pcoupl            = no
Pcoupltype        = isotropic
tau_p             = 2.0        ; relaxation time
compressibility    = 4.5e-5     ; isothermal compressibility
ref_p             = 1.0        ; ref pressure
;
gen_vel           = yes
gen_temp          = 298.15
gen_seed          = 173529
;
constraint_algorithm = LINCS
lincs_order       = 4
constraints       = none
;
fourierspacing    = 0.12      ; grid spacing
pme_order         = 4         ; order interpolation
ewald_rtol        = 1e-5
optimize_fft      = yes

```

APPENDIX B4

```
integrator      = md      ; (NPT production simulation)
dt             = 0.002      ; ps integration time steps
nsteps        = 5000000
nstcomm       = 1
nstxtcout     = 500
xtc-precision = 1000
nstxout       = 500
nstvout       = 100
nstfout       = 0
nstlog        = 500
nstenergy     = 500
nstlist       = 5          ; update every steps
ns_type       = grid
pbc           = xyz
rlist         = 1.2       ; neighbor searching
coulombtype   = PME      ; long-range electrostatic interaction
rcoulomb      = 1.2
vdwtype       = cut-off
rvdw          = 1.2
Tcoupl        = Berendsen
tc-grps       = system
tau_t         = 0.1       ; temperature coupling constant
ref_t         = 298.15    ; ref temperature
energygrps    = system
Pcoupl        = Berendsen
Pcoupltype    = isotropic
tau_p         = 2.0       ; relaxation time
compressibility = 4.5e-5  ; isothermal compressibility
ref_p         = 1.0       ; ref pressure
;
gen_vel       = no
gen_temp      = 298.15
gen_seed      = 173529
;
constraint_algorithm = LINCS
lincs_order   = 4
constraints   = none
;
fourierspacing = 0.12    ; grid spacing
pme_order     = 4        ; order interpolation
ewald_rtol    = 1e-5
optimize_fft   = yes
```


APPENDIX B5

```

integrator          = md      ;NVT non-equilibration for viscosity
dt                 = 0.002    ; ps integration time steps
nsteps             = 5000000
nstcomm            = 1
nstxtcout          = 500
xtc-precision      = 1000
nstxout            = 500
nstvout            = 100
nstfout            = 0
nstlog             = 500
nstenergy          = 500
nstlist            = 5        ; update every steps
ns_type            = grid
pbc                = xyz
rlist              = 1.2      ; neighbor searching
coulombtype        = PME      ;long-range electrostatic interaction
rcoulomb           = 1.2
vdwtype            = cut-off
rvdw               = 1.2
Tcoupl             = Berendsen
tc-grps            = system
tau_t              = 0.1      ; temperature coupling constant
ref_t              = 298.15   ; ref temperature
energygrps         = system
Pcoupl             = no
Pcoupltype         = isotropic
tau_p              = 2.0      ; relaxation time
compressibility     = 4.5e-5   ; isothermal compressibility
ref_p              = 1.0      ; ref pressure
gen_vel            = no
gen_temp           = 298.15
gen_seed           = 173529
constraint_algorithm = LINCS
lincs_order        = 4
constraints         = none
fourierspacing     = 0.12     ; grid spacing
pme_order          = 4        ; order interpolation
ewald_rtol         = 1e-5
optimize_fft       = yes
;
; Non-equilibrium MD
cos_acceleration   = 0.02

```

APPENDIX C1

```
; Energy Minimization
; Steepest Descent Method
;
integrator          = steep
emtol              = 50.0
emstep            = 0.002
nstcgsteep        = 500
nsteps            = 5000
nstenergy         = 10
;
; Electrostatics and van der Waals
;
nstlist           = 5
ns_type          = grid
pbc              = xyz
rlist            = 1.2
coulombtype      = PME
rcoulomb         = 1.2
vdwtype         = cut-off
rvdw            = 1.2
constraints      = none
;
; Free energy control stuff
;
free_energy      = yes
init_lambda     = 0.00
delta_lambda    = 0
foreign_lambda  = 0.05
sc-alpha        = 0.5
sc-power       = 2.0
sc-sigma       = 0.3
couple-moltype  = ADE ;name of moleculetype to decouple
couple-lambda0  = vdW-q ; only van der Waals interactions
couple-lambda1  = none ;turn off everything, in this case
only vdW
couple-intramol = no
nstdhdl        = 1
```

APPENDIX C2

```
; Energy Minimization
; Conjugate Gradient Method
;
integrator           = cg
emtol               = 50.0
emstep              = 0.002
nstcgsteep          = 500
nsteps              = 5000
nstenergy           = 10
;
; Electrostatics and van der Waals
;
nstlist              = 5
ns_type             = grid
pbc                  = xyz
rlist                = 1.2
coulombtype         = PME
rcoulomb             = 1.2
vdwtype              = cut-off
rvdw                 = 1.2
constraints          = none
;
; Free energy control stuff
;
free_energy          = yes
init_lambda          = 0.00
delta_lambda         = 0
foreign_lambda       = 0.05
sc-alpha             = 0.5
sc-power             = 2.0
sc-sigma             = 0.3
couple-moltype       = ADE ;name of moleculetype to decouple
couple-lambda0       = vdw-q ; only van der Waals interactions
couple-lambda1       = none ; turn off everything, in this case
only vdW
couple-intramol      = no
nstdhdl              = 1
```

APPENDIX C3

```
integrator          = sd          ; stochastic dynamics NVT
dt                 = 0.002        ; ps integration time steps
nsteps             = 50000        ; 100 ps
nstcomm            = 1
;
nstxtcout          = 500
xtc-precision      = 1000
nstxout            = 500
nstvout            = 100
nstfout            = 0
nstlog             = 500
nstenergy          = 500
;
nstlist            = 5            ; update every stpes
ns_type            = grid
pbc                = xyz
rlist              = 1.2         ; neighbor searching
;
coulombtype        = PME         ; long-range electrostatic interaction
rcoulomb           = 1.2
vdwtype            = cut-off
rvdw               = 1.2
;
; tcoupl is implicitly handled by the sd integrator
;
tc_grps            = system
tau_t              = 0.1
ref_t              = 298
;
DispCorr           = EnerPres
energygrps         = system
;
pcoupl             = no
pcoupltype         = isotropic
tau_p              = 2.0         ; relaxation time
compressibility    = 4.5e-5      ; isothermal compressibility
ref_p              = 1.0         ; ref pressure
;
gen_vel            = yes
gen_temp           = 298
gen_seed           = 173529
;
constraint_algorithm = LINCS
```

```

lincs_order          = 4
constraints          = all-bonds
;
fourierspacing      = 0.12          ; grid spacing
pme_order           = 4             ; order interpolation
ewald_rtol          = 1e-5
optimize_fft        = yes
;
; Free energy control stuff
;
free_energy          = yes
init_lambda         = 0.0
delta_lambda        = 0
foreign_lambda      = 0.05
sc-alpha            = 0.5
sc-power            = 2.0
sc-sigma           = 0.3
couple-moltype      = ADE          ; name of molecule type to decouple
couple-lambda0      = vdw-q        ; only van der Waals interactions
couple-lambda1      = none         ; turn off everything, in this case
only vdW
couple-intramol     = no
nstdhdl             = 1
;

```

APPENDIX C4

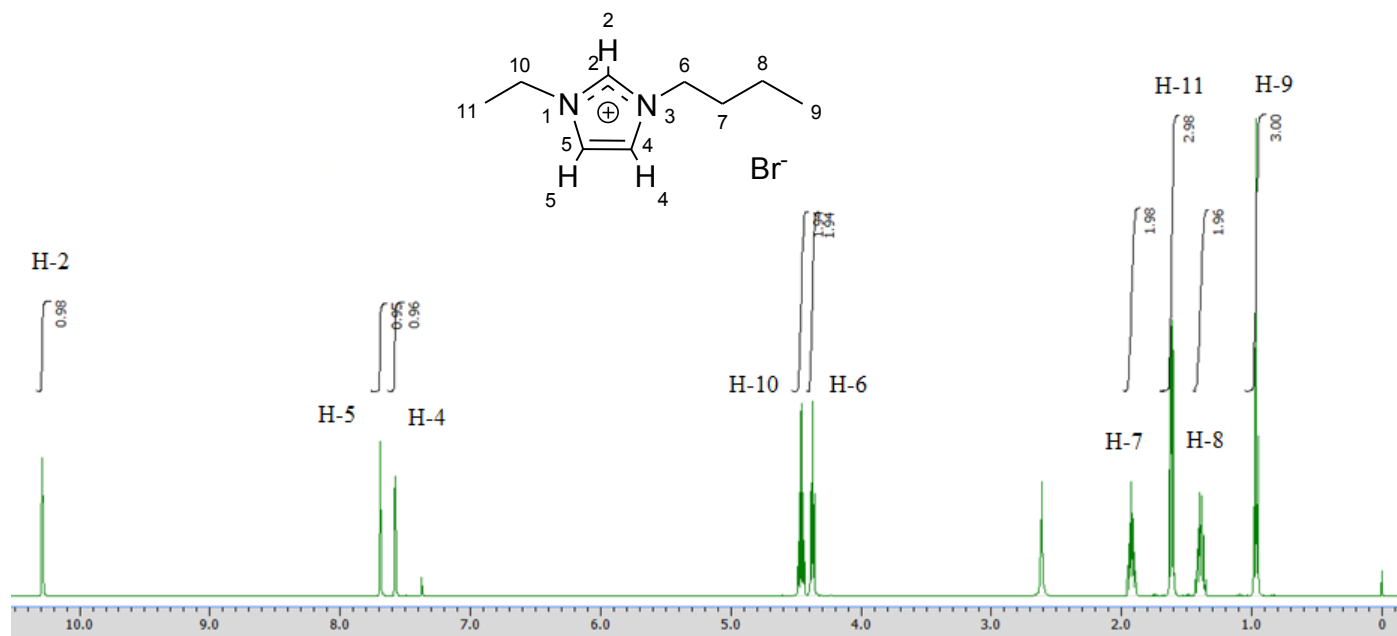
```
integrator          = sd          ; stochastic dynamics NPT
dt                 = 0.002        ; ps integration time steps
nsteps             = 1000000     ; 2 ns
nstcomm           = 1
;
nstxtcout          = 500
xtc-precision      = 1000
nstxout            = 500
nstvout            = 100
nstfout            = 0
nstlog             = 500
nstenergy          = 500
;
nstlist            = 5           ; update every stpes
ns_type            = grid
pbc                = xyz
rlist              = 1.2        ; neighbor searching
;
coulombtype        = PME         ; long-range electrostatic interaction
rcoulomb           = 1.2
vdwtype            = cut-off
rvdw               = 1.2
;
; tcoupl is implicitly handled by the sd integrator
;
tc_grps            = system
tau_t              = 0.1
ref_t              = 298
;
DispCorr           = EnerPres
energygrps         = system
;
pcoupl             = Berendsen
pcoupltype         = isotropic
tau_p              = 2.0        ; relaxation time
compressibility    = 4.5e-5     ; isothermal compressibility
ref_p              = 1.0        ; ref pressure
;
gen_vel            = no
gen_temp           = 298
gen_seed           = 173529
;
constraint_algorithm = LINCS
```

```

lincs_order          = 4
constraints          = all-bonds
;
fourierspacing      = 0.12          ; grid spacing
pme_order           = 4             ; order interpolation
ewald_rtol          = 1e-5
optimize_fft        = yes
;
; Free energy control stuff
;
free_energy         = yes
init_lambda         = 0.0
delta_lambda        = 0
foreign_lambda      = 0.05
sc-alpha            = 0.5
sc-power            = 2.0
sc-sigma            = 0.3
couple-moltype      = ADE          ; name of molecule type to decouple
couple-lambda0      = vdw-q        ; only van der Waals interactions
couple-lambda1      = none         ; turn off everything, in this case
only vdW
couple-intramol     = no
nstdhdl             = 1
;

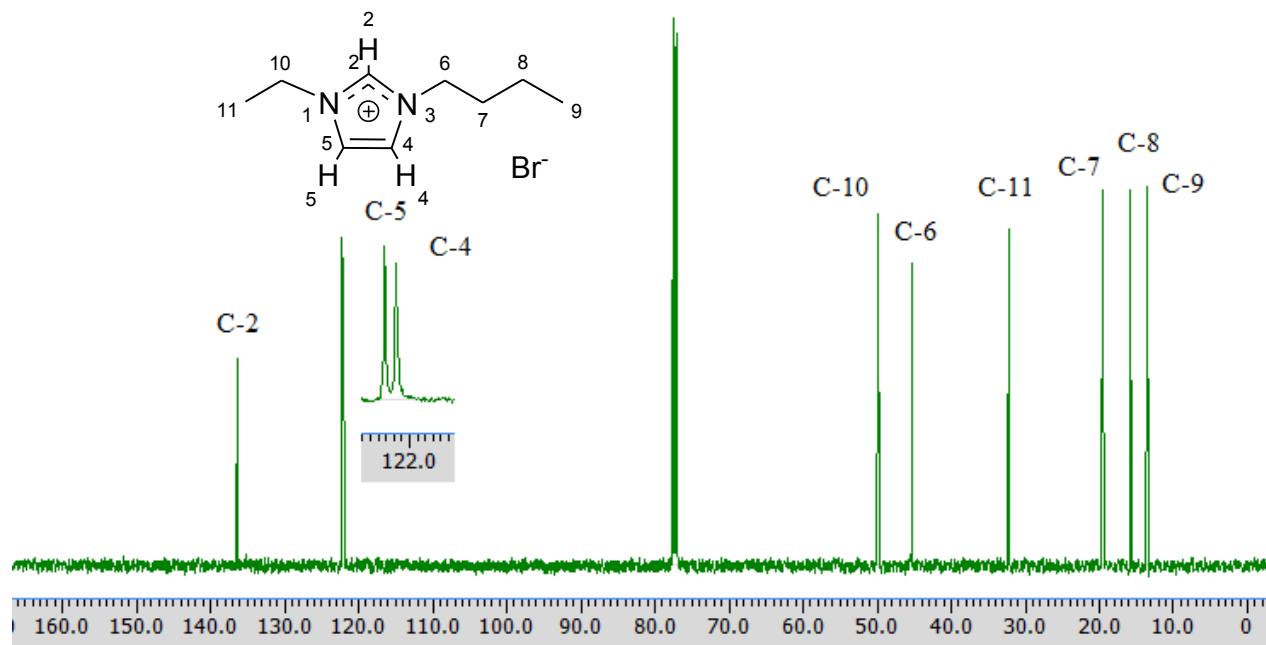
```

APPENDIX D1



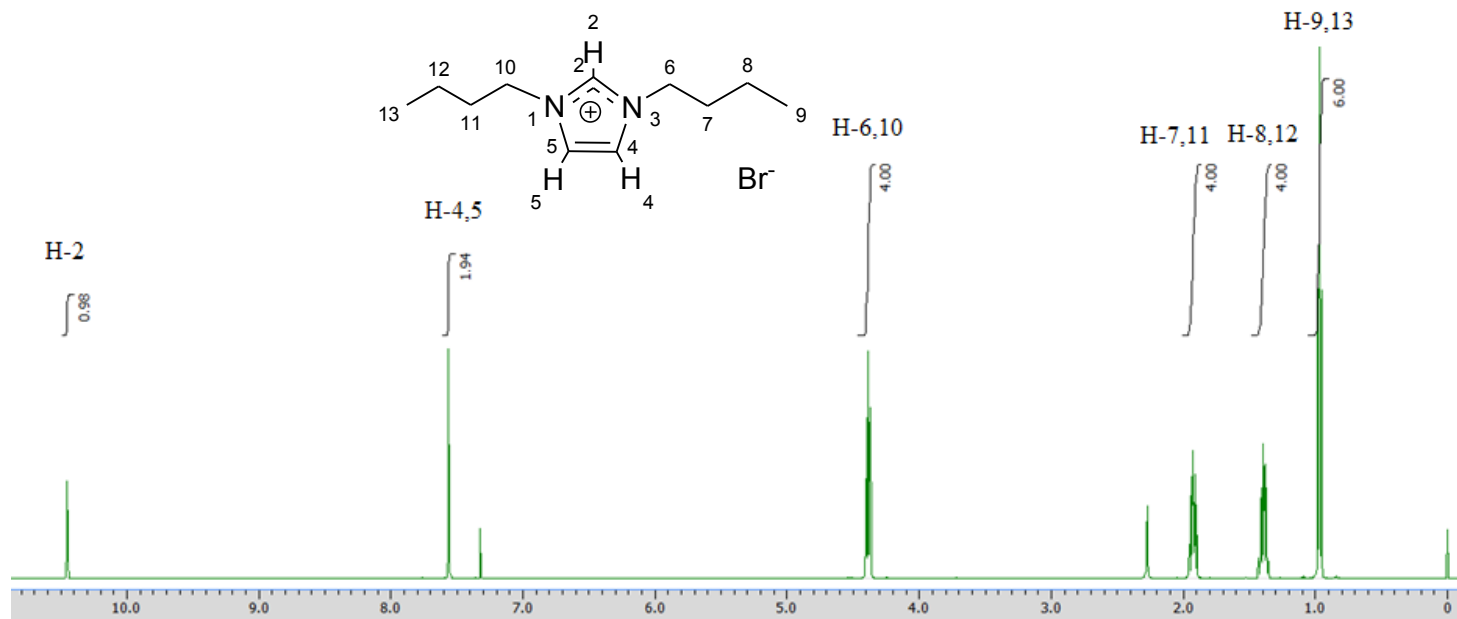
¹H NMR spectrum of 1-ethyl-3-butylimidazolium bromide ([C₂bim][Br])

APPENDIX D2



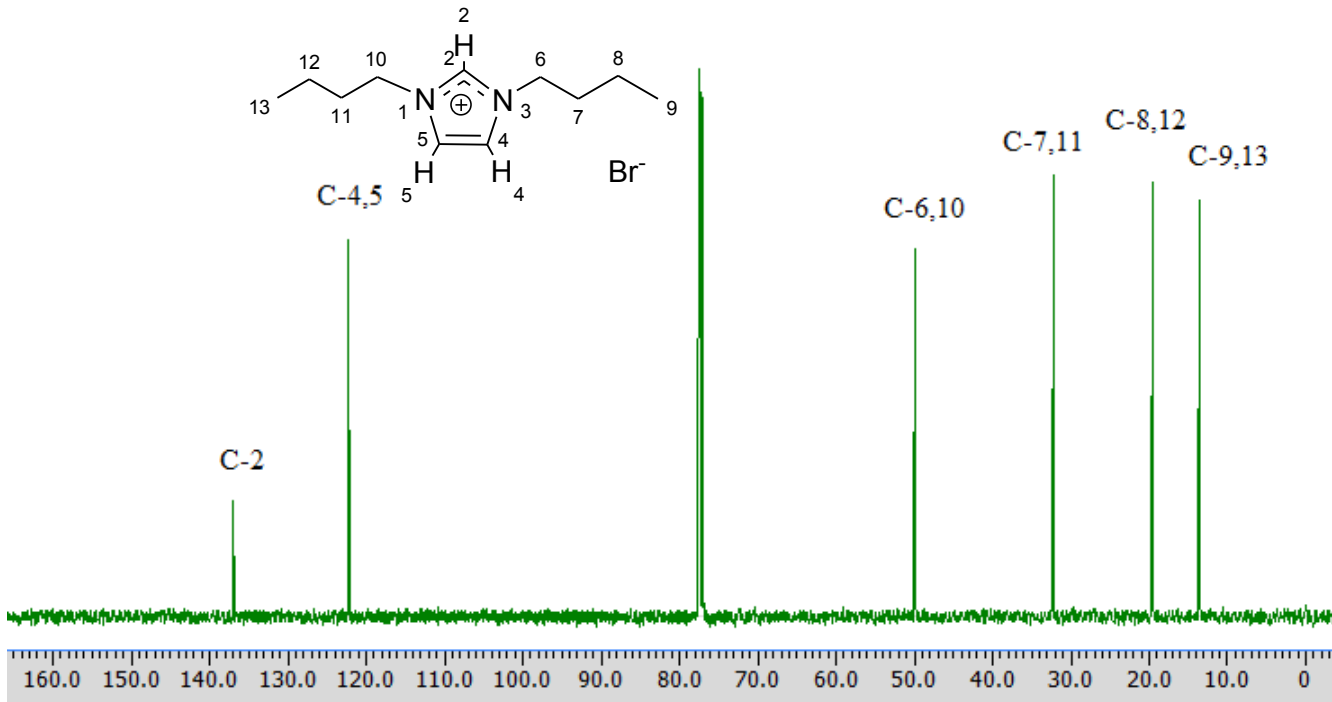
^{13}C NMR spectrum of 1-ethyl-3-butylimidazolium bromide ($[\text{C}_2\text{bim}][\text{Br}]$)

APPENDIX D3



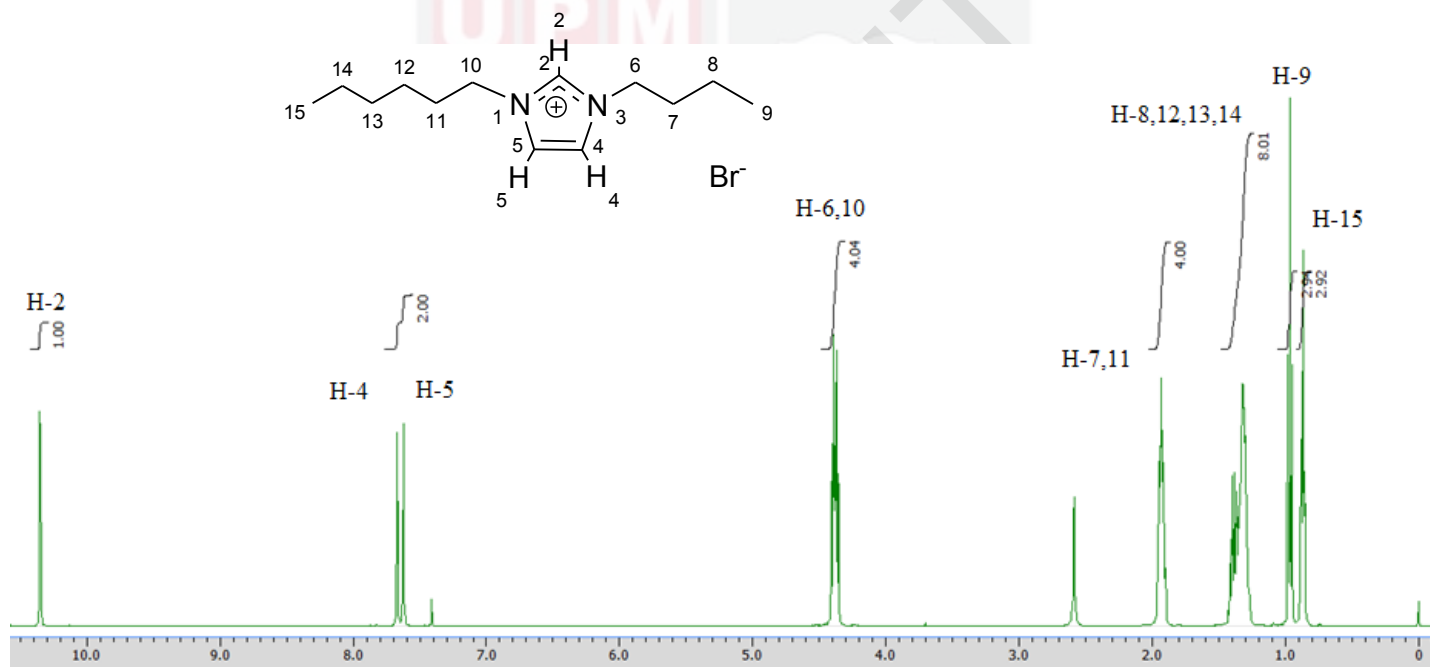
¹H NMR spectrum of 1,3-dibutylimidazolium bromide ([C₄bim][Br])

APPENDIX D4



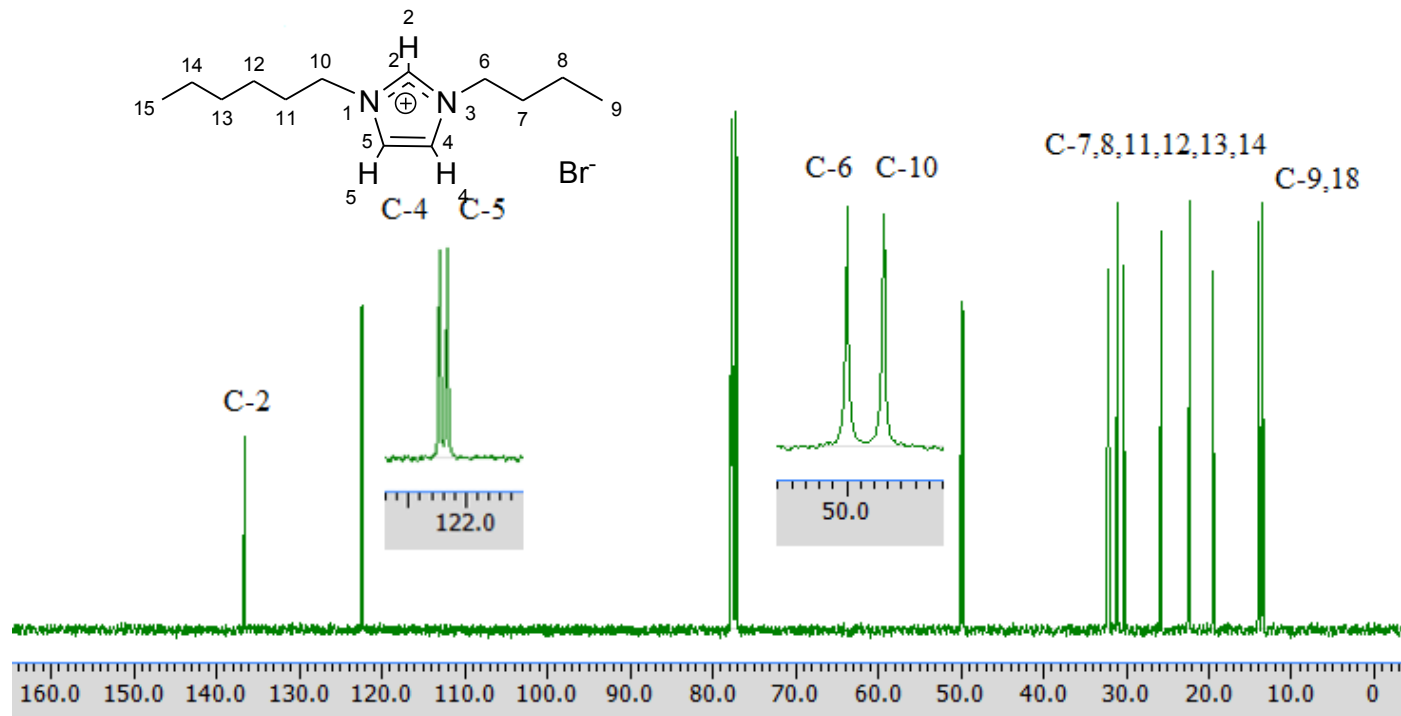
¹³C NMR spectrum of 1,3-dibutylimidazolium bromide ([C₄bim][Br])

APPENDIX D5

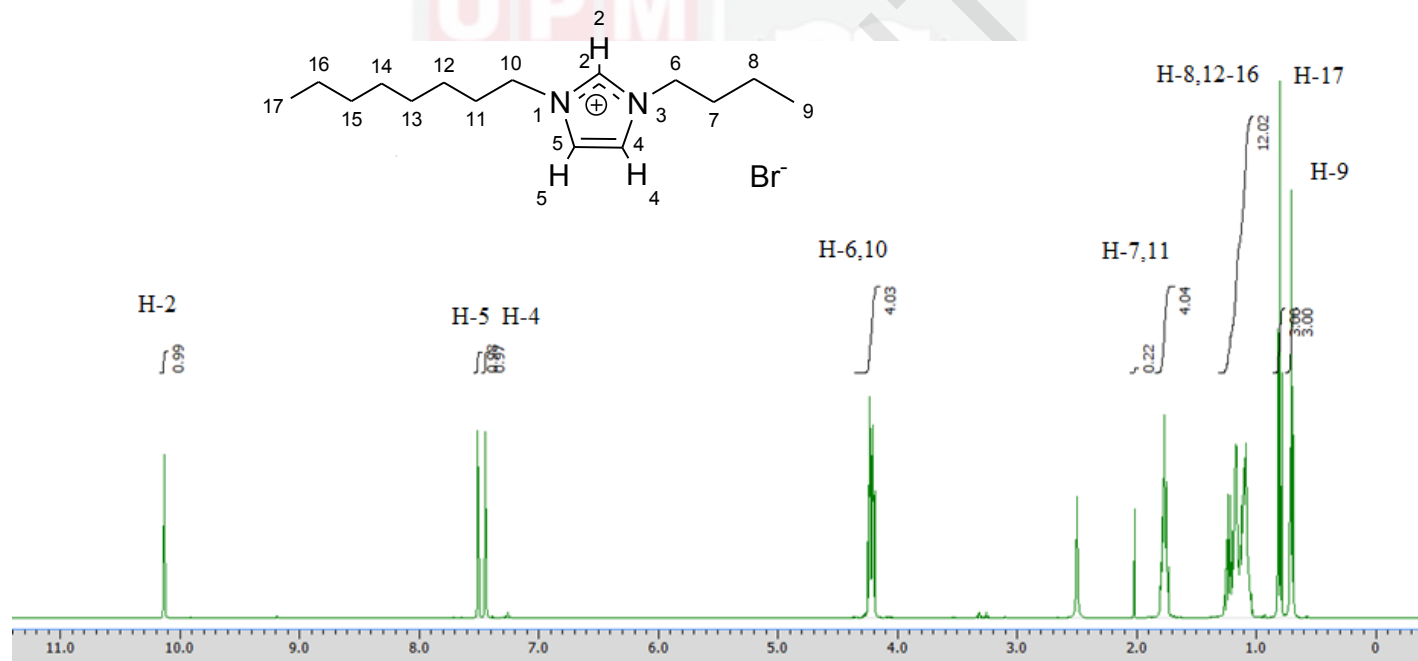


¹H NMR spectrum of 1-hexyl-3-butylimidazolium bromide ([C₆bim][Br])

APPENDIX D6

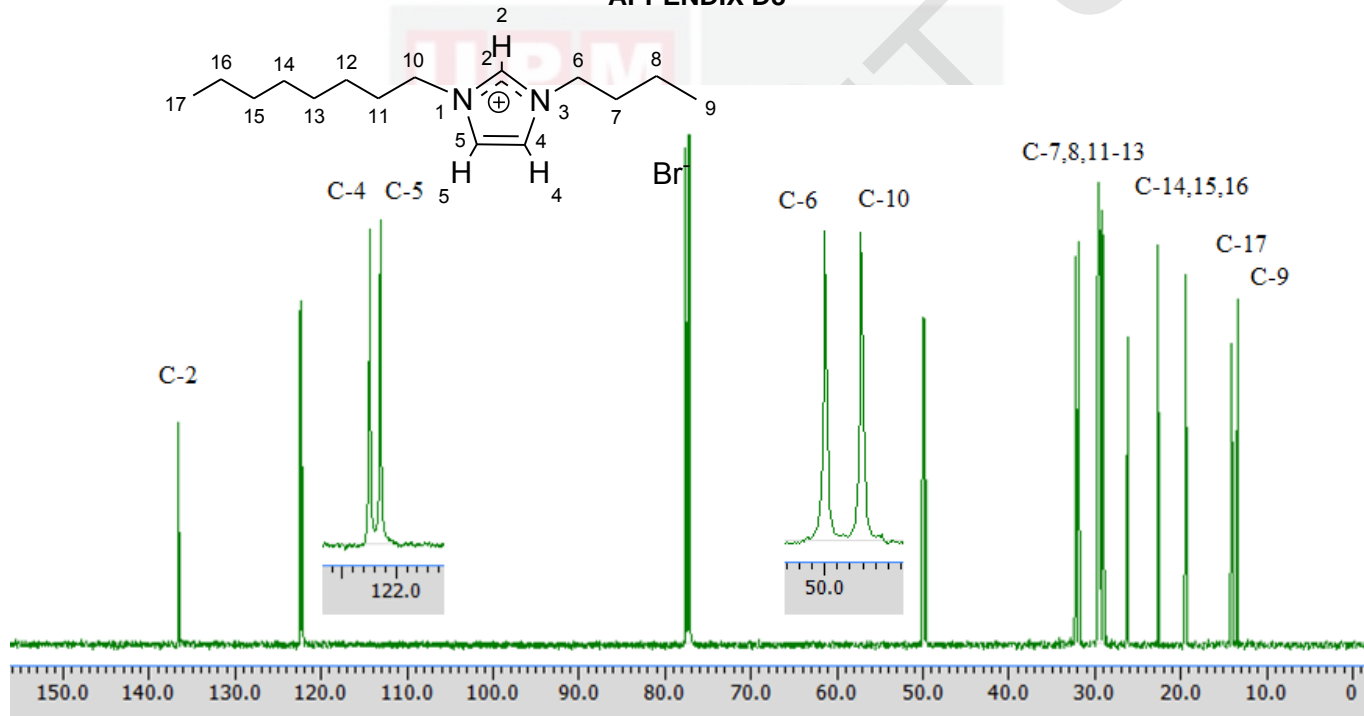
 ^{13}C NMR spectrum of 1-hexyl-3-butylimidazolium bromide ($[\text{C}_6\text{bim}][\text{Br}^-]$)

APPENDIX D7



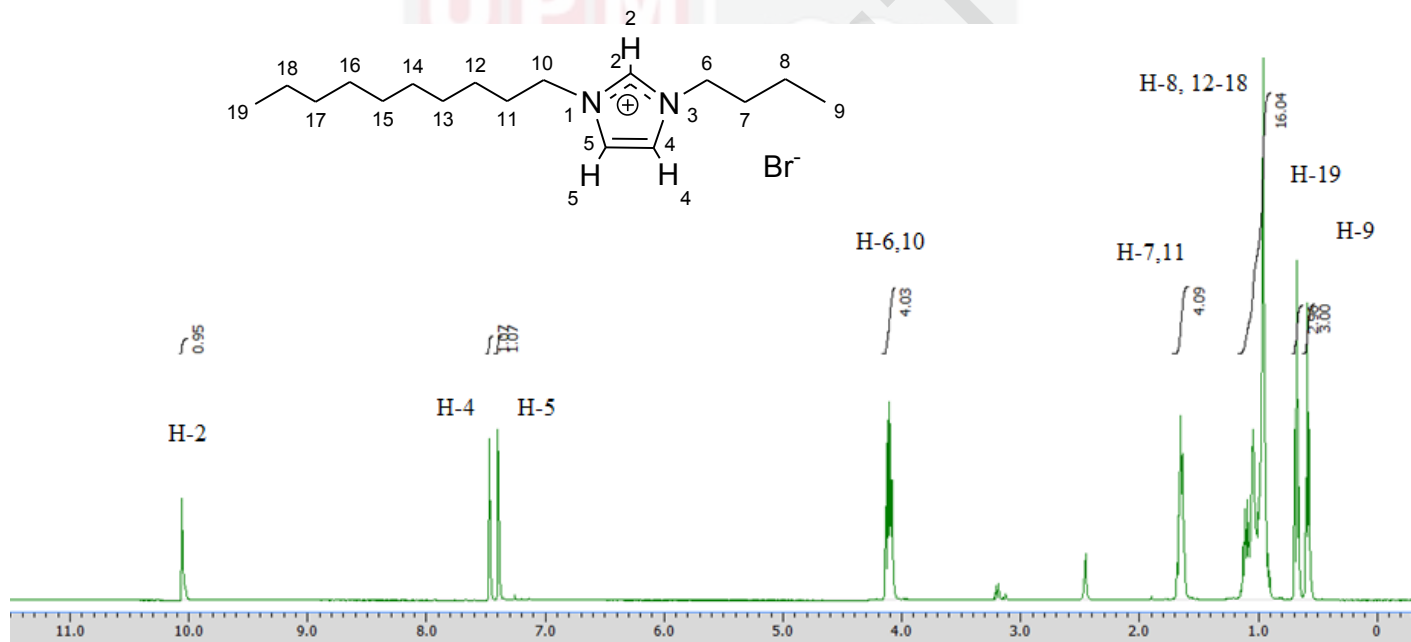
1H NMR spectrum of 1-octyl-3-butylimidazolium bromide ($[C_8bim][Br]$)

APPENDIX D8



^{13}C NMR spectrum of 1-octyl-3-butylimidazolium bromide ($[\text{C}_8\text{bim}][\text{Br}]$)

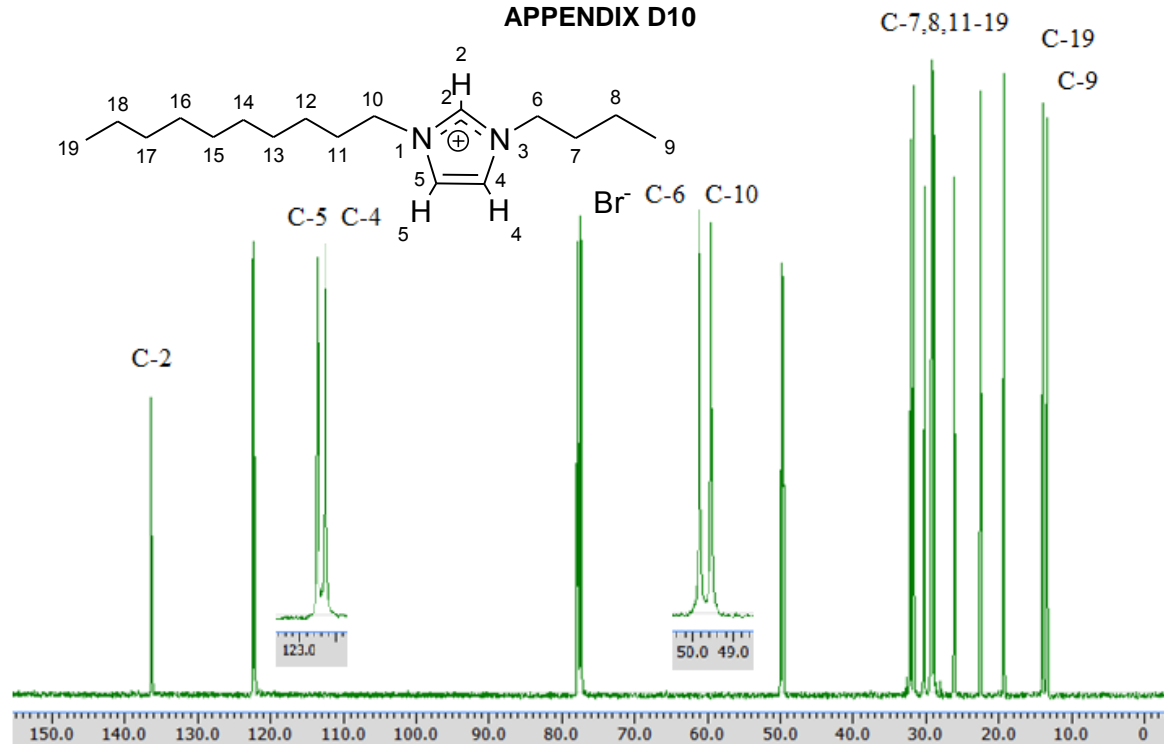
APPENDIX D9



1H NMR spectrum of 1-decyl-3-butylimidazolium bromide ($[C_{10}bim][Br]$)

DM

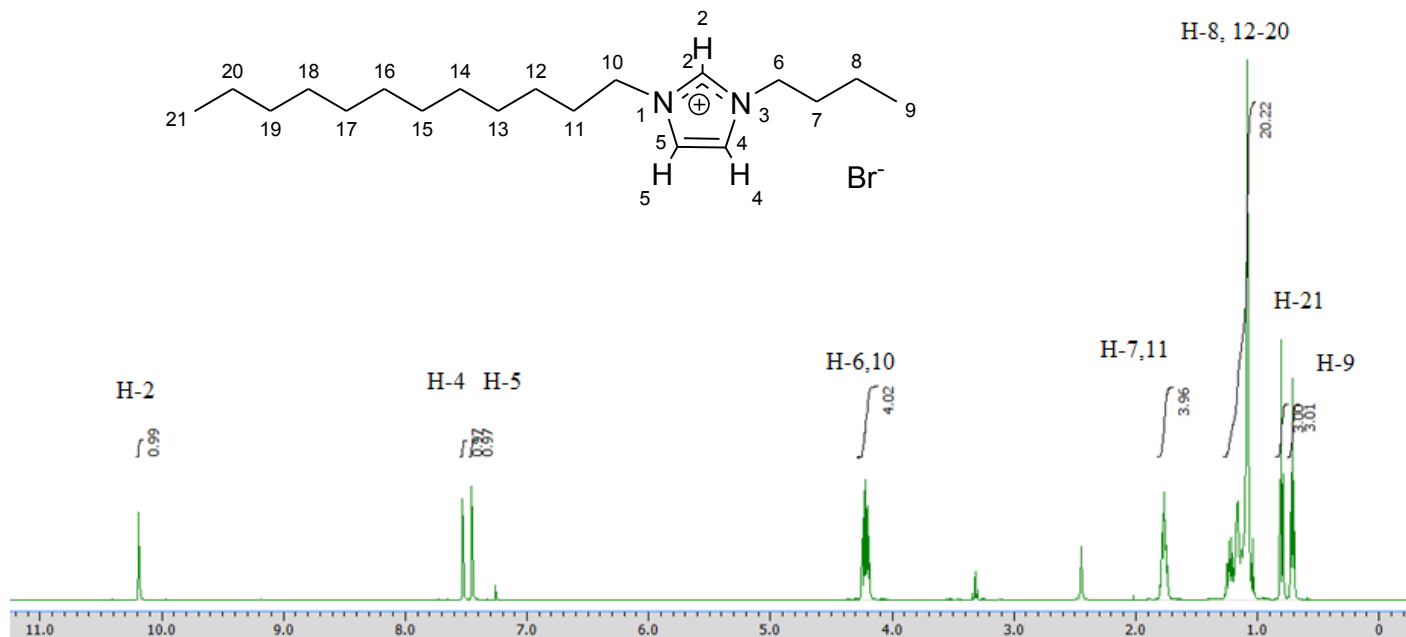
APPENDIX D10



¹³C NMR spectrum of 1-decyl-3-butylimidazolium bromide ([C₁₀bim][Br])



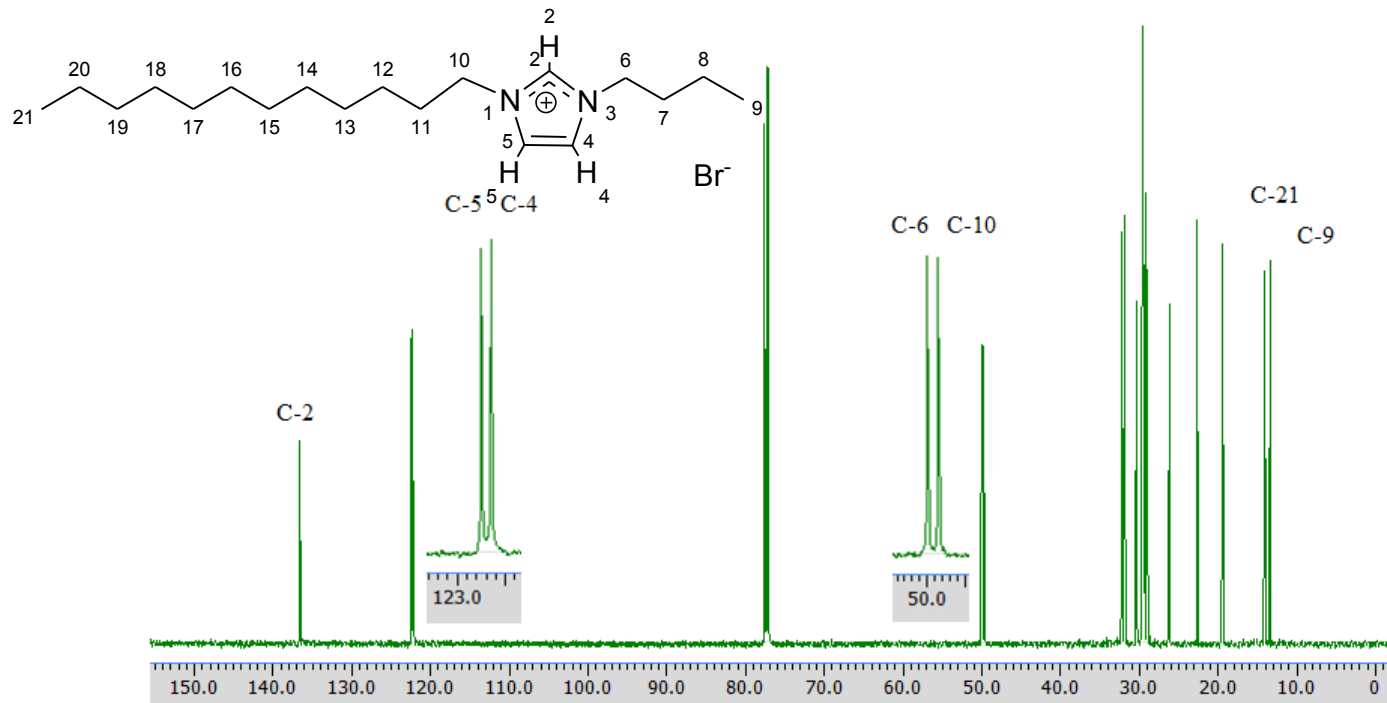
APPENDIX D11



^1H NMR spectrum of 1-dodecyl-3-butylimidazolium bromide ($[\text{C}_{12}\text{bim}][\text{Br}]$)

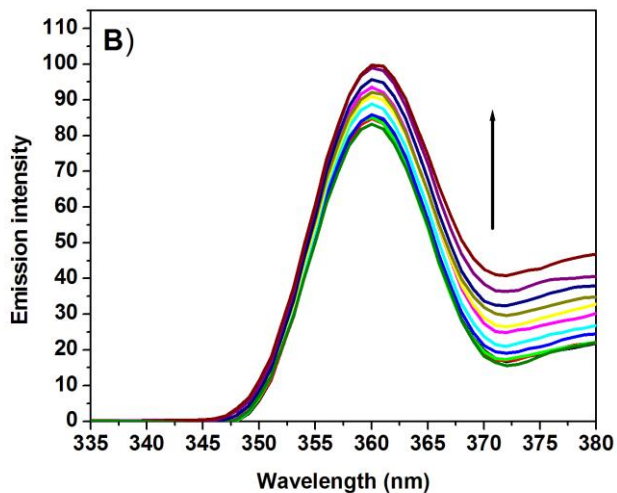
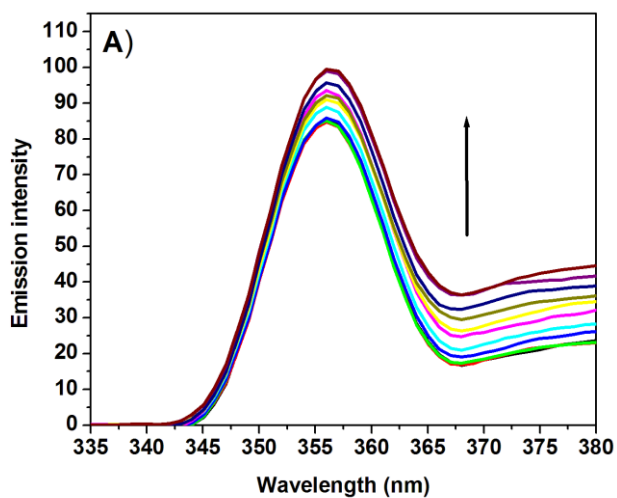
APPENDIX D12

C-7,8, 11-21



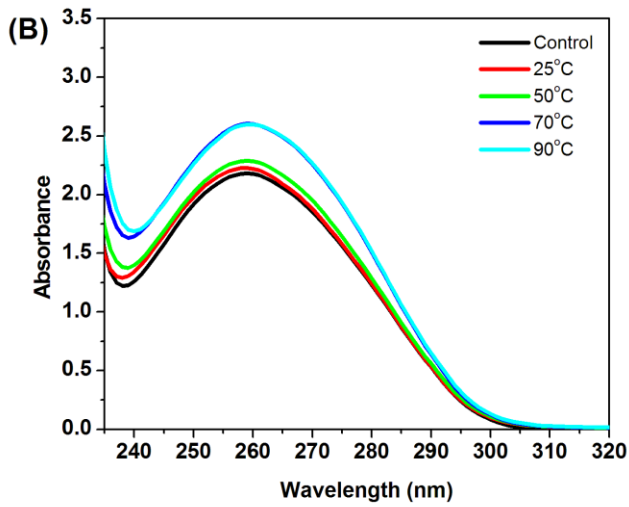
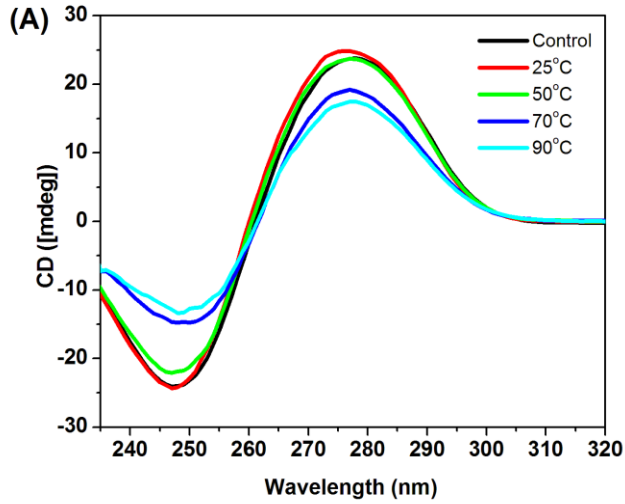
¹³C NMR spectrum of 1-dodecyl-3-butylimidazolium bromide ([C₁₂bim][Br])

APPENDIX E



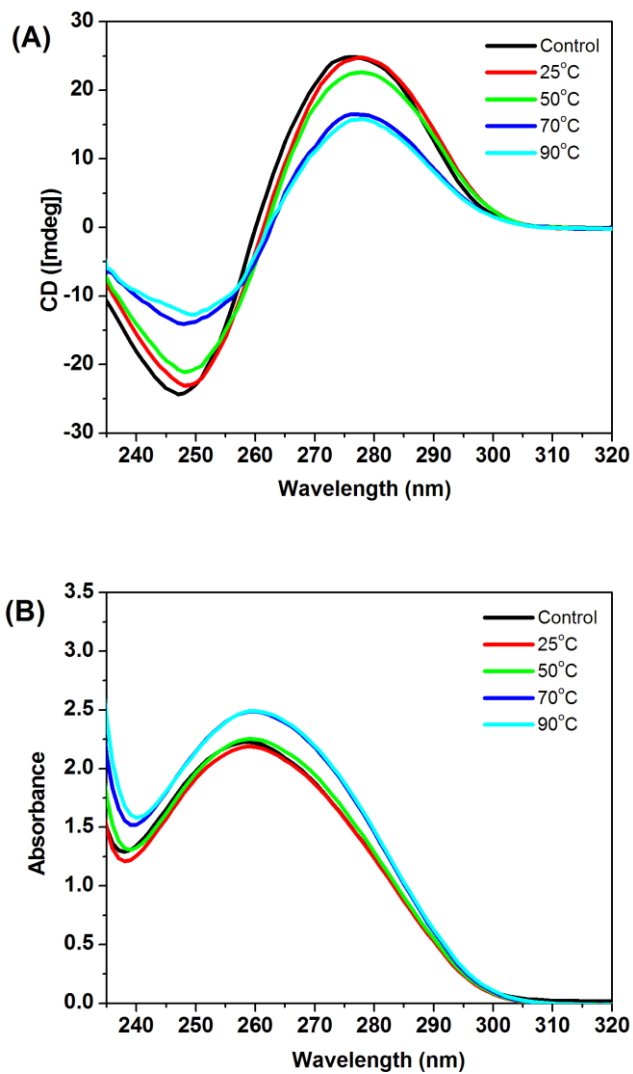
Fluorescence emission spectra of A) $[C_2bim][Br]$ and B) $[C_6bim][Br]$ in the absence (bottom curve) and presence of calf thymus DNA in aqueous solution of deionized water. The arrow indicates that the emission intensity of increases with the addition of DNA. Excitation wavelength was set at 320 nm.

APPENDIX F1



Circular dichroism (A) and UV absorbance (B) spectra of 60 μM Calf thymus DNA in the presence of $[\text{C}_2\text{bim}][\text{Br}]$ at different temperatures. Concentration $[\text{C}_2\text{bim}][\text{Br}]$ was fixed at 0.1 M.

APPENDIX F2



Circular dichroism (A) and UV absorbance (B) spectra of 60 μM Calf thymus DNA in the presence of $[\text{C}_6\text{bim}][\text{Br}]$ at different temperatures. Concentration $[\text{C}_6\text{bim}][\text{Br}]$ was fixed at 0.1 M.

LIST OF PUBLICATIONS / SEMINAR / CONFERENCE

A) Publication (Published / Submitted / Draft)

1. Khairulazhar Jumbri, Mohd Basyaruddin Abdul Rahman, Emilia Abdul Malek, Haslina Ahmad and Nuno M. Micaelo. An insight into structure and stability of DNA in ionic liquids from molecular dynamics simulation and experimental studies. *Phys. Chem. Chem. Phys.*, 2014; 16: 14036-14046.
2. Khairulazhar Jumbri, Emilia Abdul Malek, Haslina Ahmad and Mohd Basyaruddin Abdul Rahman. Binding Energy of Ionic Liquid-DNA Complex: Understanding the Role of Hydrophobic Interactions. *J. Phys. Chem. B* 2015 (Submitted).
3. Khairulazhar Jumbri, Mohd Basyaruddin Abdul Rahman and Nuno M. Micaelo. Predicted Solvation Free Energies of Nucleobases in Ionic Liquids. *Chem. Phys. Lett.* 2015 (Submitted).
4. Khairulazhar Jumbri, Emilia Abdul Malek, Haslina Ahmad and Mohd Basyaruddin Abdul Rahman. Biophysical Properties of Ionic Liquid-DNA Complex. *J. Fluoresc.* 2015 (Submitted).
5. Khairulazhar Jumbri, Emilia Abdulmalek, Haslina Ahmad and Mohd Basyaruddin Abdul Rahman. Synthesis and Properties of New 1-Alkyl-3-Butylimidazolium Bromide Ionic Liquids. (Manuscript in preparation).

B) SEMINAR / CONFERENCE / WORKSHOP

1. Regional Symposium of Malaysia Analytical Sciences (SKAM) "DNA in Hydrated Ionic Liquids", 9–10 Dec 2014, KSL Resort, Johor Bharu. Organized by Universiti Teknologi Malaysia. (Best Poster Presenter Award).
2. Exhibition of Invention, Research & Innovation (PRPI) for the research of "Molecular Insight into Structure and Stability of DNA in Ionic Liquids", 30 Sept–1st Oct 2014, Universiti Putra Malaysia. (Gold Medal Award).

3. Molecular Dynamics Simulation Workshop: Non-Aqueous Biocatalysis and Peptidomimetics (NABP 2013), 17–21 June 2013, Malaysia Genome Institute.
4. 1st ASEAN Workshop on X-Ray Absorption Spectroscopy (XAS), 29–31 July 2010, Synchrotron Light Research Institute (SLRI), Nakhon Ratchasima, Thailand.
5. 3rd National Seminar and Workshop on Computer Aided Drug Design: Virtual Screening, 2–8 Dec 2010, Universiti Sains Malaysia and Institute Pharmaceutical and Nutraceutical Malaysia (IPharm).



BIODATA OF AUTHOR



Khairulazhar Jumbri was born in Kuala Kurau, Perak on 28th May 1984. He received his primary education at Sekolah Kebangsaan Kuala Kurau and then continued his secondary education at Sekolah Menengah Kebangsaan Alang Iskandar (SMKAI), Bagan Serai, Perak. He completed his Matriculation of Science under Ministry of Education Malaysia (KPM) in 2003. Then he was offered to pursue his studies at UPM and three years later in 2006 he obtained Bachelor of Science (Honours) degree in Petroleum Chemistry. Upon his graduation, he was offered as temporary teacher at his old school, SMKAI. Starting of December 2006, he enrolled his Master of Science at Department of Chemistry, Faculty of Science, UPM under supervision Prof. Dr. Mohd. Basyaruddin Abdul Rahman. He was offered National Science Fellowship scholarship (NSF) from Ministry of Science, Technology and Innovation (MOSTI) Malaysia during his study. In 2010, he was offered a NSF scholarship for the second time for his PhD's programme.



UNIVERSITI PUTRA MALAYSIA

**STATUS CONFIRMATION FOR THESIS / PROJECT REPORT
AND COPYRIGHT**

ACADEMIC SESSION : 2014 / 2015

TITLE OF THESIS / PROJECT REPORT:

DESIGN AND SYNTHESIS OF NEW 1-ALKYL-3-BUTYLIMIDAZOLIUM BROMIDE IONIC LIQUIDS AS ALTERNATIVE MEDIA FOR DNA SOLVATION

NAME OF STUDENT :

KHAIRULAZHAR BIN JUMBRI

I acknowledge that the copyright and other intellectual property in the thesis/project report belonged to Universiti Putra Malaysia and I agree to allow this thesis/project report to be placed at the library under the following terms:

1. This thesis/project report is the property of Universiti Putra Malaysia.
2. The library of Universiti Putra Malaysia has the right to make copies for educational purposes only.
3. The library of Universiti Putra Malaysia is allowed to make copies of this thesis for academic exchange.

I declare that this thesis is classified as:

*Please tick (✓)

CONFIDENTIAL

(Contain confidential information under Official Secret Act 1972).

RESTRICTED

(Contains restricted information as specified by the organization / institution where research was done).

OPEN ACCESS

I agree that my thesis/project report to be published as hard copy or online open access.

This thesis is submitted for:

PATENT

Embargo from _____
until _____ (date)
_____ (date)

Approved by:

(Signature of Student)

New IC No: 840528-08-5463

Date :

(Signature of Chairman
of Supervisory Committee)

Name:

Date :

[Note : If the thesis is CONFIDENTIAL or RESTRICTED, please attach with the letter from the organization/institution with period and reasons for confidentially or restricted.]